Discovering Poncelet Invariants in the Plane

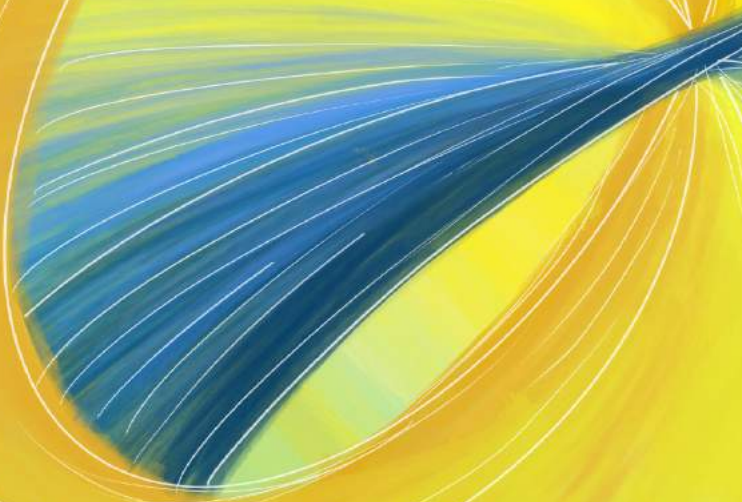

Ronaldo A. Garcia
Dan S. Reznik

impa

33º Colóquio Brasileiro de Matemática

Discovering Poncelet Invariants in the Plane

Discovering Poncelet invariants in the plane
Primeira impressão, julho de 2021

Publicado no Brasil / Published in Brazil.

ISBN 978-65-89124-43-6
MSC (2020) Primary: 37M05, Secondary: 14H70, 37C83, 51M15, 51N20, 14Q05

Coordenação Geral Carolina Araujo

Produção Books in Bytes **Capa** Izabella Freitas & Jack Salvador

Realização da Editora do IMPA
IMPA
Estrada Dona Castorina, 110
Jardim Botânico
22460-320 Rio de Janeiro RJ

www.impa.br
editora@impa.br

Preface

Since the discovery of Poncelet's porism in the 1810s, a steady stream of proofs has been put forth, drawing upon the ever-evolving language and abstraction of mathematics. These started in the 19th century with Poncelet's own synthetic/analytic proof, passing through Jacobi's treatment with elliptic functions, all the way to our era where the phenomenon is understood on an abstract torus. See Del Centina (2016a,b) for the historical background.

Indeed, for the past 200 years, the focus has been on refining proofs and understanding ramifications of the porism with respect to other areas of Mathematics. One consequence has been that the ambient, dynamic planar geometry of Poncelet polygons has been mostly unexplored.

In this book we take this less-traveled road, i.e., utilizing tools of interactive simulation, we set off to discover curious phenomena manifested by Poncelet polygons in the Euclidean plane. These include invariant metric quantities, the shape of loci of certain points, etc. Luckily, we have stumbled upon many interesting phenomena. Whenever possible, we illustrate the results with pictures and/or animations. To further engage the reader, we propose many exercises and research questions.

This research started in 2011 following lively conversations with Jair Koiller about the path of light rays in an ellipse. This resulted in several Mathematica simulations and a few videos uploaded to YouTube. After an 8-year hiatus, we resumed the work in early 2019 following a few very auspicious events: (i) one of the authors learned other mathematicians had watched our videos and published proofs of phenomena therein, (ii) Sergei Tabachnikov's invitation for us to pub-

lish an article (jointly with Jair Koiller) in the Mathematical Intelligencer, and (ii) our expository talk at IMPA's 32nd colloquium of Brazilian mathematics (see this video). Following this process our research sped up and we ended up producing dozens of papers and hundreds of experimental videos, which form the basis of this book.

We are indebted to several mathematicians and friends who have answered hundreds of our emails, and shared with us much needed insights: Arseniy Akopyan, Michael Bialy, Ana Chávez-Caliz, Mário Jorge Carneiro, Manish Chakrabarti, Ethan Cotterill, Marcos Craizer, Iverton Darlan, Carlos Esperança, Robert Ferréol, Corentin Fierobe, Sergey Galkin, Liliana Gheorghe, Bernard Gibert, João Gondim, Darij Grinberg, Mark Helman, Daniel Jaud, Clark Kimberling, Jair Koiller, Dominique Laurain, Nicholas McDonald, Peter Moses, Oliver Nash, Boris Odehnal, Matt Perlmutter, Pedro Roitman, Olga Romaskevich, Richard Schwartz, Hellmuth Stachel, Sergei Tabachnikov, Israel Vainsencher, Daniel Weller, Jorge Zubelli, and others.

We also thank IMPA for the opportunity to publish this book supporting our course in the 33rd Colloquium of Brazilian Mathematics (2021), and Paulo Ney de Souza for his encouragement, and editorial support.

Ronaldo Garcia & Dan Reznik

Goiânia & Rio de Janeiro, Brazil

July, 2021

Contents

1 Introduction

1.1 Poncelet preliminaries

Poncelet's closure theorem is illustrated in Figure 1.1. It is based on a simple geometric iteration. Given two nested ellipses[1] $\mathcal{E}$ and $\mathcal{E}_c$, pick a point P_1 on the boundary of $\mathcal{E}$. Let P_2 be where a ray shot from P_1 along one of the tangents to $\mathcal{E}_c$ meets $\mathcal{E}$ again. Repeat this from P_2, yielding P_3, etc. This produces a piecewise-linear Poncelet *trajectory*.

For most choices of $(\mathcal{E}, \mathcal{E}_c)$, the trajectory will never close, i.e., it will never meet P_1 again. In fact, it will fill a region between the two conics. However, for certain choices [2], the trajectory will indeed close. Let N, and integer greater than 2, be the number of steps required for P_1 to be met again. We call such polygonal trajectories "N-periodic".

Still referring to Figure 1.1, Poncelet's theorem states that if a trajectory departing from some point P_1 on $\mathcal{E}$ closes after N steps, then a *porism* is triggered which prescribes a 1d family of N-gons: a trajectory departing from *any* other point on the boundary of $\mathcal{E}$ will also close in N steps. We say such a pair "admits" a 1d family of N-periodic trajectories.

[1] The theorem is projective, i.e., it works for any pair of conics, nested or not.

[2] Those which satisfy Cayley's conditions, see Dragović and Radnović (2011).

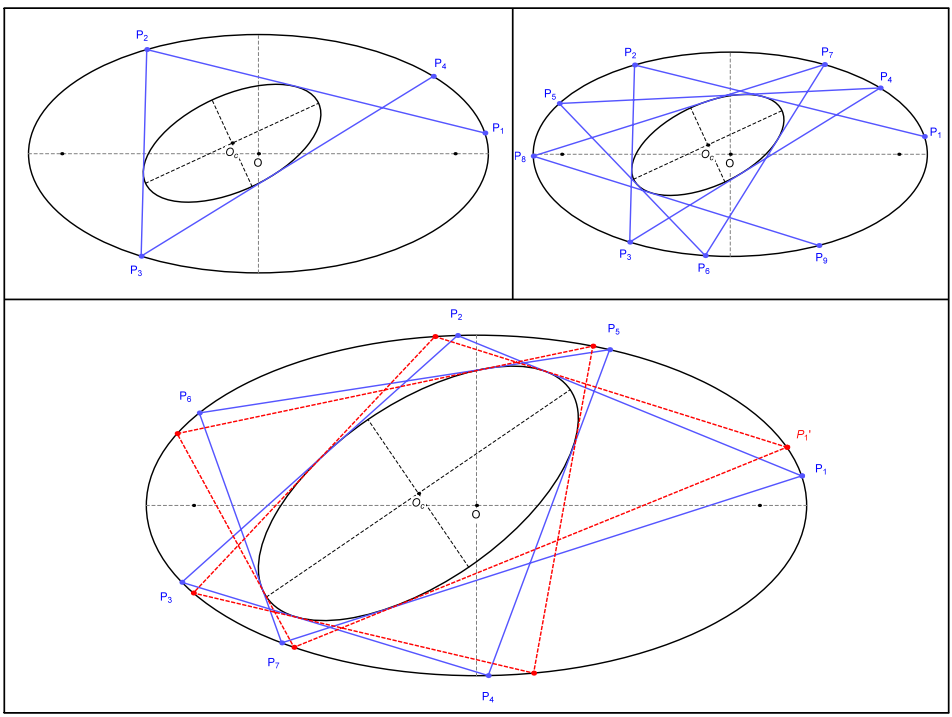

Figure 1.1: **Top left**: 3 Poncelet iterations within a pair of ellipses in general position; their centers are labeled O and O_c, respectively. Top right: 5 more iterations executed (starting at P_4), showing the trajectory is not likely to close. **Bottom:** a new ellipse pair for which an iteration departing from P_1 closes after 7 steps (blue polygon). Poncelet's porism guarantees that if the iteration were to start anywhere else on the outer ellipse, e.g., P_1', it will also yield a closed, 7-gon (dashed red). Video, Live

Poncelet's theorem has been widely studied for over 2 centuries. It is regarded as a fundamental result in algebraic geometry, see the surveys in Bos, Kers, and Raven (1987), Del Centina (2016b), and Dragović and Radnović (2014).

1.2 The elliptic billiard

A special case with remarkable properties is when $\mathcal{E}$ and $\mathcal{E}_c$ are constrained to be *confocal*, i.e., to have coinciding foci, see Figure 1.2. As a corollary to Graves' theorem described in Tabachnikov (2005), consecutive segments of a trajectory (open or closed) are bisected by the normal to $\mathcal{E}$. Thus, the iteration can be regarded as the path of a small billiard ball undergoing elastic collisions against the boundary of $\mathcal{E}$. For this reason, the confocal pair is also termed the *elliptic billiard*. An elliptic billiard trajectory can also be interpreted as the path of a light ray reflecting in a mirrored elliptic cavity. Since all rays are tangent to an internal, virtual ellipse, one borrows a term from optics and calls the latter the *caustic*[3]. From a dynamical systems' point of view, the path of the billiard ball is constrained by two *integrals of motion*, namely, linear and angular momentum. This renders the system *integrable*: the trajectory can be fully computed from initial conditions. For a more formal definition, see Tabachnikov (ibid.). Indeed, the elliptic billiard is conjectured as the *only* integrable planar billiard, see Kaloshin and Sorrentino (2018).

Assume a pair of confocal ellipses has been chosen which admits an N-periodic family. A first remarkable property is that in the confocal case, the family *conserves* perimeter, i.e., perimeter is *invariant*. This is all the more impressive[4] given the non-linearities constraining the dynamic geometry of billiard N-periodics.

1.3 Focusing on 3-periodics

Though invariant perimeter is a prime example of a clearly inspectable metric phenomenon, little attention has been paid as to whether confocal (or other Poncelet families) may manifest any additional, interesting, euclidean phenomena. Here, partly owing to our limitations, we did get a head start exploring that less-traveled road, i.e., using simulation to probe the dynamic geometry of Poncelet families for any salient Euclidean properties.

[3] In optics, this term refers to the *envelope* of rays reflected from a curved mirror.

[4] In fact, this result is rooted on the fact that billiard trajectories are extrema of the perimeter function, see Tabachnikov (2005).

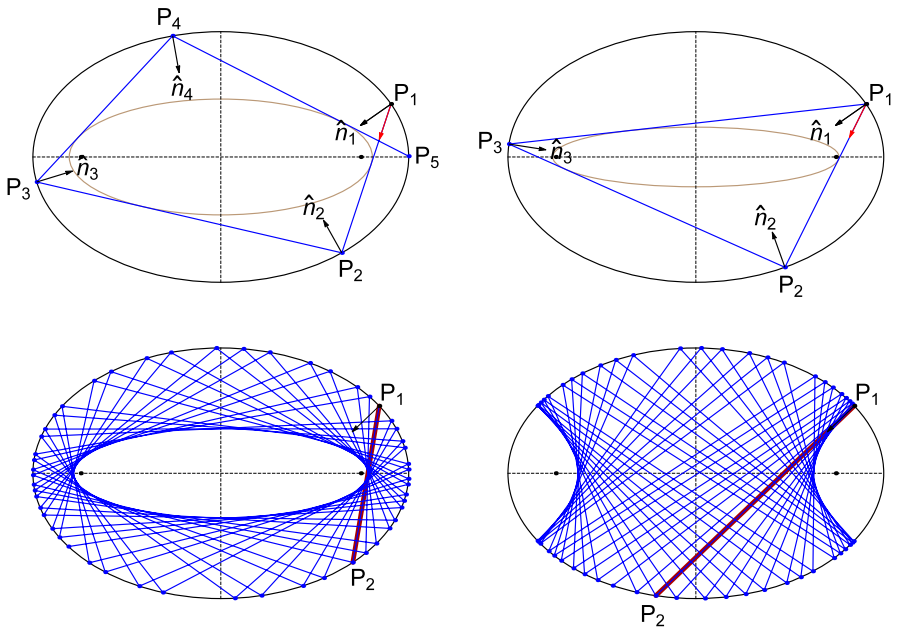

Figure 1.2: **Top left**: A confocal pair of ellipses; shown are the first four Poncelet iterations departing from P_1. Graves' theorem guarantees that each two consecutive segments are bisected by the ellipse normal $\hat{n}_i$. **Top right**: A closing 3-periodic trajectory. **Bottom left**: The first 50 segments of a non-periodic trajectory starting at P_1 and directed toward P_2, notice P_1P_2 does not pass between the two foci. **Bottom right**: a confocal pair comprising an ellipse and a hyperbola. All trajectory segments pass between the foci and are tangent to the hyperbola. Early Video 1, Video 2, Video 3

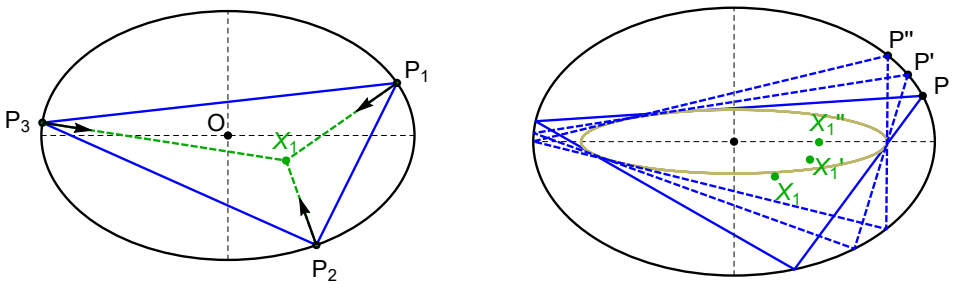

Figure 1.3: **Left:** An $N = 3$ *orbit*. Its incenter X_1 is where angular bisectors (black arrows) concur. **Right**: Three billiard 3-periodics tangent to a confocal caustic (brown). Over positions P, P', P'' of a first vertex. Also shown are the corresponding incenters X_1, X_1', X_1''. Video 1, Video2

At a first moment, we further restricted our search to $N = 3$ families only, confocal or not. Indeed, this book is a tale of the offspring – properties and invariants – of the unlikely marriage of triangle geometry and Poncelet constraints.

The literature covering triangle geometry is extensive, though have often referred to Gallatly (1914) and Johnson (1960). For informal use we have relied on Weisstein (2009, 2019).

1.4 Asking simple questions

An early observation is illustrated in Figure 1.3. Consider a confocal ellipse pair admitting a 3-periodic family. These are triangles whose internal angles are bisected by ellipse normals (see above). Known to the Greeks was the fact that the bisectors of a triangle concur (i.e., they meet) at a point known as the *incenter*. Immediately one is compelled to ask: "what could be the path, or locus, of the incenter, over the family of triangles in the confocal pair?" As it turns out, and despite all non-linearities, it is pure ellipse[5].

A second observation is illustrated in Figure 1.4. Directly associated with both a triangle and its incenter is the *incircle*, the unique circle tangent to each side of a triangle. The points of tangency are known as the *intouchpoints*. Again a natural question is "what is the locus of the intouchpoints over billiard 3-periodics?" As

[5]We later realized this is a very rare occurrence. The space of ellipse pair choices is 5d. That of confocal pairs 1d. There is growing evidence the locus of the incenter can only be an ellipse if the pair is confocal.

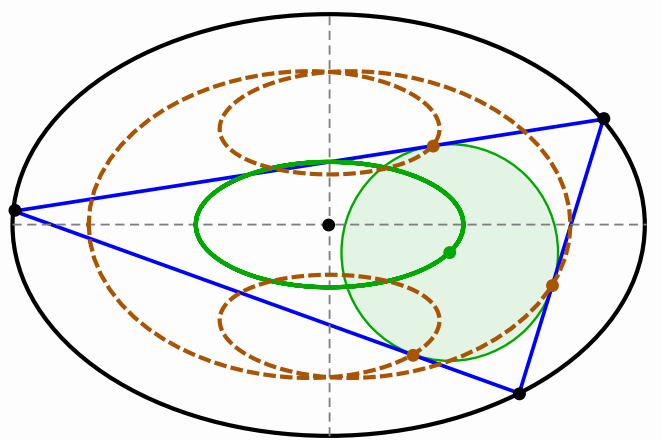

Figure 1.4: An $N = 3$ orbit (blue), its Incircle (transparent green), Incenter (green dot) and Intouch Points (brown dots). Over the $N = 3$ family, the Incenter locus is a perfect ellipse (green), while the Intouchpoints produce a self-intersecting sextic (dashed brown). Video, Live

shown in the figure, it turns out this locus is not as simple: it is a two-lobed, self-intersecting curve.

As one plays with other locus phenomena, one is quickly led to ask "what determines locus shape?" In this book we will explore these and many other related questions.

1.5 On to more confocal results

Upon a more systematic probing of confocal 3-periodics, there emerges a list of surprising facts:

- There is a special center of the triangle – the *mittenpunkt* – which remains *stationary* over the family at the common center.
- The ratio of the radii of two classic circles associated with a triangle – the circumcircle and incircle – is *invariant* over the family.
- In turn, the previous observation implies (via a well-known theorem) that the sum of internal angle cosines is also invariant. Interestingly, this fact

remains true[6] for $N > 3$ families!

1.6 Branching out to non-confocal families

Beyond confocal 3-periodics, we also investigate a few other "famous" concentric ellipse pairs, shown in Figure 1.5. These include a pair (i) with an incircle, (ii) with circumcircle, (iii) of homothetic ellipses, (iv) of "dual" ellipses, and (v) of the *excentral* triangles to the confocal pair itself. As it turns out, each aforementioned family maintains a specific *triangle center*[7] stationary at the common center. Experiments quickly identify special euclidean quantities each family conserves. For example, both the circumcircle and homothetic families conserves the sum of their *squared sidelengths*. While the former conserves the product of internal angle cosines, the latter conserves the sum of internal angle cotangents! Compare these with the confocal family, whose perimeter (i.e., the sum of sidelengths), and *sum* of its internal angle cosines are conserved.

Indeed, as properties, invariants, and loci types for each family were unearthed, we began to organize families in groups with shared "behaviors".

1.7 Analysis methods

We have used a number of methods to analyze and prove some of the facts detected experimentally. These include: (i) analytic geometry often assisted by a computer algebra system (CAS), (ii) synthetic and/or inversive geometry of conics, often relying on Akopyan and Zaslavsky (2007), Coxeter and Greitzer (1967), and Glaeser, Stachel, and Odehnal (2016), (iii) the theory of resultants to classify loci as algebraic, (iv) family parametrizations of various kinds, such as standard, elliptic-function-based, and one based on Blaschke products, as described in Daepp et al. (2019), etc.

In fact, the latter has also helped us approach two central questions: (i) what determines whether the locus of a triangle center is an ellipse or not, and (ii) whether the locus of the incenter (and/or excenters) can be an ellipse in a pair other than the confocal one. Experiments suggest it cannot, and a comprehensive proof is still lacking.

[6] Indeed, to us this opened a Pandora's box, since many properties of $N = 3$ systems continue to hold for $N > 3$.

[7] These are special points on a triangle, thousands of which are catalogued in Kimberling (2019).

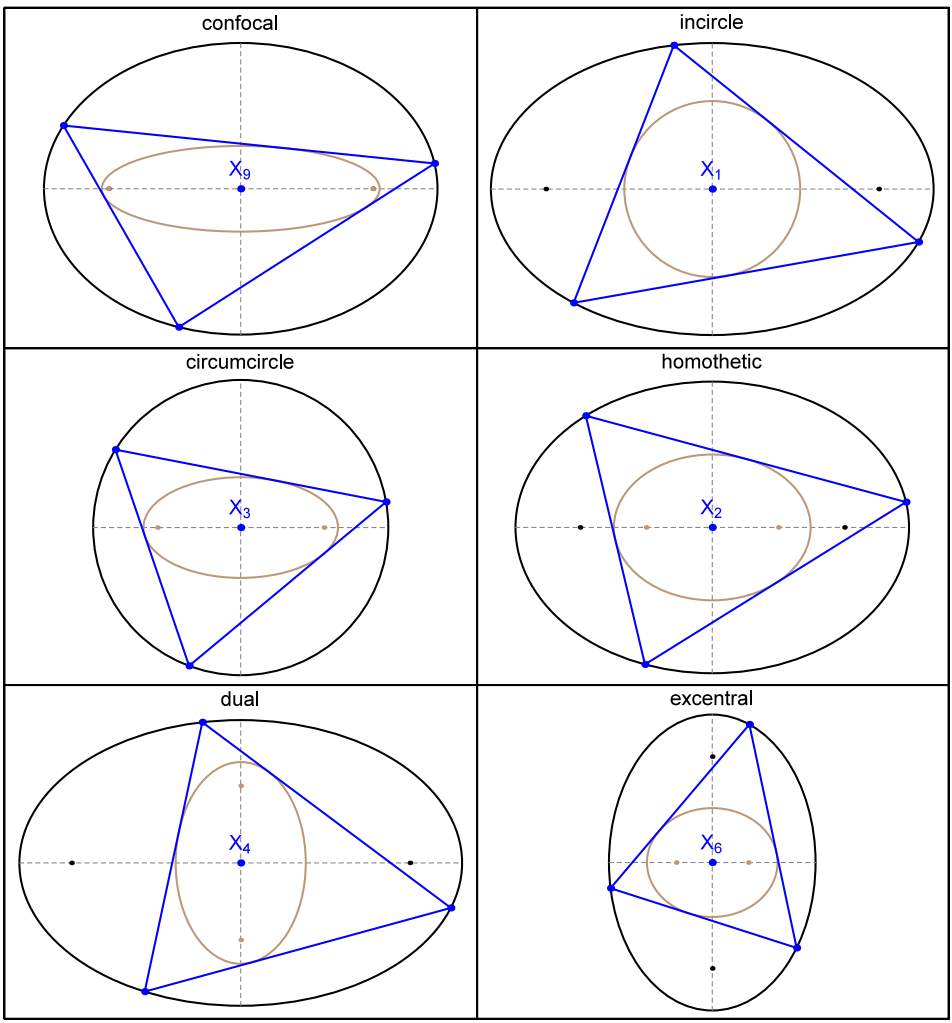

Figure 1.5: The confocal family is shown at the top left. Also shown are 5 other "famous" concentric families. Video

1.8 Related work

Loci of triangle centers over the $N = 3$ "poristic" family (interscribed between two circles) were studied by Odehnal (2011). In Schwartz and Tabachnikov (2016a) the loci of vertex, perimeter, and area centroids are studied over a generic Poncelet family indicating that the first and last are always ellipses while in general the perimeter one is not a conic. The locus of the "circumcenter-of-mass" (a generalization of the circumcenter for N-gons), studied in Tabachnikov and Tsukerman (2014), is shown to be a conic over Poncelet N-periodics in Chavez-Caliz (2020).

Over confocal 3-periodics, the elliptic locus of (i) the incenter was proved in Fierobe (2021), Garcia (2019), and Romaskevich (2014); (ii) of the barycenter in Garcia (2019) and Schwartz and Tabachnikov (2016a); and (iii) of the circumcenter in Fierobe (2021) and Garcia (2019). The elliptic locus of the Spieker center (which is the perimeter centroid of a triangle) was proved in Garcia (2019). Some properties and invariants of confocal N-periodics are described in Reznik, Garcia, and Koiller (2020a); $N = 3$ subcases are proved in Garcia, Reznik, and Koiller (2020b). Some invariants have been proved for all $N \geqslant 3$ in Akopyan, Schwartz, and Tabachnikov (2020), Bialy and Tabachnikov (2020), and Chavez-Caliz (2020).

1.9 Book organization

The next 3 chapters describe the basic geometry, several phenomena, and invariants of Poncelet 3-periodic families, as follows:

- Confocal family, Chapter 2: these are billiard 3-periodics, i.e., interscribed in a confocal pair of ellipses.
- Concentric, axis-parallel (CAP), Chapter 3: these are non-confocal triangle families interscribed in a pair of concentric, axis-parallel ellipses.
- Non-concentric, axis-parallel (NCAP), Chapter 4: these are triangle families interscribed in a pair of non-concentric, axis-parallel ellipses (and/or circles).

Following the above, we redirect our attention to the geometry and properties of loci of triangle centers and vertices over some of the aforementioned families. To be sure:

- Loci of the confocal family, Chapter 5.
- Loci in non-confocal CAP families Chapter 6.
- A framework for analyzing and explaining locus phenomena, based on Blashke products, Chapter 7.

In Chapter 8 we introduce a property-rich, non-Ponceletian family called the "focus inversive" family. These are images of billiard 3-periodics under an inversion with respect to a focus-centered circle.

Most figures herein will contain links to either YouTube videos or live demonstrations. The latter are rendered by a specially-built locus visualization application. Its functionality is described in Chapter 9.

At the end of every chapter we include a set of exercises and whenever possible, research questions. We very much encourage the reader to give them a try.

The following appendices are included:

- Appendix A contains some notes about triangle geometry. A more complete reference is of course Weisstein (2009).
- Appendix B contains a review of Jacobi elliptic functions used for one of our family parametrizations.
- In Appendix C we describe the loci of the Brocard points over a certain non-Ponceletian family of triangles defined with respect to an ellipse or a circle.

2 Confocal Pair

In this chapter we describe the geometry and properties of *billiard 3-periodics*, i.e., the 1d family of Poncelet triangles "interscribed"[1] in a pair of confocal ellipses. We begin by (i) reviewing some elliptic billiard preliminaries; then (ii) deriving conditions for the geometry of the inner ellipse (also known as the *caustic*); following that we review and prove some early results in regards to (iii) the elliptic loci of the incenter and excenter of the family, and (iv) the stationarity of a special triangle center known as the Mittenpunkt. Then (v) the key metric conservation of the ratio of inradius-to-circumradius is discussed. The chapter ends by proposing two alternative parameterizations for the vertices of billiard 3-periodics which we call standard and Jacobi-based.

2.1 Preliminaries

Let the confocal pair of ellipses $\mathcal{E}$ and $\mathcal{E}_c$ be given by:

$$\mathcal{E}: \frac{x^2}{a^2} + \frac{y^2}{b^2} - 1 = 0, \quad \mathcal{E}_c: \frac{x^2}{a_c^2} + \frac{y^2}{b_c^2} - 1 = 0$$

[1] This means inscribed in a first ellipse while circumscribing a second one.

where $c^2 = a^2 - b^2 = a_c^2 - b_c^2$.

Indeed, the family of billiard N-periodics classically conserve perimeter L and Joachimsthal's constant J. The latter one is equivalent to stating all trajectory segments are tangent to a confocal caustic, see Tabachnikov (2005, Thm 4.4) and Arnold and Tabachnikov (2020).

When $N = 3$, we can derive these explicitly using the vertex parametrization given in Equation (2.5).

Proposition 2.1. *For billiard 3-periodics, the perimeter and Joachimsthal's constant are given by:*

$$J = \frac{\sqrt{2\delta - a^2 - b^2}}{c^2}, \quad L = 2(\delta + a^2 + b^2)J$$

where $\delta = \sqrt{a^4 - a^2b^2 + b^4}$*, called here Darboux's constant.*

Proof. We compute the values considering an isosceles 3-periodic with $P_1 = [a, 0]$, and

$$P_2 = \left[\frac{a\left(b^2 - \delta\right)}{a^2 - b^2}, \frac{b^2\sqrt{2\delta - a^2 - b^2}}{a^2 - b^2}\right], \quad P_3 = \left[\frac{a\left(b^2 - \delta\right)}{a^2 - b^2}, -\frac{b^2\sqrt{2\delta - a^2 - b^2}}{a^2 - b^2}\right] \tag{2.1}$$

We have that

$$L = |P_2 - P_3| + 2|P_1 - P_2|, \quad J = \left\langle \frac{P_1 - P_3}{|P_1 - P_3|}, \left[\frac{1}{a}, 0\right]\right\rangle$$

Straightforward calculations using the vertex parametrization in Equation (2.5), leads to the stated result. □

Henceforth the oft-occurring quantity δ will be referred to as the Darboux constant. An interesting geometric interpretation for it appears in Proposition 2.5.

2.2 Caustic semiaxes

The Cayley condition for a concentric, axis parallel (CAP) pair of ellipses to admit a 3-periodic family is given by:

$$\frac{a_c}{a} + \frac{b_c}{b} = 1 \tag{2.2}$$

In turn, this constrains the semiaxes of the confocal caustic.

Proposition 2.2. *The semiaxes a_c, b_c of the confocal caustic are given by:*

$$a_c = \frac{a\left(\delta - b^2\right)}{c^2}, \quad b_c = \frac{b\left(a^2 - \delta\right)}{c^2}.$$

When $a = b$, we have that $a_c = b_c = a/2$.

Proposition 2.3. *The semiaxes a and b of the ellipse in terms of the semiaxes a_c and b_c of the confocal ellipse are given by:*

$$a = -\frac{1}{2}\sqrt{w_1} + \frac{1}{2}\sqrt{w_2 - \frac{2a_c^3 - 4c^2 a_c}{\sqrt{w_1}}} + \frac{a_c}{2}, \quad b = \sqrt{a^2 - c^2}$$
$$w_1 = a_c^2 - (4ca_c b_c)^{\frac{2}{3}}, \quad w_2 = 2a_c^2 + (4ca_c b_c)^{\frac{2}{3}}$$

The implicit equation that defines a above is the quartic given by

$$c^2(a_c^2 - 2a_c a) + a^2(2a_c a - a^2) = 0$$

2.3 Incenter and excenter loci

An intriguing phenomenon is that over billiard 3-periodics, the locus of both incenter and the excenters are ellipses, as was initially detected experimentally (see an early Video). This was proved in Romaskevich (2014) and Garcia (2019). Indeed, we haven't yet found another Poncelet pair where this is the case[2], see Conjecture 2 and Conjecture 3.

Referring to Figure 2.1:

Theorem 2.1. *Over billiard 3-periodics, the locus of the incenter X_1 and excenter are ellipses $\mathcal{E}_1$ and $\mathcal{E}_e$ concentric and axis-parallel with the confocal pair whose axes (a_1, b_1) and (a_e, b_e) are given by:*

$$a_1 = \frac{\delta - b^2}{a}, \quad b_1 = \frac{a^2 - \delta}{b}$$
$$a_e = \frac{b^2 + \delta}{a}, \quad b_e = \frac{a^2 + \delta}{b}$$

Furthermore, $\mathcal{E}_1$ and $\mathcal{E}_e$ have reciprocal aspect ratios, i.e., $a_1/b_1 = b_e/a_e$.

[2]One exception is the *poristic* family, for which the locus of the excenters is a circle and that of the incenter is a point.

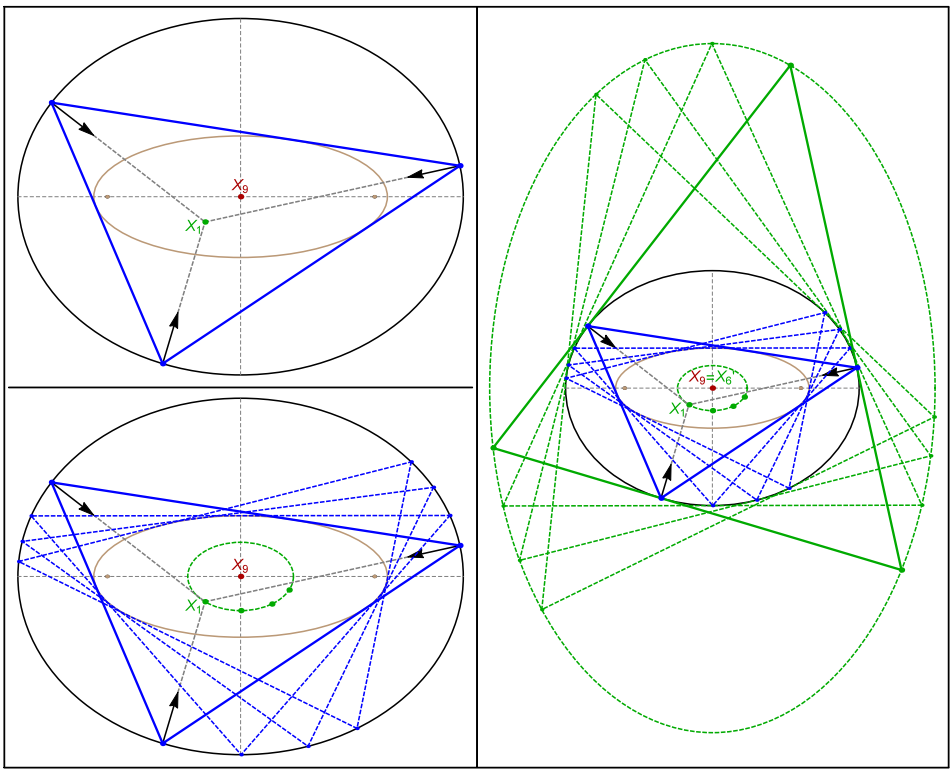

Figure 2.1: **Top Left:** An elliptic billiard 3-periodic (solid blue) is shown inscribed in an outer ellipse (black) and a confocal caustic (brown). Graves' theorem implies its internal angles will be bisected by ellipse normals (black arrows). Also shown is the incenter X_1 defined as the intersection of said bisectors. **Bottom Left:** Poncelet's porism implies a 1d family of such triangles exists. Some samples are shown (dashed blue). A classic invariant is perimeter. The Mittenpunkt X_9 remains stationary at the center. The incenter X_1 sweeps an ellipse (dashed green). **Right:** The excentral triangle (solid green) has sides perpendicular to the bisectors. Over billiard 3-periodics, the excentral is of variable perimeter. Its vertices (known as the "excenters") also sweep an ellipse (dashed green) whose aspect ratio is the reciprocal of that of the incenter locus. The symmedian point X_6' of the excentral triangle coincides with X_9 of the reference and is therefore stationary. Live

Proof. It follows from the vertex parametrization in Equation (2.5) and the definition of incenter and excenters. We have that

$$X_1 = \frac{s_1 P_1 + s_2 P_2 + s_3 P_3}{s_1 + s_2 + s_3} = \frac{1}{L}(s_1 P_1 + s_2 P_2 + s_3 P_3)$$

where $s_1 = |P_2 - P_3|$, $s_2 = |P_1 - P_3|$ and $s_3 = |P_1 - P_2|$. A careful symbolic analysis shows that $\mathcal{E}_1(X_1) = 0$. A similar analysis considering the excenters shows that the locus of the three points is the ellipse $\mathcal{E}_e$ stated. □

A more general treatment to the above is given in Chapter 7.

Corollary 2.1. *The pair $\{\mathcal{E}, \mathcal{E}_e\}$ is Ponceletian.*

Proof. Direct from Cayley condition

$$\frac{a}{a_e} + \frac{b}{b_e} = \frac{a^2}{b^2 + \delta} + \frac{b^2}{a^2 + \delta} = 1$$

□

2.4 A stationary point

The Mittenpunkt X_9 is a triangle center where lines from each excenter thru the side midpoint meet. Referring to Figure 2.2:

Theorem 2.2. *Over the family of 3-periodics in the elliptic billiard, X_9 is stationary at the common center.*

An elegant synthetic proof was kindly contributed by Romaskevich (2019):

Proof. Let $\mathcal{E}$ be the outer ellipse in the confocal pair, O. By definition, the Mittenpunkt X_9 is where lines from the excenters E_i through the side midpoints M_i concur. Notice each side is an ellipse chord between tangents to $\mathcal{E}$ seen from the E_i (this is because in the confocal pair the excentral triangle is tangent to $\mathcal{E}$). Consider the image of lines $E_i M_i$ under an affine transform which sends $\mathcal{E}$ to a circle $\mathcal{C}'$, let O' be its center. The transformed lines will pass through the midpoints of chords of $\mathcal{C}'$ between tangents seen from E_i' (the affine image of E_i). By circular symmetry, such lines must also pass through O', and therefore remain stationary. But O' is the affine image of O, so the result follows. □

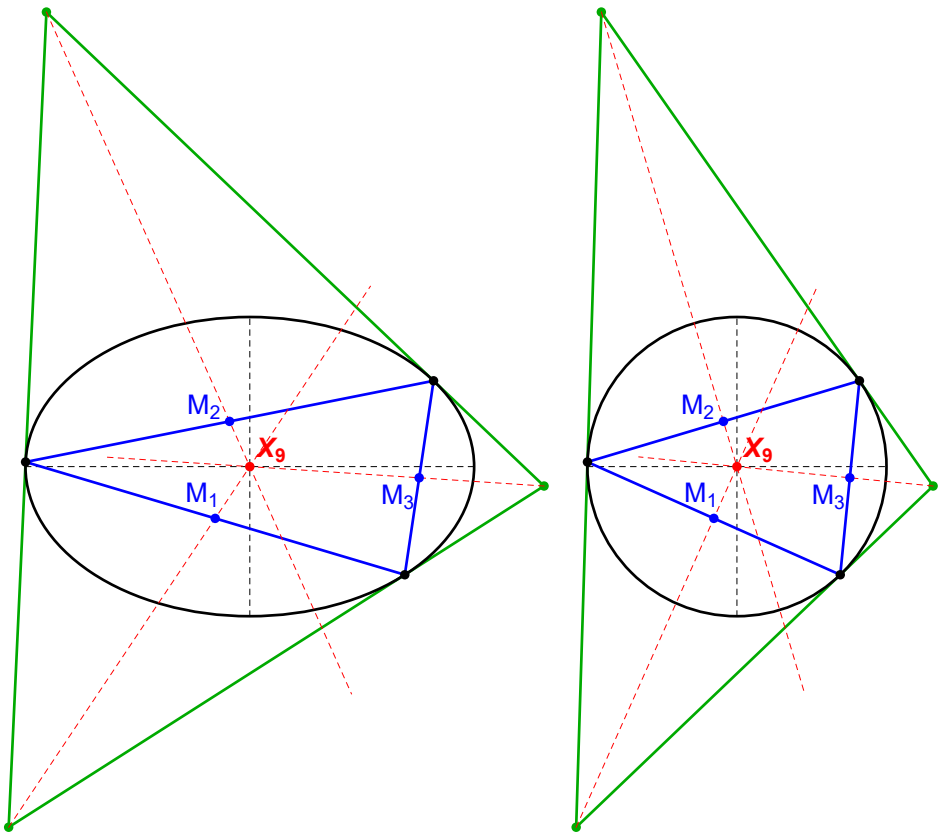

Figure 2.2: **Left**: 3-periodic billiard triangle (blue), its excentral triangle (green). The Mittenpunkt X_9 is the point of concurrence of lines drawn from the excenters through sides' midpoints M_i. **Right**: the affine image which sends the billiard to a circle. Lines from imaged excenters through sides' midpoints must pass through the origin. Since the latter is stationary, so must be its pre-image X_9, which is stationary at the billiard center. Video

2.5 Conserved quantities

Given a triangle, let r and R denote the radius of its incircle and circumcircle, known as the *inradius* and *circumradius*, respectively. Over billiard 3-periodics, note these two radii are variable. Referring to Figure 2.3:

Theorem 2.3. *r/R is invariant over billiard 3-periodics and given by:*

$$\frac{r}{R} = \frac{2(\delta - b^2)(a^2 - \delta)}{c^4}.$$

Proof. The following relation, found in Johnson (1960), holds for any triangle:

$$rR = \frac{s_1 s_2 s_3}{2L},$$

where $L = s_1 + s_2 + s_3$ is the perimeter, constant over billiard 3-periodics. Therefore:

$$\frac{r}{R} = \frac{1}{2L}\frac{s_1 s_2 s_3}{R^2}. \tag{2.3}$$

Next, let $P_1 = (a, 0)$ be a vertex of an isosceles 3-periodic. Obtain a candidate expression for r/R. This yields (2.3) exactly. Using the vertex parametrization in Equation (2.5), derive an expression for the square of the right-hand side of (2.3) as a function of x_1 and subtract from it the square of (2.3). In Garcia, Reznik, and Koiller (2020b) it is shown $\left(s_1 s_2 s_3/R^2\right)^2$ is rational on x_1. For simplification, use $R = s_1 s_2 s_3/(4A)$, where A is the triangle area. With a CAS, show said difference is identically zero for all $x_1 \in (-a, a)$. □

Let θ_i, r, R, and A denote the ith internal angle, inradius, circumradius, and area of a reference triangle. Primed quantities refer to the excentral triangle. The relations below, appearing in Johnson (1960), hold for any triangle:

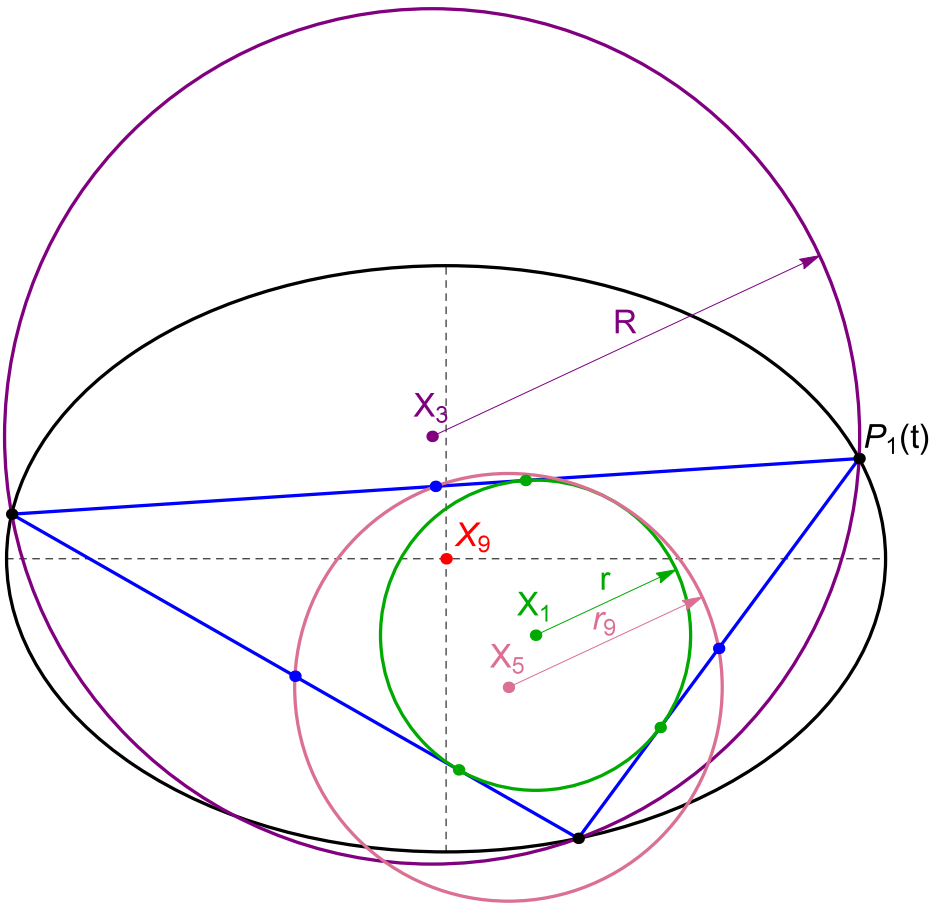

Figure 2.3: The incircle (green), circumcircle (purple), and 9-point (Euler's) circle (pink) of a billiard triangle (blue). These are centered on X_1, X_3, and X_5, respectively. Their radii are the inradius r, circumradius R, and 9-point circle radius $r_9 = 2R$. Over the family, the ratio r/R is invariant. In turn this implies an invariant sum of cosines. Live

$$\sum_{i=1}^{3} \cos\theta_i = 1 + \frac{r}{R} \tag{2.4}$$
$$\prod_{i=1}^{3} \cos\theta_i' = \frac{r}{4R}$$
$$\frac{A}{A'} = \frac{r}{2R}$$

Corollary 2.2. *Over billiard 3-periodics, also invariant are the sum of 3-periodic cosines, the product of excentral cosines, and the ratio of excentral-to-3-periodic areas.*

Direct calculations yields an expression for the invariant sum of cosines in terms of elliptic billiard constants J and L.

Corollary 2.3. $\sum_{i=1}^{3} \cos\theta_i = JL - 3$

Indeed in Akopyan, Schwartz, and Tabachnikov (2020) it is shown that for all N the sum of cosines is invariant and equal to $JL - N$.

Let P_i be a billiard 3-periodic vertex and $d_{j,i} = |P_i - f_j|$ its distance to billiard focus f_j.

Proposition 2.4. *Over billiard 3-periodics, the following sum is invariant:*

$$\sum \frac{1}{d_{1,i}} = \sum \frac{1}{d_{2,i}} = \frac{a^2 + b^2 + \delta}{ab^2}$$

Proof. Direct computation with CAS using vertex parametrization given in Section 2.7. □

Let $P = (x, y)$ be a point on an ellipse with semiaxes a, b. In Weisstein (2019, Ellipse), the curvature at P is expressed both in terms of its coordinates and the distances d_1, d_2 to the foci as follows:

$$\kappa = \frac{1}{a^2 b^2}\left(\frac{x^2}{a^4} + \frac{y^2}{b^4}\right)^{-3/2} = \frac{ab}{(d_1 d_2)^{3/2}}$$

Let κ_i denote the billiard ellipse curvature at vertex P_i of a Poncelet 3-periodic. From the above and Proposition 2.4 obtain:

Corollary 2.4. *Over billiard 3-periodics, the following quantity is conserved:*

$$\sum_{i=1}^{3} \kappa_i^{\frac{2}{3}} = \frac{a^2+b^2+\delta}{(ab)^{\frac{4}{3}}}$$

2.6 An interpretation for Darboux's constant

Darboux's constant δ appearing above has a curious geometric interpretation. Recall the power of a point Q with respect to a circle $\mathcal{C} = (C_0, R_0)$ is given by $|Q - C_0|^2 - R_0^2$, see Weisstein (2019, Circle Power). Let $\mathcal{C}$ denote the (moving) circumcircle of billiard 3-periodic, and $O = X_9$ the billiard center.

Proposition 2.5. *The power of O with respect to $\mathcal{C}$ is constant and equal to $-\delta$.*

Proof. Consider an isosceles billiard 3-periodic given by Equation (2.1). Its circumcircle will be centered at $C_0 = [\frac{b^2-\delta}{2b}, 0]$ with circumradius $R_0 = \frac{b^2+\delta}{2b}$. Therefore, the power of the center of the ellipse with respect to the circumcircle is given by

$$|OC_0|^2 - R_0^2 = \left(\frac{b^2-\delta}{2b}\right)^2 - \left(\frac{b^2+\delta}{2b}\right)^2 = -\delta.$$

The stated invariance is confirmed with a CAS using the vertex parametrization in Equation (2.5). □

2.7 Confocal vertex parametrization

We describe two parametrizations for billiard 3-periodic vertices: (i) standard and (ii) Jacobi.

2.7.1 Standard

We call "standard" parametrization that where a first vertex $P_1(t)$ of the billiard 3-periodic is parametrized as $P_1(t) = [x_1, y_1] = [a\cos t, b\sin t]$.

As derived in Garcia (2019), $P_2 = (x_2, y_2)/q_2$ and $P_3 = (x_3, y_3)/q_3$ where:

$$
\begin{aligned}
x_2 =& -b^4\left(\left(a^2+b^2\right)\cos^2\alpha - a^2\right)x_1^3 - 2a^6\,\cos\alpha\sin\alpha\,y_1^3\\
&+ a^4\left(\left(a^2-3\,b^2\right)\cos^2\alpha + b^2\right)x_1\,y_1^2 - 2\,a^4b^2\cos\alpha\,\sin\alpha x_1^2 y_1,\\
y_2 =& 2b^6\,\cos\alpha\sin\alpha\,x_1^3 - a^4\left(\left(a^2+b^2\right)\cos^2\alpha - b^2\right)y_1^3\\
&+ 2\,a^2b^4\cos\alpha\sin\alpha\,x_1 y_1^2 + b^4\left(\left(b^2-3\,a^2\right)\cos^2\alpha + a^2\right)x_1^2 y_1\\
q_2 =& b^4\left(a^2-\left(a^2-b^2\right)\cos^2\alpha\right)x_1^2 + a^4\left(b^2+\left(a^2-b^2\right)\cos^2\alpha\right)y_1^2\\
&- 2\,a^2b^2\left(a^2-b^2\right)\cos\alpha\sin\alpha\,x_1\,y_1.
\end{aligned}
\tag{2.5}
$$

$$
\begin{aligned}
x_3 =& \,b^4\left(a^2-\left(b^2+a^2\right)\cos^2\alpha\right)x_1^3 + 2\,a^6\cos\alpha\,\sin\alpha\,y_1^3\\
&+ a^4\left(\cos^2\alpha\left(a^2-3\,b^2\right)+b^2\right)x_1\,y_1^2 + 2\,a^4b^2\cos\alpha\sin\alpha\,x_1^2 y_1\\
y_3 =& -2\,b^6\cos\alpha\sin\alpha\,x_1^3 + a^4\left(b^2-\left(b^2+a^2\right)\cos^2\alpha\right)\,y_1^3\\
&- 2\,a^2b^4\cos\alpha\sin\alpha\,x_1 y_1^2 + b^4\left(a^2+\left(b^2-3\,a^2\right)(\cos\alpha)^2\right){x_1}^2 y_1,\\
q_3 =& \,b^4\left(a^2-\left(a^2-b^2\right)\cos^2\alpha\right)x_1^2 + a^4\left(b^2+\left(a^2-b^2\right)\cos^2\alpha\right)y_1^2\\
&+ 2\,a^2b^2\left(a^2-b^2\right)\cos\alpha\sin\alpha\,x_1\,y_1.
\end{aligned}
$$

where:

$$
\cos\alpha = \frac{a^2b\,\sqrt{-a^2-b^2+2\,\sqrt{a^4-b^2c^2}}}{c^2\sqrt{a^4-c^2x_1^2}} = \frac{a^2b^2\,\sqrt{2\delta-a^2-b^2}}{c^2\sqrt{a^4y_1^2+b^4x_1^2}}
$$

$$
\sin\alpha = \frac{\sqrt{b^4\left(a^2-\delta\right)^2x_1^2 + a^4\left(b^2-\delta\right)^2y_1^2}}{c^2\sqrt{a^4y_1^2+b^4x_1^2}}
$$

Note that in Section 3.6 we generalize the above to any concentric, axis-parallel pair.

2.7.2 Jacobi's universal measure

Under the standard parametrization, we can obtain the "position" t of $P = [x, y]$ on an ellipse:

$$
t = \tan^{-1}\frac{ay}{bx}.
$$

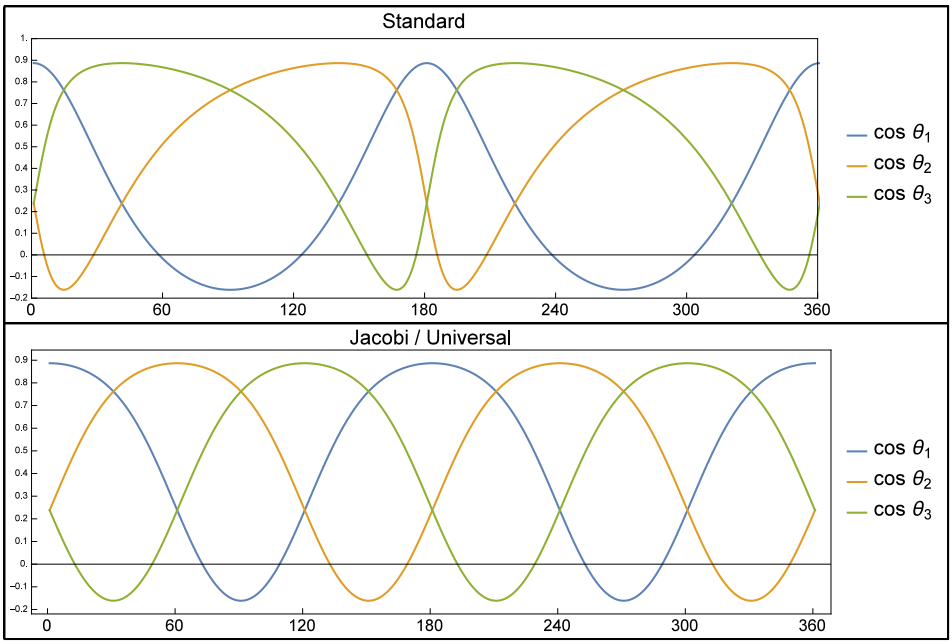

Figure 2.4: The cosines cos($theta_i$) of billiard 3-periodic internal angles for the standard (top) and Jacobi parametrizations (bottom). While in the former case the three curves are distinct, in the latter case all cosines follow the same curve at different phases.

As shown in Figure 2.5(top), when a first vertex $P_1(t)$ in a billiard 3-periodic is parametrized in the standard way, though its position is linear on the t parameter, it will drive motions of the other two vertices $P_2(t)$ and $P_3(t)$ which are both distinct and non-linear.

Fortunately, a uniform parametrization exists, which goes back to Jacobi, for all Poncelet families, based on the so-called "universal measure", which linearizes the Poncelet map, see Koiller, Reznik, and Garcia (2021). Specifically, vertices are obtained at fixed multiples of a constant Δu in the argument of certain Jacobi elliptic functions. This parametrization, adapted to the elliptic billiard case, appears in Stachel (2021a,b) and is reproduced below. First let's recall a few useful definitions.

The notation adopted below takes after Armitage and Eberlein (2006).

Definition 2.1. *The incomplete elliptic integral of the first kind* $K(\varphi, k)$ *is given*

by:

$$K(\varphi, k) = \int_0^{\varphi} \frac{d\theta}{\sqrt{1 - k^2 \sin^2 \theta}} \tag{2.6}$$

The complete elliptic integral of the first kind $K(k)$ is simply $K(\pi/2, k)$.

Definition 2.2. *The elliptic sine sn, cosine cn, and delta-amplitude dn are given by:*

$$\begin{aligned} sn(u,k) &= \sin\varphi \\ cn(u,k) &= \cos\varphi \\ dn(u,k) &= \sqrt{1 - k^2 \sin^2 \varphi} \end{aligned}$$

where $\varphi = am(u, k)$ is known as the amplitude, i.e., the upper-limit in the integral in Equation (2.6) such that $K(\varphi, k) = u$.

A review of these functions appears in Appendix B.

Remark 2.1. *Note to the reader: Mathematica (resp. Maple) expects $m = k^2$ (resp. k) as the second parameter to elliptic functions.*

Theorem 2.4. *A billiard 3-periodic P_i $(i = 1, \ldots, N)$ of period N with turning number τ, where $\gcd(N, \tau) = 1$, is parametrized on u with period $4K$ where:*

$$P_i = \left[-a \,\mathrm{sn}\left(u + i\,\Delta u, m\right), b \,\mathrm{cn}\left(u + i\,\Delta u, m\right)\right]$$

where,

$$m = k^2 = \frac{a_c^2 - b_c^2}{a_c^2}, \quad \Delta u = \frac{4\tau K}{N}$$

$$a = \sqrt{b^2 + a_c^2 - b_c^2}, \quad b = \frac{b_c}{\mathrm{cn}(\frac{\Delta u}{2}, m)}$$

Proof. See Stachel (2021b). □

Since in this chapter we are considering billiard 3-periodics, so above $N = 3$, and $\tau = 1$. As shown in Figure 2.5, under the Jacobi parametrization each of the 3 vertices of billiard 3-periodics follows the exact same curve, albeit with a 120-degree phase.

Recall the sum of cosines is constant for billiard 3-periodics. Figure 2.4 shows how individual cosines follow either (i) 3-distinct curves, or (ii) the same exact curve (at different phases) if the parametrization is standard or Jacobi, respectively.

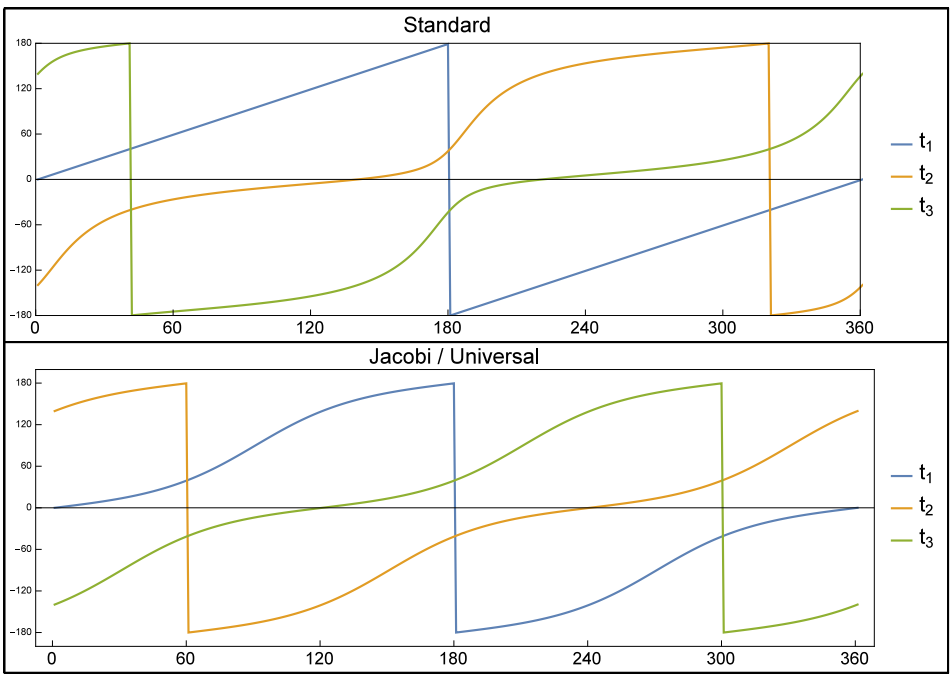

Figure 2.5: The "position" θ_i (vertical axis) of a point on an ellipse with semiaxes a, b vs the billiard 3-periodic parameter (horizontal axis). **Top:** vertex under "standard parametrization", i.e., $P_1(t) = [a\cos t, b\sin t]$. Notice while P_1's position evolves linearly, those of P_2 and P_3 are different curves. **Bottom:** Said positions under Jacobi's parametrization. Notice the three positions are 120-degree delayed copies of one another.

.

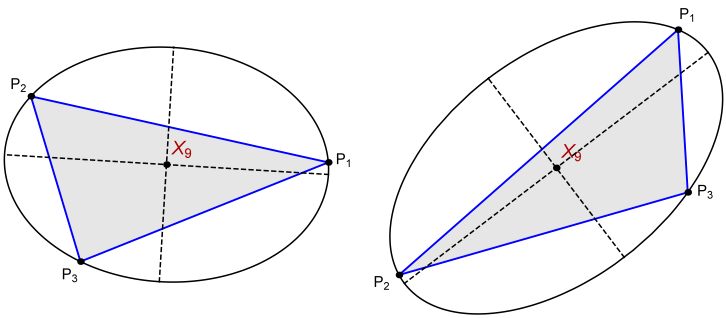

Figure 2.6: Two random triangles shown with their circumbilliards. Video

2.8 Exercises

Exercise 2.1. *Referring to Figure 2.6, show that every triangle has a circumbilliard, i.e., an ellipse to which it is inscribed and to which it is a billiard 3-periodic. Compute the axes of said circumbilliard with respect to triangle vertices.*

Exercise 2.2. *A pair of circles uniquely defines a* pencil *of coaxial circles, see Weisstein (2019, Limiting Points). The pencil contains exactly two circles which degenerate to a point, known as* limiting points*. Derive the location of such points for the poristic pair obtained from the image of two confocal ellipses centered at* $[0,0]$ *and with axes* a, b *and* a', b'*.*

Exercise 2.3. *Let* ℓ_1, ℓ_2 *be the limiting points of the two circles which are polar images of a confocal pair* $\mathcal{E}, \mathcal{E}'$ *with respect to a circle centered on* f_1*. At what aspect ratio* a/b *of* $\mathcal{E}$ *will* ℓ_2 *coincide with* f_2*?*

Exercise 2.4. *A well-known result is that the inversion of a circle pair* $\mathcal{C}, \mathcal{C}'$ *with respect to a circle* $\mathcal{C}_1$ *centered on* ℓ_1 *(resp.* $\mathcal{C}_2$ *centered on* ℓ_2*) is a pair of concentric circles* $\mathcal{C}_1'$ *and* $\mathcal{C}_1''$ *(resp.* $\mathcal{C}_1'$ *and* $\mathcal{C}_1''$*). Prove the following lesser known result: the ratio of radii between* $\mathcal{C}_1'$ *and* $\mathcal{C}_1''$ *is the same as the ratio between* $\mathcal{C}_2'$ *and* $\mathcal{C}_2''$*.*

Exercise 2.5. *Referring to Figure 8.9, let* $\mathcal{C}, \mathcal{C}'$ *be the pair of circles which are the polar image of a confocal pair of ellipses* $\mathcal{E}, \mathcal{E}'$*. Let* $\mathcal{C}_1', \mathcal{C}_1''$ *be the inversive images of* $\mathcal{C}, \mathcal{C}'$ *wrt to a circle centered on a focus of the ellipse pair. Prove that: (i)* $\mathcal{C}_1'$ *and* $\mathcal{C}_1''$ *are concentric with the ellipse pair and (ii)* $\mathcal{C}_1'$ *(resp.* $\mathcal{C}_1''$*) is externally tangent to* $\mathcal{E}$ *(resp.* $\mathcal{E}'$*) at its left and right major vertices.*

Exercise 2.6. *Prove the inversive image of billiard 3-periodics with respect to a focus-centered circle is a non-Ponceletian family inscribed in Pascal's Limaçon whose Gergonne point X_7 is stationary; see it Live. Indeed, this family has constant perimeter (to be shown later).*

Exercise 2.7. *Consider the ellipse $x^2/a^2 + y^2/b^2 = 1$. For a 3-periodic billiard orbit with vertices $P_i = [x_i, y_i]$ (i=1,2,3) show that:*

$$(x_2\, y_3 - x_3\, y_2)\, x_1\, y_1 + (x_3\, y_1 - x_1\, y_3)\, x_2\, y_2 + (x_1\, y_2 - x_2\, y_1)\, x_3\, y_3 = 0$$

Exercise 2.8. *For a 3-periodic billiard orbit with vertices $P_i = [x_i(t), y_i(t)]$ (i=1,2,3) Let $C_i(t) = [1/x_i(t), 1/y_i(t)]$.*

Show that the polygon $\{C_1(t), C_2(t), C_3(t)\}$ is a segment that can be bounded or unbounded.

Exercise 2.9. *Which simple or self-intersected N- gon (closed polygon with N vertices and N sides) can be an orbit on an elliptic billiard?*

For $N = 4$ only the parallelogram can be a non self-intersected orbit on an elliptic billiard, see Connes and Zagier (2007). See Garcia and Reznik (2020) for the analysis of self-intersected $4 - gons$.

Exercise 2.10. *Consider a 3-periodic billiard orbit and its antipodal orbit. Show that the six points of intersections of the two triangles are contained in a stationary confocal ellipse $\mathcal{E}_h$: $x^2/a_h^2 + y^2/b_h^2 = 1$ where:*

$$a_h = \frac{\left(\delta - b^2\right)\left(a^2 + b^2 + 2\,\delta\right)\sqrt{2\delta - a^2 - b^2}}{3\left(a^2 - b^2\right)^2}$$
$$b_h = \frac{\left(a^2 - \delta\right)\left(a^2 + b^2 + 2\,\delta\right)\sqrt{2\delta - a^2 - b^2}}{3\left(a^2 - b^2\right)^2}$$

Conclude that the pair of ellipses $\{\mathcal{E}_h, \mathcal{E}_1\}$ is a billiard pair having all orbits of period 6. Also show that the pair $\{\mathcal{E}, \mathcal{E}_h\}$ defines a zig-zag billiard and that the orbits have period 12 and that the perimeter is constant. See Live

2.9 Research questions

Question 2.1. *Weisstein (2019, Extouch triangle) defines the extouch triangle as having vertices at the points of contact of the excircles with a triangle's sidelines. In Chapter 5 we show that the vertices of the extouch triangles of billiard 3-periodics coincide with the caustic touchpoints, see it Live. Show that said extouch family is also Ponceletian and concentric with the elliptic billiard; derive expressions for the semiaxes of its elliptic caustic. Is its center a triangle center?*

3 Concentric, Axis-Parallel (CAP)

Below we introduce, five additional notable 3-periodic Poncelet families inscribed between a pair of concentric, axis-parallel (CAP) ellipses. They were shown in Figure 1.5 and we name them (i) incircle, (ii) circumcircle, (iii) homothetic, (iv) dual, and (v) excentral (their geometry is defined below). As before, the Cayley condition Equation (2.2) will be used to constrain the ellipse pair. For each family we derive geometric properties and invariants. The chapter concludes with a parameterization which is general for any CAP pair and is used to support several proofs. In Section 3.7 we summarize properties, fixed points, and other traits of the families treated herein.

3.1 Excentral family

This is the Ponceletian family of excentral triangles to billiard 3-periodics. If the axes of its caustic are a, b, this family is inscribed in an ellipse with a_e, b_e given in Theorem 2.1; see Figure 3.1(left). Indeed, by inverting the relations in the latter, we can express a, b[1] in terms of a_e, b_e:

[1] There is a slight abuse of notation in that these should have been labeled a_c, b_c. However we maintained these as a, b since the caustic to the excentral family is the elliptic billiard.

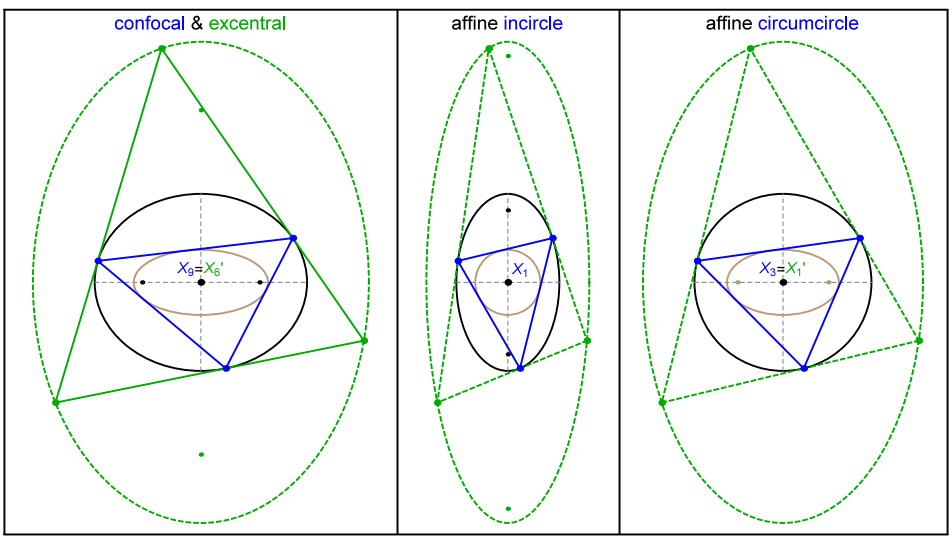

Figure 3.1: **Left:** billiard 3-periodic (blue) and its excentral triangle (green). The former conserves the sum of its cosines. The latter is inscribed in an ellipse (dashed green) and conserves the product of its cosines. **Middle:** Affine image of confocal family which sends caustic (brown) to a circle. This family also conserves the sum of cosines, equal to that conserved by its confocal pre-image. **Right:** Affine image of confocal family which sends billiard ellipse (black) to a circle. This family also conserves the product of cosines, equal to that conserved by the excentral family of its pre-image. Video

Proposition 3.1. *Given the semiaxes a_e, b_e of $\mathcal{E}_e$ the semi axis of the caustic $\mathcal{E}$ are given by:*

$$a = \frac{(\delta_e - a_e^2 - 3b_e^2)a_e}{2c_e^2}, \quad b = \frac{(3a_e^2 + b_e^2 - \delta_e)b_e}{2c_e^2}$$

where $c_e^2 = a_e^2 - b_e^2$ and $\delta_e = \sqrt{a_e^4 + 14a_e^2b_e^2 + b_e^4}$.

The symmedian point X_6 of the excentral triangle coincides with the mittenpunkt of its reference, see Kimberling (2019, X(6)). Therefore:

Corollary 3.1. *Over excentral 3-periodics, the symmedian point X_6 of the excentral family is stationary.*

Recall that in Corollary 2.2 two other notable invariants are mentioned: product of internal angle cosines, and ratio of its area by billiard 3-periodics.

Corollary 3.2. *The invariant product of cosines of excentral 3-periodics is a quarter of the quantity in Corollary 2.2. Furthermore the area ratio of billiard 3-periodics by excentrals is half the quantity in Corollary 2.2.*

Let s_i' denote the variable sidelengths of the excentral family, $i = 1, 2, 3$. Here is an additional curious invariant:

Proposition 3.2. *Over the excentral family, the sum squared sidelines divided by the product of sidelines is constant. Furthermore it is equal to Joachimsthal's constant J of its parent 3-periodic billiard family. Explicitly:*

$$\frac{\sum (s_i')^2}{\prod s_i'} = \frac{\sqrt{2\delta - a^2 - b^2}}{c^2} = J$$

Proof. Derive explicit expressions for excentral sidelengths and arrive at claim via CAS simplification. □

Referring to Figure 3.2, Weisstein (2019, Cosine Circle) defines the *cosine circle* as centered on the symmedian point X_6, and passing through the 6 intersections of lines through X_6 parallel to the sides of the orthic triangle. Its radius r^* is given by the product of sidelengths divided by the sum of their squares.

Corollary 3.3. *The cosine circle of the excentral family is stationary with radius $r^* = 1/J$.*

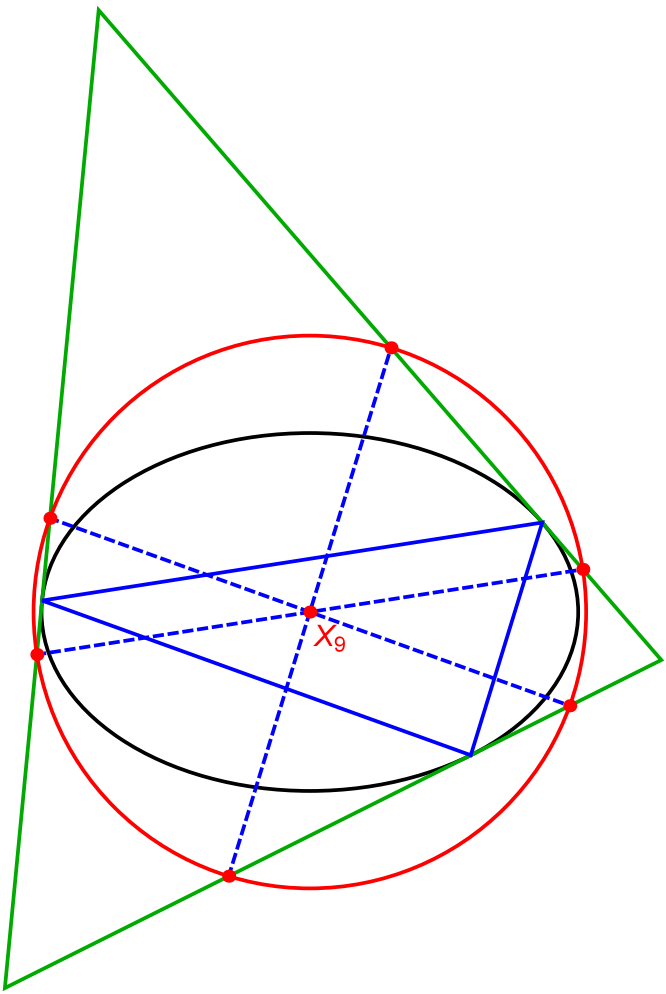

Figure 3.2: The cosine circle (red) of the excentral family (green) is stationary. It contains the 6 intersections of lines (dashed blue) through the common center (family's X_6 and billiard periodics' X_9) which are parallel to their orthic, i.e., side-lines of billiard 3 periodics. Video

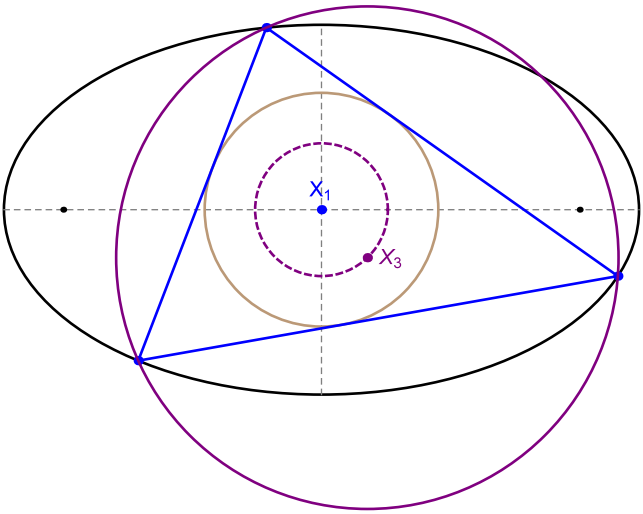

Figure 3.3: A 3-periodic (blue) in the incircle family, and its fixed-radius circumcircle (purple). The locus of the circumcenter X_3 is a concentric circle (dashed purple). Live

3.2 Incircle family

The incircle family, shown in Figure 3.1(middle), is the Poncelet family in a CAP pair for which the caustic is a circle (let r denote its radius). It follows immediately that the family's incenter X_1 is stationary. Let a, b be the axes of the ellipse the family is inscribed in. Cayley yields:

Proposition 3.3. *The inradius r of the incircle family is given by:*

$$r = a_c = b_c = \frac{ab}{a+b}$$

As shown in Figure 3.3:

Proposition 3.4. *The incircle family has invariant circumradius given by $R = (a+b)/2$. Furthermore, the locus of its circumcenter X_3 is a circle of radius $d = R - b = a - R$ centered on the common center $O = X_1$.*

Proof. Let $P_1 = (x_1, y_1)$ be a first vertex of the incircle family. Using an explicit parametrization for P_2 and P_3, obtain via CAS the following coordinates for the moving circumcenter X_3:

$$X_3 = \frac{a-b}{2}\left[-\frac{x_1\left(-x_1^2(a+b)^2+a^2b(2a+b)\right)}{a\left((a^2-b^2)x_1^2+a^2b^2\right)}, \frac{y_1\left(x_1^2(a+b)^2-a^2b^2\right)}{b\left(a^2x_1^2+b^2(a^2-x_1^2)\right)}\right]$$

And circumradius $R = |P_1 - X_3| = (a+b)/2$. Also obtain that the locus of X_3 is a circle concentric with the incircle and of radius $(a-b)/2$. □

Referring to Equation (2.4):

Corollary 3.4. *The incircle family conserves its sum of cosines given by:*

$$\sum \cos\theta_i = 1 + \frac{r}{R} = \frac{a^2+4ab+b^2}{(a+b)^2}$$

3.2.1 Confocal affine image

As Figure 3.1(middle) depicts, the incircle family can also be obtained from an affine image of billiard 3-periodics which sends the confocal caustic to a circle. Let α, β be the semiaxes of its billiard ellipse pre-image.

Lemma 3.1. *The confocal family is sent to the incircle family by scaling it along the major axis by an amount s given by:*

$$s = \frac{\beta(\bar{\delta}-\alpha^2+\beta^2)}{\alpha^3}, \quad \bar{\delta} = \sqrt{\alpha^4-(\alpha\beta)^2+\beta^4}$$

Proof. The scaled family will be inscribed in an ellipse with semiaxes $a = s\alpha$, and $b = \beta$. Its caustic will be the circle $r = b_c$, where $b_c = \beta\left(\alpha^2-\bar{\delta}\right)/(\alpha^2-\beta^2)$ is the confocal caustic minor axis given in Proposition 2.2. The Cayley condition for the incircle family imposes that $r = b_c = (ab)/(a+b)$, i.e., the result follows from solving $b_c = (s\alpha\beta)/(s\alpha+\beta)$ for s.

□

Surprisingly:

Proposition 3.5. *The sum of cosines conserved by the incircle family is identical to that conserved by billiard 3-periodics which are its affine pre-image.*

Proof. Let s be the scaling along the major axis in Lemma 3.1. Plug $a = s\alpha$ and $b = \beta$ into Corollary 3.4, subtract one (to obtain r/R for the incircle family) and verify it yields the expression in Theorem 2.3. □

3.3 Circumcircle family

The circumcircle family, shown in Figure 3.1(right), is the Poncelet family in a CAP pair for which the outer ellipse is a circle (let R denote its radius). It follows immediately that the family's circumcenter X_3 is stationary. Let a_c, b_c be the axes of its inellipse and s_i the sidelengths. Cayley imposes $a_c + b_c = R$.

Lemma 3.2. *Poncelet triangles in the circumcircle family are always acute.*

Proof. Since the stationary circumcenter X_3 is interior to the caustic caustic, it will be interior to circumcircle family triangles, and the result follows. □

Proposition 3.6. *The circumcircle family conserves the sum of squared sidelengths. This is given by:*

$$\sum_{i=1}^{3} s_i^2 = 4(a_c + 2b_c)(2a_c + b_c)$$

Proof. CAS-assisted simplification from the vertex parametrization in Proposition 3.17. □

Proposition 3.7. *The circumcircle family conserves the product of its internal angle cosines. This is given by:*

$$\prod_{i=1}^{3} \cos\theta_i = \frac{a_c b_c}{2(a_c + b_c)^2} = \frac{a_c b_c}{2R^2}$$

Proof. CAS-assisted simplification from vertex parametrization. □

Recall the orthic triangle has vertices at the feet a triangle's altitudes. Let R_h denote its circumradius. The well-known identity $R_h = R/2$ appears in Weisstein (2019, Orthic Triangle, Eqn 7). Therefore R_h is invariant over the circumcircle family. Let r_h denote the orthic's inradius. Referring to Figure 3.4:

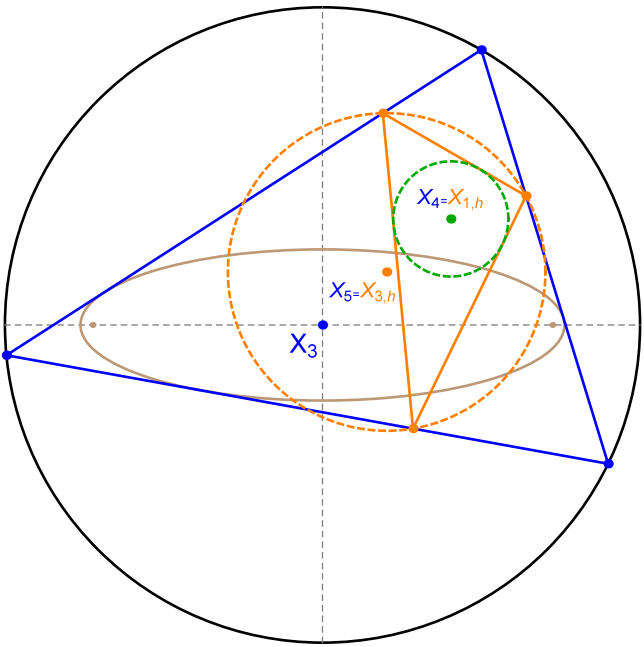

Figure 3.4: A circumcircle family 3-periodic (blue) and its orthic triangle (orange). Over the family the orthic's circumcircle (dashed orange) and incircle (dashed green) have invariant radii. Also shown are their centers $X_{3,h}$ and $X_{1,h}$ which, for any reference triangle, correspond the nine-point center X_5 and orthocenter X_1. Video, Live

Proposition 3.8. *Over the circumcircle family r_h is invariant and given by $r_h = a_c b_c/(a_c + b_c)$.*

Proof. In Weisstein (ibid., Orthic Triangle, Eqn. 5) one finds the identity $r_h = 2R\prod_{i=1}^{3}\cos\theta_i$. Recalling $R = a_c + b_c$, substitution into Proposition 3.7 yields the claim. □

Referring to Figure 3.4, it can be shown (see Exercise 3.3):

Lemma 3.3. *Over the circumcircle family, the locus of the orthic circumcenter (i.e., the 9-point center X_5 of the family) is a circle concentric with the pair.*

Let κ_i' denote the curvature of the inner ellipse at the points of contact of circumcircle 3-periodics (the proof is left to the reader in Question 3.10):

Proposition 3.9. *Over circumcircle 3-periodics, the following quantity is conserved:*

$$\sum_{i=1}^{3}(\kappa_i')^{\frac{2}{3}} = \frac{a_c^2 + a_c b_c + b_c^2}{(a_c b_c)^{\frac{4}{3}}}$$

3.3.1 Confocal affine image

As Figure 3.1(right) depicts, the circumcircle family can also be obtained from an affine image of billiard 3-periodics which sends the billiard ellipse with semiaxes α, β to a circle with radius $R = \beta$. Therefore billiard 3-periodics are sent to the circumcircle family by scaling it along the major axis by an amount $s' = \beta/\alpha$. Therefore Proposition 2.2 implies:

Lemma 3.4. *The caustic semiaxes a_c, b_c of the circumcircle family which is the s'-affine image of the confocal family are given by:*

$$a_c = \frac{\beta}{\alpha}\alpha_c = \frac{\beta(\bar{\delta} - \beta^2)}{\alpha^2 - \beta^2}, \quad b_c = \beta_c = \frac{\beta(\alpha^2 - \bar{\delta})}{\alpha^2 - \beta^2}$$

where α_c, β_c are the caustic semiaxes of the confocal pre-image, and $\alpha, \beta, \bar{\delta}$ are as previously defined.

Note that the s'-affine image of billiard excentrals becomes a Poncelet family with fixed incircle; see Figure 3.1(right, dashed green triangles). We have seen above such a family conserves its sum of cosines. Surprisingly, the following invariant "role reversal" takes place:

Proposition 3.10. *The sum of cosines conserved by billiard 3-periodics is the same as the one conserved by the s'-affine image of billiard excentrals. Furthermore product of cosines conserved by billiard excentrals is the same as the one conserved by the s'-affine image of billiard 3-periodics (circumcircle family).*

Proof. For the first statement it suffices to show that the s'-affine image of billiard excentrals has sides parallel to those of the s-image of billiard 3-periodics, i.e., the incircle family and use Proposition 3.5. The second statement can be proved algebraically from vertex parametrization. □

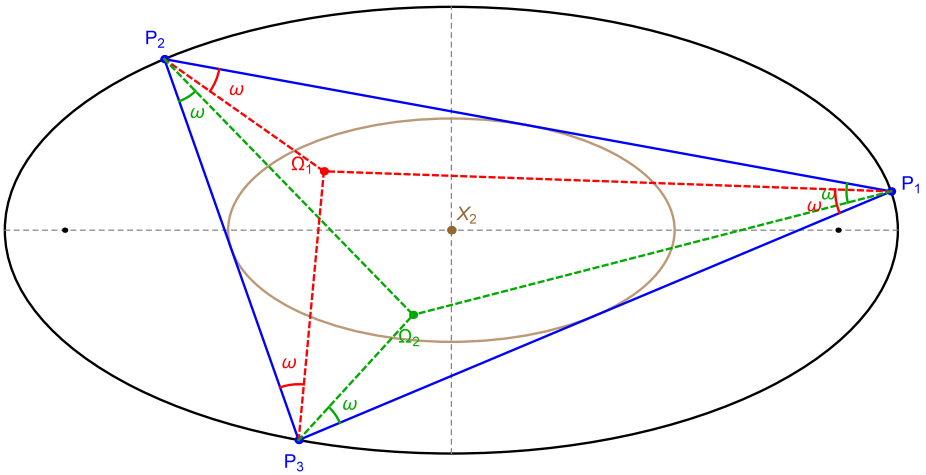

Figure 3.5: A 3-periodic (blue) interscribed between two homothetic ellipses (black, brown). Since this family is an affine image of one of equilaterals interscribed between two concentric circles, (i) the barycenter X_2 is stationary at the common center, and (ii) the area is conserved. Also conserved is (iii) the sum of squared sidelengths. (ii) and (iii) imply the Brocard angle ω is invariant. Also shown are the two (moving) the Brocard points Ω_1 and Ω_2. Video, Live

3.4 Homothetic family

The homothetic family, shown in Figure 3.5, is the Poncelet family in a CAP pair for which the outer and inner ellipse are homothetic to each other, i.e., $a = ka_c$ and $b = kb_c$, where a, b and a_c, b_c are outer and inner ellipse semiaxes, respectively. Cayley implies:

Proposition 3.11. *The semiaxes of a CAP pair of homothetic ellipses which admits a 3-periodic are given by:*

$$a_c = \frac{a}{2}, \quad b_c = \frac{b}{2}$$

Proposition 3.12. *The barycenter X_2 is stationary at the common center and area A is invariant and given by:*

$$A = \frac{3\sqrt{3}}{4}ab$$

Proof. Consider an affine transformation that sends both outer and inner ellipse to a unit circle, e.g., by scaling the system along the major (resp. minor) axis by $1/a$ (resp. $1/b$). Uniquely amongst all triangle centers, the barycenter X_2 is invariant under affine transformations. By symmetry of the equilateral centroid, it will be identified with the center of the homothetic pair. Affine transformations preserve area ratios, so A will be the the area of an equilateral triangle inscribed in a unit circle scaled by the inverse Jacobian ab. This completes the proof. □

Curiously, the homothetic family shares the following invariant with the circumcircle family:

Proposition 3.13. *Over the homothetic family, the sum of squared sidelengths s_i^2 is invariant and given by:*

$$\sum_{i=1}^{3} s_i^2 = \frac{9}{2}\left(a^2 + b^2\right)$$

The proof below was kindly contributed by Tabachnikov (2020).

Proof. Invariant sum of squared sidelengths follows from the fact that the average of the harmonics of degree 1 and 2 over the group of rotations of order 3 is zero. Namely, consider a unit vector $v(\varphi) = (\cos\varphi, \sin\varphi)$ and a matrix $\mathcal{A}$ taking concentric circles to homothetic ellipses. Then $|\mathcal{A}v(\varphi)|^2$ is a trigonometric polynomial of degree 2. Average it over $\mathbb{Z}_3$ by adding $2\pi/3$ and $4\pi/3$ to φ. The result is independent of φ, as needed. The actual value is obtained via CAS simplification from vertex parametrization. □

Referring to Figure 3.5, recall the definition of a triangle's Brocard angle ω, given in Weisstein (2019, Brocard Angle): sidelines $P_i P_{i+1}$ rotated about P_i by some angle θ will only concur (at the first Brocard point Ω_1) if $\theta = \omega$. A second, distinct Brocard point Ω_2 exists if sidelines $P_i P_{i-1}$ are rotated about P_i by $-\omega$.

A known relation appearing in Weisstein (ibid., Brocard Angle, Eqn. 2) is $\cot\omega = (\sum_{i=1}^{3} s_i^2)/(4A)$. Therefore:

Corollary 3.5. *Over the homothetic family, the Brocard angle ω is invariant. Its cotangent is given by:*

$$\cot\omega = \frac{\sqrt{3}}{2}\frac{a^2 + b^2}{ab}$$

Proof. Direct calculations using the explicit parametrization of homothetic vertices. □

Another known relation valid for any triangle is $\cot\omega = \sum \cot\theta_i$:

Corollary 3.6. *The homothetic family conserves the sum of its internal angle cotangents.*

As in Corollary 2.4, let κ_i denote the curvature of the outer ellipse at vertex P_i.

Proposition 3.14. *Over homothetic 3-periodics, the following quantities are conserved:*

$$\sum_{i=1}^{3} \kappa_i^{-\frac{2}{3}} = \frac{3}{2}\frac{(a^2+b^2)}{(ab)^{\frac{2}{3}}}$$
$$\sum_{i=1}^{3} \kappa_i^{-\frac{4}{3}} = \frac{3}{8}\frac{(3a^4+a^2b^2+3b^4)}{(ab)^{\frac{4}{3}}}$$

Proof. In the homothetic pair, a 3-periodic orbit is given by:

$$P_i = [a\cos(u+\frac{2i\pi}{3}), b\sin(u+\frac{2i\pi}{3})]$$

and $k_i^{-\frac{2}{3}}$ is the following

$$k_i^{-\frac{2}{3}} = \frac{b^4x_i^2 + a^4y_i^2}{(ab)^{\frac{8}{3}}}$$

The result follows by direct computation using CAS. □

3.5 Dual family

The dual family, shown in Figure 3.6, is the Poncelet family in a CAP pair such that the outer and inner ellipses are "duals" curves of each other, i.e., tangents to one are sent to points on the other and vice versa. For ellipses, this simply implies their aspect ratios a/b and a_c/b_c will be reciprocals of one another. Cayley yields:

Proposition 3.15. *The caustic semiaxes of the dual family are given by:*

$$a_c = \lambda\, b, \quad b_c = \lambda\, a, \quad \lambda = \frac{ab}{a^2+b^2}$$

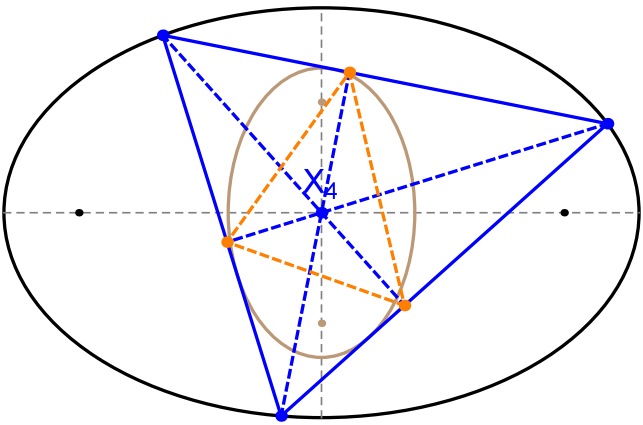

Figure 3.6: A Dual family 3-periodic (blue) interscribed in a pair of "dual" ellipse (black, brown). Their aspect ratios are reciprocals of each other. No invariants have yet been detected for this family other than the fact that the orthocenter X_4 is stationary at the common center. Also shown is the orthic triangle (dashed orange) whose vertices lie at the feet of the altitudes (dashed blue). Live

Remarkably:

Proposition 3.16. *The orthocenter X_4 of the dual family is stationary.*

Proof. Follows directly from the vertex parametrization in Proposition 3.17.

In terms of the vertices of a triangle $A = [x_a, y_a]$, $B = [x_b, y_b]$, $C = [x_c, y_c]$ the orthocenter $X_4 = [x_{4n}/A_4, y_{4n}/A_4]$ is given by the following rational functions

$$\begin{aligned} x_{4n} &= (x_c - x_b)\, x_a\, y_a + (x_b\, y_b - x_c\, y_c)\, x_a + (y_c - y_b)\, y_a^2 + \left(y_b^2 - y_c^2\right) y_a \\ &\quad + x_c x_b\, (y_c - y_b)) + y_b y_c (y_c - y_b) \end{aligned}$$

$$\begin{aligned} y_{4n} &= (x_b - x_c)\, x_a^2 + (y_b - y_c)\, x_a\, y_a + \left(x_c^2 - x_b^2\right) x_a + (-x_b\, y_b + x_c\, y_c)\, y_a \\ &\quad + x_b x_c (x_b - x_c) + y_b\, y_c (x_b - x_c) \\ A_4 &= (y_b - y_c)\, x_a + (-x_b + x_c)\, y_a + x_b\, y_c - x_c\, y_b \end{aligned}$$

The results follows from CAS-assisted simplification from the vertex parametrization in Proposition 3.17. □

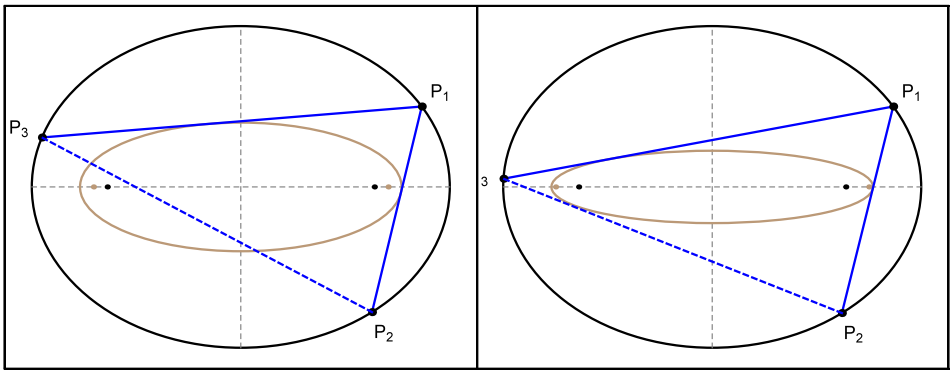

Figure 3.7: **Left:** Two CAP ellipses (black and brown), and a point P_1 on the outer one. The lines thru P_1 tangent to the inner ellipse intersect the outer one at P_2 and P_3. Notice that P_2P_3 cut thru the inner ellipse, i.e., the pair of ellipses does not satisfy Cayley's conditions. **Right:** the minor axis of the inner ellipse has been scaled such that $P_1P_2P_3$ is now a Poncelet triangle.

Despite much searching, no invariant quantities have yet been found for this family.

3.6 Vertex parametrization for a generic CAP pair

Consider a general CAP pair of ellipses denoted $\mathcal{E}$ and $\mathcal{E}_c$. We will derive a generic parametrization for the vertices of 3-periodics in such a pair. A first calculation will be helpful. Referring to Figure 3.7(left):

Proposition 3.17. *The intersections P_2 and P_3 on $\mathcal{E}$ of the two tangents to $\mathcal{E}_c$ seen from a point $P_1 = [x_1, y_1]$ also on $\mathcal{E}$ are given by:*

$$P_2 = [x_2, y_2] = \frac{1}{k_2}\left[\frac{p_1x_1 + p_2y_1}{b}, \frac{-w_1x_1 + w_2y_1}{a}\right]$$
$$P_3 = [x_3, y_3] = \frac{1}{k_2}\left[\frac{p_1x_1 - p_2y_1}{b}, \frac{w_1x_1 + w_2y_1}{a}\right]$$

CAP family	a_c	b_c	note
confocal	$a\left(\delta - b^2\right)/c^2$	$b\left(a^2 - \delta\right)/c^2$	Proposition 2.2
incircle	$(ab)/(a+b)$	$(ab)/(a+b)$	Proposition 3.3
circumcircle	choose $a_c < R$	$R - a_c$	$R = a = b$
homothetic	$a/2$	$b/2$	Proposition 3.11
dual	$(ab^2)/(a^2+b^2)$	$(a^2b)/(a^2+b^2)$	Proposition 3.15
conf. excentrals	$\frac{(\delta_e - a_e^2 - 3b_e^2)a_e}{2c_e^2}$	$\frac{(3a_e^2 + b_e^2 - \delta_e)b_e}{2c_e^2}$	Proposition 3.1

Table 3.1: Values for the caustic semiaxes a_c, b_c to be used in the generic vertex parametrization for a CAP pair in Proposition 3.17

$$
\begin{aligned}
p_1 &= b\left(a^4 b_c^4 - (a^2 - a_c^2)^2 b^4\right) \\
p_2 &= 2a\left((a^2 + a_c^2)b^2 - a^2 b_c^2\right) k_1 \\
k_1 &= \sqrt{b^2 b_c^2 (a^2 - a_c^2) x_1^2 + a_c^2 a^2 (b^2 - b_c^2) y_1^2} \\
k_2 &= \left(\frac{a^2(b^2 + b_c^2) - a_c^2 b^2}{a} x_1\right)^2 + \left(\frac{a^2(b^2 - b_c^2) + a_c^2 b^2}{b} y_1\right)^2 \\
w_1 &= 2b\left((b^2 + b_c^2)a^2 - a_c^2 b^2\right) k_1 \\
w_2 &= a\left(a_c^4 b^4 - a^4 (b^2 - b_c^2)^2\right)
\end{aligned}
$$

Parametrizations for specific CAP families can be obtained from Proposition 3.17 by setting the caustic semiaxes a_c, b_c as in Table 3.1.

3.7 Summary

Fixed points and (known) conserved quantities for the concentric, axis-parallel (CAP) families in this chapter appear in Table 3.2.

Also of interest is data about caustics, regarded as a family's fixed inconic, shown in Table 3.3.

Family	Fixed	Conserves	Notes
Confocal	X_9	$L,\ J,\ r/R,$ $\sum \cos\theta_i,\ \kappa_i^{2/3}$	i.e., billiard 3-periodics
Incircle	X_1	$R,\ \sum \cos\theta_i$	sum of cosines same as confocal affine pre-image
Circumcircle	X_3	$\sum s_i^2,\ \prod \cos\theta_i,$ $r_h, R_h, (\kappa_i')^{2/3}$	product of cosines same as excentrals' in confocal affine pre-image
Confocal Excentrals	X_6	$A'/A,\ \prod \cos\theta_i',$ $\sum (s_i')^2 / \prod s_i'$	primed quantities refer to those of the excentral family
Homothetic	X_2	$A,\ \sum s_i^2,\ \omega,$ $\sum \cot\theta_i,\ \kappa_i^{-2/3},\ \kappa_i^{-4/3}$	affine image of concentric circles
Dual	X_4	n/a	

Table 3.2: Summary of fixed points and (known) conserved quantities for the concentric, axis-parallel (CAP) families mentioned in this chapter.

Poncelet family	center	caustic (inconic)	Brianchon point	caustic contact tri	contact tri `bit.ly/*`
incircle	X_1	incircle	X_7	intouch	`3tYYu3h`
homothetic	X_2	Steiner	X_2	medial	`3474753`
circumcircle	X_3	?	X_{69}	X_{69}-cev.	`2T3qu9f`
dual	X_4	?	X_{253}	X_{253}-cev.	`2SUfomB`
excentral	X_6	orthic	X_4	orthic	`3uXXI7H`
confocal	X_9	Mandart	X_8	extouch	`3wiBeyv`

Table 3.3: Information about the caustic to various CAP families, regarded as a fixed inconic. The Brianchon point is the perspector to the triangle whose vertices are at the touchpoints with the inconic, see Weisstein (2019, Brianchon point). When named, this triangle appears in the "caustic contact tri" column. An link to an animation for each case is provided.

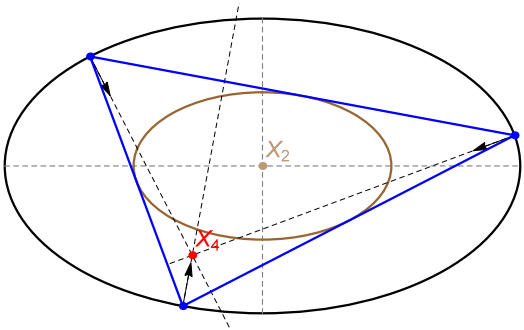

Figure 3.8: Normals to the ellipse at vertices of 3-periodics in the homothetic family concur at the orthocenter X_4.

3.8 Exercises

Exercise 3.1. *Prove that the power of the circumcircle with with respect to the common center in each of the following 3-periodic families is constant and given by the listed expressions. (i) incircle: $-a_e b_e$; (ii) homothetic: $-(a_e^2 + b_e^2)/2$, and (iii) excentral: $-a^2 - b^2 - 2\delta$.*

Exercise 3.2. *Prove the radius r^* of the stationary cosine circle of the excentral family is larger than the major axis a of its caustic.*

Exercise 3.3. *Prove Lemma 3.3.*

Exercise 3.4. *Derive the proof details to the 2nd part of Proposition 3.10.*

Exercise 3.5. *(contributed by L. Gheorghe) Prove that ellipse normals at vertices of 3-periodics in the homothetic family are concurrent at the orthocenter X_4, see Figure 3.8. Derive the semiaxes of the elliptic locus of X_4 as a function of a, b of the outer ellipse, see it Live.*

Exercise 3.6. *The Thomson cubic is the locus of centers of circumconics such that normals at the vertices concur (on the Darboux cubic), see Gibert (2021a, Darboux and Thomson cubics). Prove that vertex normals off of the X_1- and X_6-centered circumconics concur on X_{84} and X_{64}, respectively. This readily implies normals to the outer ellipse at the incircle and excentral family vertices will concur on said points; see Table 3.4.*

Poncelet family	center	norms. concur	concur bit.ly/*
incircle	X_1	X_{84}	3eVuCQY
homothetic	X_2	X_4	3eXSRhC
circumcircle	X_3	X_3	2RqMqul
dual	X_4	X_{3346}	n/a
excentral	X_6	X_{64}	3hwCTfN
confocal	X_9	X_1	3uTvqLI

Table 3.4: CAP families studied herein. Coincidentally, their centers lie on the Thomson cubic which is the loci of circumconic centers such that normals at vertices concur, see Gibert (2021a, Thomson Cubic). The third column lists the experimentally-found concurrence points. These lie on the Darboux cubic described in Gibert (2021a, Darboux cubic).

Exercise 3.7. *Recall the dual family has stationary orthocenter X_4. Prove that the inversive image of the dual family wrt to a circle concentric with the ellipse pair is a non-Ponceletian family with incenter X_1' stationary at the common center. This inversive family is inscribed in Booth's curve and its caustic can contain multiple spikes; see it Live.*

Exercise 3.8. *Given a reference triangle T, its tangential triangle T' has sides tangent to the circumcircle at the vertices of T. A known fact is that the sides of T' are parallel to those of the orthic T_h of T, see Weisstein (2019, Tangential Triangle). For any acute triangle T, the Gergonne point X_7' of the tangential triangle coincides with the symmedian X_6 of T, see Weisstein (ibid., Contact Triangle).*

Let T denote the Poncelet family of excentral triangles. We've seen above that (i) this family is all acute, and that (ii) its symmedian point X_6 is stationary. Let T' denote their tangential triangles. This family will be non-Ponceletian: its vertices do not sweep a conic nor do its sides envelop one.

Since the T are all acute, they can be thought of as the contact triangles of the T'. Therefore the Gergonne point X_7' of the tangentials to the excentrals will coincide with X_6 of the excentrals and be stationary, see Weisstein (ibid., Contact Triangle).

Prove that the ratio of homothety between the orthics (billiard 3-periodics) and the tangentials is invariant. Corollaries: (i) the T' conserve perimeter; (ii) they conserve the same r/R as the excentral orthics, i.e., the corresponding billiard 3-periodics. See it Live.

Also prove that the locus of X_9' of the T' is an ellipse.

Derive equations for the curves swept by the vertices of T' as well as their caustic.

3.9 Research questions

Question 3.1. *Referring to Figure 3.6, are there any conserved quantities for the dual family besides stationarity of X_4 at the common center?*

Question 3.2. *Referring to the dashed green triangle in Figure 3.1(middle), are there any conserved quantities and/or fixed triangle centers for the family which is an s-affine image of billiard excentrals?*

Question 3.3. *Consider the homothetic family and its polar image with respect to a focus of the outer ellipse $\mathcal{E}$. Prove that (i) the caustic is a circle, derive its location and radius. (ii) the family is inscribed in a conic, namely, below (resp. above) a certain aspect ratio a/b of $\mathcal{E}$, the conic is an an ellipse (resp. hyperbola). (iii) the Gergonne point X_7 of the family is stationary. Live: family inscribed in ellipse, hyperbola.*

Question 3.4. *Prove that a necessary condition for a triangle center to be stationary over Poncelet 3-periodics is that it lies on the Thomson Cubic, defined in Gibert (2021b).*

Question 3.5. *X_k, $k = 1, 2, 3, 4, 6, 9$ lie on the Thomson cubic K_{002} and as seen above, are stationary over Poncelet families centered on them. Referring to Figure 3.9, prove that X_{1249}, also on K_{002}, is stationary over Poncelet 3-periodics centered on it. Show that in the X_{1249}-centered system, X_4 (resp. X_{20}) is the perspector of the circumconic (resp. inconic).*

Question 3.6. *The perspector of a circumconic centered on X is the X_2-Ceva conjugate of X. Likewise, the perspector (Brianchon point) of an inconic centered on X is the isotomic conjugate of the anticomplement of X. Given a triangle, let C and I be the X-centered circumconic and inconic. Show that for a triangle, the inconic perspector (i.e., the Brianchon point) is the anticomplement of the circumconic one.*

Question 3.7. *In Gibert (ibid.), it is stated that if X_k lies on the Thomson cubic K_{002}, circumconic normals at the vertices (and inconic normals at the contact points) concur. Consider the (axis-parallel, concentric) circumconic and inconic*

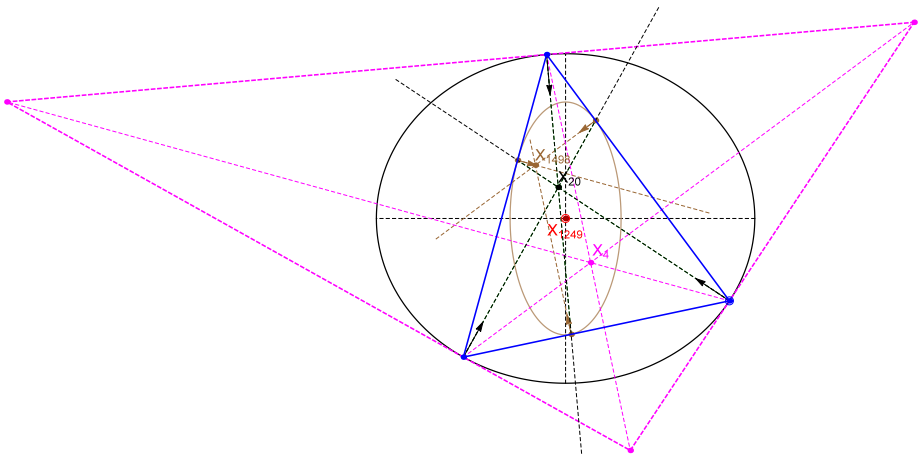

Figure 3.9: A Poncelet 3-periodic (blue) interscribed between the X_{1249}-centered circumconic $\mathcal{C}$ (black) and inconic $\mathcal{I}$ (brown); over the family, said center remains stationary. Since the center lies on the Thomson cubic, (i) $\mathcal{C}$ and $\mathcal{I}$ are axis-parallel, (ii) the normals to $\mathcal{C}$ at the vertices concur (at X_{20} in this case), and (iii) the normals to $\mathcal{I}$ at the contact points also concur (at X_{1498}). It turns out X_{20} doubles up as the Brianchon point of $\mathcal{I}$, and X_4 is the perspector of $\mathcal{C}$, i.e., the perspector of its polar triangle (magenta) with respect to $\mathcal{C}$. Video

pair centered on X_{1249}. Prove that the circumconic (resp. inconic) normals at the vertices (resp. contact points) meet at X_{20} (resp. X_{1498}).

Question 3.8. *Gibert (ibid.) lists the following triangle centers as lying on the Thomson cubic: X_k, k =57, 223, 282, 1073, 3341, 3342, 3343, 3344, 3349, 3350, 3351, 3352, 3356, 14481. Experimentally they are not stationary over Poncelet 3-periodics centered on them. Why is that? Conversely, why is it that X_k, k =1,2,3,4,6,9,1249 , also on the Thomson, can be stationary?*

Question 3.9. *Given a triangle, compute its X_7-centered inconic and circumconic. Prove that 3-periodics interscribed in said conics will not maintain X_7 stationary. Prove the same by taking the conic pair's center to be X_8 and X_{10}, i.e., in neither of these cases will the original center remain stationary. Report the Brianchon point for all said inconics.*

Question 3.10. *Prove Proposition 3.9.*

4 Non-concentric, Axis-Parallel (NCAP)

Here we introduce a few Poncelet triangle families interscribed in non-concentric, axis-parallel (NCAP) ellipse pairs. These are known as (i) the poristic family (interscribed between two non-concentric circles), (ii) the poristic "excentral" family, comprising the excentral triangles to the poristic family, and (iii) the Brocard porism, a special family whose Brocard points remain stationary (defined and explained below). In each case we describe their geometry, present properties and invariants, and propose a vertex parameterization. In Section 4.5, properties and fixed points for the families treated herein are summarized. In Figure 4.11 we organize all families studied in this chapter and in Chapters 2 and 3, grouping them by "similarity" of properties and invariants.

4.1 Poristic family (Bicentric triangles)

Poristic triangles, shown in Figure 4.1, are the simplest case of Poncelet's porism: a 1d family of triangles with fixed incircle and circumcircle. They are also known as the ($N = 3$) bicentric family.

First described by Chapple (1746), the family was later studied by both Euler

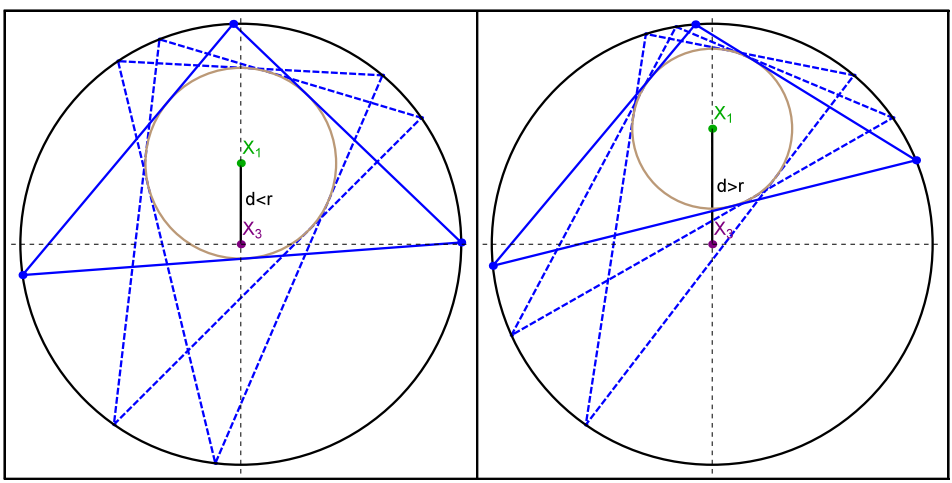

Figure 4.1: Poristic Triangle family (blue): fixed incircle (green) and circumcircle (purple). **Left**: a few poristic triangles (blue and dashed blue) in a pair of circles such that $d < r$, i.e., all poristic triangles are acute. **Right**: the same but with $d > r$; since X_3 can be either interior or exterior to the family, both acute and obtuse triangles will be present. Live

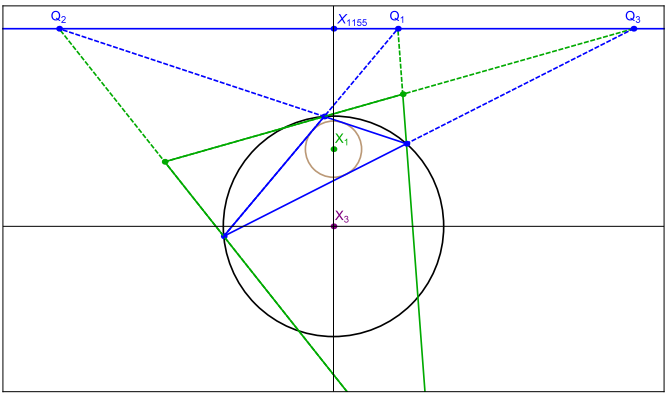

Figure 4.2: Over the poristic family, the antiorthic axis (solid blue) is stationary and perpendicular to X_1X_3. Video.

and Poncelet. The so-called Euler's triangle formula[1], constrains the distance d between incenter X_1 and circumcenter X_3 as follows:

$$d^2 = R(R-2r) \tag{4.1}$$

where r, R are the radii of outer and inner circle. Referring to Figure 4.1:

Proposition 4.1. *The Poristic family will contain obtuse triangles iff $d > r$.*

Proof. This stems from the fact that when $d < r$, X_3 is always interior to the incircle, i.e., the caustic of the Poncelet family. □

In consonance with both billiard 3-periodics and the incircle family:

Proposition 4.2. *The poristic family conserves the sum of its internal angle cosines.*

Proof. Direct application of Equation (2.4), noting by definition r/R is constant. □

In Weisstein (2019, Antiorthic axis), the antiorthic axis is defined as containing the three intersections of a triangle's sidelines with those of the excentral triangle. As illustrated in Figure 4.2, the following was proved by Weaver (1927):

[1] Chapple had stated it in 1746, Euler in 1765, and Poncelet's porism was published in 1822, see Del Centina (2016a).

Proposition 4.3. *The antiorthic family is stationary over the poristic family and perpendicular to* X_1X_3.

Let a first vertex P_1 of the poristic family be parametrized by $P_1(t) = R[\cos t, \sin t]$.

Proposition 4.4. *The perimeter* $L(t)$ *of poristic triangles is given by:*

$$L(t) = \frac{\left(3\,R^2 - 4\,dR\cos t + d^2\right)\sqrt{3\,R^2 + 2\,dR\cos t - d^2}}{R\sqrt{R^2 - 2\,dR\cos t + d^2}}$$

Proof. Follows directly computing the 3-vertices explicitly and using $L(t) = |P_1 - P_2| + |P_2 - P_3| + |P_3 - P_1|$ and simplifying it with a CAS. □

It turns out that poristic triangles can be regarded as the image of billiard 3-periodics (and vice versa) under (i) a variable similarity transform, and (ii) a polar transformation wrt to a focus-centered circle. We now proceed to prove these results, but first we will need a couple of lemmas. In Odehnal (2011, page 17), one finds the following result, illustrated in Figure 4.3:

Lemma 4.1. *Over the poristic family, the locus of the Mittenpunkt* X_9 *is a circle with radius is* $Rd^2R/(9R^2-d^2)$ *centered on* $X_1+(X_1-X_3)(2R-r)/(4R+r) = d(3R^2 + d^2)/(9R^2 - d^2)$.

In fact we can derive $X_9(t)$ explicitly:

Lemma 4.2.

$$X_9(t) = \left[\frac{d\left(4\,d\,\mathbf{c}^2\,(R\mathbf{c}_t - d) - r\,(3\,d\,\mathbf{c}_t + R) - r^2\right)}{(4\,R + r)\,(d\,\mathbf{c}_t - R + r)}, \frac{4Rd^2\mathbf{s}_t\left(R^2 - (2\,R\mathbf{c}_t - d)^2\right)}{(R^2 + d^2 - 2\,dR\mathbf{c}_t)\,(9\,R^2 - d^2)}\right]$$

where $\mathbf{c}_t$ *and* $\mathbf{s}_t$ *are shorthand for* $\cos(t)$ *and* $\sin(t)$ *respectively.*

Let $P_i = [x_i, y_i]$ denote the vertices of billiard 3-periodics and $P_i' = [x_i', y_i']$ those of a poristic family, $i = 1, 2, 3$.

Theorem 4.1. *The* P_i' *are an image of the* P_i *under a variable similarity transform comprising of (i) a rigid rotation by* $\theta(t)$*, (ii) a rigid translation by* $X_9(t)$*, and (iii) uniform scaling by* $L(t)$*. These are given by:*

$$\begin{aligned} x_i' &= L(t)(\cos\theta(t)x_i + \sin\theta(t)y_i + x_9(t)) \\ y_i' &= L(t)(-sin\theta(t)x_i + \cos\theta(t)y_i + y_9(t)) \\ \tan\theta(t) &= \frac{(1-\cos t)(R + d - 2R\cos t)}{(2R\cos t + R - d)\sin t} \end{aligned}$$

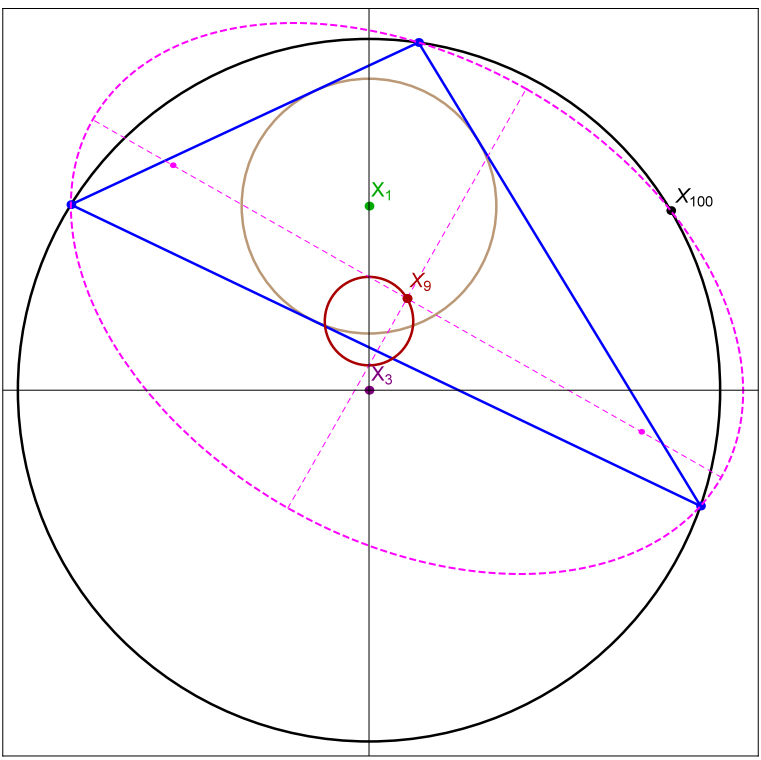

Figure 4.3: A poristic triangles (blue) is shown along as its circumbilliard (dashed magenta) whose aspect ratio is invariant. The locus of the Mittenpunkt X_9 is a circle (red). Video, Live

Proof. CAS-assisted simplification. □

Reznik and Garcia (2021a) defines the "circumbilliard" E_9 of a triangle as the circumellipse centered on X_9. Let a_9, b_9 its semiaxes. CAS manipulation yields:

Corollary 4.1. *Over the poristic family, $a_9(t)$ and $b_9(t)$ are given by:*

$$\begin{aligned} a_9 &= L(t)\frac{R\sqrt{3\,R^2+2\,dR-d^2}}{9\,R^2-d^2} \\ b_9 &= L(t)\frac{R\sqrt{R-d}}{\sqrt{3\,R+d}\,(3\,R-d)} \\ c_9 &= \sqrt{a_9^2-b_9^2} = L(t)\frac{2R\sqrt{dR}}{9R^2-d^2}. \end{aligned}$$

Corollary 4.2. *The ratios $a_9(t)/L(t)$, $b_9(t)/L(t)$, and $c_9(t)/L(t)$ are invariant over the Poristic family.*

Corollary 4.3. *Over the poristic family, the aspect ratio of the (varying) circumbilliard is invariant and given by:*

$$\frac{a_9(t)}{b_9(t)} = \sqrt{\frac{(R+d)\,(3R-d)}{(R-d)\,(3\,R+d)}}$$

Recall the definition of the *polar* of a point P with respect to a circle $\mathcal{C}$, mentioned in Weisstein (2019, Polar): it is defined as the line perpendicular to OP which contains the inversion of P wrt to $\mathcal{C}$. Dually, the pole of a line L with respect to $\mathcal{C}$ is the inversion of the foot of the perpendicular dropped from O onto P wrt to $\mathcal{C}$. So given a smooth curve, we can speak of its *polar image* with respect to a circle as the set of poles of the curve's tangents with respect to $\mathcal{C}$.

The fact that the polar image of an ellipse with respect to a focus is a circle is a well-known result, mentioned in Akopyan and Zaslavsky (2007) and Glaeser, Stachel, and Odehnal (2016).

Let $\mathcal{E}$ and $\mathcal{E}'$ be a confocal ellipse pair centered at $[0, 0]$, with major axes along x. Let a, b and a', b' denote their major and minor semiaxes, respectively. The foci f_1 and f_2 are at $[\pm c, 0]$, where $c^2 = a^2 - b^2$. A known classical result which we reproduce below is:

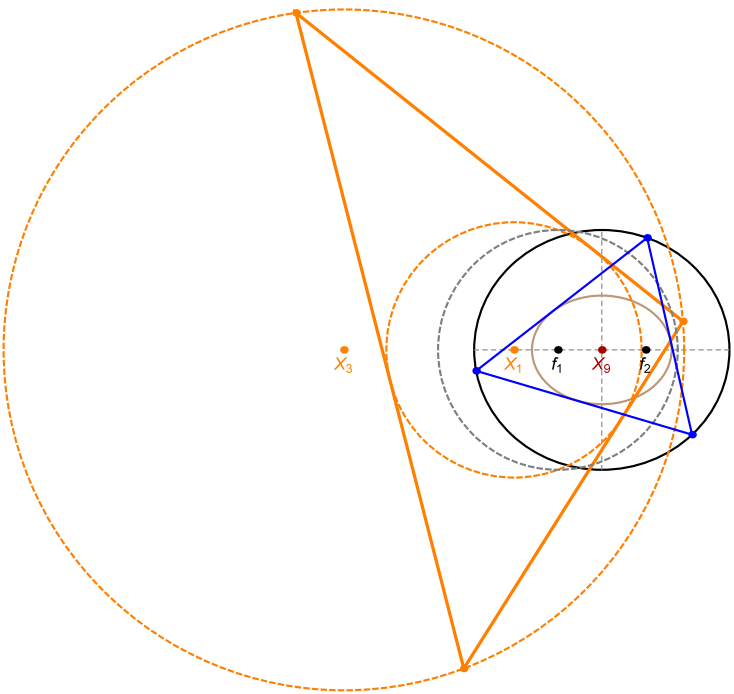

Figure 4.4: The poristic family (orange) is the polar image of billiard 3-periodics (blue) with respect to a circle (dashed gray) centered on one of the foci of the confocal pair (f_1 in the picture). Live

Lemma 4.3. *The polar image of the $\mathcal{E}, \mathcal{E}'$ pair with respect to a circle of radius ρ centered on f_1 is a pair of nested circles $\mathcal{C}_{int}, \mathcal{C}_{ext}$ with centers given by:*

$$\mathcal{O}_{int} = [-c - \rho^2 \frac{c}{b^2}, 0], \quad \mathcal{O}_{ext} = [-c - \rho^2 \frac{c}{b'^2}, 0]$$

Their radii r, R and distance d between their centers are given by:

$$r = \rho^2 \frac{a}{b^2}, \quad R = \rho^2 \frac{a'}{b'^2}, \quad d = \rho^2 \frac{c\,(a^2 - a'^2)}{b^2\, b'^2}$$

Referring to Figure 4.4:

Corollary 4.4. *The poristic family is the polar image of billiard 3-periodics with respect to a circle centered on a focus.*

Corollary 4.5. *The sum of cosines of the polar image of billiard 3-periodics with respect to a focus-centered circle is given by:*

$$\sum \cos\theta' = 1 + \frac{r}{R} = 1 + \frac{ab'^2}{a'b^2} \tag{4.2}$$

Given a triangle, an inconic is is fully defined by its center and is tangent to the three sidelines, see Weisstein (2019, Inconic).

Referring to Figure 4.5, let E_1 be the X_1-centered circumconcic to the poristic family, i.e., it contains the vertices. Let μ_1, and ν_1 denote its semiaxes. Interestingly:

Proposition 4.5. *$\mu_1 = R + d$ and $\nu_1 = R - d$ are invariant over the poristic family, i.e., E_1 rigidly rotates about X_1.*

A proof appears in Garcia and Reznik (2021, Appendix C).

4.2 Poristic excentrals

The family of excentral triangles to the poristic family, shown in Figure 4.6 is also Ponceletian: in Odehnal (2011), it is shown to be inscribed in a circle of radius $2R$ where R is the circumradius of its reference poristic family, centered on X_{40}, the Bevan point, or X_3' of the family in questions (to avoid confusion, we will be priming quantities associated with this family).

Proposition 4.6. *The barycenter X_2' of poristic excentrals is stationary.*

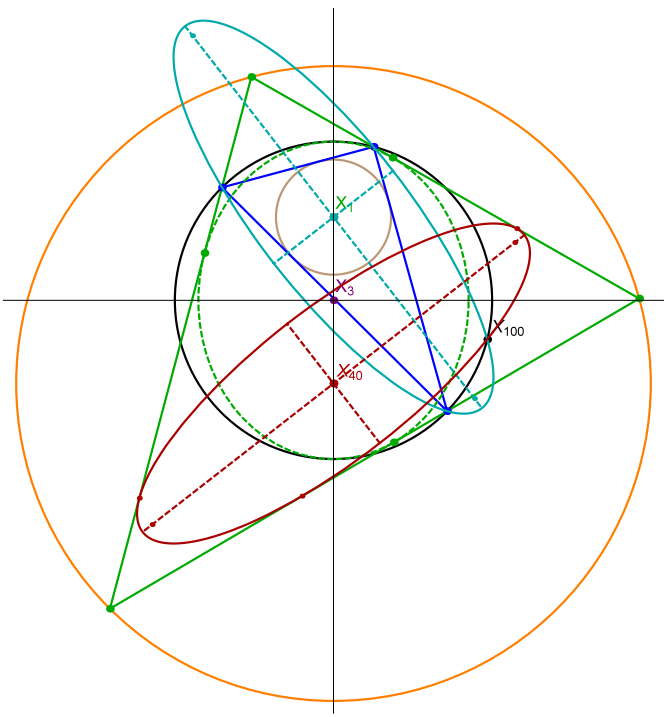

Figure 4.5: A poristic triangle (blue) is shown, as well as I_1, the X_1-centered inconic (light blue). Also shown is the excentral triangle (green), the circle (orange) the excentral family is inscribed in and their MacBeath caustic (dashed green). Also shown is I_3' (dark red), the X_3'-centered excentral inconic (red). Note $X_3' = X_{40}$. Over the poristic family, both I_1 and I_3' rotated rigidly at 90-degrees from each other. Video

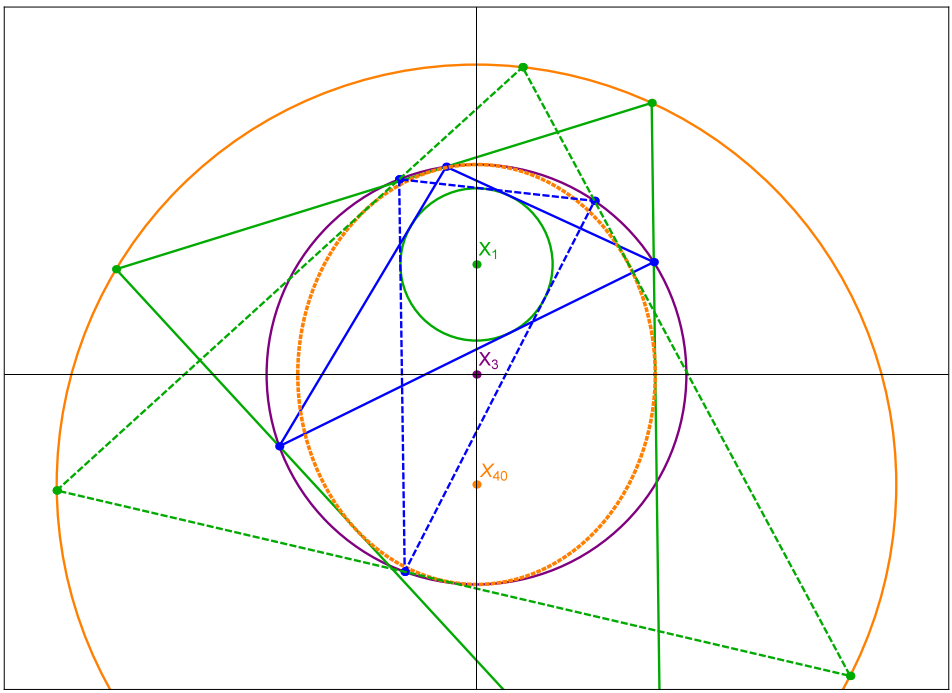

Figure 4.6: The poristic family (blue) is interscribed between two fixed circles, i.e., their circumcenter X_3 and incenter X_1 are stationary. The family of its excentral triangles (solid green) are inscribed in a circle (orange) centered on the Bevan point X_{40} and of radius twice the original circumradius. This family circumscribes the MacBeath inellipse (dashed orange), centered on X_3 with foci on X_1 and X_{40}. A second for both poristics and excentrals configuration is also shown (dashed blue and dashed green). Video, Live

excentral MacBeath	excentral center	reference center
center	X_5'	X_3
focus	X_4'	X_1
focus	X_3'	X_{40}

Table 4.1: Center and foci of the MacBeath inconic of an excentral triangle and the corresponding triangle center of the reference.

Proof. Recall a triangle's barycenter X_2 is a third of the way from the circumcenter to the orthocenter, see Weisstein (2019, Euler Line, Eqn. 6). The result follows from the fact that both $X_3' = X_{40}$ and $X_4' = X_1$ are stationary. □

The MacBeath inconic, defined in Weisstein (ibid., MacBeath Inconic), is an ellipse centered on a triangle's 9-point center X_5, with foci at the circumcenter X_3 and orthocenter X_5. Poristic excentrals are Ponceletian since:

Proposition 4.7. *The MacBeath inconic to the excentral poristics is stationary and is therefore the caustic. Let μ_5' and ν_5' denote its major and minor semiaxes. These are given by:*

$$\mu_5' = R, \quad \nu_5' = \sqrt{R^2 - d^2}$$

Proof. It is straightforward to verify the sidelines of poristic excentrals are dynamically tangent to the ellipse:

$$\frac{(x-d)^2}{R^2} + \frac{y^2}{R^2 - d^2} = 1$$

with center $X_3 = (d, 0)$ and foci $X_{40} = (0, 0)$ and $X_1 = (2d, 0)$. □

Correspondences between the centers and foci of the excentral MacBeath inconic and those of the reference triangle appear in Table 4.1.

Since $\mu_5'/\nu_5' = R/\sqrt{R^2 - d^2}$, use Equation (4.1) to obtain:

Corollary 4.6. *The aspect ratio of the caustic to the excentral poristics is given by:*

$$\frac{\mu_5'}{\nu_5'} = \sqrt{\frac{R}{2r}}$$

As shown in Figure 4.5, let I_3' be the X_3'-centered inconic to poristic excentrals. Let μ_3' and ν_3' denote its major and minor semiaxes, respectively.

Proposition 4.8. *Over poristic excentrals, $\mu_3' = R + d$ and $\nu_3' = R - d$ are invariant, i.e., I_3' rigidly rotates about X_3'.*

We omit the long proof kindly contributed by B. Odehnal and appearing in Garcia and Reznik (2021, Appendix C).

Interestingly:

Theorem 4.2. *Excentral poristics are the image of the circumcircle family under a variable rigid rotation. The rigidly-rotating I_3' is identified with the caustic of the circumcircle family.*

Proof. Recall Proposition 3.8: the orthic triangles of the circumcircle family has invariant inradius and circumradius. Also recall Lemma 3.3: the locus of the orthic circumcenter is a circle concentric with the common center. Also notice in the circumcircle family, the caustic is the stationary inconic centered on X_3. □

4.3 The Brocard porism

A property-rich family of Poncelet triangles is the so-called "Brocard porism", introduced in Bradley (2011), Bradley and Smith (2007), and Shail (1996). It is inscribed in a circle and circumscribes the so-called *Brocard inellipse*. Remarkably, its foci coincide with the stationary Brocard points Ω_1 and Ω_2 of the family; see Figure 4.7.

Let R denote the radius of the outer circle and a', b' the caustic semiaxes, with $(c')^2 = (a')^2 - (b')^2$. Let also, $d = |X_3 - X_{39}|$ the distance between the centers of the circle and of the caustic.

Proposition 4.9. *A pair of circle (outer) $(x-x_0)^2+y^2 = R^2$ and ellipse (caustic) $(x - x_1)^2/(a')^2 + y^2/(b')^2 = 1$ admit a 1d family of Poncelet triangles if and only if*

$$(a')^2 - 2Ra' - (b')^2 + R^2 - d^2 = 0, \quad d = |x_1 - x_0|$$

Proof. Follows from Cayley condition for 3-periodics in an NCAP pair. □

Proposition 4.10. *For any triangle T, the circumcircle and Brocard inellipse are Ponceletian, they admit a 1d family of Poncelet triangles. Furthermore, their Brocard inellipse is stationary.*

Proof. Follows from vertex parametrization for the Brocard family and/or from stationarity of X_6, see Proposition 4.13. □

Proposition 4.11. *The stationary circumcenter X_3 and circumradius R are given by:*

$$X_3 = \left[0, -\frac{c'\delta_1}{b'}\right], \quad R = \frac{2(a')^2}{b'}$$

where $\delta_1 = \sqrt{4(a')^2 - (b')^2}$.

The following is a known requirement for the Brocard porism to be possible, appearing in Shail (1996, Eqs. 15–17):

Corollary 4.7. $R \geqslant 2c'$

Remarkably, and echoing a property seen above for the homothetic family, leaving the proof as an exercise:

Proposition 4.12. *Over the Brocard porism, the Brocard angle ω is invariant and given by:*

$$\cot\omega = \frac{\delta_1}{b'} \geqslant \sqrt{3}$$

Henceforth, we shall use symbol ш for $\cot\omega$. Recall for any triangle $\text{ш} = \sum_{i=1}^{3} \cot\theta_i$, i.e.:

Corollary 4.8. *The Brocard porism conserves the sum of its internal angle cotangents.*

Shail (ibid.) derives the distance between Brocard points (the foci of the Brocard inellipse), in terms of invariant R and ω:

$$|\Omega_1 - \Omega_2|^2 = 4R^2 \sin^2\omega(1 - 4\sin^2\omega) = (c')^2 \tag{4.3}$$

Corollary 4.9.

$$c' = R\sin\omega\sqrt{1 - 4\sin^2\omega}$$

Referring to Figure 4.7, all of Ω_1, Ω_2, X_3, and X_6 are concyclic on the so-called Brocard circle, see Weisstein (2019, Brocard Circle), whose center is X_{182}. The Brocard axis is defined in Weisstein (ibid., Brocard Axis) as the line containing the circumcenter X_3 and symmedian point X_6 of a triangle.

Proposition 4.13. *Over the Brocard porism, the following 3 objects are stationary: (i) the Brocard circle, (ii) the Brocard axis, and (iii) the symmedian point X_6 are stationary.*

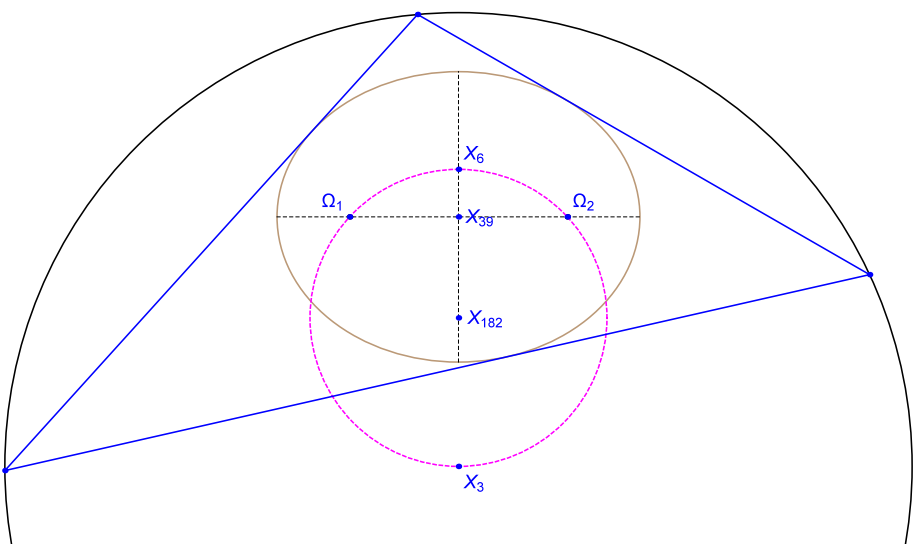

Figure 4.7: A triangle (blue) in the Brocard porism is shown inscribed in an outer circle (black) and having the Brocard inellipse (brown) as its caustic, with foci at the stationary Brocard points Ω_1 and Ω_2 of the family, and centered on the Brocard midpoint X_{39}. The Brocard points as well as the stationary circumcenter X_3 and symmedian point X_6 are concyclic on the Brocard circle (dashed magenta), whose center is X_{182}. Live

Proof. The Brocard circle is stationary since it passes through 3 stationary points: Ω_1, Ω_2, X_3 are stationary. The Brocard axis is stationary since it contains stationary X_3 and stationary Brocard midpoint X_{39}. For any triangle, X_6 is antipodal to X_3 on the Brocard circle. □

Recall the two isodynamic points X_{15} and X_{16} of a triangle as the two unique intersections of the 3 Apollonius circles[2]. X_{15} (resp. X_{16}) is interior (resp. exterior) to the circumcircle. In fact they are inverse images of each other with respect to the latter, see Weisstein (2019, Isodynamic Points).

Proposition 4.14. *Over the Brocard porism, the two Isodynamic points X_{15} and X_{16} are stationary and given by:*

$$X_{15} = \left[0, \frac{R(\sqrt{3} - \text{ш})}{\sqrt{\text{ш}^2 - 3}}\right], \quad X_{16} = \left[0, -\frac{R(\sqrt{3} + \text{ш})}{\sqrt{\text{ш}^2 - 3}}\right]$$

Proof. Let P and U be finite points on a triangle's plane with normalized barycentric coordinates (p, q, r) and (u, v, w), respectively. Let f and g be homogeneous functions of the sidelengths. The (f, g) *barycentric combo* of P and U, also denoted $f * P + g * U$, is the point with barycentric coordinates $(f\ p + g\ u,\ f\ q + g\ v,\ f\ r + g\ w)$. In Kimberling (2019, X(15), X(16)), the following combos (see below), derived by Peter Moses, are provided:

$$\begin{aligned} X_{15} &= \sqrt{3} * X_3 + \text{ш} * X_6 \\ X_{16} &= \sqrt{3} * X_3 - \text{ш} * X_6 \end{aligned}$$

With all involved quantities invariant, the result follows. □

Proposition 4.15. *The semiaxes a' and b' and center X_{39} of the Brocard inellipse are given by:*

$$\begin{aligned} [a', b'] &= R\left[\sin\omega, 2\sin^2\omega\right] = R\left[\frac{1}{\sqrt{1 + \text{ш}^2}}, \frac{2}{1 + \text{ш}^2}\right] \\ X_{39} &= \left[0, -\frac{R\text{ш}\sqrt{\text{ш}^2 - 3}}{\text{ш}^2 + 1}\right] \end{aligned}$$

[2] These are circles which contain a vertex and the intersection of the corresponding internal and external bisectors with the opposite side.

Proof. Consider a triangle T with sidelengths s_1, s_2, s_3, area A, and circumradius R. The following identities appear in Bradley and Smith (2007) and Shail (1996):

$$R = \frac{s_1 s_2 s_3}{4A}, \quad \sin\omega = \frac{2A}{\sqrt{\Gamma}} \tag{4.4}$$

where $\Gamma = (s_1 s_2)^2 + (s_2 s_3)^2 + (s_3 s_1)^2$. Bringing in Equation (4.3), the result follows from combining the above into expressions for the Brocard inellipse semiaxes, given in Weisstein (2019, Brocard Inellipse):

$$a' = \frac{s_1 s_2 s_3}{2\sqrt{\Gamma}}, \qquad b' = \frac{2 s_1 s_2 s_3 A}{\Gamma} \tag{4.5}$$

□

With the results above, we can derive the following quantities and centers explicitly:

$$X_6 = \left[0, -\frac{R\sqrt{\text{ш}^2 - 3}}{\text{ш}}\right]$$
$$|X_3 - X_6| = \frac{R\sqrt{\text{ш}^2 - 3}}{\text{ш}}$$
$$\Omega_{1,2}(R, \text{ш}) = \frac{R\sqrt{\text{ш}^2 - 3}}{\text{ш}^2 + 1}\,[\pm 1, -\text{ш}]$$

Let a' be the major axis of a generic triangle's Brocard inellipse. Interestingly, we have:

Lemma 4.4.

$$\sum_{i=1}^{3} \frac{1}{s_i^2} = \frac{1}{4(a')^2}$$

Proof. As

$$\frac{1}{s_1^2} + \frac{1}{s_2^2} + \frac{1}{s_3^2} = \frac{s_2^2 s_3^2 + s_1^2 s_3^2 + s_1^2 s_2^2}{s_1^2 s_2^2 s_3^2}$$

the result follows from Equation (4.5). □

Therefore, we have:

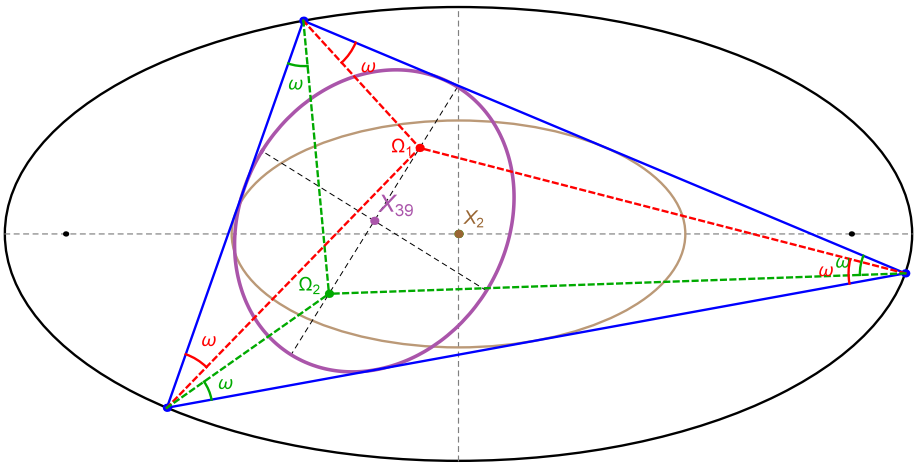

Figure 4.8: Over the homothetic family, the Brocard inellipse has semiaxes of variable lengths but invariant aspect ratio. Video

Corollary 4.10. *Over the Brocard porism, the sum of inverse squared sidelengths is invariant*

Similarity and Polar image: As it will be seen below, the Brocard porism is the image of the Homothetic family under two different transformations: variable similarity and polar.

Referring to Figure 4.8, we will first prove a handy lemma, introduced in Reznik and Garcia (2021b):

Lemma 4.5. *Over the homothetic family, though the semiaxes of the Brocard inellipse have variable lengths, their ratio β is invariant and given by:*

$$\beta = \frac{\sqrt{3a^4 + 10a^2b^2 + 3b^4}}{4ab} > 1$$

Proof. The result follows from combining Equation (4.4) with Equation (4.5), using the sidelengths s_i of the homothetic family using the parametrization in Section 2.7.1. □

The result below was introduced in Reznik and Garcia (ibid., Thm 4.1):

Proposition 4.16. *The Brocard family is the image of the homothetic one under a variable similarity transform.*

Proof. Consider the following similarity transform which sends points X in the plane of the homothetic family to new ones X':

$$X' = Scale(1/b'').Rot(-\theta).Transl(-X_{39}).X$$

where b'' is the variable minor semiaxis length of the the (moving) Brocard inellipse $\mathcal{E}''$ in the homothetic pair, θ the angle between said minor axis and the horizontal, and X_{39} the moving center of $\mathcal{E}''$. Clearly, $\mathcal{E}''$ will be sent to an origin-centered ellipse which is axis-parallel to the homothetic ones. By Lemma 4.5, the aspect ratio β of $\mathcal{E}''$ is invariant over the homothetic family, implying the transformed inellipse will have fixed axes $(\beta, 1)$. Notice its circumcenter and circumradius are prescribed by the semiaxes of the caustic (see Proposition 4.11). This completes the proof. □

Referring to Figure 4.9, let a, b be the semiaxes of the outer ellipse in the homothetic pair.

Proposition 4.17. *The Brocard porism is the polar image of the homothetic family with respect to a circle centered on a caustic focus f'. The symmedian point X_6 of the image coincides with f'. Its outer circle and ellipse are given by:*

$$\begin{aligned}
&\mathcal{C}: \ (x-x_0)^2 + y^2 = R^2 \\
&\mathcal{E}: \ \frac{(x-x_1)^2}{(a')^2} + \frac{y^2}{(b')^2} = 1 \\
&x_0 = -\frac{c(b^2+4\rho^2)}{2b^2}, \quad x_1 = -\frac{c(4a^2-c^2+4\rho^2)}{2(4a^2-c^2)} \\
&(a') = \frac{4a\rho^2}{4a^2-c^2}, \quad (b') = \frac{2a\rho^2}{b\sqrt{4a^2-c^2}}, \quad R = \frac{2a\rho^2}{b^2}
\end{aligned}$$

Here $b' > a'$.

Proof. Proof is left as an exercise. □

Remark 4.1. *From the relations obtained in Proposition 4.17 it follows that*

$$a = \rho^2 \frac{(4(b')^2 - (a')^2)}{3a'(b')^2}, \quad b = \rho^2 \frac{\sqrt{4(b')^2 - (a')^2}}{\sqrt{3}(b')^2}$$

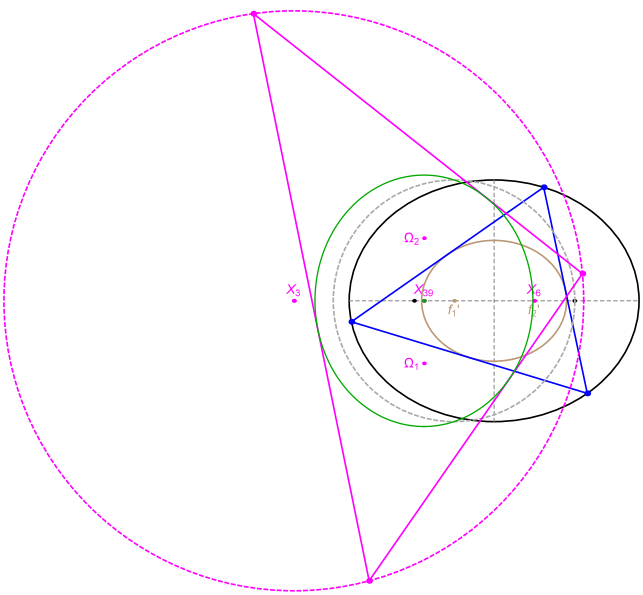

Figure 4.9: The Brocard family (magenta) is the polar image of the homothetic family (solid blue) with respect to a circle (dashed gray) centered on a focus of the homothetic caustic (light brown) which is sent to the Brocard circumcircle (dashed magenta). The outer ellipse (black) is sent to the Brocard inellipse (green). Live

Since two polar transformations with respect to the same circle is the identity:

Corollary 4.11. *The homothetic family is the polar image of the Brocard family with respect to its stationary symmedian point X_6.*

Corollary 4.12. *In terms of the homothetic pre-image semiaxes a, b, the invariant sum of inverse squared sidelengths and Brocard angle are given by:*

$$\sum_{i=1}^{3} \frac{1}{s_i^2} = \frac{1}{4(b')^2} = \frac{b^2(3a^2+b^2)}{16\rho^4 a^2}$$
$$\cot\omega = \text{ш} = \sqrt{3}\frac{a}{b}$$

Proof. By Proposition 4.15 and Proposition 4.17 it follows that $\sin\omega = (a')/(2b') = b/\sqrt{4a^2-c^2}$. Using that $\csc^2\omega - \cot^2\omega = 1$ the result follows. □

4.3.1 A digression: equilateral isodynamic pedals

Referring to Figure 4.10, the pedal (resp. antipedal) triangles of the isodynamic points X_{15} and X_{16} (resp. isogonic points X_{13} and X_{14}) are equilateral triangles centered on X_{396} and X_{395} (resp. X_{5463} and X_{5464}). These facts appear in Kimberling (2019).

Let A denote the area of a triangle and A_k, $k = 13, 14, 15, 16$ denote the area of said equilaterals. Moses (2020) has kindly contributed the following expressions:

Proposition 4.18.

$$A_{13}/A = 2 + \frac{2\text{ш}}{\sqrt{3}}, \quad A_{14}/A = 2 - \frac{2\text{ш}}{\sqrt{3}}$$
$$A_{15}/A = \frac{-3+\sqrt{3}\text{ш}}{2(\csc^2\omega - 4)}, \quad A_{16}/A = \frac{-3-\sqrt{3}\text{ш}}{2(\csc^2\omega - 4)}$$

Corollary 4.13. *For any triangle:*

$$\frac{A_{13}}{A_{14}} = \frac{A_{16}}{A_{15}} = \frac{\text{ш}+\sqrt{3}}{\text{ш}-\sqrt{3}}$$

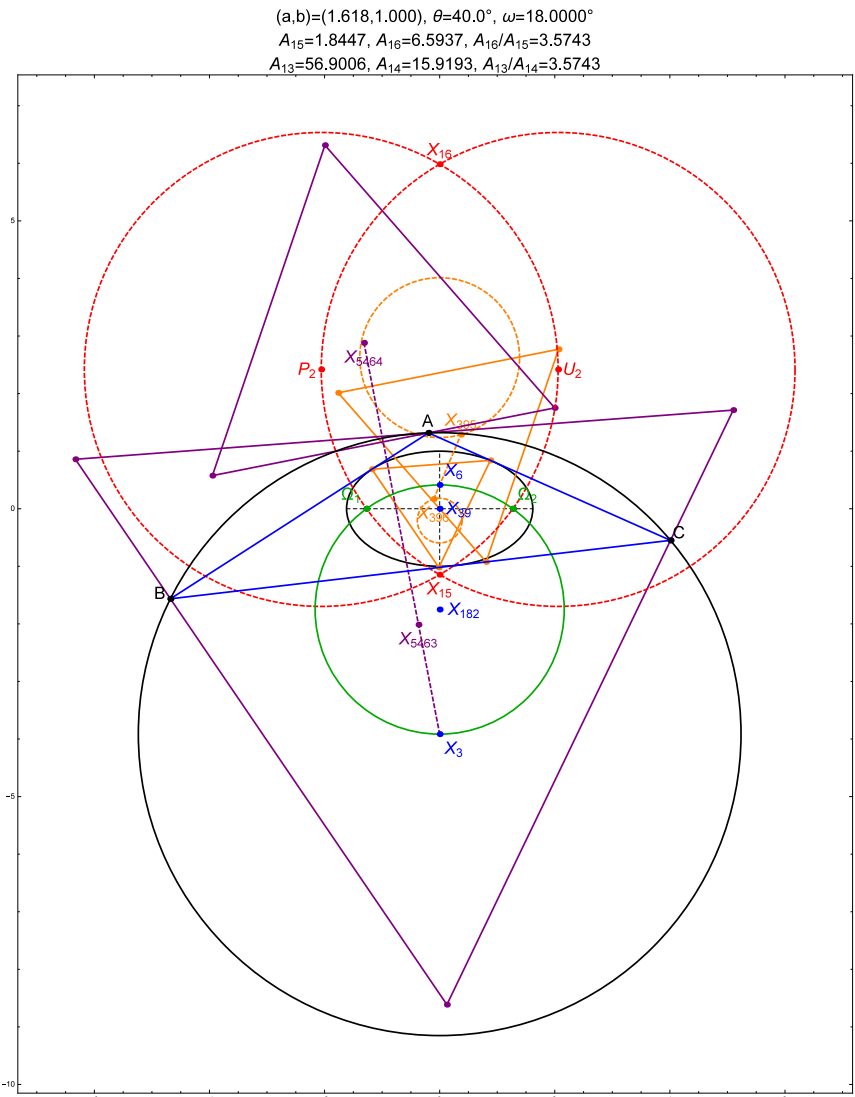

Figure 4.10: The pedal (resp. antipedal) triangles (orange, resp. purple) of the isodynamic points X_{15} and X_{16} (resp. isogonic points X_{13} and X_{14}) are equilaterals centered on X_{396} and X_{395}, collinear with X_6 (resp. X_{5463} and X_{5464}, collinear with X_3), see Kimberling (2019). Over the porism, the area ratios A_{16}/A_{15} and A_{13}/A_{14} are invariant and identical. The loci of X_{396} and X_{395} are circles (dashed orange) as are those of X_{5463} and X_{5464} (not shown). Video

Corollary 4.14. *The Brocard porism conserves A_{13}/A_{14} and A_{16}/A_{15}.*

The centroid of the pedal triangle of X_{15} (resp. X_{16}) is X_{396} (resp. X_{395}).

Proposition 4.19. *The locus of X_{15} and X_{16} pedal centroids X_{396} and X_{395} are the following circles:*

$$C_{395} = \left[0, \frac{R\left(3(ш^2+1) - 2\sqrt{3}\,ш\right)\left(ш + \sqrt{3}\right)}{3\sqrt{ш^2-3}\,(ш^2+1)}\right], \quad r_{395} = \frac{R(\sqrt{3}ш+3)}{3(ш^2+1)}$$

$$C_{396} = \left[0, \frac{R\left(3\,(ш^2+1) + 2\sqrt{3}\,ш\right)\left(ш - \sqrt{3}\right)}{3\sqrt{ш^2-3}\,(ш^2+1)}\right], \quad r_{396} = \frac{R(\sqrt{3}ш-3)}{3(ш^2+1)}$$

Proof. Obtained via CAS. □

Remark 4.2. *Notice the ratio r_{395}/r_{396} is equal to A_{396}/A_{395}.*

Still referring to Figure 4.10:

Proposition 4.20. *The locus of X_{13} and X_{14} antipedal centroids X_{5463} and X_{5464} are the following circles:*

4.4 Vertex parametrization

4.4.1 Poristic family

Consider a pair of circles $x^2+y^2 = R^2$, $(x-d)^2+y^2 = r^2$, with $d^2 = R(R-2r)$. Then a 3-periodic orbit is parametrized by:

$$\begin{aligned}
P_1 &= [x_1, y_1]\\
P_2 &= \frac{1}{w^2}\left[-4Rr^2qy_1 - w_1w_2, -2rRw_1y_1 + 2rqw_2\right]\\
P_3 &= \frac{1}{w^2}\left[4Rr^2qy_1 - w_1w_2, -2rRw_1y_1 - 2rqw_2\right]\\
q &= \sqrt{R^2 - r^2 - 2dx_1 + d^2}, \quad w = R^2 - 2dx_1 + d^2\\
w_1 &= R^2 - 2r^2 - 2dx_1 + d^2, \quad w_2 = (R^2+d^2)x_1 - 2R^2d
\end{aligned}$$

4.4.2 Poristic excentrals

Its vertices sweep a circle centered on X_{40} of the original poristic family, so we omit the parametrization.

4.4.3 Brocard porism

Consider an isosceles Poncelet triangle $\mathcal{T} = ABC$ in the Brocard porism, where AB is tangent to $\mathcal{E}$ at one of its minor vertices. Let $|AB| = 2d$ and the height be h. Let $\zeta = d^2 + h^2$. Let the origin $(0, 0)$ be at its circumcenter X_3. Its vertices will be given by:

$$A = \left[-d, \frac{d^2 - h^2}{2h}\right], \quad B = \left[d, \frac{d^2 - h^2}{2h}\right], \quad \left[0, \frac{\zeta}{2h}\right]$$

Proposition 4.21. *The Brocard porism containing $\mathcal{T}$ as a Poncelet triangle is defined by the following circumcircle $\mathcal{K}_0$ and Brocard inellipse $\mathcal{E}$:*

$$\begin{aligned}\mathcal{K}_0 &: x^2 + y^2 - R^2 = 0, \quad R = \frac{\zeta}{2h}\\ \mathcal{E} &: -64d^2h^4x^2 - 4h^2(9d^2 + h^2)\zeta y^2 + 4h(3d^2 + h^2)(3d^2 - h^2)\zeta y\\ &\quad - (d^2 - h^2)(9d^2 - h^2)\zeta^2 = 0\end{aligned}$$

Proof. The proof follows from $\mathcal{T}$, and isosceles Poncelet triangle. Recall that the Brocard inellipse is centered at X_{39}. Its perspector is X_6, i.e., it will be tangent to $\mathcal{T}$ where cevians through X_6 intersect it, see Weisstein (2019, Brocard inellipse). □

Consider the pair: circle $x^2 + y^2 = R^2 = (d^2 + h^2)^2/(4h^2)$ and ellipse $x^2/a^2 + (y - y_0)^2/b^2 = 1$, with semiaxes

$$(a, b) = \left(\frac{d\sqrt{d^2 + h^2}}{9d^2 + h^2}, \frac{4d^2}{9d^2 + h^2}\right)$$

and center $(0, y_0)$, $y_0 = (9d^4 - h^4)/(2h(9d^2 + h^3))$.

Vertices $P_i = [x_i, y_i]$, $i = 1, 2, 3$ of Brocard porism triangles are given by:

Family	Fixed	Conserves	Notes
Poristic (bicentric)	$X_1, X_3, X_{40}, \ldots$	$\sum \cos\theta_i$, a_9/b_9	polar image of Confocal family wrt to a focus
Poristic Excentrals	X_2, X_3, X_4, X_5	$\sum s_i^2$, $\prod \cos\theta_i$	Inscribed in circle; caustic is MacBeath inconic
Brocard	$X_3, X_6, X_{15}, X_{16}, X_{39}, X_{182}, \ldots, \Omega_1, \Omega_2$	$\sum s_i^{-2}$, ω, $\sum \cot\theta_i$	polar image of Homothetic family wrt caustic focus; inscribed in circle; caustic is Brocard inellipse

Table 4.2: Summary of fixed points and (known) conserved quantities for the non-concentric, axis-parallel (NCAP) families in this chapter.

$$
\begin{aligned}
x_1 &= \cos t/q_1\\
y_1 &= \sin t/q_1\\
x_2 &= -d(d^2+h^2)((3d^2+h^2)\sin t + 2dh\cos t - 3d^2 + h^2)/q_2\\
y_2 &= -(d^2+h^2)((9d^4-2d^2h^2+h^4)\sin t - 2dh(3d^2+h^2)\cos t - 9d^4 + h^4)/(2bq_2)\\
x_3 &= d(d^2+h^2)(2dh\cos t - (3d^2+h^2)\sin t + 3d^2 - h^2)/q_3\\
y_3 &= (d^2+h^2)(2dh(3d^2+h^2)\cos t + (9d^4-2d^2h^2+h^4)\sin t - 9d^4 + h^4)/(2bq_3)\\
q_1 &= (2h)/(d^2+h^2)\\
q_2 &= 2dh(3d^2-h^2)\cos t - (9d^4-h^4)\sin t + 9d^4 + 2d^2h^2 + h^4\\
q_3 &= 2dh(3d^2-h^2)\cos t + (9d^4-h^4)\sin t - 9d^4 - 2d^2h^2 - h^4
\end{aligned}
$$

4.5 Summary

Fixed points and (known) conserved quantities for the non-concentric (NCAP) families in this chapter appear in Table 4.2 (compare with Table 3.2).

A diagram depicting how certain pairs of families are interrelated by either similarity or polar transformations appears in in Figure 4.11.

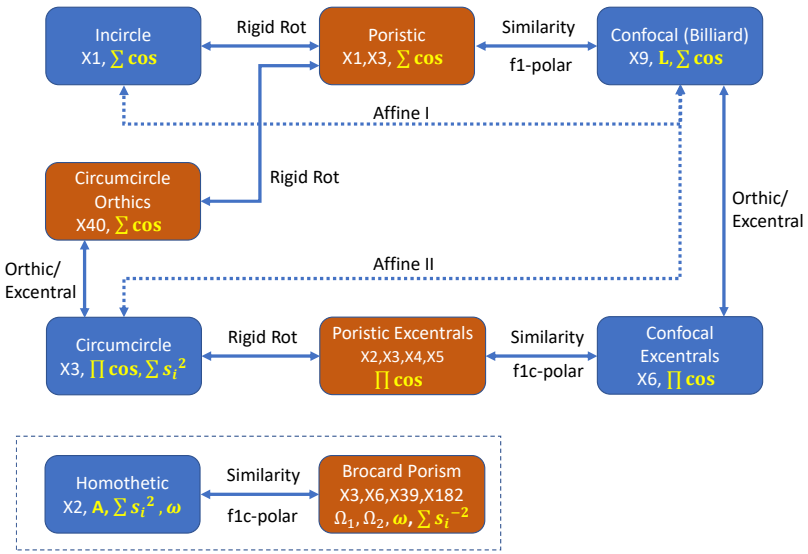

Figure 4.11: Families mentioned in this chapter (blue ones are concentric, tan ones are non-concentric), as well as the transformations under which certain families are interrelated.

4.6 Exercises

Exercise 4.1. *Show that over the poristic family, the locus of the foci of the X_9-centered circumconic (the circumbilliard) is a circle.*

Exercise 4.2. *Prove Proposition 4.3. Furthermore, prove the intersection point of X_1X_3 with the antiorthic axis is the Schröder point X_{1155}.*

Exercise 4.3. *Prove that over the poristic family the inconic centered on X_1 is axis-parallel with the circumconic centered on X_9 (i.e., the circumbilliard), see this Video.*

Exercise 4.4. *Recall the cosine circle $\mathcal{C}$ (also known as the second Lemoine circle) is centered on a triangle's symmedian point X_6. Let $\mathcal{E}'$ be the Brocard ellipse of some triangle T. Let β be the aspect ratio of $\mathcal{E}'$, i.e., a'/b'. Show that for any T, above (resp. below) a certain β, $\mathcal{C}$ is tangent to $\mathcal{E}'$ at two distinct points (resp. it is exterior to $\mathcal{E}'$). See it Live.*

Exercise 4.5. *Show that the poristic excentral family is also the polar image of billiard excentrals wrt to a circle centered on a billiard (i.e., the caustic) focus. See it Live.*

Exercise 4.6. *Show that over the Brocard porism the radius r^* of the cosine circle is invariant.*

Exercise 4.7. *Show that the first Lemoine circle (centered on X_{182} is stationary over the Brocard porism. Above a certain a'/b', this circle is tangent to one of the minor vertices of the caustic. See it Live.*

Exercise 4.8. *Ehrmann's "third" Lemoine circle is studied in Grinberg (2012). It is centered on X_{576}, is defined as follows: for each vertex, consider the 3 circles containing pairs of vertices and the symmedian point X_6. The third Lemoine circle contains the 6 intersections of said circles (2 each) with the sidelines. Prove this circle is also stationary over the Brocard porism, i.e., all three Lemoine circles are; see it Live.*

Exercise 4.9. *Prove the expression and inequality for* $\cot\omega$ *in Proposition 4.12.*

Exercise 4.10. *That the Brocard axis X_3X_6 is stationary over the Brocard porism is established. Prove that the Lemoine axis, which intersects the Brocard axis at the Schoutte point X_{187}, is also stationary; see it Live.*

Exercise 4.11. *The so-called "second" Brocard triangle, defined in Weisstein (2019, Second Brocard Triangle), has vertices at the intersections of symmedians (cevians through X_6) with the Brocard circle. Show that over the Brocard porism, the family of second Brocard triangles is a new, smaller Brocard porism which shares the isodynamic points X_{15} and X_{16} with the original family. Prove that if this is iterated, the shrinking porisms converge to X_{15}. See it Live.*

4.7 Research questions

Question 4.1. *Show that (i) the family of tangential triangles to the Brocard porism is also Ponceletian (caustic is the Brocard circumcircle).(ii) Derive the axes for the ellipse it is inscribed in. and that (iii) its Gergonne point X_7 is stationary and coincides with the symmedian point X_6 of the Brocard porism; (iv) the locus of X_{20} of the tangentials is a segment along the Brocard axis of the original family. Live*

Question 4.2. *The 3 Apollonius' circles of a triangle pass through a vertex and its two isodynamic points X_{15} and X_{16}, see Weisstein (2019, Isodynamic points). Prove that over the Brocard porism, the sum of the inverse squared radii of the three Apollonius circles is invariant, see them Live.*

Question 4.3. *Prove that the polar image of the Brocard porism with respect to a circle centered on a caustic focus is another (tilted, smaller) Brocard porism whose Brocard inellipse shares a focus with the original one. Where does the sequence of Porisms converge? See it Live.*

Question 4.4. *Prove that over the poristic family, the barycenter X_2 of the intouch triangles is stationary. Derive its coordinates. See it Live.*

5 Locus Phenomena in the Confocal Family

When we consider Poncelet 3-periodic families, a natural (and indeed early) question was "what are the loci of certain triangle centers". Recall one of our early experimental finds: that over billiard 3-periodics, the locus of the incenter X_1 is an ellipse (as is that of the excenters), see Section 2.3. Also an early find was that the "locus" of the Mittenpunkt X_9 is a point, see Section 2.4.

In this chapter we expand this exploration by touring a gallery of interesting locus-related phenomena. Our hope is to give the reader an appreciation for the beauty and variety of loci obtainable. These include:

- The loci of some notable centers of a triangle, showing they are ellipses;
- Billiard 3-periodics which can be both acute and obtuse;
- A triangle center with a non-elliptic (quartic) locus nearly identical to an ellipse;
- Two special triangle centers railed to either the billiard or the confocal caustic;

- A non-smooth locus with four singularities;
- A self-intersecting locus;
- A non-compact, non-elliptic locus;
- An elliptic locus whose aspect ratio is the golden ratio φ;
- A triangle center railed to the elliptic billiard whose motion with respect to 3-periodic vertices is "non-monotonic";
- The non-elliptic loci of the vertices of certain derived triangles.
- The "triple-winding" of triangle center loci over themselves.

5.1 Kimberling centers with elliptic loci

The semiaxes a_1, b_1 for the elliptic locus of the incenter X_1 were given in Theorem 2.1. As shown in Figure 5.1, it turns the loci of the next four centers on Kimberling (2019) are also ellipses. These are the barycenter X_2, the circumcenter X_3, the orthocenter X_4, and the center of the 9-point circle (also known as Euler's circle) X_5. Their semiaxes are given by:

$$
\begin{aligned}
(a_2, b_2) &= k_2\,(a, b)\,, \text{ with } k_2 = \frac{2\delta - a^2 - b^2}{3c^2} \\
(a_3, b_3) &= \left(\frac{a^2 - \delta}{2a}, \frac{\delta - b^2}{2b}\right) \\
(a_4, b_4) &= \left(\frac{k_4}{a}, \frac{k_4}{b}\right), \text{ with } k_4 = \frac{(a^2 + b^2)\delta - 2\,a^2 b^2}{c^2} \\
(a_5, b_5) &= \left(\frac{-w_5'(a,b) + w_5''(a,b)\delta}{w_5(a,b)}, \frac{w_5'(b,a) - w_5''(b,a)\delta}{w_5(b,a)}\right)
\end{aligned}
$$

where $w_5'(u, v) = u^2(u^2 + 3v^2)$, $w_5''(u, v) = 3u^2 + v^2$, and $w_5(u, v) = 4u(u^2 - v^2)$. Note that (i) $a_2/b_2 = a/b$ and (ii) $b_4/a_4 = a/b$.

As it turns out, the locus of 49 out of the first 200 centers on Kimberling (ibid.) are ellipses. These are: $X_k, k =$1, 2, 3, 4, 5, 7, 8, 10, 11, 12, 20, 21, 35, 36, 40, 46, 55, 56, 57, 63, 65, 72, 78, 79, 80, 84, 88, 90, 100, 104, 119, 140, 142, 144, 145, 149, 153, 162, 165, 190, 191, 200. Links to live animations as well as expressions for their semiaxes are provided in Garcia, Reznik, and Koiller (2021).

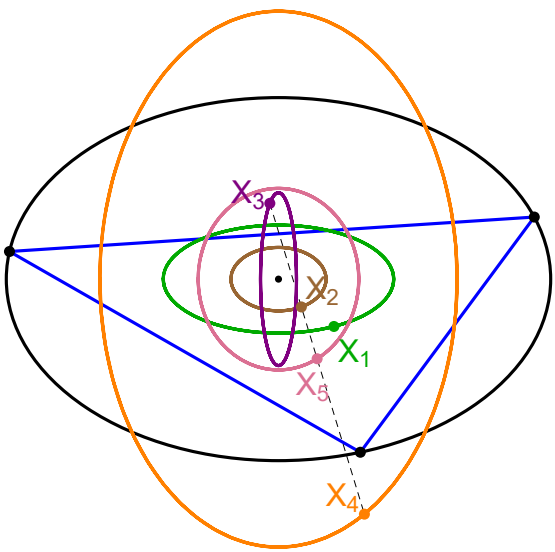

Figure 5.1: Over billiard 3-periodics, the loci of incenter X_1, barycenter X_2, circumcenter X_3, orthocenter X_4, and 9-point center X_5 are all ellipses. The Euler line (dashed black) is shown passing through all but the first center. Video, Live

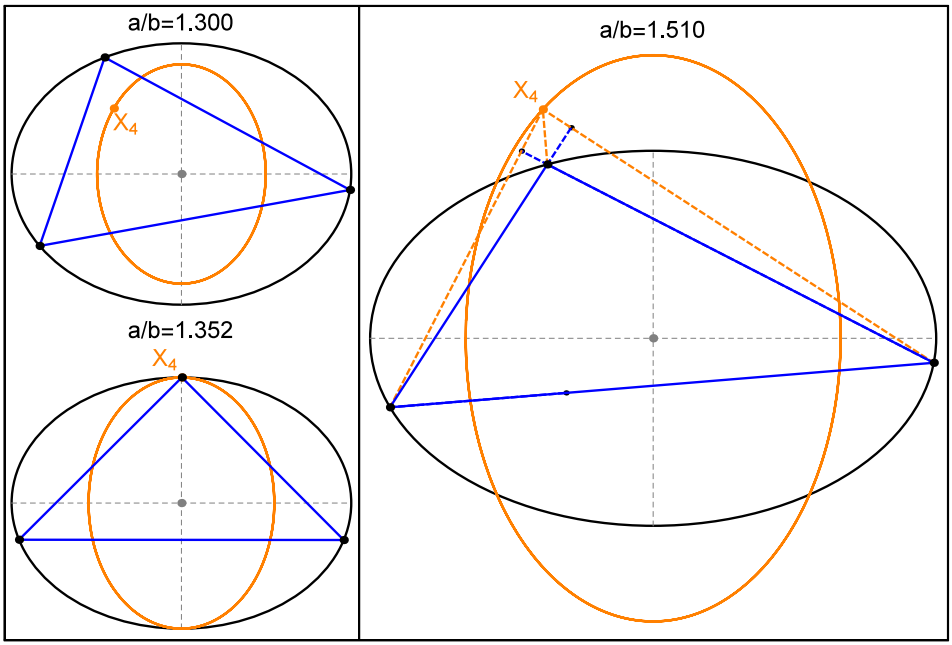

Figure 5.2: Locus of the orthocenter (orange) over elliptic billiards with different aspect ratios. If a/b is (i) less than (resp. (ii) equal, (iii) greater than) $\alpha_4 \simeq 1.352$, the locus of the orthocenter X_4 (orange) is (i) interior (resp. (ii) internally tangent, (iii) intersecting) with the elliptic billiard. In (i) and (ii) all 3-periodics are acute, whereas in (iii) some will be obtuse.

5.2 When billiard 3-periodics are obtuse

It turns out the locus of X_4 can be used to determine if the billiard 3-period family will contain obtuse triangles. Referring to Figure 5.2:

Proposition 5.1. *The locus of X_4 is internally tangent to the elliptic billiard at its top and bottom vertices when $a/b = \alpha_4$ given by:*

$$\alpha_4 = \sqrt{2\sqrt{2}-1} \simeq 1.352.$$

Proof. The equation $b_4 = b$ is equivalent to $a^4 + 2a^2b^2 - 7b^4 = 0$. Therefore, as $a > b > 0$, it follows that $a/b = \sqrt{2\sqrt{2}-1}$. □

Let α_4^* be the positive root of $x^6 + x^4 - 4x^3 - x^2 - 1 = 0$, i.e., $\alpha_4^* = \simeq 1.51$.

Proposition 5.2. *When $a/b = \alpha_4^*$, then $a_4 = b$ and $b_4 = a$, i.e., the locus of X_4 is identical to a rotated copy of Billiard.*

Proof. The condition $a_4 = b$, or equivalently $b_4 = a$, is defined by $a^6 + a^4b^2 - 4a^3b^3 - a^2b^4 - b^6 = 0$. Graphic analysis shows that $x^6 + x^4 - 4x^3 - x^2 - 1 = 0$ has only one positive real root which we call α_4^*. □

Theorem 5.1. *If $a/b < \alpha_4$ (resp. $a/b > \alpha_4$) the 3-periodic family will not (resp. will) contain obtuse triangles.*

Proof. If the 3-periodic is acute, X_4 is in its interior, therefore also internal to the EB. If the 3-periodic is a right triangle, X_4 lies on the right-angle vertex and is therefore on the EB. If the 3-periodic is obtuse, X_4 lies on exterior wedge between sides incident on the obtuse vertex (feet of altitudes are exterior). Since the latter is on the EB, X_4 is exterior to the EB. □

Another way to think of this is depicted in Figure 5.3: $a/b > \alpha_4$, opens up two "zones" along the top and bottom halves of the elliptic billiard. A 3-periodic will be obtuse if and only if one of its vertices is on either zone. These zones are precisely portions of the elliptic billiard which are interior to the locus of X_4; see Figure 5.2(right). When $a/b = \alpha_4$ said zones collapse to the top and bottom vertices of the elliptic billiard; see Figure 5.2(bottom left).

5.3 Quartic locus of the symmedian point X_6

The symmedian point X_6 is replete with properties. Honsberger (1995, Ch. 7) calls it "one of the crown jewels of triangle geometry". Its construction is deceptively simple: the point where a triangle's *symmedians* concur; these are reflections of medians on the bisectors. Its trilinear coordinates could not be simpler: $[a : b : c]$. However, it is the first Kimberling center whose locus over billiard 3-periodics is *not* an ellipse.

In fact, when $1 < a/b < 2$, its locus is visually indistinguishable from a true ellipse; see Figure 5.4. Fortunately, its fit error is easily detectable with numerical methods. Indeed:

Proposition 5.3. *The locus of X_6 is a convex quartic given by:*

$$\mathcal{X}_6(x, y) = c_1x^4 + c_2y^4 + c_3x^2y^2 + c_4x^2 + c_5y^2 = 0$$

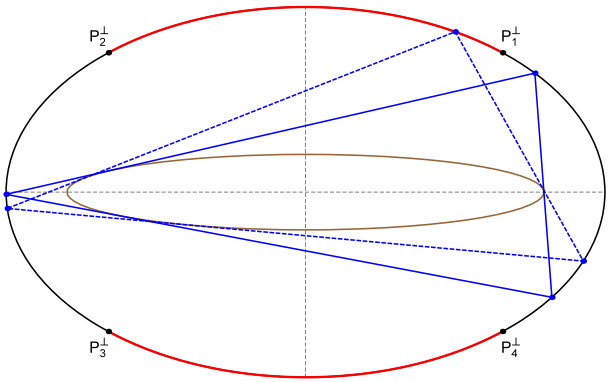

Figure 5.3: Both acute (blue) and obtuse (dashed blue) billiard 3-periodics are shown. In this case $a/b = 1.618 > \alpha_4$. If a 3-periodic vertex is located in the red arcs along the top and bottom halves of the elliptic billiard, the 3-periodic will be obtuse.

where:

$$\begin{aligned} c_1 &= b^4(5\delta^2 - 4(a^2-b^2)\delta - a^2b^2) & c_2 &= a^4(5\delta^2 + 4(a^2-b^2)\delta - a^2b^2) \\ c_3 &= 2a^2b^2(a^2b^2 + 3\delta^2) & c_4 &= a^2b^4(3b^4 + 2(2a^2-b^2)\delta - 5\delta^2) \\ c_5 &= a^4b^2(3a^4 + 2(2b^2-a^2)\delta - 5\delta^2) & \delta &= \sqrt{a^4 - a^2b^2 + b^4} \end{aligned}$$

Proof. Using a CAS, obtain symbolic expressions for the coefficients of a quartic symmetric about both axes (no odd-degree terms), passing through 5 known-points. Still using a CAS, verify the symbolic parametric for the locus satisfies the quartic. □

Note the above is also satisfied by a degenerate level curve $(x, y) = (0, 0)$, which we ignore.

Remark 5.1. *We term the "best-fit" ellipse $\mathcal{E}_6$ the one internally-tangent to $\mathcal{X}_6(x, y) = 0$ at its four vertices. Its semiaxes are given by:*

$$a_6 = \frac{\left[(3\,a^2 - b^2)\delta - (a^2 + b^2)b^2\right]a}{a^2b^2 + 3\delta^2}, \quad b_6 = \frac{\left[(a^2 - 3\,b^2)\delta + (a^2 + b^2)a^2\right]b}{a^2b^2 + 3\delta^2}$$

Table 5.1 shows the above coefficients numerically for a few values of a/b.

a/b	a_6	b_6	c_1/c_3	c_2/c_3	c_4/c_3	c_5/c_3	$A(\mathcal{E}_6)/A(\mathcal{X}_6)$
1.25	0.433	0.282	0.211	1.185	−0.040	−0.095	0.9999
1.50	0.874	0.427	0.114	2.184	−0.087	−0.399	0.9998
2.00	1.612	0.549	0.052	4.850	−0.134	−1.461	0.9983
3.00	2.791	0.620	0.020	12.423	−0.157	−4.769	0.9949

Table 5.1: Coefficients c_i/c_3, $i = 1, 2, 4, 5$ for the quartic locus of X_6 as well as the axes a_6, b_6 for the best-fit ellipse, for various values of a/b. The last-column reports the area ratio of the internal ellipse $\mathcal{E}_6$ (with axes a_6, b_6) to that of the quartic locus $\mathcal{X}_6$, showing an almost exact match.

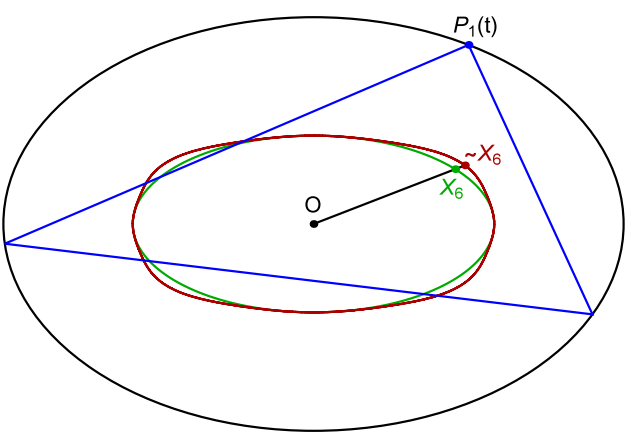

Figure 5.4: Over billiard 3-periodics (blue), the locus of the symmedian point X_6 is a quartic (green). At the billiard aspect ratio shown, it is visually identical to an ellipse. Also shown is a copy of the quartic (red) such that the distance to a best-fit ellipse (green) is scaled 1000 fold. Live

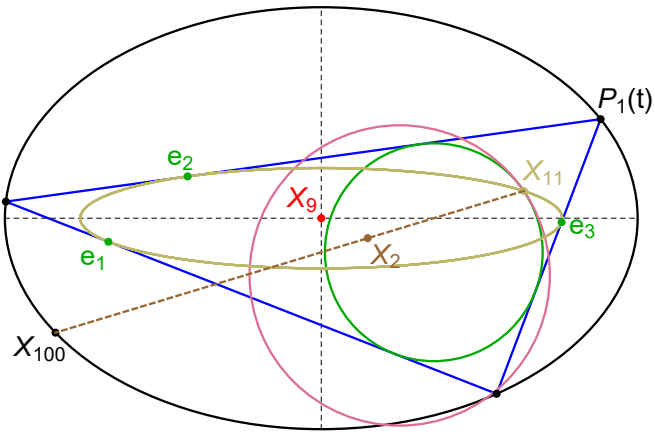

Figure 5.5: A billiard 3-periodic (blue). Also shown are the incircle (green) and 9-point circle (pink) which touch at the Feuerbach point X_{11}. Also shown is the latter's *anticomplement* X_{100}, and the three extouchpoints e_1, e_2, e_3. Over the billiard family, X_{100} sweep the billiard while both X_{11} and the extouchpoints sweep the caustic (though in opposite directions). Video, Live

5.4 The locus of the Feuerbach point and its anticomplement

Referring to Figure 5.5, the Feuerbach point X_{11} is the single point of contact between the incircle and the 9-point circle, see Weisstein (2019, X(11)). X_{11} is known to lie on the X_9-centered inconic, called the Mandart inellipse, see Weisstein (ibid., Mandart inellipse). Since the latter is unique:

Observation 5.1. *The confocal caustic is the stationary Mandart inellipse of billiard 3-periodics.*

Therefore:

Proposition 5.4. *Over billiard 3-periodics, X_{11} sweeps the confocal caustic.*

The anticomplement of a point P is its double-length reflection about the barycenter X_2, i.e., $A(P) = X_2 + 2X_2 - P$. Still referring, Figure 5.17, X_{100} is the anticomplement of X_{11}. This point is known to lie on (i) the circumcircle, (ii) the Steiner circumellipse (centered on X_2), and most relevantly here, (iii) on

the X_9-centered circumellipse, see Kimberling (2019, X(9)). Since the latter is unique:

Observation 5.2. *The elliptic billiard is the stationary X_9-centered circumconic of billiard 3-periodics.*

Therefore (proof is left as Exercise 5.8):

Proposition 5.5. *Over billiard 3-periodics, the locus of X_{100} is the elliptic billiard. It sweeps it in the direction opposite to that of the 3-periodic vertices along the billiard.*

The vertices of the so-called *extouch triangle* are the points of contact of the excircles with a triangle's sidelines, see Weisstein (2019, Extouch triangle). These are also known as *extouchpoints*. A known fact is that the Mandart inellipse (i.e., the caustic) touches a triangle's sidelines at the extouchpoints, see Weisstein (ibid., Mandart inellipse). Therefore:

Proposition 5.6. *Over billiard 3-periodics, the locus of the extouchpoints is the confocal caustic.*

This is also illustrated in Figure 5.17. A curious dynamic phenomenon is that while the extouchpoints follow the direction of motion of billiard 3-periodics along the outer ellipse (e.g., counter- or clockwise), X_{11} rotates in the opposite direction; see this Live.

5.5 A locus with singularities

Loci considered thus far have been smooth, regular curves. Here we give an example of one with four corners. Recall that given a triangle T, the orthic triangle has vertices at the feet of T's altitudes.

Referring to Figure 5.6, it is easy to see that if a triangle T is acute (resp. obtuse), all three vertices (only one vertex) of the orthic will lie on a sideline. In the obtuse case, the other two will lie on extensions of two sidelines, i.e., they will be exterior to T.

An interesting result is the "switching" behavior of the incenter of the orthic triangle, mentioned in Coxeter and Greitzer (1967, Chapter 1):

Lemma 5.1. *If a triangle is acute (resp. obtuse), the incenter of the orthic will coincide with the orthocenter (resp. the obtuse vertex of T).*

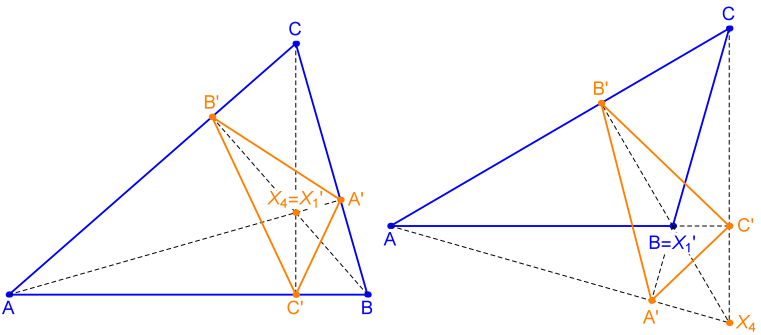

Figure 5.6: **Left**: the orthic triangle (orange) is shown of an acute reference triangle T (blue), for with an interior orthocenter X_4. In this case, the orthic incenter X_1' coincides with X_4. **Right**: When T (blue) is obtuse, X_4 is exterior. Furthermore, two orthic vertices are outside of T and X_1' coincides with the obtuse vertex, B in the picture. Video

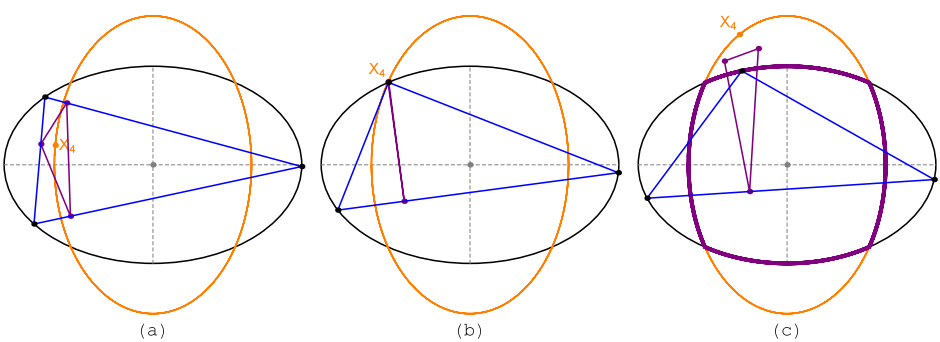

Figure 5.7: From left to right: the orthic triangle (purple) of billiard 3-periodics (blue) is shown at 3 different positions. The locus of X_4 (orange ellipse) intersects the billiard, i.e., $a/b > \alpha_4$. When a 3-periodic is acute (left), the orthic incenter coincides with X_4. When it is a right triangle (middle), X_4 is on the elliptic billiard and the orthic is a degenerate segment. When it is obtuse (right), the orthic incenter remains "pinned" to the obtuse vertex. The end result is that the locus of the orthic incenter is a quadrilateral with four elliptic arcs (thick purple, right) with four corners. Video, Live

Recall that for billiard 3-periodics to include obtuse triangles, $a/b > \alpha_4$; see Proposition 5.1. Referring to Figure 5.7:

Corollary 5.1. *If $a/b > \alpha_4$, the locus of the incenter of the orthic triangle of billiard 3-periodics is an elliptic arc "quadrilateral" with four corners.*

5.6 A self-intersecting locus

Consider the curious case of a triangle center which is the isogonal conjugate of the Feuerbach point, listed on Kimberling (2019) as X_{59}. We revisit its intriguing locus.

As shown in Figure 5.8, this is a continuous curve with four self-intersections, internally tangent to the elliptic billiard on its four vertices independently of a/b. Since it intersects a line parallel to and infinitesimally away from either axis at six points, its degree must be at least 6.

We propose leave it as a research question (below) the derivation of this locus (as an implicit and/or parametric equation) and of its critical points.

5.7 A non-compact locus

Given a triangle T, Weisstein (2019, Tangential triangle) defines the *tangential triangle* T' as having sides tangent to the circumcircle at the vertices. Notice T' is unbounded for a right triangle since the hypotenuse is a diameter of the circumcircle. Consider a smooth deformation of an acute triangle to an obtuse one: one of the vertices of the tangential triangle will undergo a discontinuous jump. Recall that the family of billiard 3-periodics with $a/b > \alpha_4$ (resp. $a/b < \alpha_4$) contains both acute and obtuse (resp. only acute) triangles. Therefore the family of T' will (will not) undergo discontinuous jumps, and the locus of triangle centers thereof will be non-compact (resp. compact).

As an example, consider the locus of the circumcenter of the tangential triangle, listed as X_{26} on Kimberling (2019). It can be shown it is non-elliptic. As shown in Figure 5.9, it is non-compact (resp. compact) when $a/b > \alpha_4$ (resp. $a/b < \alpha_4$). In the former case, the locus is compactified by an inversion with respect to the center.

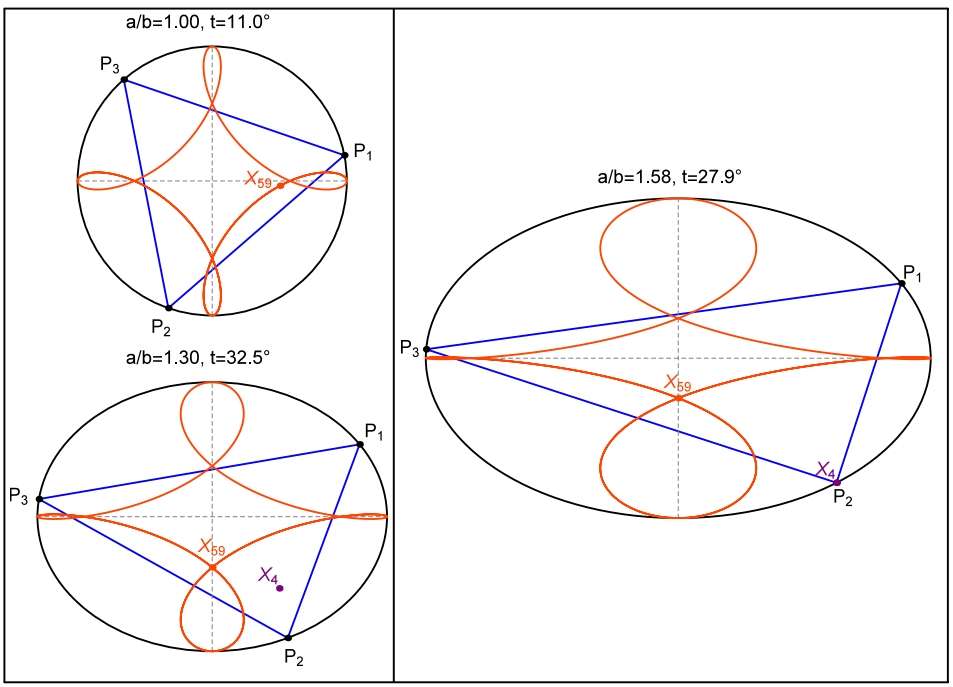

Figure 5.8: Over billiard 3-periodics, the locus of X_{59} is a continuous curve with four self-intersections, tangent to the billiard at its four vertices. **Top Left**: if a/b is slightly above 1, the locus of X_{59} is nearly four-fold symmetric. Not shown: if $a/b = 1$, X_{59} will be on the line at infinity. **Bottom Left**: An acute 3 periodic $a/b < \alpha_4$, and an acute 3-periodic. **Right**: a right-angle 3-periodic in an $a/b > \alpha_4$ elliptic billiard. Video, Live

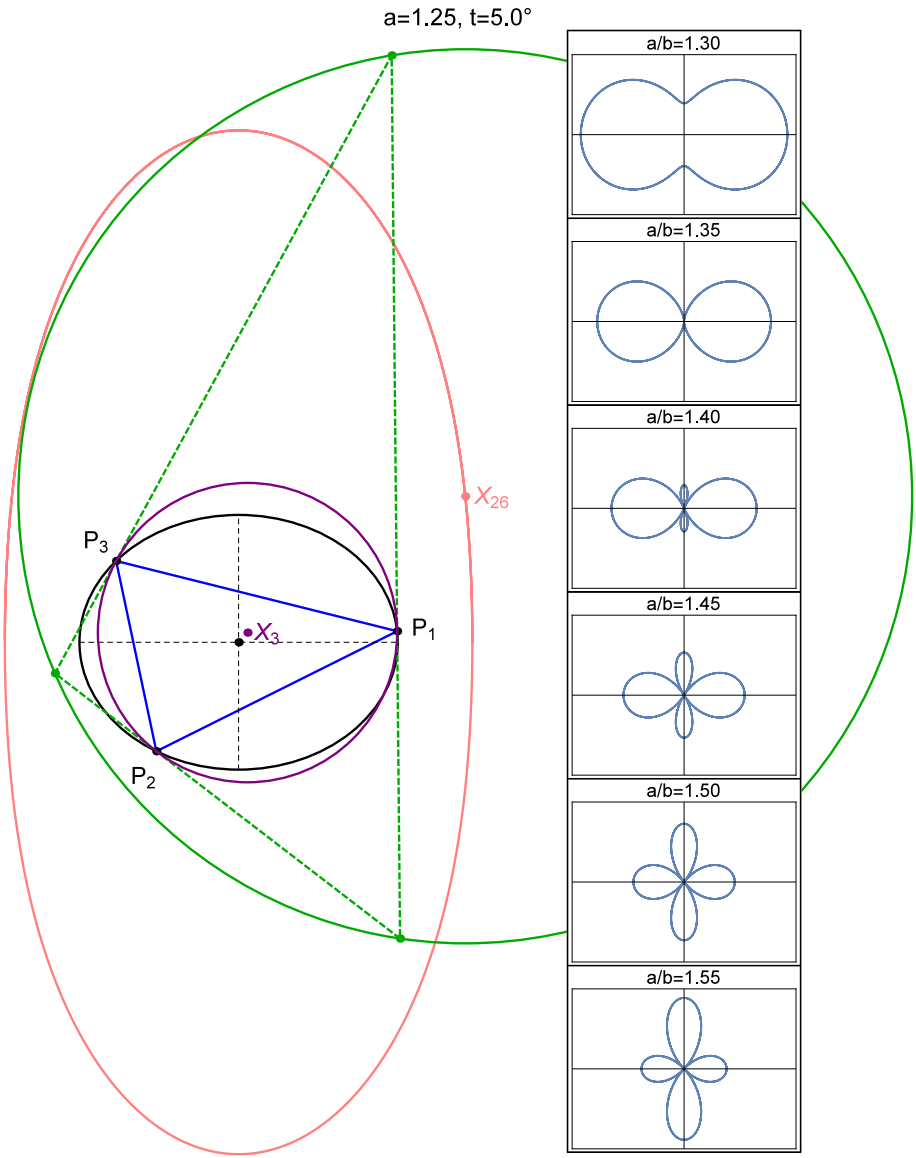

Figure 5.9: **Left:** The tangential triangle (dashed green) is shown for a 3-periodic in an $a/b < \alpha_4$ elliptic billiard. The center of the tangential circumcircle (green) is X_{26}. In this case all 3-periodics are acute, and the locus of X_{26} is compact (and non-elliptic). **Right inset:** the image of the (non-compact) locus of X_{26} under an inversion with respect to a circle concentric with the billiard, for various values

5.8 A golden locus

The circumcenter of the excentral Triangle is known as the *Bevan point* X_{40}, see the corresponding entry on Kimberling (2019). The following was shown in Garcia, Reznik, and Koiller (2020a):

Proposition 5.7. *Over billiard 3-periodics, the locus of X_{40} is an ellipse similar to a rotated copy of the elliptic billiard. Its semiaxes are given by*

$$a_{40} = c^2/a, \quad b_{40} = c^2/b.$$

Corollary 5.2. *At $a/b = \sqrt{2}$, the top and bottom vertices of the locus of X_{40} touches the top and bottom vertices of the elliptic billiard. .*

Referring to Figure 5.10, the following is a harmonious fact associated with the locus of X_{40}:

Corollary 5.3. *At $a/b = (1+\sqrt{5})/2 = \varphi$, the Golden Ratio, the locus of X_{40} is identical to a $90°$-rotated copy of the elliptic billiard.*

5.9 When the billiard is swept non-monotonically

In Proposition 5.5, we saw that X_{100} sweeps the elliptic billiard in the direction opposite to the motion of billiard 3-periodic vertices.

The next triangle center on Kimberling (2019) which is on the X_9-centered circumconic is X_{88}, known to be collinear with X_1 and X_{100}. Assume a monotonic traversal of billiard 3-periodic vertices along the billiard. It turns out at a certain aspect ratio, the "motion" of X_{88} can be made to stop.

Proposition 5.8. *At $a/b = \alpha_{88}$, the y velocity of X_{88} vanishes when the 3-periodic is a sideways isosceles, where*

$$\alpha_{88} = (\sqrt{6+2\sqrt{2}})/2 \simeq 1.485$$

Proof. Parametrize a 3-periodic vertex $P_1(t) = [a\cos t, b\sin t]$. At $t = 0$, $P_1 = (a, 0)$ it can be easily checked that $X_{88} = (-a, 0)$. Solve $y'_{88}(t)|_{t=0} = 0$ for a/b. After some algebraic manipulation, this equivalent to solving $4x^4 - 12x^2 + 7 = 0$, whose positive roots are $(\sqrt{6 \pm 2\sqrt{2}})/2$. α_{88} is the largest of the two. □

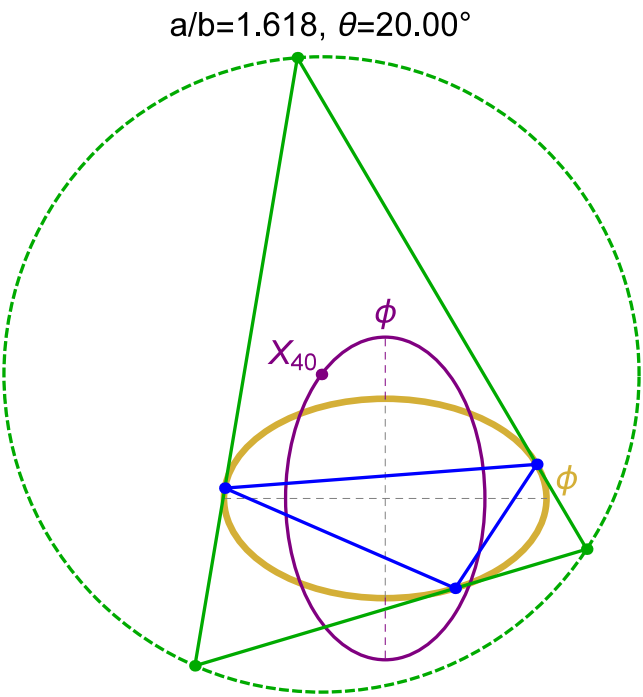

Figure 5.10: A 3-periodic (blue) is shown within an $a/b = \varphi$ elliptic billiard (gold) as well as its excentral triangle (green). At this aspect ratio, the locus of the Bevan point X_{40} (purple) is a 90°-rotated copy of the billiard. Recall this point is the circumcenter of the excentral triangle. Video, Live

Indeed, there are three types of X_{88} motion with respect to $P_1(t)$: (i) $a/b < \alpha_{88}$: monotonic and opposite to $P_1(t)$; (ii) $a/b = \alpha_{88}$: monotonic and opposite, but with full stop at the billiard major vertices; (iii) $a/b < \alpha_{88}$: non-monotonic, containing two retrograde phases.

An equivalent statement, illustrated in Figure 5.11, is that the line family X_1X_{100} is instantaneously tangent to its *envelope* at X_{88}. Referring to Figure 5.11:

Proposition 5.9. *Over billiard 3-periodics, the envelope of X_1X_{100} is (i) entirely inside, (ii) touches at vertices of, or (iii) intersects the billiard, for a/b (i) less than, (ii) equal to, or (iii) greater than α_{88}, respectively.*

Interestingly:

Proposition 5.10. *The motion of X_{88} is instantaneously (i) opposite to P_1, (ii) stationary, or (iii) in the direction of P_1, if the tangency E of X_1X_{100} with the envelope lies inside, on, or outside the billiard.*

5.10 The dance of the swans

Several triangle centers were identified by Peter Moses which lie on the X_9-centered circumconic of any triangle. These are listed on Kimberling (2019, X(9)) as follows: X_k, k =88, 100, 162, 190, 651, 653, 655, 658, 660, 662, 673, 771, 799, 823, 897, 1156, 1492, 1821, 2349, 2580, 2581, 3257, 4598, 4599, 4604, 4606, 4607, 8052, 20332, 23707, 24624, 27834, 32680.

In Reznik, Garcia, and Koiller (2020b) we called such centers *swans*, since over billiard 3-periodics they will elegantly glide along the margins of an elliptic "pond". The first four centers on said list are X_k, k =88, 100, 162, and 190, and are shown in Figure 5.12.

Above we saw that the motion of X_{100} is "monotonic" whereas that with $a/b > \alpha_{88}$ that of X_{88} isn't. The next two swans on Kimberling (2019) are X_{162} and X_{190}.

Proposition 5.11. *The motion of X_{162} with respect to $P_1(t)$ is non-monotonic if $a/b > \alpha_{162}$ where $\alpha_{162} \simeq 1.1639$ is the only positive root of:*

$$5x^8 + 3x^6 - 32x^4 + 52x^2 - 36$$

Proof. The trilinear coordinates of X_{162} are given by

$$\frac{1}{\left(s_2^2 - s_3^2\right)\left(s_2^2 + s_3^2 - s_1^2\right)} : \frac{1}{\left(s_3^2 - s_1^2\right)\left(s_3^2 + s_1^2 - s_2^2\right)} : \frac{1}{\left(s_1^2 - s_2^2\right)\left(s_1^2 + s_3^2 - s_3^2\right)}.$$

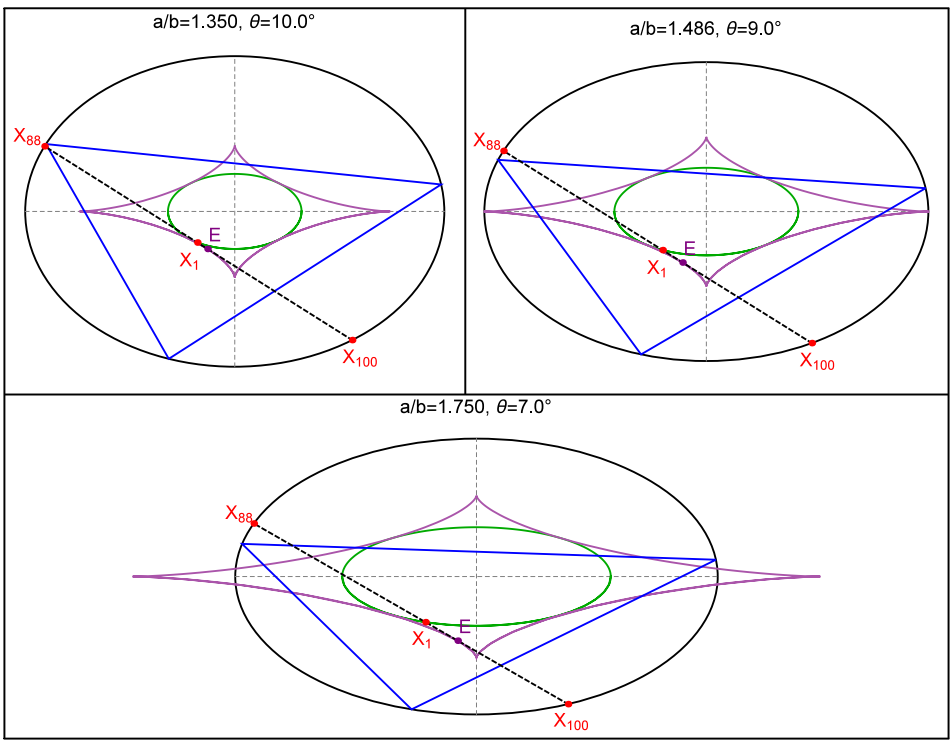

Figure 5.11: Collinear points X_1, X_{100}, X_{88} shown in an elliptic billiard with a/b (i) less than (top-left), (ii) equal to (top-right), or (iii) greater than (bottom), $\alpha_{88} \simeq 1.486$. The motion of X_{88} relative to 3-periodic vertices will be: (i) monotonic and opposite to the vertices, (ii) monotonic and opposite but will full stops at the vertices, and (iii) non-monotonic. The envelope (purple) of line X_1X_{100} intersects the billiard if $a/b > \alpha_{88}$ (bottom). The motion of X_{88} is instantaneously (i) opposite to P_1, (ii) stationary, or (iii) in the direction of P_1, if the tangency E of X_1X_{100} with the envelope lies inside, on, or outside the billiard. Video, Live

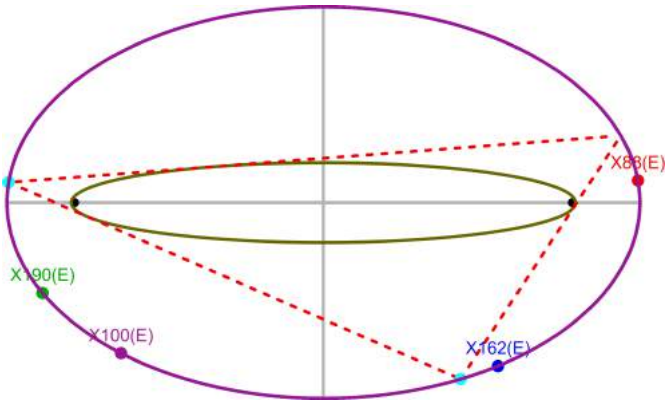

Figure 5.12: A billiard 3-periodic (blue) and the swans X_k, k =88, 100, 162, and 190. Live. This Video shows 29 swans from Moses' list on Kimberling (2019, X(9)).

We use the standard parametrization for vertices of the confocal family found in Section 2.7.1. Using the trilinear coordinates above, we have

$$X_{162}(t) = (x_{126}(t), y_{126}(t))$$

At $t = \frac{\pi}{2}$, $P_1 = (0, b)$ and $X_{162}(\frac{\pi}{2}) = (0, b)$.

Solve $x'_{162}(t)|_{t=\frac{\pi}{2}} = 0$ for a/b. After some long algebraic symbolic manipulation, this is equivalent to solving $5x^8 + 3x^6 - 32x^4 + 52x^2 - 36 = 0$, whose positive roots is $\alpha_{162} \simeq 1.16369$. □

Since $\alpha_{88} > \alpha_{162}$, setting $a/b > \alpha_{88}$ implies both centers will move non-monotonically. Curiously:

Proposition 5.12. *With $a/b > 1$, X_{88} and X_{162} never coincide. Therefore over the billiard 3-periodic family, they never cross each other.*

Proof. Consider an elementary triangle $P_1 = (-1, 0)$, $P_2 = (1, 0)$ and $P_3 = (u, v)$. Obtain cartesian coordinates for X_{88} and X_{162} using their trilinears. The equation $X_{88} = X_{162}$ is given by two algebraic equations $F(u, v, s_1, s_2) = G(u, v, s_1, s_2) = 0$ of degree 17 with $s_1 = \sqrt{(u-1)^2 + v^2} = | P_3 - P_2 |$ and $s_2 = \sqrt{(u+1)^2 + v^2} = | P_2 - P_1 |$. Particular solutions of these equations

are equilateral triangles with $P_3 = (0, \pm\sqrt{3})$ in which case X_{88} and X_{162} go to infinity, i.e., these centers can never meet with $a/b > 1$. □

In Figure 5.13, X_{88} and X_{162} are imagined as "swans" executing an elegant, choreographing a never-crossing dance along the margins of an elliptic "pond".

The joint motion of $P_1(t)$, X_{88}, and X_{162} can also be visualized on the surface of a torus where the meridians (circles around the smaller radius) correspond to a given t and the parallels represent a fixed location on the billiard boundary. As shown in Figure 5.14, the curves for X_{88} and X_{162} are thrice-winding, though never intersecting.

Referring to Figure 5.15, we summarize the monotonicity in the motion of the first four swans on Kimberling (2019) with respect to a vertex of billiard 3-periodics as follows:

Proposition 5.13. *Over the family of billiard 3-periodics, for any $a/b > 1$, the motion of X_{100} and X_{190} is monotonic and opposite with respect to that of a vertex in the family.*

Proposition 5.14. *Over the family of billiard 3-periodics, if a/b is below (resp. above) a certain $\alpha_{162} > 1$ (resp. $\alpha_{88} > \alpha_{162}$), the motion of X_{162} (resp. X_{88}) is monotonic and opposite (resp. non-monotonic) with respect to that of a vertex in the family.*

5.11 Locus of vertices of derived triangles

Some triangles derived from billiard 3-periodics are shown in Figure 5.16. For their constructions see Appendix A and Weisstein (2019).

Mentioned in Chapter 1 was an early experiment which showed that over billiard 3-periodics, the locus of the vertices of the intouch triangle (i.e., the intouch-points) is a 2-lobed, self-intersect curve; see Figure 1.4.

As shown in Figure 5.17, the loci of vertices of some other triangles derived from billiard 3-periodics aren't ellipses. A noteworthy exception is the extouch triangle, mentioned above.

5.12 Locus triple winding

Consider one turn of vertex $P_1(t)$ of billiard 3-periodics around the billiard. Given 3-periodic triple periodicity, over said motion a triangle center will sweep its locus

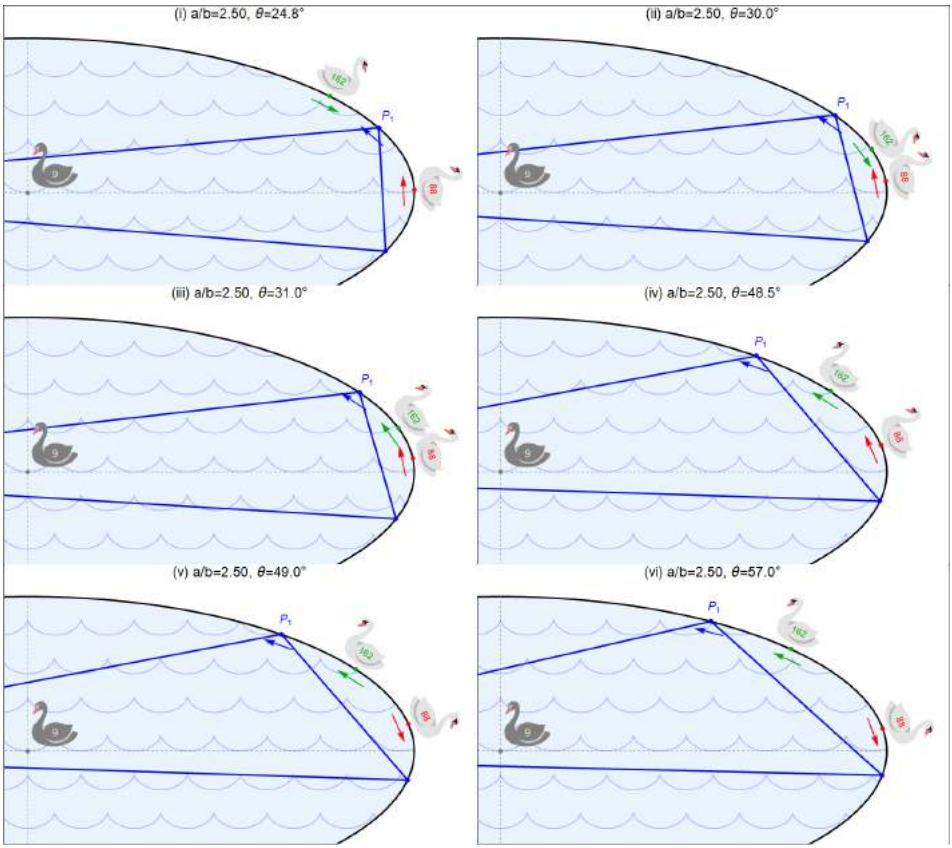

Figure 5.13: The dance of swans X_{88} and X_{162} along the margins of an elliptic pond. (i) while P_1 moves CCW, X_{88} and X_{162} approach each other; (ii) at their closest, they almost kiss. (iii) Suddenly, X_{162} reverses course, (iv) and a short-lived same-direction pursuit ensues. (v) An unswooned X_{88} also changes course, (vi) with now both swimming away from each other. The duo meets again on 2nd, 3rd and 4th quadrants, where the dance steps are played back in alternating forward and backward order. A black mittenswan guards his clutch at the center of the lake. Video, two Live swans, four Live swans.

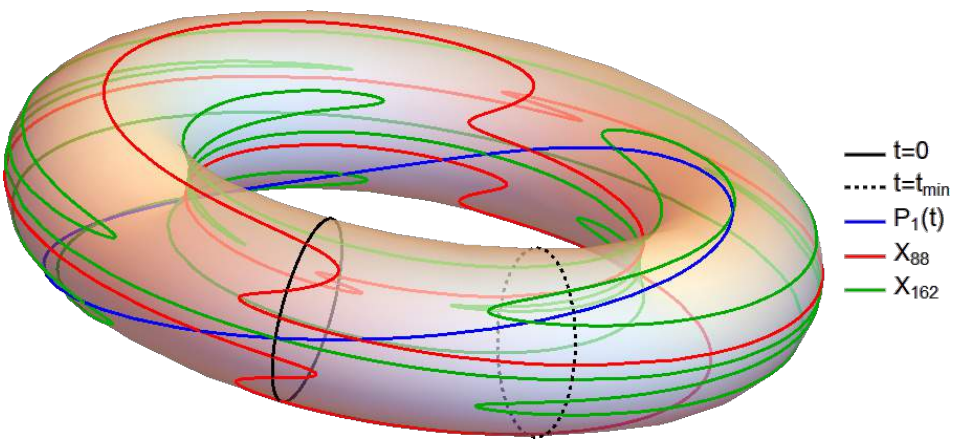

Figure 5.14: The coordinated motion of $P_1(t)$ (blue), X_{88} (red) and X_{162} (green) on the surface of a translucent torus, whose (i) meridians represent position along the elliptic billiard, and (ii) parallels the family parameter t. Notice the green and red curves are non-monotonic around the torus but never cross each other. A solid black meridian is wound at $t = 0$ and a dashed one appears at one of the 12 instants of closest distance between X_{88} and X_{162}, see Question 5.5.

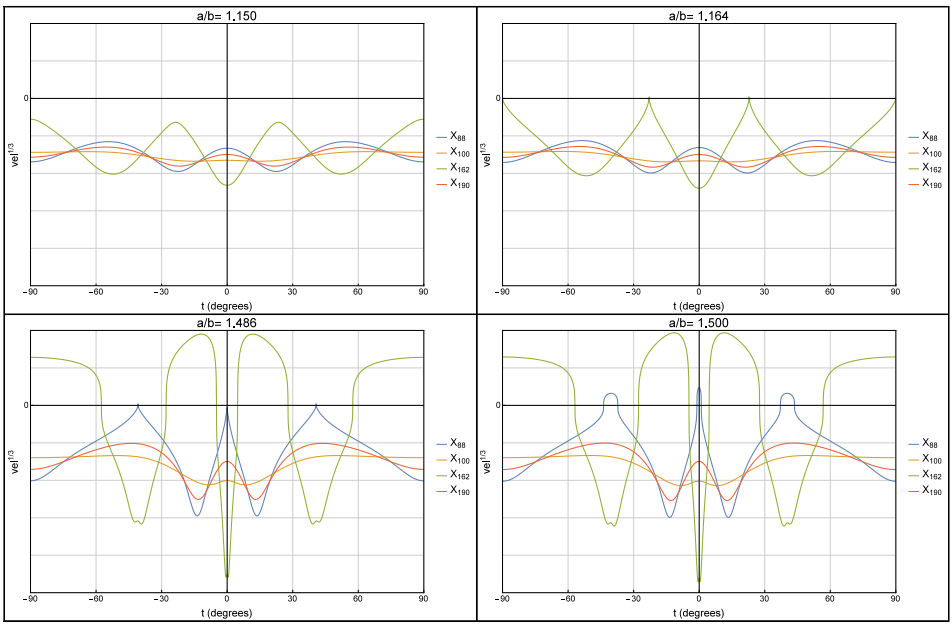

Figure 5.15: Signed angular velocities of swans X_k, k =88,100,162,190 vs the parameter t of $P_1(t) = [a\cos(t), b\sin(t)]$ of a billiard 3-periodic vertex, for various values of a/b. Cubic roots of the velocities are shown for better visualization near zero. **Top left:** $a/b = 1.15$ is sufficiently small such that all centers move with variable, negative velocity (monotonic). **Top right:** At $a/b = \alpha_{162} \geqslant 1.164$, the motion of X_{162} comes to a stop at discrete values of t. **Bottom left:** At $a/b = \alpha_{88} \geqslant 1.486$, it is X_{88}'s turn to touch zero velocity at discrete moments. **Bottom right:** at $a/b = 1.5 > \alpha_{88} > \alpha_{162}$, both X_{162} and X_{88} are engaged in non-monotonic motion. Notice X_{100} and X_{190} remain monotonic (negative velocity).

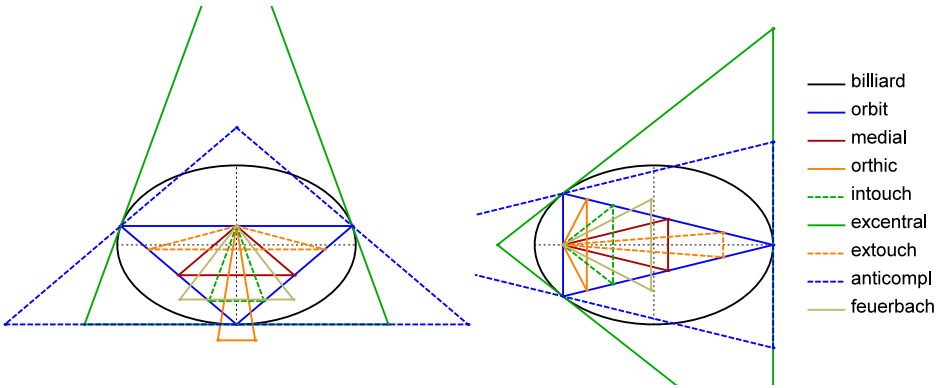

Figure 5.16: Triangles derived from an isosceles billiard 3-periodic (blue). These contain one vertex on the axis of symmetry. Video, Live

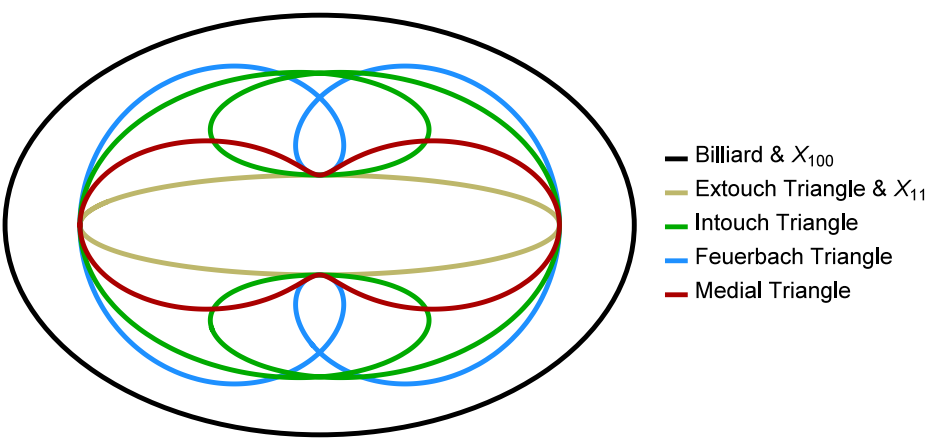

Figure 5.17: Non-elliptic loci of the vertices of triangles derived from billiard 3-periodics: the (i) intouch (green), (ii) Feuerbach (not to be confused with the Feuerbach *point*) (blue), (iii) medial (red), triangles. A noteworthy excpetion is the extouch triangle (light brown), whose vertices sweep the confocal caustic. Video, Live

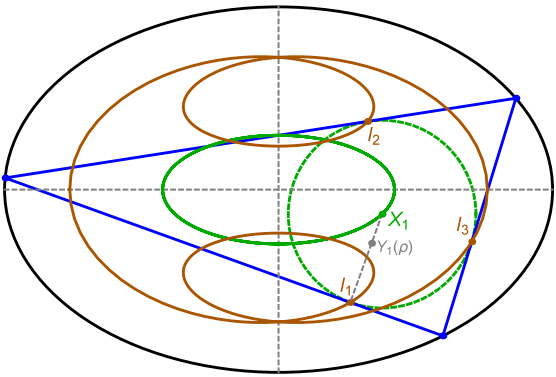

Figure 5.18: Depicted is the convex combination $Y_1(\rho)$ of the incenter X_1 and an intouchpoint I_1 of a billiard 3-periodic. app, Video 1, Video 2.

thrice (excluding X_9 which doesn't move).

Referring to Figure 5.18, consider the convex combination $Y_1(t)$ of incenter X_1 and an intouch point $I_1(t)$, namely:

$$Y_1(t) = (1-\rho)X_1(t) + \rho I_1(t)$$

where ρ is a real number.

Loci obtained for Y_1 at different values of ρ are shown in Figure 5.19. At $\rho = 1$ (top-left), $Y_1(t)$ is the recognizable two-lobe locus of the intouchpoints. As ρ decreases, the two lobes approach each other. At some critical ρ they will touch each other at single point. Decreasing ρ further causes the lobes to self-intersect and contain the center of the confocal ellipse pair,. which entails that the turning number about the origin of the locus suddenly jumps from 1 to 3. As ρ approaches zero, the lobes further interpenetrate, and when $\rho = 0$, they collapse to the elliptic locus of the incenter which by continuity, will thrice wind over itself.

5.13 Exercises

Exercise 5.1. *Calculate the elliptic billiard aspect ratio a/b such that top and bottom vertices of the elliptic locus of X_3 coincide each with the billiard top and bottom vertices. Repeat for the locus of X_5.*

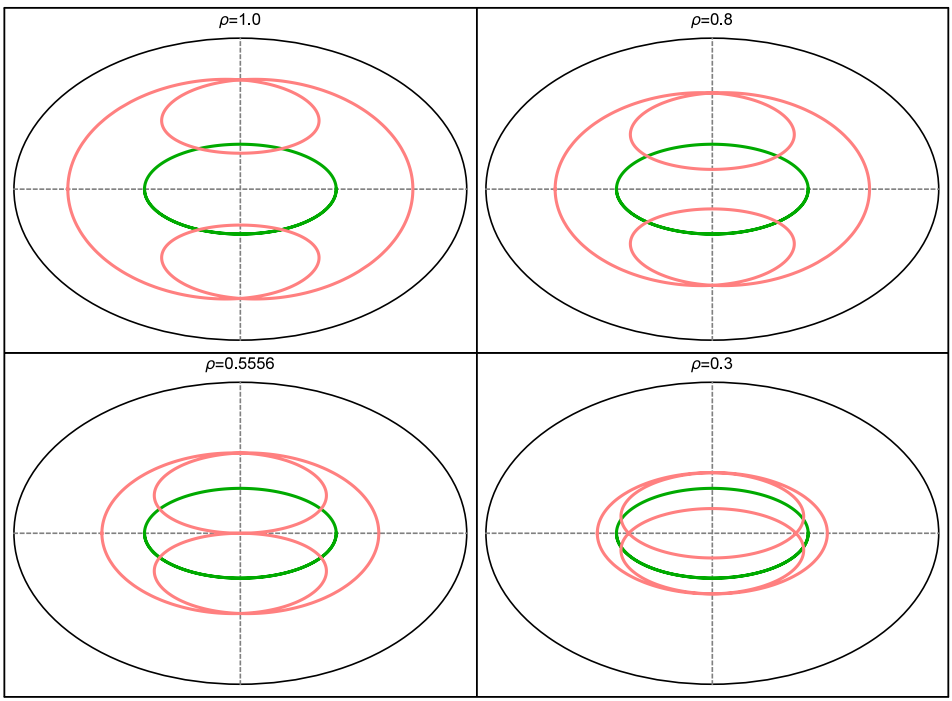

Figure 5.19: The locus (pink) of convex combination Y_1 of the incenter and an intouchpoint at different values of ρ. The elliptic locus of the incenter appears in all four frames (green). When $\rho = 1$ (top left), one obtains the original two-lobed locus of the intouchpoints (pink). As ρ decreases (top right, bottom left), the two lobes approach each other and at some point touch. Decreasing ρ further still causes loves to self-intersect and contain the ellipse pair center. As ρ approaches zero (bottom right), the lobes further interpenetrate and when $\rho = 0$ (not shown), they collapse to the elliptic locus of the incenter (green). Video 1, Video 2

Exercise 5.2. *Calculate the elliptic billiard aspect ration a/b such that the locus of X_4 is identical to a $90°$ rotated copy of billiard.*

Exercise 5.3. *Over billiard 3-periodics, the envelope of the Euler line is an astroidal-like curve with four cusps, see it Live. Derive its equation. Also, find the elliptic billiard aspect ratio a/b such that the top and bottom cusps of said curve coincide each with top and bottom vertices of the elliptic billiard.*

Exercise 5.4. *Referring to Figure 5.6(right), let T_h denote the orthic triangle of an obtuse triangle T. Is there another (acute) triangle T' whose orthic is also T_h?*

Exercise 5.5. *Express in terms of a, b of the elliptic billiard, the coordinates of the endpoints of the obtuse "zones" labeled $P_i^{\perp}$, $i = 1, 2, 3, 4$ in Figure 5.3.*

Exercise 5.6. *Prove Corollaries 5.2 and 5.3.*

Exercise 5.7. *Let A be area of the four-corner region common to an ellipse and its $90°$-rotated copy and $A_{ell} = \pi ab$ be the area of the ellipse. Show that $A/A_{ell} = 4\csc^{-1}\left[\sqrt{1+(a/b)^2}\right]/\pi$. What is this ara ratio for $a/b = \varphi$?*

Exercise 5.8. *Prove that the motion of X_{100} along the elliptic billiard is opposite to that of the vertices of billiard 3-periodics.*

Exercise 5.9. *Assume $a/b > \alpha_{88}$. Find t in $P_1(t) = [a\cos t, b\sin t]$ where the motion of X_{88} changes direction.*

Exercise 5.10. *Prove that X_{88} coincides with a 3-periodic vertex if and only if $s_2 = (s_1 + s_3)/2$. In this case, X_1 is the midpoint between X_{100} and X_{88}*

Exercise 5.11. *Prove Proposition 5.9.*

Exercise 5.12. *Find the unique aspect ratio $a/b > \alpha_4$ of an elliptic billiard which contains right-triangle 3-periodics with sides as 3:4:5. Find aspect ratios for billiards with the next up Pythagorean 3-periodics: 5:12:13, 8:15:17, 7:24:25, 20:21:29.*

Exercise 5.13. *Let T be a billiard 3-periodic, and T' its anticomplementary triangle.Recall its sides contain each of the vertices of T and are parallel to the latter's opposite sides, see Weisstein (2019). Let T'' be the intouch triangle of T'. Show that the vertices of T'' (the intouchpoints) are always on the elliptic billiard. See it Live. Bonus: prove that the motion of the intouchpoints of T'' is non-monotonic assuming $P_1(t) = [a\cos t, b\sin t]$ is monotonic along the billiard.*

Exercise 5.14. *Referring to Figure 5.19, compute the ρ such that the lobes of $Y(t)$ touch.*

5.14 Research questions

Question 5.1. *Concerning the locus of X_{59} over billiard 3-periodics (Figure 5.8, determine:*

- *An implicit and/or parametric equation;*
- *The locations of its four self-intersections;*
- *The a/b such that if X_{59} is on a self-intersections on the elliptic billiard minor axis, the 3-periodic is a right triangle? (it is close to* 1.58*, see Figure 5.8(right).*

Question 5.2. *Prove that over billiard 3-periodics traversed continuously, the vertices of the extouch triangle, i.e., the 3 extouchpoints, will move in the same direction as 3-periodic vertices, whereas the Feuerbach point will move in the opposite direction.*

Question 5.3. *Derive an expression (implicit and/or parametric) for the locus of X_{26} in either the compact or non-compact case.*

Question 5.4. *Derive an expression of the non-elliptic locus of the vertices of the anticomplementary triangle over billiard 3-periodics. Show it is always external to the elliptic billiard. Derive its inflection points. See it Live.*

Question 5.5. *Derive an expression for t where X_{88} and X_{162} are closest (there are 12 solutions). In Figure 5.14, the dashed meridian represents one such minimum which for $a/b = 2$ occurs at $t \simeq 41°$. Notice it does not coincide with any critical points of motion.*

Question 5.6. *Show that the locus of the inversion of X_1 with respect to the moving circumcircle of billiard 3-periodics is also an ellipse. See it Live.*

Question 5.7. *Show that the locus of the inversion of X_3 with respect to the moving incircle of billiard 3-periodics is also an ellipse. See it Live.*

Question 5.8. *Prove Proposition 5.13.*

Question 5.9. *Prove Proposition 5.14, and derive α_{162} and α_{88}. Numerically, these are approximately* 1.164 *and* 1.486*, respectively, see Figure 5.15 (top right and bottom left).*

6 Locus Phenomena in other CAP Families

In the previous chapter we toured loci phenomena over billiard 3-periodics. Here we continue this exploration over the five concentric, axis-parallel (CAP) families depicted in Figure 1.5. In Section 6.6, we review and discuss locus phenomena for each such family, organizing them according to similarity in locus curve types (for various triangle centers). Interestingly, the following 3 groups emerge:

- Confocal, incircle, and poristics
- Excentrals, circumcircle, and poristic excentrals
- Homothetic pair and Brocard porism.

For reference, and as we march toward a theory for locus ellipticity (next chapter), at the chapter's end we provide a list of triangle centers which over each of the families studied so far are either stationary, trace out a circle, or an ellipse.

In the discussion below, recall Cayley's condition for a CAP pair to admit a Poncelet 3-periodic family: $a_c/a + b_c/b = 1$, where $a > b > 0$, $a_c > 0$, and $b_c > 0$.

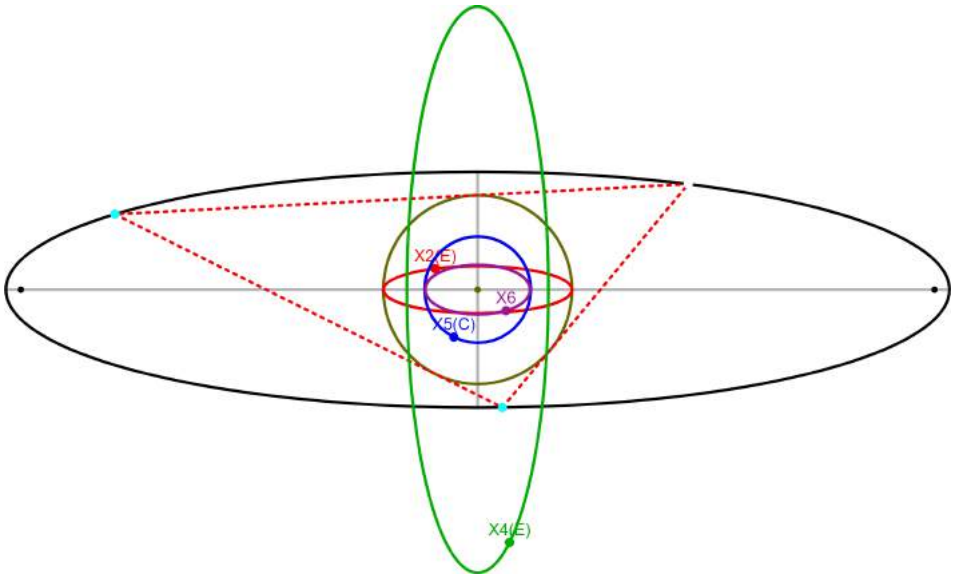

Figure 6.1: Loci of X_k, k =2,4,5,6 over incircle 3-periodics. These are ellipses for all but X_5 whose locus is a circle. Live 1, Live 2

6.1 Incircle family

A 3-periodic interscribed in a CAP pair with incircle is shown in Figure 1.5(top middle).

Recall that for this pair, Cayley implies the inradius $r = \frac{ab}{a+b}$. Also recall that in Proposition 3.4, we show that incircle 3-periodics have invariant circumradius $R = (a + b)/2$ and that the locus of the circumcenter X_3 is a circle of radius $d = (a - b)/2$ centered on X_1, see Figure 3.3.

The next 4 propositions are illustrated in Figure 6.1.

Proposition 6.1. *Over incircle 3-periodics, the locus of the barycenter X_2 is an ellipse with axes $a_2 = a(a-b)/(3a+3b)$ and $b_2 = b(a-b)/(3a+3b)$ centered on $O = X_1$.*

Proof. Follows from Section 3.6. □

Proposition 6.2. *Over incircle 3-periodics, the locus of the orthocenter X_4 is an ellipse of axes $a_4 = (a - b)b/(a + b)$ and $b_4 = (a - b)a/(a + b)$ centered on $O = X_1$.*

Proposition 6.3. *Over incircle 3-periodics, the locus of the center X_5 of the nine-point circle is a circle of radius $d = \frac{(a-b)^2}{4(a+b)}$ centered on $O = X_1$.*

Proof. Direct, analogous to Garcia, Reznik, and Koiller (2020b, Thm.3). □

Proposition 6.4. *Over incircle 3-periodics, the locus of X_6 is a quartic given by the following implicit equation:*

$$\left(b\,(b+2\,a)\left(a^2+2\,ab+3\,b^2\right)x^2+a\,(a+2\,b)\left(3\,a^2+2\,ab+b^2\right)y^2\right)^2 \\ -a^2b^2\,(a-b)^2\left(b^2\,(b+2\,a)^2\,x^2+a^2\,(a+2\,b)^2\,y^2\right)=0$$

6.2 Circumcircle family

This family is inscribed in a circle of radius R centered on $O = X_3$ and circumscribes a concentric ellipse with semiaxes a, b; see Figure 1.5(top right). Recall that the Cayley condition implies $R = a + b$.

Proposition 6.5. *Over circumcircle 3-periodics, the locus of the barycenter X_2 is a concentric circle with radius r_2 given by:*

$$r_2 = \frac{1}{3}(a-b)$$

Referring to Figure 6.2:

Proposition 6.6. *Over circumcircle 3-periodics, the loci of both the orthocenter X_4 and the center X_5 of the 9-point circle are concentric circles centered on X_3, with radii $2d'$ and d' respectively, where $d' = (a-b)/2$.*

Proof. Based on 3-periodic vertex parametrization and CAS-assisted algebraic simplification. □

In Section 2.3 (resp. Section 5.3) we showed that over the confocal family, the locus of X_1 (resp. X_6) is an ellipse (resp. quartic). Interestingly:

Proposition 6.7. *Over circumcircle 3-periodics, the locus of the symmedian point X_6 (resp. the incenter X_1) is an ellipse (resp. the convex component of a quartic*

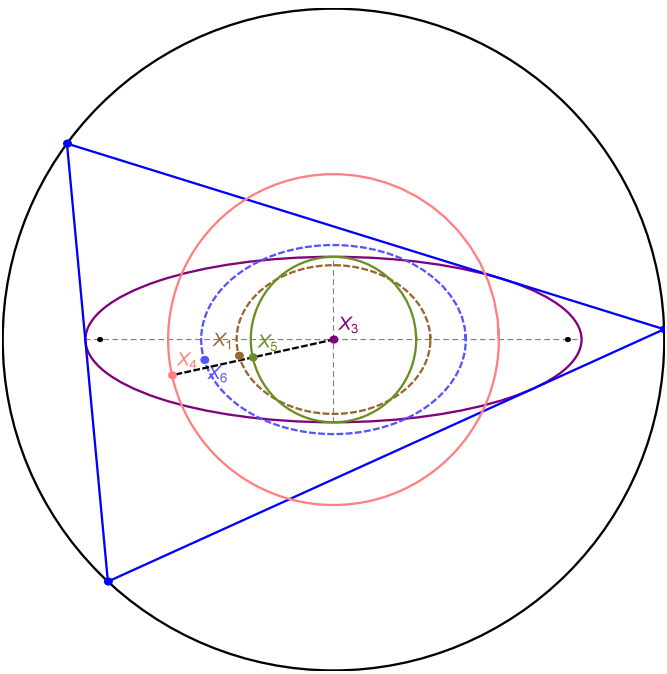

Figure 6.2: A circumcircle 3-periodic: The loci of both orthocenter X_4 (pink) and nine-point center X_5 (olive green) are concentric with the external circle (black). Their radii are $2d'$ and d', respectively where $d' = |X_4 - X_5|$. In contradistinction to the elliptic billiard, the locus of the incenter X_1 (dashed brown) is non-elliptic while that of the symmedian point X_6 (dashed blue) is an ellipse. Video, Live

– note the other component corresponds to the locus of the 3 excenters which can be concave). These are given by:

$$\text{locus of } X_6: \frac{x^2}{a_6^2}+\frac{y^2}{b_6^2}=1,\ a_6=\frac{a^2-b^2}{a+2b},\ \ b_6=\frac{a^2-b^2}{2a+b},$$
$$\text{locus of } X_1: \left(x^2+y^2\right)^2-2\,(a+3\,b)\,(a+b)\,x^2-2\,(a+b)\,(3\,a+b)\,y^2 + \left(a^2-b^2\right)^2=0.$$

Proof. CAS-assisted simplification. □

6.3 Homothetic family

The family of 3-periodics interscribed in a pair of homothetic ellipses is depicted in Figure 1.5(bottom left). Let a, b be the semiaxes of the outer ellipse. The Cayley condition for this pair implies that $a_c = a/2$ and $b_c = b/2$, see Proposition 3.11.

Recall the barycenter X_2 is stationary at the common center and the area $A = (3ab\sqrt{3})/4$ is invariant.

Recall that over the confocal family, the locus of the incenter X_1 (resp. symmedian point X_6) was an ellipse (resp. a quartic). Referring to Figure 6.3, this is reversed in the homothetic family:

Proposition 6.8. *Over homothetic 3-periodics, the locus of the incenter X_1 (resp. symmedian point X_6) is a quartic (resp. an ellipse). These are given by:*

$$\text{locus of } X_1: 16\left(a^2y^2+b^2x^2\right)\left(a^2x^2+b^2y^2\right)-8\,b^2\left(a^4+5\,a^2b^2+2\,b^4\right)x^2 - 8\,a^2\left(2\,a^4+5\,a^2b^2+b^4\right)y^2+a^2b^2\left(a^2-b^2\right)^2=0,$$
$$\text{locus of } X_6: \frac{x^2}{a_6^2}+\frac{y^2}{b_6^2}=1,\ a_6=\frac{a(a^2-b^2)}{2(a^2+b^2)},\quad b_6=\frac{b(a^2-b^2)}{2(a^2+b^2)}.$$

Proof. CAS-assisted simplification. □

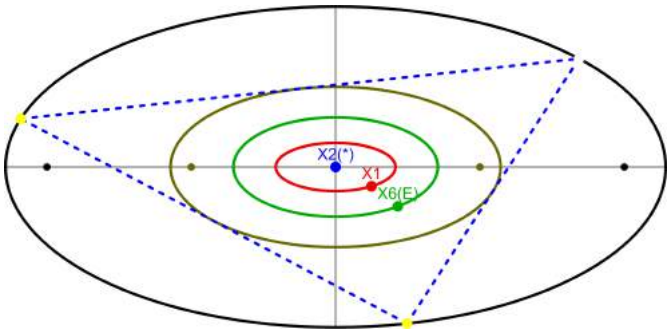

Figure 6.3: A homothetic 3-periodic and the quartic (resp. elliptic) locus of the incenter X_1 (resp. symmedian point X_6). Live

6.3.1 Four circular loci

The two Fermat points X_{13} and X_{14} as well as the two isodynamic points X_{15} and X_{16} have trilinear coordinates which are irrational on the sidelengths of a triangle, see Kimberling (2019). Indeed, over billiard 3-periodics, their loci are non-elliptic.

Referring to Figure 6.4:

Proposition 6.9. *Over homothetic 3-periodics, the loci of X_k, k =13,14,15,16 are four distinct circles. Their radii are $(a-b)/2$, $(a+b)/2$, $(a-b)^2/z$, and $(a+b)^2/z$, respectively, where $z = 2(a+b)$.*

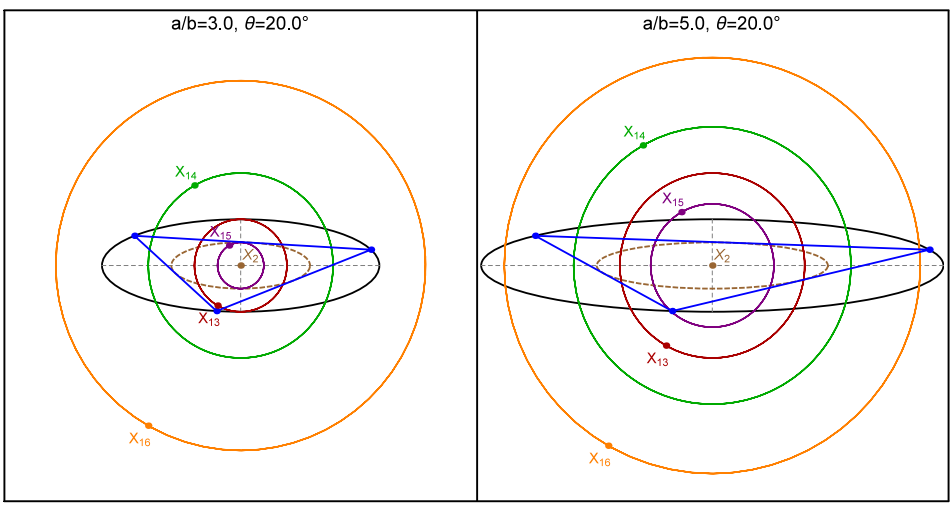

Figure 6.4: Circular loci of the first and second Fermat points X_{13} and X_{14} (red and green) as well as the first and second isodynamic points X_{15} and X_{16} (purple and orange) for two aspect ratios of the homothetic pair: $a/b = 3$ (left) and $a/b = 5$ (right). The radius of the X_{16} locus is minimal at the first case. Video, Live

6.3.2 Loci of the Brocard points

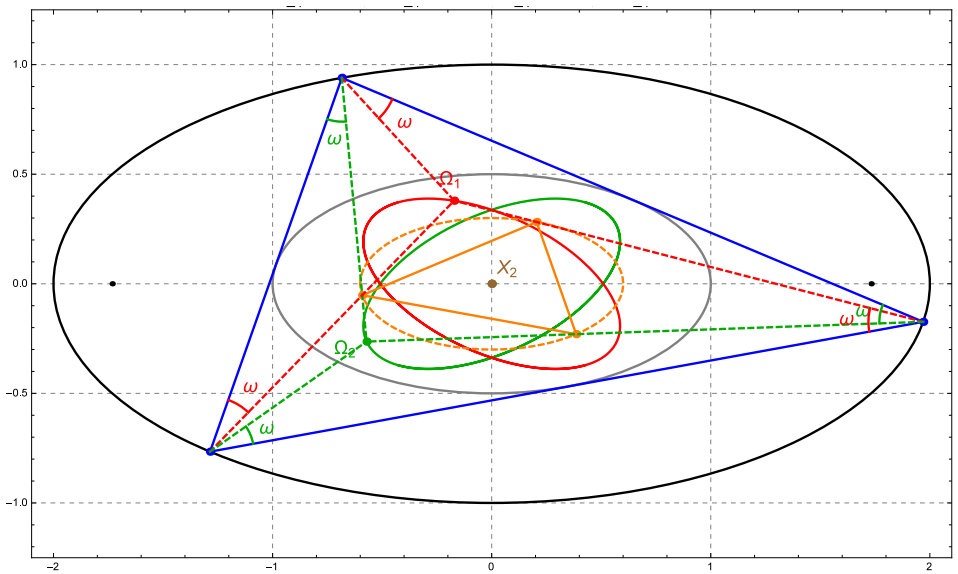

Figure 6.5: Over homothetic 3-periodics, the loci of the two Brocard points Ω_1 and Ω_2 are tilted ellipses (red and green) of aspect ratio equal to those in the pair, see Video. Also shown (dashed orange) is the locus of the vertices of the first Brocard triangle (orange): this is an axis-aligned ellipse also homothetic to the pair.Video, Live

Referring to Figure 6.5:

Proposition 6.10. *Over homothetic 3-periodics, the loci of the Brocard points Ω_1 and Ω_2 are ellipses $\mathcal{E}_1$ and $\mathcal{E}_2$ which modulo rotation are homothetic to the ellipses in the pair. The loci are reflected images of each other about either the x or y axis.*

Proof. The loci are given by

$$\mathcal{E}_1 = \frac{\left(7\,a^4+6\,a^2b^2+3\,b^4\right)x^2}{a^2\left(a^2-b^2\right)^2}+\frac{\left(3\,a^4+6\,a^2b^2+7\,b^4\right)y^2}{b^2\left(a^2-b^2\right)^2}-\frac{4\sqrt{3}\left(a^2+b^2\right)xy}{ab\left(a^2-b^2\right)}-1$$

$$\mathcal{E}_2 = \frac{\left(7\,a^4+6\,a^2b^2+3\,b^4\right)x^2}{a^2\left(a^2-b^2\right)^2}+\frac{\left(3\,a^4+6\,a^2b^2+7\,b^4\right)y^2}{b^2\left(a^2-b^2\right)^2}+\frac{4\sqrt{3}\left(a^2+b^2\right)xy}{ab\left(a^2-b^2\right)}-1$$

The angle θ between the axes of ellipses $\mathcal{E}_1$ and $\mathcal{E}_2$ is given by

$$\tan\theta = \frac{4\sqrt{3}(a^2+b^2)ab}{3a^4+2a^2b^2+3b^4}.$$

□

In no other CAP family so far studied, is the locus of either Brocard point an ellipse. This informs:

Conjecture 1. *Over 3-periodics in a CAP family, the locus of the Brocard points is an ellipse if and only if the ellipses are homothetic.*

In Appendix C we describe the loci of the Brocard points over a certain non-Ponceletian family of triangles with two vertices affixed to the boundary of an ellipse (or circle) and the other one which sweeps it.

6.3.3 First Brocard triangle: vertex locus

Consider a triangle $T = P_1P_2P_3$ with Brocard points Ω_1 and Ω_2. Referring to Figure 6.6:

Definition 6.1 (First Brocard Triangle)**.** *The vertices P_1', P_2', P_3' of the First Brocard Triangle T_1 are defined as follows: P_1' (resp. P_2', P_3') is the intersection of $P_2\Omega_1$ (resp. $P_3\Omega_1$, $P_1\Omega_1$) with $P_3\Omega_2$ (resp. $P_1\Omega_2$, $P_2\Omega_2$).*

Know properties of the T_1 include that (i) it is inversely similar to T, (ii) its barycenter X_2 coincides with that of the reference triangle, and (iii) its vertices are concyclic with Ω_1, Ω_2, X_3, and X_6 on the Brocard circle, defined in Weisstein (2019, Brocard Circle), whose center is X_{182}. Referring to Figure 6.5:

Proposition 6.11. *Over 3-periodics in the homothetic pair, the locus of the vertices of T_1 is an axis-aligned, concentric ellipse, homothetic to the ones in the pair and interior to the caustic. Its axes are given by:*

$$a' = \frac{a(a^2-b^2)}{2(a^2+b^2)}, \quad b' = \frac{b(a^2-b^2)}{2(a^2+b^2)}$$

Proof. The locus must be an ellipse since T_1 is inversely similar to the 3-periodics whose vertices are inscribed in an ellipse and their barycenters coincide. A vertex of the Brocard triangle is parametrized by

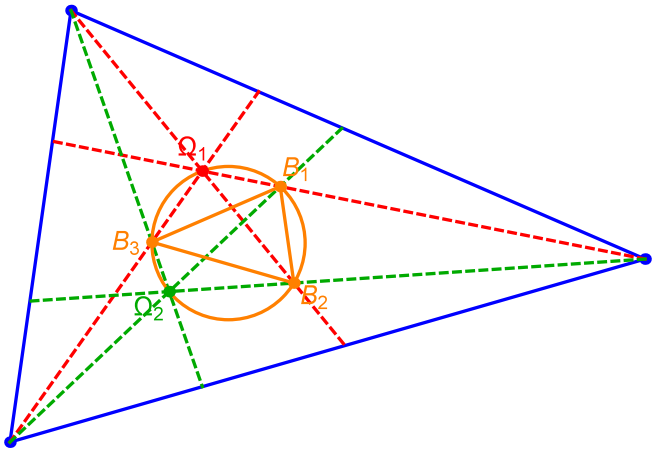

Figure 6.6: Construction for the First Brocard Triangle (orange) taken from Weisstein (2019, First Brocard Triangle). It is inversely similar to the reference one (blue), and their barycenters X_2 are common. Its vertices B_1, B_2, B_3 are concyclic with the Brocard points Ω_1 and Ω_2 on the Brocard circle (orange).

$$\frac{x^2}{a'^2} + \frac{y^2}{b'^2} = 1$$

□

Since homothetic 3-periodics conserve area (they are the affine image of regular polygons interscribed in two concentric circles, see Reznik and Garcia (2021b)), so must T_1 (inversely similar). Its area can be computed explicitly:

Proposition 6.12. *Over 3-periodics in the homothetic pair, the area of T_1 is invariant and given by*

$$\frac{3\sqrt{3}ab\left(a^2-b^2\right)^2}{16\left(a^2+b^2\right)^2}$$

6.3.4 Loci of Fermat and isodynamic equilaterals

As seen in Section 4.3.1, the pedal triangles from either the Fermat X_{13}, X_{14} and Isodynamic X_{15}, X_{16} points are equilateral. Since the homothetic family conserves $\text{ш} = \cot\omega$, Proposition 4.18 implies:

Corollary 6.1. *Over homothetic 3-periodics, the areas A_k, $k = 13, 14, 15, 16$ of the equilateral pedals from the Fermat and Isodynamic points are invariant.*

Over the Brocard porism, the loci of said equilaterals, were shown to be circles, see Figure 4.10. Interestingly, and referring to Figure 6.7:

6.4 Dual family

The dual family (bottom middle in Figure 1.5) is interscribed between two CAP ellipses with reciprocal aspect ratios. Its orthocenter X_4 is stationary. Referring to Figure 6.8:

Proposition 6.13. *Over dual 3-periodics, the loci of X_2, X_3, and X_5 are ellipses.*

6.5 Excentral family

Recall in Theorem 2.1, we derived the semiaxes of the locus of the excenters, i.e., the ellipse in which the excentral family is inscribed.

Also recall Section 5.8 where it was noted that over the excentral family, the locus its circumcenter (X_{40} in terms of billiard 3-periodics) was identical to a rotated copy of caustic (i.e., the elliptic billiard) when the latter's aspect ratio is φ the golden ratio.

Referring to Figure 6.9:

Proposition 6.14. *Over excentral 3-periodics the locus of X_2, X_3 and X_4 are ellipses.*

6.6 Summary

Table 6.1 summarizes the types of loci (point, circle, ellipse, etc.) for some triangle centers for families analyzed in this and previous chapters (including non-concentric such as poristic triangles and Brocard's porism). Families are grouped according to similar patterns in their loci types.

The first row reveals that out of the 8 families considered only in the confocal case is the locus of the incenter X_1 an ellipse, suggesting this is a rare phenomenon.

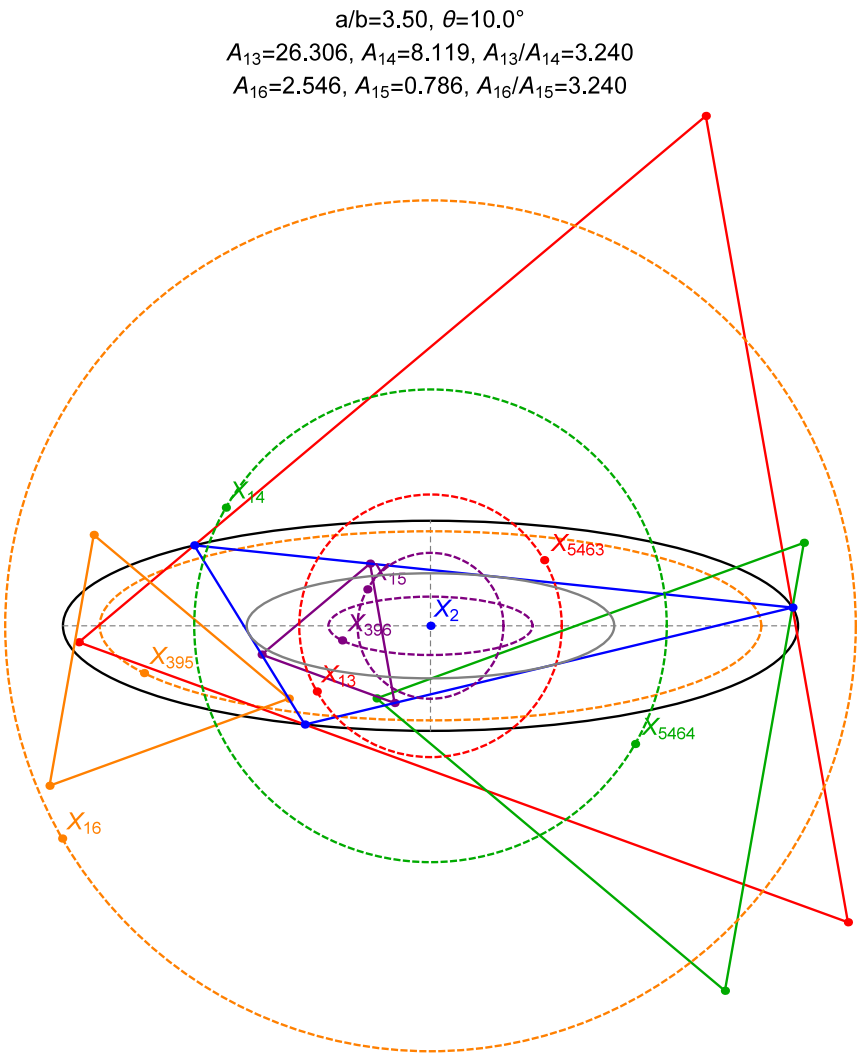

Figure 6.7: The homothetic Poncelet family (stationary X_2) is equibrocardal (conserves ω) and its triangles (blue) have invariant area. The loci of $X_k, k = 13, 14, 15, 16$ are circles concentric with the ellipses Video. Since areas A_{15}, A_{16}, A_{13}, A_{14} only depend on $\cot\omega$, they are individually invariant. The loci of X_{396} and X_{395} are ellipses whereas those of X_{5463} and X_{5464} are circles. Video

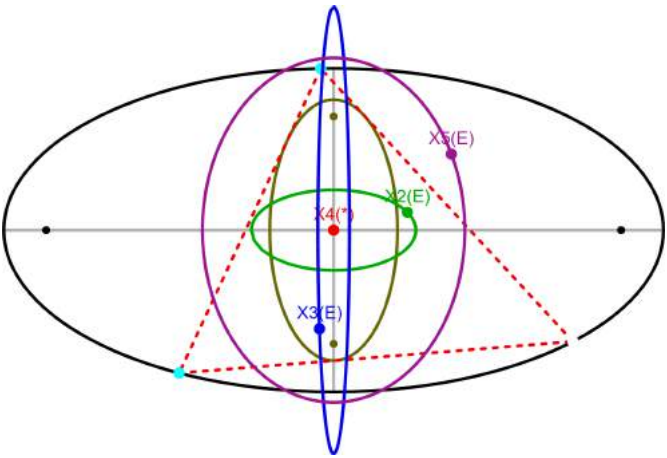

Figure 6.8: Over dual 3-periodics (stationary X_4), the loci of X_2, X_3, and X_5 are ellipses. Live

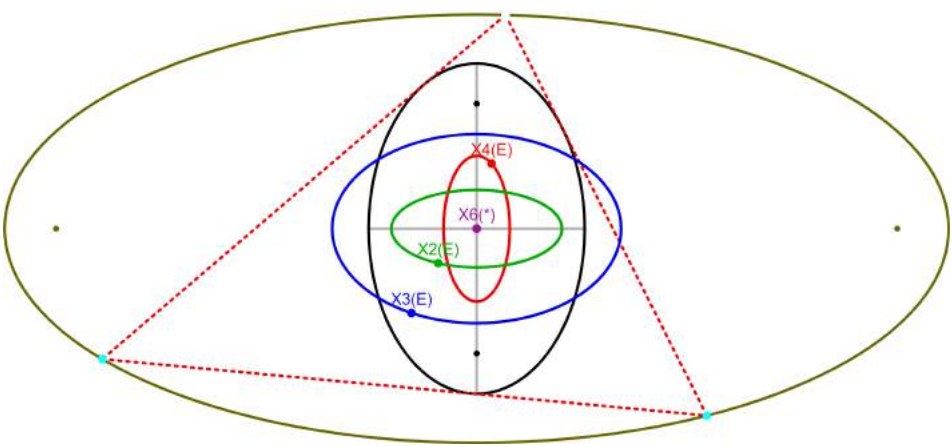

Figure 6.9: Elliptic loci of X_k, k =2,3,4 over excentral 3-periodics (the symmedian X_6 is stationary at the center). Live

	Group A			Group B			Group C	
	Conf.	Inc.	Por.	Exc.	Circ.	Por. Exc.	Hom.	Broc.
X_1	E	P	P	X	X	X	4	X
X_2	E	E	C	E	C	P	P	C
X_3	E	C	P	E	P	P	E	P
X_4	E	E	C	E	C	P	E	C
X_5	E	C	C	E	C	P	E	C
X_6	4	4	**E**	P	E	C	E	P
X_7	E	E	C	X	X	X	X	X
X_8	E	E	C	X	X	X	X	X
X_9	P	E	C	X	X	X	X	X
X_{10}	E	E	C	X	X	X	X	X
X_{11}	E″	C″	C″	X	X	**C_5**	X	X
X_{12}	E	C	C	X	X	X	X	X
X_{13}	X	X	X	X	X	X	C	C
X_{14}	X	X	X	X	X	X	C	C
X_{15}	X	X	X	X	X	X	C	P
X_{16}	X	X	X	X	X	X	C	P
X_{99}	X	X	C′	**X**	C′	C′	E′	C′
X_{100}	E′	E′	C′	**X**	C′	C′	**X**	C′
X_{110}	X	X	C′	E′	C′	C′	**X**	C′

Table 6.1: Loci types (P, C, E, X indicate point, circle, ellipse, and non-elliptic (degree not yet derived) loci, respectively) of some triangle centers over 3-periodic families. These are clustered in in 3 groups A,B,C sharing many metric phenomena: (i) confocal, incircle, poristic; (ii) excentral, circumcircle, poristic-excentral; (iii) homothetic and Brocard porism. A numeric entry indicates the degree of the non-elliptic implicit, e.g., '4' for quartic. A singly (resp. doubly) primed letter indicates a perfect match with the outer (resp. inner) conic in the pair. The symbol C_5 refers to the nine-point circle. The boldface entries indicate a discrepancy in the cluster. Note: X_n for the confocal and poristic excentral triangles refer to triangle centers of the family itself (not of their reference triangles).

The plethora of circles in the poristic family had already been shown in Odehnal (2011). A significant occurrence of ellipses in the confocal pair was signalled in Garcia, Reznik, and Koiller (2020a). As mentioned above, irrational centers X_k, $k \in [13, 16]$ sweep out circles for the homothetic pair. X_{15} and X_{16} are known to be stationary over the Brocard family studied in Bradley and Smith (2007). However, the locus of X_{13} and X_{14} are circles. Also noticeable is the fact that (i) though in the confocal pair the locus of X_1 (resp. X_6) is an ellipse (resp. quartic), locus types are swapped for both circumcircle and homothetic families.

It is well-known that there is a projective transformation that takes any Poncelet family to the the confocal pair, see Dragović and Radnović (2011). In this case only projective properties are preserved.

As mentioned above, the confocal family is the affine image of either the incircle or circumcircle family. In the first (resp. second) case the caustic (resp. outer ellipse) is sent to a circle. Though the affine group is non-conformal, we showed above that both families conserve the sum of cosines. One way to see this is that there is an alternate, conformal path which takes incircle 3-periodics to confocal ones, namely through a rigid rotation (yielding poristic triangles), followed by a variable similarity (yielding the confocal family).

A similar argument is valid for circumcircle triangles: there is an affine path (non-conformal) to the confocal family though both conserve the product of cosines. Notice there is also an alternate conformal composition of rotation (yielding poristic excentral triangles) and a variable similarity (yielding confocal excentral triangles). All in this path conserve the product of cosines.

Finally, homothetic and Brocard porism 3-periodics form an isolated clique. As mentioned in Reznik and Garcia (2021b), though these are variable similarity images of one another, they are not affinely-related.

6.6.1 Loci types, CAP families

Below we list triangle centers such that their loci types are either points or conics. These are obtained via numerical simulation amongst the first 200 centers on Kimberling (2019).

- Confocal pair (stationary X_9)
  - Ellipses: 1, 2, 3, 4, 5, 7, 8, 10, 11, 12, 20, 21, 35, 36, 40, 46, 55, 56, 57, 63, 65, 72, 78, 79, 80, 84, 88, 90, 100, 104, 119, 140, 142, 144, 145, 149, 153, 162, 165, 190, 191, 200.
  - Circles: n/a

- Incircle: (stationary X_1)
  - Ellipses: 2, 4, 7, 8, 9, 10, 20, 21, 63, 72, 78, 79, 84, 90, 100, 104, 140, 142, 144, 145, 149, 153, 191, 200.
  - Circles: 3, 5, 11, 12, 35, 36, 40, 46, 55, 56, 57, 65, 80, 119, 165.
- Circumcircle: (stationary X_3)
  - Ellipses: 6, 49, 51, 52, 54, 64, 66, 67, 68, 69, 70, 113, 125, 141, 143, 146, 154, 155, 159, 161, 182, 184, 185, 193, 195.
  - Circles: 2, 4, 5, 20, 22, 23, 24, 25, 26, 74, 98, 99, 100, 101, 102, 103, 104, 105, 106, 107, 108, 109, 110, 111, 112, 140, 156, 186.
- Homothetic: (stationary X_2)
  - Ellipses: 3, 4, 5, 6, 17, 20, 32, 39, 62, 69, 76, 83, 98, 99, 114, 115, 140, 141, 147, 148, 182, 183, 187, 190, 193, 194.
  - Circles: 13, 14, 15, 16.
- Dual: (stationary: X_4)
  - Ellipses: 2, 3, 5, 20, 64, 107, 122, 133, 140, 154.
  - Circles n/a
- Excentral: (stationary: X_6)
  - Ellipses: 2, 3, 4, 5, 20, 22, 23, 24, 25, 26, 49, 51, 52, 54, 64, 66, 67, 68, 69, 70, 74, 110, 113, 125, 140, 141, 143, 146, 154, 155, 156, 159, 161, 182, 184, 185, 186, 193, 195.
  - Circles n/a

Expressions for the semiaxes of the elliptic loci for many triangle centers are available in Garcia, Reznik, and Koiller (2021).

6.6.2 Loci types, NCAP families

For completeness, included below are point and/or conic loci for both Poristic and Brocard triangles. These include many stationary centers as well as segment and hyperbolic loci.

- Poristic, see Odehnal (2011)
  - Points (11): 1, 3, 35, 36, 40, 46, 55, 56, 57, 65, 165.
  - Segments (2): 44, 171.
  - Circles (46): 2, 4, 5, 7, 8, 9, 10, 11, 12, 20, 21, 23, 63, 72, 74, 78, 79, 80, 84, 90, 98, 99, 100, 101, 102, 103, 104, 105, 106, 107, 108, 109, 110, 111, 112, 119, 140, 142, 143, 144, 145, 149, 153, 186, 191, 200.
  - Ellipses (39): 6, 19, 22, 24, 25, 28, 31, 33, 34, 37, 38, 41, 42, 43, 45, 47, 48, 51, 52, 54, 58, 59, 60, 71, 73, 77, 81, 88, 89, 169, 170, 181, 182, 184, 185, 195, 197, 198, 199.
  - Hyperbolas (7): 26, 49, 64, 154, 155, 156, 196.
- Brocard porism
  - Points (10): 3, 6, 15, 16, 32, 39, 61, 62, 182, 187.
  - Segments (3): 50, 52, 58.
  - Circles (38): 2, 4, 5, 13, 14, 17, 18, 20, 23, 69, 74, 76, 83, 98, 99, 100, 101, 102, 103, 104, 105, 106, 107, 108, 109, 110, 111, 112, 114, 115, 140, 141, 147, 148, 183, 186, 193, 194.
  - Ellipses (6): 24, 25, 51, 143, 157, 18.
  - Hyperbolas (5): 26, 49, 64, 154, 159.

6.7 Exercises

Exercise 6.1. *Prove that over incircle 3-periodics, the power of the center with respect to the (fixed radius) circumcircle is invariant and equal to* $-ab$.

Exercise 6.2. *Compute* a/b *of the external ellipse in the incircle CAP family such that (i) the circular locus of* X_3 *coincides with the incircle, (ii) the elliptic locus of* X_4 *touches the outer ellipse at its top and bottom vertices, and (iii) the circular locus of* X_5 *coincides with the incircle. See it Live1, Live2.*

Exercise 6.3. *Derive the radius of the circumcircle in the same-named family such that the quartic locus of* X_1 *and the circular locus of* X_4 *intersect at four points on the inner ellipse, see it Live.*

Exercise 6.4. *Prove Proposition 6.9.*

Exercise 6.5. *Prove that over homothetic 3-periodics, the radius of the circular locus of X_{16} is minimum when $a/b = 3$.*

Exercise 6.6. *Prove that at $a/b = \sqrt{5}$, the elliptic loci of the Brocard points over homothetic 3-periodics are internally tangent to the inner ellipse. See it Live.*

Exercise 6.7. *Derive the a/b such that the elliptic loci of the Brocard points over the homothetic family intersect the y axis at $b/2$, i.e., at the top vertex of the caustic. See it Live.*

Exercise 6.8. *Prove that over homothetic 3-periodics, the locus of the Brocard midpoint X_{39} is an ellipse, derive its axis.*

Exercise 6.9. *Show that over homothetic 3-periodics, the elliptic locus of the vertices of the first Brocard triangle is interior to the inner ellipse.*

Exercise 6.10. *Compute the invariant similarity ratio of homothetic 3-periodics to the first Brocard triangles.*

Exercise 6.11. *Derive expressions for the areas in Corollary 6.1.*

Exercise 6.12. *Synthesize a triangle center such that over billiard 3-periodics its locus is a circle? Hint: it will be an affine combination of X_2 and X_3.*

Exercise 6.13. *Derive the semiaxes for the dual family elliptic loci of X_2, X_3, and X_5 in Proposition 6.13.*

Exercise 6.14. *As shown in Section 6.6.2, over poristic triangles, the locus of X_{44}, and X_{171} are segments. Derive their data. Do the same for the segment-loci of X_{50}, X_{52}, X_{58} over Brocard porism 3-periodics.*

Exercise 6.15. *Given an ellipse $\mathcal{E}$ with semiaxes a, b, consider a non-Ponceletian family of triangles with two vertices fixed on the foci of $\mathcal{E}$ and a third one which sweeps the boundary. Show the locus of the incenter of this family is an ellipse. See it Live.*

Exercise 6.16. *Prove that over the Brocard porism, the locus of X_{114} is a circle concentric with, and exterior to, the Brocard inellipse. Derive its radius. Live*

Exercise 6.17. *Prove that over the Brocard porism, the locus of X_{115} is a circle concentric with the Brocard inellipse of radius equal to the latter's minor semiaxis. Live*

Exercise 6.18. *Over the Brocard porism, the locus of X_{185} is an ellipse which intersects the major axis of the Brocard inellipse $\mathcal{E}'$ in two points A and B, see it Live. In the $1 < a/b < 2$ range, A, B appear to lie between the foci of $\mathcal{E}'$, however for larger a/b, e.g., $a/b = 3$, the locus seems to pass through the foci, see it Live. Prove or disprove this statement. Derive the center and semiaxes of the locus.*

6.8 Research questions

Question 6.1. *Prove (or disprove) Conjecture 1.*

Question 6.2. *Prove that over homothetic 3-periodics, the locus of center X_{5463} (resp. X_{5464}) of the first (resp. second) isogonic equilateral antipedal coincides with the circular locus of X_{13} (resp. X_{14}).*

Question 6.3. *Prove that over homothetic 3-periodics, the locus of the centers X_{396} (resp. X_{395}) of the isodynamic equilateral pedals are two ellipses, and derive their semiaxes.*

Question 6.4. *Can a triangle center be found such that over excentral (or dual) 3-periodics its locus is a circle?*

Question 6.5. *Show that over the poristic family (see Section 4.1), the locus of X_{59} is an ellipse whose major vertices are internally tangent to the outer circle poristics are inscribed in. See it Live.*

Question 6.6. *Prove Proposition 6.14 and derive the semiaxes of the elliptic loci of the named centers.*

7 Analyzing Loci

In Chapters 5 and 6, we took an informal, observational approach in describing interesting locus-related phenomena. In this chapter we take a first step at analyzing such phenomena. Namely, we attempt to answer the following questions:

- When are loci algebraic?
- What type of curve is swept by the incenter (and excenters) in a generic concentric, axis-parallel (CAP) pair?
- Given 3-periodics in a generic pair of ellipses, when is the locus of a triangle center an ellipse?
- We consider the special case of 3-periodics in the circumcircle family, showing that many such loci are circles.

Half through the chapter, we review Blaschke products, described in Daepp et al. (2019), since they will be used to answer some of the above questions.

Section 7.6 closes the chapter by presenting a theory for locus ellipticity in the confocal pair, as initially described in Helman, Laurain, Reznik, et al. (2021). This theory can be easily generalizable to any other pair. We also derive conditions under which a given locus in the confocal pair is a perfect circle or degenerates into a segment.

7.1 When are loci algebraic?

Consider a Triangle Center X whose Trilinears $p : q : r$ are rational on the sidelengths s_1, s_2, s_3, i.e., the Triangle Center Function h is rational, see Equation (A.1)

Theorem 7.1. *The locus of a rational triangle center over 3-periodics in a CAP pair is an algebraic curve.*

Our proof is based on the following 3-steps which yield an algebraic curve $\mathcal{L}(x, y) = 0$ which contains the locus. We refer to Lemma 7.1 and Lemma 7.2 appearing below.

Proof.

Step 1. *Introduce the symbolic variables* u, u_1, u_2

$$u^2 + u_1^2 = 1, \quad u_2^2 = r_1 u^2 + r_2.$$

Let sidelengths $s_1 = |P_3 - P_2|$, $s_2 = |P_1 - P_3|$, $s_3 = |P_2 - P_1|$. *Define* $g_1 = s_1^2 - |P_3 - P_2|^2$, $g_2 = s_2^2 - |P_3 - P_1|^2$ *and* $g_3 = s_3^2 - |P_2 - P_1|^2$. *Therefore,* g_i *(i=1,2,3) are polynomial expressions on* s_i *and* (u, u_1, u_2)*:*

$$\begin{aligned} g_1 &= -h_1 s_1^2 + h_0 \\ g_2 &= -h_1 s_2^2 - h_2 u_1 u_2 + h_3 \\ g_3 &= -h_1 s_3^2 + h_2 u_1 u_2 + h_3 \end{aligned}$$

Here h_i *are polynomials in the variable* u. *The long expressions will be omitted, but can be evaluated from the vertex parametrization given in Proposition 3.17.* The vertices will be given by rational functions of u, u_1, u_2

$$P_1 = (a\,u, b\,u_1), \quad P_2 = (p_{2x}, p_{2y})/p_3, \quad P_3 = (p_{3x}, p_{3y})/p_3$$

Equations $g_i = 0 \;\; (i = 1, 2, 3)$, are polynomial in (s_i, u, u_1, u_2).

Step 2. *Express the locus* X *as a rational function on* $u, u_1, u_2, s_1, s_2, s_3$.

Convert $p : q : r$ to Cartesians $X = (x, y)$ via Equation (A.1). From Lemma 7.1, it follows that (x, y) is rational on $u, u_1, u_2, s_1, s_2, s_3$.

$$x = \mathcal{Q}/\mathcal{R}, \quad y = \mathcal{S}/\mathcal{T}$$

To obtain the polynomials $\mathcal{Q}, \mathcal{R}, \mathcal{S}, \mathcal{T}$ on said variables $u, u_1, u_2, s_1, s_2, s_3$, one substitutes the p, q, r by the corresponding rational functions of s_1, s_2, s_3 that define a specific Triangle Center X. Other than that, the method proceeds identically.

Step 3. *Computing resultants. Our problem is now cast in terms of the polynomial equations:*

$$E_0 = \mathcal{Q} - x\,\mathcal{R} = 0, \quad F_0 = \mathcal{S} - y\,\mathcal{T} = 0$$

Firstly, compute the resultants, in chain fashion:

$$\begin{aligned} E_1 &= \mathrm{Res}(g_1, E_0, s_1) = 0, \quad F_1 = \mathrm{Res}(g_1, F_0, s_1) = 0 \\ E_2 &= \mathrm{Res}(g_2, E_1, s_2) = 0, \quad F_2 = \mathrm{Res}(g_2, F_1, s_2) = 0 \\ E_3 &= \mathrm{Res}(g_3, E_2, s_3) = 0, \quad F_3 = \mathrm{Res}(g_3, F_2, s_3) = 0 \end{aligned}$$

It follows that $E_3(x, u, u_1, u_2) = 0$ and $F_3(y, u, u_1, u_2) = 0$ are polynomial equations. In other words, s_1, s_2, s_3 have been eliminated.

Now eliminate the variables u_1 and u_2 by taking the following resultants:

$$\begin{aligned} E_4(x, u, u_2) &= \mathrm{Res}(E_3, u_1^2 + u^2 - 1, u_1) = 0 \\ F_4(y, u, u_2) &= \mathrm{Res}(F_3, u_1^2 + u^2 - 1, u_1) = 0 \\ E_5(x, u) &= \mathrm{Res}(E_4, u_2^2 + \rho_1 u^2 - 1, u_2) = 0 \\ F_5(y, u) &= \mathrm{Res}(F_4, u_2^2 + \rho_1 u^2 - 1, u_2) = 0 \end{aligned}$$

This yields two polynomial equations $E_5(x, u) = 0$ and $F_5(y, u) = 0$.

Finally compute the resultant

$$\mathcal{L} = \mathrm{Res}(E_5, F_5, u) = 0$$

that eliminates u and gives the implicit algebraic equation for the locus X. □

Remark 7.1. *In practice, after obtaining a resultant, a human assists the CAS by factoring out spurious branches (when recognized), in order to get the final answer in more reduced form.*

When not rational in the sidelengths, except a few cases[1], Triangle Centers in Kimberling's list have explicit Trilinears involving fractional powers and/or terms

[1] For instance Hofstadter points $X(359)$, $X(360)$.

containing the triangle area. Those can be made implicit, i.e, given by zero sets of polynomials involving p, q, r, s_1, s_2, s_3. The chain of resultants to be computed will be increased by three, in order to eliminate the variables p, q, r before (or after) s_1, s_2, s_3.

Theorem 7.2. *In the family of 3-periodic orbits in a generic Poncelet pair of conics the locus of a rational triangle center is an algebraic curve.*

Proof. The analysis follow the same steps as in the case of a Poncelet pair of ellipses. See proof of Theorem 7.1. □

Supporting lemmas

Lemma 7.1. *Let* $P_1 = (au, b\sqrt{1-u^2})$. *The coordinates of* P_2 *and* P_3 *of the 3-periodic billiard orbit are rational functions in the variables* u, u_1, u_2, *where* $u_1 = \sqrt{1-u^2}$, $u_2 = \sqrt{r_1 + r_2 u^2}$ *and* $r_1 = a_c^2(b^2 - b_c^2)a^2b^2$, $r_2 = a^2b^2(a^2b_c^2 - a_c^2b^2)$.

Proof. Follows directly from the vertex parametrization in Proposition 3.17. □

Lemma 7.2. *Let* $P_1 = (au, b\sqrt{1-u^2})$. *Let* s_1, s_2 *and* s_3 *the sides of the triangular orbit* $P_1P_2P_3$. *Then* $g_1(u, s_1) = 0$, $g_2(s_2, u_2, u) = 0$ *and* $g_3(s_3, u_2, u) = 0$ *for polynomial functions* g_i.

Proof. Using the parametrization of the 3-periodic Poncelet orbit it follows that $s_1^2 - |P_2 - P_3|^2 = 0$ is a rational equation in the variables u, s_1. Simplifying, leads to $g_1(s_1, u) = 0$.

Analogously for s_2 and s_3. In this case, the equations $s_2^2 - |P_1 - P_3|^2 = 0$ and $s_3^2 - |P_1 - P_2|^2 = 0$ have square roots $u_2 = \sqrt{r_1 + r_2u^2}$ and $u_1 = \sqrt{1-u^2}$ and are rational in the variables s_2, u_2, u_1, u and s_3, u_2, u_1, u respectively. It follows that the degrees of g_1, g_2, and g_3 are 10. Simplifying, leads to $g_2(s_2, u_2, u_1, u) = 0$ and $g_3(s_3, u_2, u_1, u) = 0$. □

7.2 Review: Blaschke products

As a tool for further results in this chapter, we will use a special parametrization of Poncelet 3-periodics based on em Blaschke Products, which we originally used in Helman, Laurain, Garcia, et al. (2021).

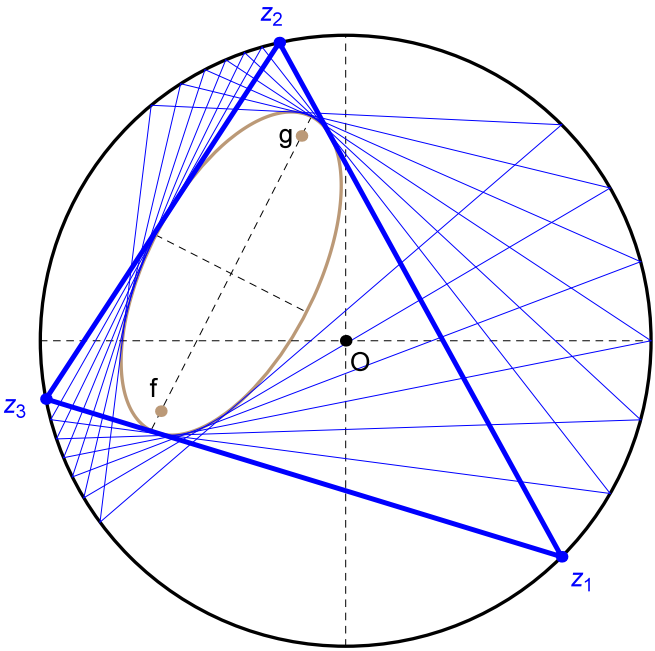

Figure 7.1: Blaschke complex parametrization of Poncelet 3-periodics (blue). Vertices are z_1, z_2, z_3. The foci of the caustic are f, g.

Here we consider 3-periodics inscribed in a unit circle and circumscribing a non-concentric ellipse. We will work in the complex plane. Under the Blaschke parametrization, Poncelet 3-periodic vertices become symmetric with respect to the information of the circle-ellipse pair.

Let $\mathbb{T} = \{z \in \mathbb{C} : |z| = 1\}$ the unit circle and $\mathbb{D} = \{z \in \mathbb{C} : |z| < 1\}$ the open unit disk bounded by $\mathbb{T}$.

Consider a Moebius map $M_{w_0} = (w_0 - z)/(1 - \overline{w_0} z)$ and the Blaschke product of degree 3 given by

$$B = M_{w_1} M_{w_2} M_{w_3}$$

Referring to Figure 7.1, let $z_1, z_2, z_3 \in \mathbb{C}$ denote the vertices of Poncelet 3-periodics in a generic $N = 3$ family with fixed (unit) circumcircle denoted $\mathbb{T} = \{z \in \mathbb{C} : |z| = 1\}$. Let f, g be the foci of the caustic. Using Viète's formula, we obtain the following parametrization of the elementary symmetric polynomials

on z_1, z_2, z_3:

Definition 7.1 (Blaschke's Parametrization)**.**

$$\begin{aligned}\sigma_1 &:= z_1 + z_2 + z_3 = f + g + \lambda\overline{f}\,\overline{g}\\ \sigma_2 &:= z_1z_2 + z_2z_3 + z_3z_1 = fg + \lambda(\overline{f} + \overline{g})\\ \sigma_3 &:= z_1z_2z_3 = \lambda\end{aligned}$$

where $\lambda \in \mathbb{T}$ is the varying parameter.

Note that the concentric case occurs when $g = -f$.

For each $\lambda \in \mathbb{T}$, the three solutions of $B(z) = \lambda$ are the vertices of a 3-periodic orbit of the Poncelet family of triangles in the complex plane, see Daepp et al. (2019, Chapter 4). Furthermore, as λ varies in $\mathbb{T}$, the whole family of triangles is covered. Clearing the denominator in this equation and passing everything to the left-hand side, we get

$$z^3 - (f + g + \lambda\overline{f}\,\overline{g})z^2 + (fg + \lambda(\overline{f} + \overline{g}))z - \lambda = 0$$

Lemma 7.3. *If $u, v, w \in \mathbb{C}$ and λ is a parameter that varies over the unit circle $\mathbb{T} \subset \mathbb{C}$, then the curve parametrized by*

$$F(\lambda) = u\lambda + \frac{v}{\lambda} + w$$

is an ellipse centered at w, with semiaxis $|u| + |v|$ and $\big||u| - |v|\big|$, rotated with respect to the horizontal axis of $\mathbb{C}$ by an angle of $(\arg u + \arg v)/2$.

Proof. If either $u = 0$ or $v = 0$, the curve $h(\mathbb{T})$ is clearly the translation of a multiple of the unit circle $\mathbb{T}$, and the result follows. Thus, we may assume $u \neq 0$ and $v \neq 0$.

Choose $k \in \mathbb{C}$ such that $k^2 = u/v$. Write k in polar form, as $k = r\mu$, where $r > 0$ ($r \in \mathbb{R}$) and $|\mu| = 1$. We define the following complex-valued functions:

$$R(z) := \mu z,\ S(z) := rz + (1/r)\overline{z},\ H(z) := kvz,\ T(z) := z + w$$

It is straightforward to check that $F = T \circ H \circ S \circ R$.

Since $|\mu| = 1$, R is a rotation of the plane, thus R sends the unit circle $\mathbb{T}$ to itself. Since $r \in \mathbb{R}$, $r > 0$, if we identify $\mathbb{C}$ with $\mathbb{R}^2$, S can be seen as a linear transformation that sends $(x, y) \mapsto ((r + 1/r)\,x, (r - 1/r)\,y)$. Thus, S sends $\mathbb{T}$

to an axis-aligned, origin-centered ellipse $\mathcal{E}_1$ with semiaxis $r + 1/r$ and $|r - 1/r|$. H is the composition of a rotation and a homothety. H sends the ellipse $\mathcal{E}_1$ to an origin-centered ellipse $\mathcal{E}_2$ rotated by an angle of $\arg(kv) = \arg(k) + \arg(v) = (\arg(u) - \arg(v))/2 + \arg(v) = (\arg(u) + \arg(v))/2$. The semiaxis of $\mathcal{E}_2$ have length

$$|kv|(r + 1/r) = r|v|(r + 1/r) = |r^2 v| + |v| = |k^2 v| + |v| = |u| + |v|, \text{ and}$$
$$|kv||r - 1/r| = r|v||r - 1/r| = \big||r^2 v| - |v|\big| = \big||k^2 v| - |v|\big| = \big||u| - |v|\big|$$

Finally, T is a translation, thus T sends $\mathcal{E}_2$ to an ellipse $\mathcal{E}_3$ centered at w, rotated by an angle $(\arg(u) + \arg(v))/2$ from the axis, with semiaxis lengths $|u| + |v|$ and $\big||u| - |v|\big|$, as desired. □

Theorem 7.3. *Let B be a Blaschke product of degree 3 with zeros $0, f, g$. For $\lambda \in \mathbb{T}$, let z_1, z_2, z_3 denote the three distinct solutions to $B(z) = \lambda$. Then the lines joining z_j and z_k, $(j \neq k)$ are tangent to the ellipse given by*

$$|w - f| + |w - g| = |1 - \overline{f}\, g|.$$

Proof. See Daepp et al. (ibid., Theorem 2.9, page 37). □

Theorem 7.4. *Given two points $f, g \in \mathbb{D}$. Then there exists a unique conic $\mathcal{E}$ with the foci f, g which is 3-Poncelet caustic with respect to $\mathbb{T}$. Moreover, $\mathcal{E}$ is an ellipse. That ellipse is the Blaschke ellipse with the major axis of length $|1 - \overline{f}\, g|$.*

Proof. See Daepp et al. (ibid., Corollary 4.4, page 44) and Dragović and Radnović (2021). □

7.3 Locus of the incenter in a generic pair

Recall the locus of the incenter and excenters are ellipses if the pair is confocal, see Theorem 2.1. Here we expand the analysis, starting with the circumcircle family. The techniques developed here will help us expand the result to any generic pair.

Proposition 7.1. *Over Poncelet 3-periodics in the pair with an outer circle and an ellipse in generic position, the locus X_1 is given by:*

$$\begin{aligned} X_1 : z^4 &- 2((\bar{f} + \bar{g})\lambda + fg)z^2 + 8\lambda z \\ &+ (\bar{f} - \bar{g})^2\lambda^2 + 2(|f|^2 g + f|g|^2 - 2f - 2g)\lambda + f^2 g^2 = 0 \\ &: z^4 - 2\beta z^2 + 8\lambda z + (\beta^2 - 4\alpha\lambda) = 0 \end{aligned}$$

Proof. The incenter of a triangle with vertices $\{z_1, z_2, z_3\}$ is given by:

$$X_1 = \frac{\sqrt{s_1}\, z_1 + \sqrt{s_2}\, z_2 + \sqrt{s_3}\, z_3}{\sqrt{s_1} + \sqrt{s_2} + \sqrt{s_3}}$$
$$s_1 = |z_2 - z_3|^2,\ s_2 = |z_1 - z_3|^2,\ \ s_3 = |z_2 - z_1|^2$$

Using that $z_i \in \mathbb{T}$ it follows that

$$s_1 = 2 - \left(\frac{z_3}{z_2} + \frac{z_2}{z_2}\right),\ \ s_2 = 2 - \left(\frac{z_1}{z_3} + \frac{z_3}{z_1}\right),\ \ s_3 = 2 - \left(\frac{z_1}{z_2} + \frac{z_2}{z_1}\right)$$

Eliminating the square roots in the equation $X_1 - z = 0$ and using the relations σ_i (i=1,2,3) given in Blaschke's parametrization the result follows. □

Note that for $z_i \in \mathbb{T}^1$ we have that $X_1 : -\sqrt{z_1 z_2} - \sqrt{z_1 z_3} - \sqrt{z_2 z_3}$, see Exercise 7.5.

Using techniques similar to those in the last proof, we derive the following expression for the locus of the incenter and the excenters over 3-periodics in any ellipse pair:

Proposition 7.2. *Over Poncelet 3-periodics in a generic nested ellipse pair, the locus of X_1 and the excenters are the roots of the following quartic polynomial in z:*

$$\begin{aligned}
&(p^2 - q^2)^2 \lambda^2 z^4 - 4\,\lambda\, pq((\lambda^2 + \beta)p^2 - (2\,\alpha\,\lambda + 2)pq + (\lambda^2 + \beta)q^2)z^3 \\
&+ (-2\,\beta\,\lambda^2 p^4 + 2\,\lambda\,(2\,\alpha\,\lambda^2 + \alpha\,\beta + 9\,\lambda)p^3 q + (-4\,\alpha^2\lambda^2 - 8\,\beta\,\lambda^2 - 20\,\alpha\,\lambda + 4\,\beta^2)p^2 q^2 \\
&+ 2\,\lambda\,(2\,\alpha\,\lambda^2 + \alpha\,\beta + 9\,\lambda)pq^3 - 2\,\beta\,\lambda^2 q^4)z^2 + (8\,\lambda^3 p^4 - 4\,\lambda\,(\beta\,\lambda^2 + 6\,\alpha\,\lambda - \beta^2)p^3 q \\
&+ (4\,\alpha\,\beta\,\lambda^2 + 16\,\alpha^2\lambda - 4\,\beta^2\alpha + 20\,\lambda^3 - 4\,\beta\,\lambda)p^2 q^2 - 4\,\lambda\,(\beta\,\lambda^2 + 6\,\alpha\,\lambda - \beta^2)pq^3 \\
&+ 8\,\lambda^3 q^4)X - \lambda^2(4\,\alpha\,\lambda - \beta^2)p^4 + 2\,\lambda\,(4\,\alpha^2\lambda - \beta^2\alpha + 2\,\lambda^3 - \beta\,\lambda)p^3 q \\
&+ (-4\,\alpha^3\lambda + \alpha^2\beta^2 - 12\,\alpha\,\lambda^3 + 2\,\beta^2\lambda^2 + 2\,\alpha\,\beta\,\lambda + \lambda^2)p^2 q^2 \\
&+ 2\,\lambda\,(4\,\alpha^2\lambda - \beta^2\alpha + 2\,\lambda^3 - \beta\,\lambda)pq^3 - \lambda^2(4\,\alpha\,\lambda - \beta^2)q^4 = 0
\end{aligned}$$

Proof. Let $p, q \in \mathbb{R}$. Consider the affine transformation $T(z) = pz + q\overline{z}$ and set $w_i = T(z_i)$. The proof is similar to that given in Proposition 7.1. Here, in order to simplify the vertices z_i it is necessary to evaluate the sums $p_k = z_1^k + z_2^k + z_3^k$ $(k = 1, \ldots, 5)$, expressing the result in terms of α, β and λ. See Figure 7.3 □

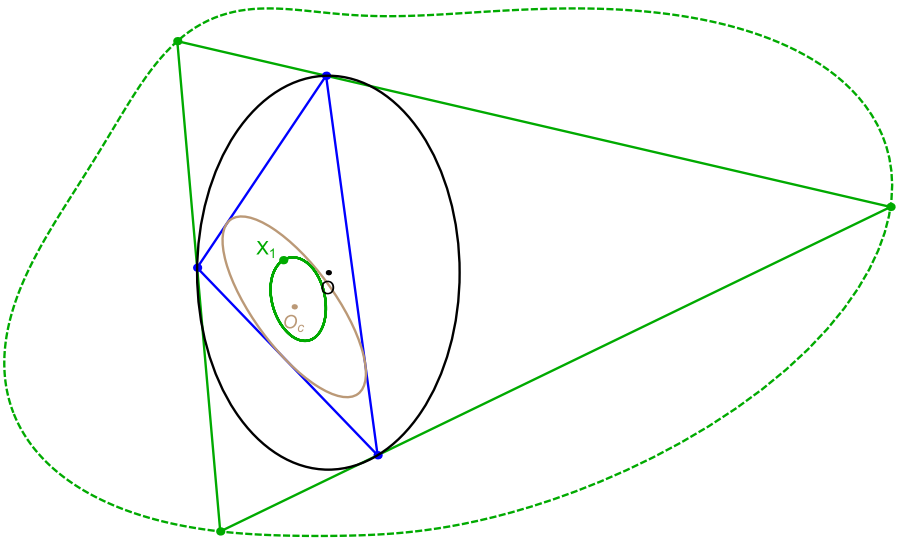

Figure 7.2: Consider a Poncelet 3-periodic family (blue) interscribed between two non-concentric, unaligned ellipses (centers O and O_c). The locus of the incenter X_1 (solid green) is non-elliptic and skewed. The locus of the excenters (dashed), i.e., the vertices of the excentral triangle (solid green), is a non-convex curve. Video

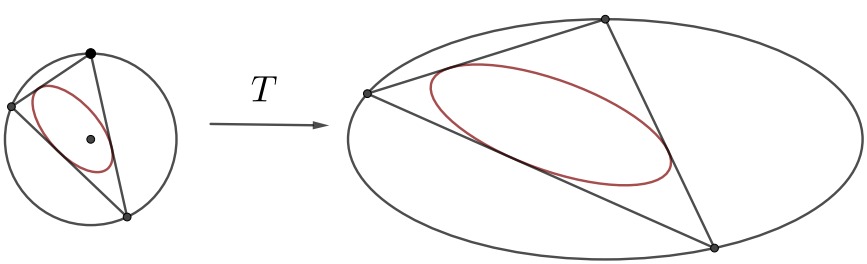

Figure 7.3: **Left:** Poncelet 3-periodic in a non-concentric pair with fixed circumcircle. **Right:** an affine image thereof.

Referring to Figure 7.2, note that in general, the locus of the incenter is not even four-fold symmetric, and that of the excenters may be non-convex.

The above entails yet another alternative proof for the ellipticity of the X_1 locus over billiard 3-periodics:

Corollary 7.1. *Over billiard 3-periodics, the locus of X_1 is given by:*

$$X_1 = z - \frac{\left(-a^4 + b^4 + c^2\delta\right)\lambda}{2\,a^2b^2} - \frac{(a^2+b^2)\delta - a^4 - b^4}{2a^2b^2\lambda} = 0$$

Proof. Let a and b be the semiaxes of the billiard. In the confocal pair we have that

$$f = \frac{1}{c}\sqrt{2\,\delta - a^2 - b^2}, \quad g = -\frac{1}{c}\sqrt{2\,\delta - a^2 - b^2}$$

This is obtained by taking an affine map $T(z) = (a+b)z/2 + (a-b)\bar{z}/2$ sending the pair with an unitary outer circle to the confocal pair, see Section 2.2.

The result follows by factorization of the quartic polynomial that defines X_1 in Proposition 7.2.

Using CAS we obtain that X_1 is factorizable as $E_1 E_2$, where

$$\begin{aligned} E_1 &= z - \frac{\left(-a^4 + b^4 + c^2\delta\right)\lambda}{2\,a^2b^2} - \frac{(a^2+b^2)\delta - a^4 - b^4}{2a^2b^2\lambda} = 0 \\ E_2 &= -2c^2\lambda\left[-2\,a^2b^2\lambda\,z^3 + \left(\left(c^2\lambda^2 - a^2 - b^2\right)\delta + \right.\right. \\ &\quad + c^2\left(a^2+b^2\right)\lambda^2 - a^4 + 4\,a^2b^2 - b^4\Big)\,z^2 \\ &\quad \left.-4\,\lambda\,c^2\left(a^2+b^2+\delta\right)z - 4\,\lambda^2\left(a^4+b^4+a^2\delta+b^2\delta\right)\right] \end{aligned}$$

□

Corollary 7.2. *The locus X_1 is the ellipse with semiaxes given by $a_1 = (a^2-\delta)/b$ and $b_1 = (\delta - b^2)/a$.*

Proof. Follows directly from Lemma 7.3 and Proposition 7.2 □

Remark 7.2. *The space of possible choices of two conics which admits a 3-periodic family is five dimensional.*

This stems from the fact that a conic has five degrees of freedom, so two conics have 10; the euclidean transformation group is 4-dimensional, and Cayley deducts one degree of freedom. Therefore: $10 - 4 - 1 = 5$.

Note that over said 5d space, the possible confocal configurations are 1-dimensional. Interestingly, experimental evidence suggests that our very first result (elliptic locus of the incenter and excenters) is actually very rare. Referring to Figure 7.4:

Conjecture 2. *Given a pair of ellipses admitting Poncelet 3-periodics, the locus of the incenter is a non-degenerate ellipse (i.e., not a point) iff the pair is confocal.*

Recall a result by Odehnal (2011), illustrated in Figure 4.6: the locus of the excenters over the poristic family is a circle twice the radius of the circumcircle. Referring to Figures 2.1 and 7.2:

Conjecture 3. *Given a pair of ellipses admitting Poncelet 3-periodics, the locus of the excenters is an ellipse iff the pair is either confocal or poristic, in which case the locus is a circle.*

7.4 Loci in generic nested ellipses

In this Section we prove the locus of a given fixed affine combination of X_2 and X_3 is an ellipse. We will use Blaschke products since, as shown in Figure 7.5, a generic non-concentric pair is always the affine image of a pair with circumcircle.

Consider the generic pair of nested ellipses $\mathcal{E} = (O, a, b)$ and $\mathcal{E}_c = (O_c, a_c, b_c, \theta)$ in Figure 7.6, where θ is the counterclockwise tilt[2] of O_c with respect to O. Let $\mathrm{s}\theta$, $\mathrm{c}\theta$ denote the sine and cosine of θ, respectively. Define $c_c^2 = a_c^2 - b_c^2$. The Cayley condition for the pair to admit a 3-periodic family is given by:

$$
\begin{aligned}
&b^4 x_c^4 + 2\,a^2 b^2 x_c^2 y_c^2 + \left(2c_c^2\left(-b^2(a^2+b^2)\right)\mathrm{c}\theta^2 - 2\left(b^2 - b_c^2\right)b^2 a^2 - 2\,b^4 b_c^2\right) x_c^2 \\
&- 8\,a^2 b^2 x_c\, y_c\, c_c^2 \mathrm{s}\theta\mathrm{c}\theta + a^4 y_c^4 + \left(2c_c^2 a^2\left(a^2+b^2\right)\mathrm{c}\theta^2 - 2\left(b_c^2 + b^2\right)a^4 + 2\,a^2 b^2 b_c^2\right) y_c^2 \\
&+ c_c^4 c^4\left(\mathrm{c}\theta^4 - 2\,c_c^2 c^2\left(a^2 a_c^2 - b^2 a^2 + b_c^2 b^2\right)\mathrm{c}\theta^2\right. \\
&+ \left.(aa_c + ab - bb_c)\,(aa_c - ab - bb_c)\,(aa_c + ab + bb_c)\,(aa_c - ab + bb_c) = 0\right.
\end{aligned}
$$

[2] Not to be confused with θ_i, used before to denote an N-periodic internal angle.

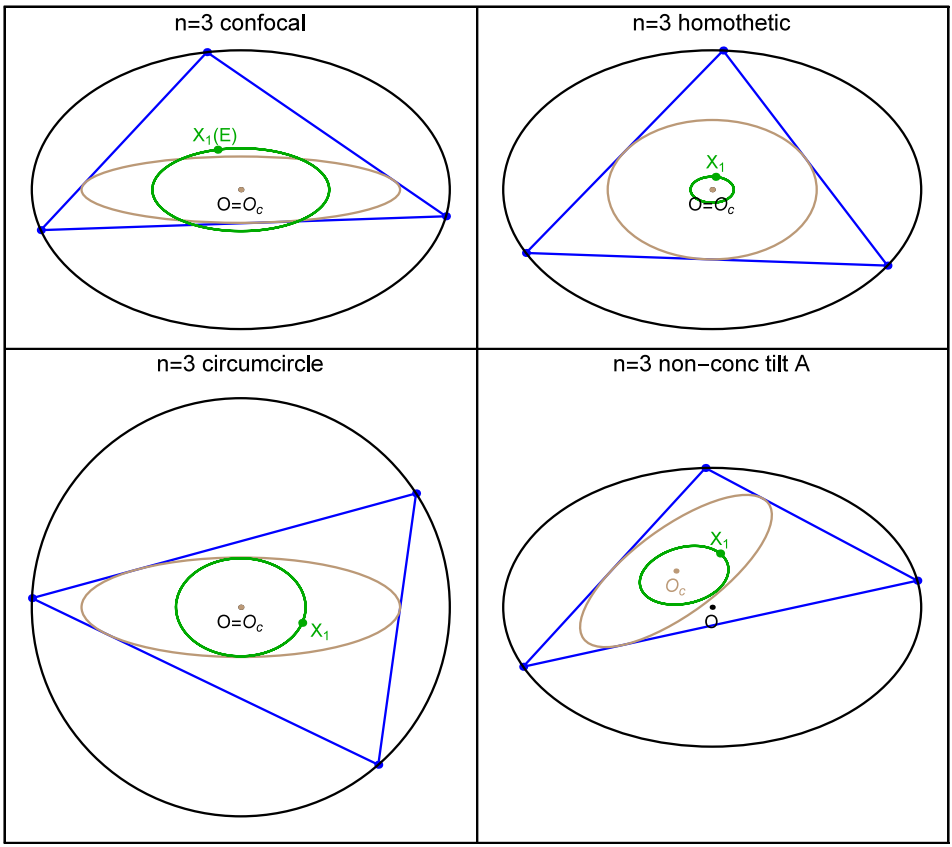

Figure 7.4: Locus of the incenter over Poncelet 3-periodics interscribed in 4 different pairs of nested ellipses. (i) confocal pair (top left): the locus of X_1 is an ellipse (this could be unique to the confocal family); (ii) homothetic (top right): the locus is non-elliptic (we know this via numerics); (iii) circumcircle family (bottom left): again, the locus is non-elliptic; (iv) 3-periodics in a non-concentric, non-axis-parallel ellipse pair (bottom right): the locus of the incenter is not even four-fold symmetric.

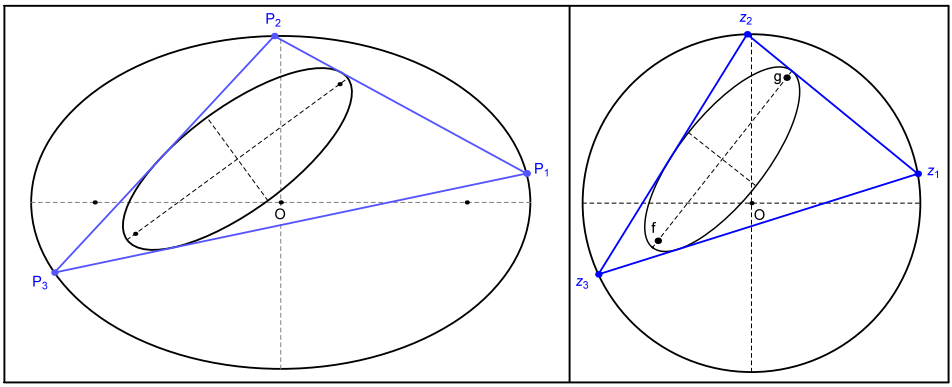

Figure 7.5: Affine transformation that sends a generic ellipse pair and its 3-periodic family (left) to a new pair with circumcircle (right). We parametrize the 3-periodic orbit with vertices z_i in the circumcircle pair using the foci of the latter's caustic f and g, and then apply the inverse affine transformation to get a parametrization of the vertices P_i of the original Poncelet pair. Video

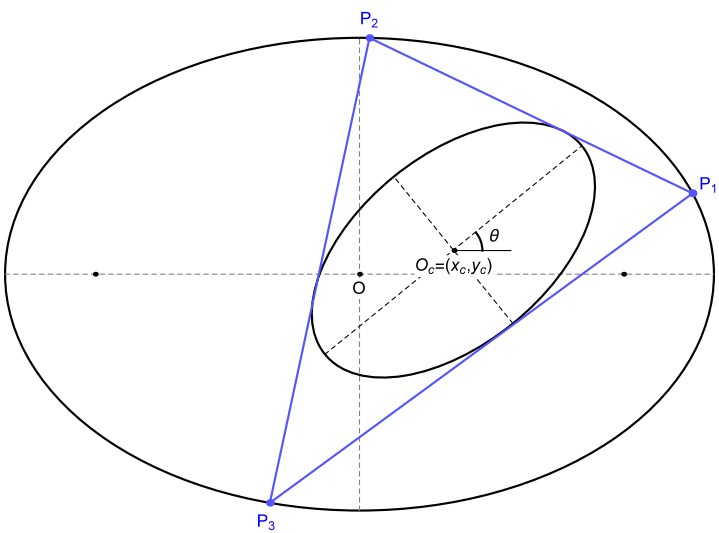

Figure 7.6: A pair of ellipses in general position which admits a Poncelet 3-periodic family (blue). Let the outer one be centered at the origin O. Their major axes are tilted by θ, and their centers displaced by $O_c = (x_c, y_c)$. Video

Referring to Figure 7.7:

Theorem 7.5. *Over the family of 3-periodics interscribed in an ellipse pair in general position (non-concentric, non-axis-aligned), if $\mathcal{X}_{\alpha,\beta}$ is a fixed linear combination of X_2 and X_3, i.e., $\mathcal{X}_{\alpha,\beta} = \alpha X_2 + \beta X_3$ for some fixed $\alpha, \beta \in \mathbb{C}$, then its locus is an ellipse.*

Proof. Consider a general $N = 3$ Poncelet pair of ellipses that forms a 1-parameter family of triangles. Without loss of generality, by translation and rotation, we may assume the outer ellipse is centered at the origin and axis-aligned with the plane $\mathbb{R}^2$, which we will also identify with the complex plane $\mathbb{C}$. Let a, b be the semi-axis of the outer ellipse, and a_c, b_c the semi-axis of the inner ellipse, as usual.

Referring to Figure 7.5, consider the linear transformation that takes $(x, y) \mapsto (x/a, y/b)$. This transformation takes the outer ellipse to the unit circle $\mathbb{T}$ and the inner ellipse to another ellipse. Thus, it transforms the general Poncelet $N = 3$ system into a pair where the outer ellipse is the circumcircle, which we can parametrize using Blaschke products. In fact, to get back to the original system, we must apply the inverse transformation that takes $(x, y) \mapsto (ax, by)$. As a linear transformation from $\mathbb{C}$ to $\mathbb{C}$, we can write it as $L(z) := pz + q\overline{z}$, where $p := (a + b)/2, q := (a - b)/2$.

Let $z_1, z_2, z_3 \in \mathbb{T} \subset \mathbb{C}$ be the three vertices of the circumcircle family, parametrized as in Definition 7.1, and let $v_1 := L(z_1), v_2 := L(z_2), v_3 := L(z_3)$ be the three vertices of the original general family. The barycenter X_2 of the original family is given by $(v_1 + v_2 + v_3)/3$, and the circumcenter X_3 is given by Tak (n.d.):

$$X_3 = \begin{vmatrix} v_1 & |v_1|^2 & 1 \\ v_2 & |v_2|^2 & 1 \\ v_3 & |v_3|^2 & 1 \end{vmatrix} \Bigg/ \begin{vmatrix} v_1 & \overline{v_1} & 1 \\ v_2 & \overline{v_2} & 1 \\ v_3 & \overline{v_3} & 1 \end{vmatrix}$$

Since $\overline{z_1} = 1/z_1, \overline{z_2} = 1/z_2, \overline{z_3} = 1/z_3$, we can write v_1, v_2, v_3 as rational functions of z_1, z_2, z_3, respectively. Thus, both X_2 and X_3 are symmetric rational functions on z_1, z_2, z_3. Defining $\mathcal{X}_{\alpha,\beta} = \alpha X_2 + \beta X_3$, we have consequently that $\mathcal{X}_{\alpha,\beta}$ is also a symmetric rational function on z_1, z_2, z_3. Hence, we can reduce its numerator and denominator to functions on the elementary symmetric polynomials on z_1, z_2, z_3. This is exactly what we need in order to use the parametrization by Blaschke products.

In fact, we explicitly compute:

$$\mathcal{X}_{\alpha,\beta} = \frac{p^2q\left(\sigma_2(\alpha+3\beta)+3\beta\sigma_3^2\right)+\alpha p^3\sigma_1\sigma_3 - pq^2(3\beta+\sigma_1\sigma_3(\alpha+3\beta))-\alpha q^3\sigma_2}{3\sigma_3(p-q)(p+q)}$$

where $\sigma_1, \sigma_2, \sigma_3$ are the elementary symmetric polynomials on z_1, z_2, z_3.

Let $f, g \in \mathbb{C}$ be the foci of the inner ellipse in the circumcircle system. Using Definition 7.1, with the parameter λ varying on the unit circle $\mathbb{T}$, we get:

$$\mathcal{X}_{\alpha,\beta} = u\lambda + v\frac{1}{\lambda} + w$$

where:

$$\begin{aligned}
u :=& \frac{p\left(\overline{f}\,\overline{g}\left(\alpha p^2 - q^2(\alpha+3\beta)\right)+3\beta pq\right)}{3(p-q)(p+q)}\\
v :=& \frac{\beta pq(q-fgp)}{(q-p)(p+q)} + \frac{1}{3}\alpha fgq\\
w :=& \frac{q\left(\overline{f}+\overline{g}\right)\left(p^2(\alpha+3\beta)-\alpha q^2\right)+p(f+g)\left(\alpha p^2 - q^2(\alpha+3\beta)\right)}{3(p-q)(p+q)}
\end{aligned}$$

By Lemma 7.3, this is the parametrization of an ellipse centered at w, as desired. As in Lemma 7.3, it is also possible to explicitly calculate its axis and rotation angle, but these expressions become very long. □

In Theorem 7.5 a linear combination of X_2 and X_3 was considered in terms of complex parameters α, β. Below this result is specialized to the case of an affine combination of said centers in terms of a real parameter γ.

Corollary 7.3. *Over the family of 3-periodics interscribed in an ellipse pair in general position (non-concentric, non-axis-aligned), if $\mathcal{X}_\gamma$ is a real affine combination of X_2 and X_3, i.e., $\mathcal{X}_\gamma = (1-\gamma)X_2 + \gamma X_3$ for some fixed $\gamma \in \mathbb{R}$, then its locus is an ellipse. Moreover, as we vary γ, the centers of the loci of the $\mathcal{X}_\gamma$ are collinear.*

Proof. Apply Theorem 7.5 with $\alpha = 1-\gamma, \beta = \gamma$ to get the elliptical loci. As in the end of the proof of Theorem 7.5, the center of the locus of $\mathcal{X}_\gamma$ can be computed

explicitly as

$$\begin{aligned} w &= w_0 + w_1\gamma, \qquad \text{where} \\ w_0 &= \frac{1}{3}\left(q\left(\overline{f}+\overline{g}\right)+p(f+g)\right) \\ w_1 &= \frac{q\left(2p^2+q^2\right)\left(\overline{f}+\overline{g}\right)-p(f+g)\left(p^2+2q^2\right)}{3(p-q)(p+q)} \end{aligned}$$

As $\gamma \in \mathbb{R}$ varies, it is clear the center w sweeps a line. □

We proved that all of the following triangle centers have elliptic loci in the general N=3 Poncelet system, including the barycenter, circumcenter, orthocenter, nine-point center, and de Longchamps point (reflection of the orthocenter about the circumcenter of a triangle):

Observation 7.1. *Amongst the 40k+ centers listed on Kimberling (2019), Kimberling (2020b) identifies about 4.9k which lie on the Euler line. Out of these, only 226 are fixed affine combinations of X_2 and X_3. For $k < 1000$, these amount to $X_k, k =$2, 3, 4, 5, 20, 140, 376, 381, 382, 546, 547, 548, 549, 550, 631, 632.*

Observation 7.2. *The elliptic loci of X_2 and X_4 are axis-aligned with the outer ellipse.*

Experimental evidence suggests the converse of Theorem 7.5 is also true:

Conjecture 4. *Over 3-periodics interscribed between two ellipses in general position, the locus of a triangle center X_k is an ellipse if and only if X_k is a fixed linear combination of X_2 and X_3.*

7.5 Circular loci in the circumcircle family

Referring to Figure 7.8:

Proposition 7.3. *If a triangle center $\mathcal{X}_{\alpha,\beta} = \alpha X_2 + \beta X_3$ is a fixed linear combination of X_2 and X_3 for some $\alpha, \beta \in \mathbb{C}$, its locus over 3-periodics in the non-concentric pair with a circumcircle is a circle centered on $\mathcal{O}_\alpha$ and of radius $\mathcal{R}_\alpha$ given by:*

$$\mathcal{O}_\alpha = \frac{\alpha(f+g)}{3}, \quad \mathcal{R}_\alpha = \frac{|\alpha f g|}{3}$$

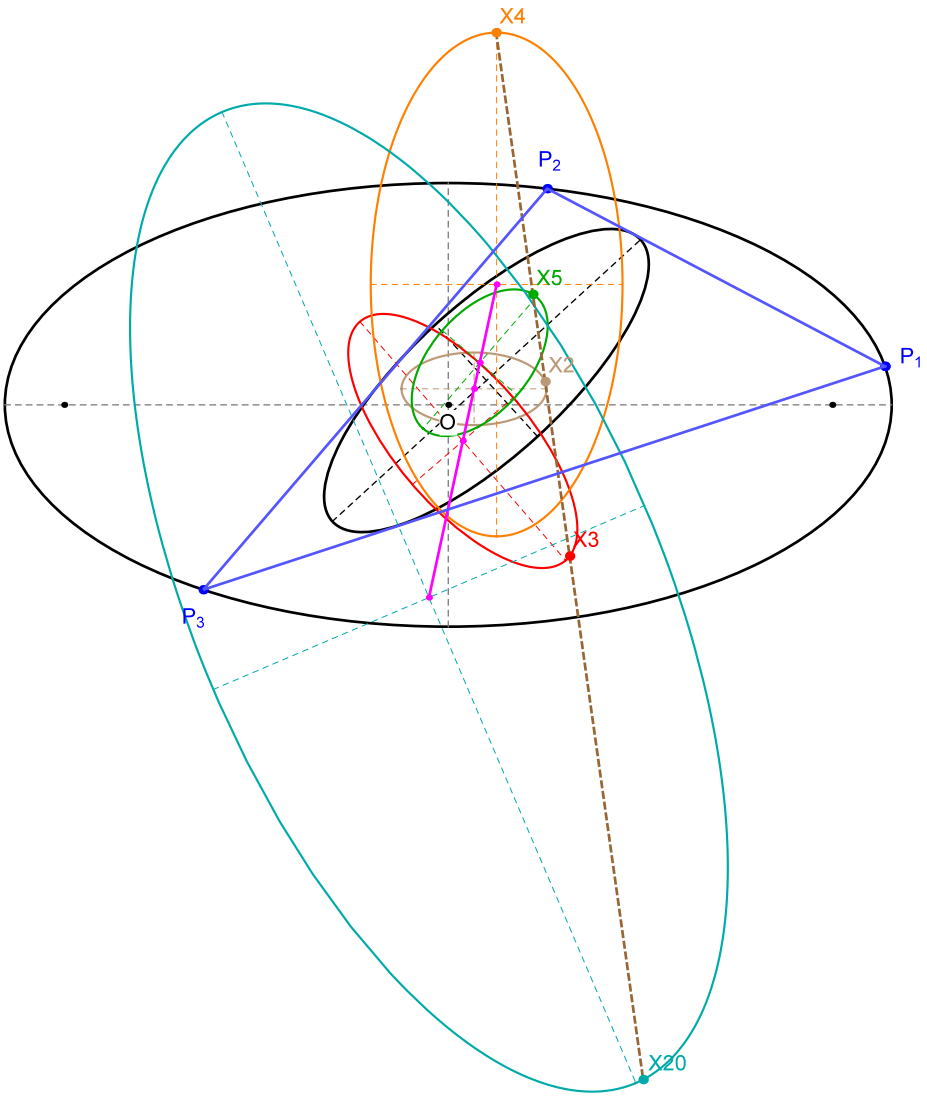

Figure 7.7: A 3-periodic is shown interscribed between two non-concentric, non-aligned ellipses (black). The loci of X_k, $k = 2, 3, 4, 5, 20$ (and many others) remain ellipses. Those of X_2 and X_4 remain axis-aligned with the outer one. Furthermore the centers of all said elliptic loci are collinear (magenta line). Video

Furthermore, the center and radius of the locus do not depend on β since the circumcenter X_3 is stationary at the origin of this system.

Proof. Since, z_1, z_2, z_3 are the 3 vertices of the Poncelet triangle inscribed in the unit circle, its barycenter and circumcenter are given by $X_2 = (z_1+z_2+z_3)/3$ and $X_3 = 0$, respectively. We define $\mathcal{X}_{\alpha,\beta} := \alpha X_2 + \beta X_3 = \alpha(z_1+z_2+z_3)/3$. Using Definition 7.1, we get $\mathcal{X}_{\alpha,\beta} = \alpha(f+g+\lambda\overline{f}\,\overline{g})/3 = \alpha(f+g)/3 + \lambda(\alpha\overline{f}\,\overline{g})/3$, where the parameter λ varies on the unit circle $\mathbb{T}$. Thus, the locus of $\mathcal{X}_\gamma$ over the Poncelet family of triangles is a circle with center $\mathcal{O}_\alpha := \alpha(f+g)/3$ and radius $\mathcal{R}_\alpha := |\alpha\overline{f}\,\overline{g}|/3 = |\alpha fg|/3$. □

Using $\alpha = 1-\gamma, \beta = \gamma$ for a fixed $\gamma \in \mathbb{R}$ in Proposition 7.3, we get:

Corollary 7.4. *If a triangle center $\mathcal{X}_\gamma = (1-\gamma)X_2 + \gamma X_3$ is a real affine combination of X_2 and X_3 for some $\gamma \in \mathbb{R}$, its locus over 3-periodics in the non-concentric pair with a circumcircle is a circle. Moreover, as we vary γ, the centers of these loci are collinear with the fixed circumcenter.*

Many triangle centers on Kimberling (2019) are affine combinations of the barycenter X_2 and circumcenter X_3. See Observation 7.1 for a partial list.

Observation 7.3. *For a generic triangle, only X_{98}, and X_{99} are simultaneously on the Euler line and on the circumcircle. However these are not linear combinations of X_2 and X_3. Still, if a triangle center is always on the circumcircle of a generic triangle (there are many of these, see Weisstein (2019, Circumcircle)), its locus over 3-periodics in the non-concentric pair with circumcircle is trivially a circle.*

Corollary 7.5. *Over the family of 3-periodics inscribed in a circle and circumscribing a non-concentric inellipse centered at O_c, the locus of X_k, k in 2,4,5,20 are circles whose centers are collinear. The locus of X_5 is centered on O_c. The centers and radii of these circular loci are given by:*

$$O_2 = \frac{f+g}{3}, \quad O_4 = f+g, \quad O_5 = \frac{f+g}{2}, \quad O_{20} = -(f+g)$$
$$r_2 = \frac{|fg|}{3}, \qquad r_4 = |fg|, \qquad r_5 = \frac{|fg|}{2}, \qquad r_{20} = |fg|$$

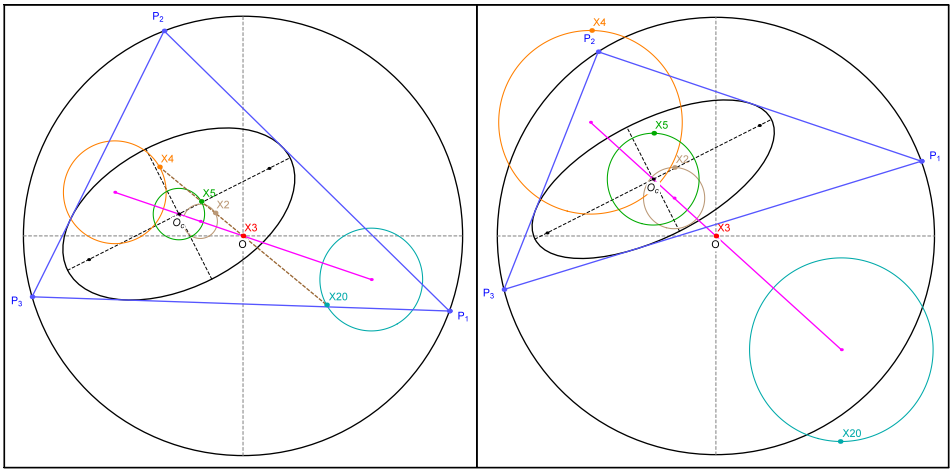

Figure 7.8: **Left:** 3-periodic family (blue) in the pair with circumcircle where the caustic contains X_3, i.e., all 3-periodics are acute. The loci of X_4 and X_{20} are interior to the circumcircle. **Right:** X_3 is exterior to the caustic, and 3-periodics can be either acute or obtuse. Equivalently, the locus of X_4 intersects the circumcircle. In both cases (left and right), the loci of X_k, k in 2,4,5,20 are circles with collinear centers (magenta line). The locus of X_5 is centered on O_c. The center of the X_2 locus is at $2/3$ along OO_c. Video

Proof. As in Corollary 7.4, we can use Proposition 7.3 with $\gamma = 0, -2, -1/2, 4$ to get the center and radius for X_2, X_4, X_5, X_{20}, respectively. All of these centers are real multiples of $f + g$, so they are all collinear. Moreover, the center O_5 of the circular loci of X_5 is $(f+g)/2$, that is, the midpoint of the foci of the inellipse, or in other words, the center O_c of the inellipse. □

Referring to Figure 7.8:

Observation 7.4. *The family of 3-periodics in the pair with circumcircle includes obtuse triangles if and only if X_3 is exterior to the caustic.*

This is due to the fact that when X_3 is interior to the caustic, said triangle center can never be exterior to the 3-periodic. Conversely, if X_3 is exterior, it must also be external to some 3-periodic, rendering the latter obtuse.

Author	Year	Technique	Reference
D. Reznik	2011	Experimental Video	Reznik (2011)
O. Romaskevich	2014	Complex Analytic Geometry	Romaskevich (2014)
R. Garcia	2016	Real Analytic Geometry	Garcia (2019)
(in this book)	2021	Specialize X_1 locus to confocal pair	Corollary 7.1
M. Helman et al.	2021	3-Center Linear Combination	see †

Table 7.1: Various proof methods for the ellipticity of X_1 over billiard 3-periodics. † Helman, Laurain, Reznik, et al. (2021)

7.6 Epilogue: a theory for elliptic loci in the confocal pair

Proposition 7.4. *If a triangle center X_k is stationary over a Poncelet 3-periodic family, then the locus of any triangle center $\mathcal{X}$ which is a fixed linear combination of X_2, X_3, X_k will be an ellipse.*

Proof. The triangle center $\mathcal{X} = \alpha X_2 + \beta X_3 + \gamma X_k$ is the linear combination $\mathcal{X}_{\alpha,\beta} := \alpha X_2 + \beta X_3$ under a fixed translation by γX_k, because both γX_k and X_k are fixed over the family. □

This entails the most compact rendition of the following result (appearing originally in Helman, Laurain, Reznik, et al. (2021)):

Corollary 7.6. *Over billiard 3-periodics, the locus of X_1 is an ellipse.*

Proof. For any triangle, X_1 can be expressed as the linear combination $X_1 = \alpha X_2 + \beta X_3 + \gamma X_9$ of X_2, X_3 and X_9 with:

$$\alpha = \frac{6}{\rho + 2}, \quad \beta = \frac{2\rho}{\rho + 2}, \quad \gamma = \frac{-\rho - 4}{\rho + 2}$$

where $\rho = r/R$, is the ratio of inradius to circumradius. In Reznik, Garcia, and Koiller (2020a) we showed that over the confocal family, X_9 is stationary and ρ is invariant, so the claim follows. □

Table Table 7.1 shows a history of proof techniques of the ellipticity of X_1 over billiard 3-periodics:

We can expand the above result to other triangle centers in the confocal pair, as many of these are fixed linear combinations of X_2, X_3, and X_9.

Proposition 7.5. *In the confocal pair, from X_1 to X_{200}, the loci of X_k are ellipses, k =1, 2, 3, 4, 5, 7, 8, 10, 11, 12, 20, 21, 35, 36, 40, 46, 55, 56, 57, 63, 65, 72, 78, 79, 80, 88†, 84, 90, 100, 104, 119, 140, 142, 144, 145, 149, 153, 162†, 165, 190†, 191, 200.*

Proof. As in the previous corollary, one can write X_1 as a fixed linear combination of X_2, X_3, and X_9, given that the ratio $\rho = r/R$ is constant in the confocal pair. In Helman, Laurain, Reznik, et al. (2021, Table 2), a table of fixed coefficients α, β, γ is provided expressing each of the triangle centers in the claim as fixed linear combinations of X_1, X_2 and X_3. Table 7.2 reproduces those results. Therefore all triangle centers in the claim (except for X_{88}, X_{162}, and X_{190}) are fixed linear combinations of X_1, X_2, and X_3, and therefore they are fixed linear combinations of X_2, X_3, and X_9 as well. By Proposition 7.4, given that X_9 is stationary over the confocal family, this implies the loci of all these triangle centers are ellipses. □

†Note: the loci of X_{88}, X_{162}, and X_{190} (called "swans" before) are also ellipses because by definition they lie on the circumconic centered on X_9, see Kimberling (2019, X(9)).

Referring to Figure 7.9:

Proposition 7.6. *In the confocal pair, the locus of $\mathcal{X} = \alpha X_2 + \beta X_3$ for $\alpha, \beta \in \mathbb{R}$ is a circle when:*

$$\left(\frac{\alpha}{\beta}\right)_{\pm} = \frac{\delta - 3ab \pm 2\left(a^2 + b^2\right)}{2ab}$$

Proof. By Lemma 7.3, this will happen when $|u| + |v| = \big||u| - |v|\big|$ with u, v from Theorem 7.5. In the confocal pair, when $\alpha, \beta \in \mathbb{R}$, both u and v are real numbers as well. Thus, this condition holds if and only if either $u = 0$ or $v = 0$. The ratios α/β that yield circular loci can then be computed directly. □

Observation 7.5. *It follows that $(\alpha/\beta)_+ + (\alpha/\beta)_- = -3$.*

Definition 7.2 (Degenerate Locus)**.** *When the elliptic locus of a triangle center is a segment, i.e., one of its axes has shrunk to zero, we will call it "degenerate".*

Proposition 7.7. *Let $\mathcal{X}$ be a fixed linear combination of X_2, X_3, and X_k, where X_k is some stationary center over the family of 3-periodics. As the vertices of the 3-periodics sweep the outer ellipse monotonically, the path of $\mathcal{X}$ in its elliptical locus is monotonic as well, except for when this locus is degenerate.*

X_k	α	β	γ
X_1	1	0	0
X_2	0	1	0
X_3	0	0	1
X_4	0	3	-2
X_5	0	$\frac{3}{2}$	$-\frac{1}{2}$
X_7	$\frac{2\rho+4}{\rho+4}$	$\frac{3\rho}{\rho+4}$	$\frac{-4\rho}{\rho+4}$
X_8	-2	3	0
X_9	$\frac{-\rho-2}{\rho+4}$	$\frac{6}{\rho+4}$	$\frac{2\rho}{\rho+4}$
X_{10}	$-\frac{1}{2}$	$\frac{3}{2}$	0
X_{11}	$\frac{1}{1-2\rho}$	$\frac{-3\rho}{1-2\rho}$	$\frac{\rho}{1-2\rho}$
X_{12}	$\frac{1}{1+2\rho}$	$\frac{3\rho}{1+2\rho}$	$\frac{-\rho}{1+2\rho}$
X_{20}	0	-3	4
X_{21}	0	$\frac{3}{2\rho+3}$	$\frac{2\rho}{2\rho+3}$
X_{35}	$\frac{1}{2\rho+1}$	0	$\frac{2\rho}{2\rho+1}$
X_{36}	$\frac{1}{1-2\rho}$	0	$\frac{-2\rho}{1-2\rho}$
X_{40}	-1	0	2
X_{46}	$\frac{1+\rho}{1-\rho}$	0	$\frac{-2\rho}{1-\rho}$
X_{55}	$\frac{1}{1+\rho}$	0	$\frac{\rho}{1+\rho}$
X_{56}	$\frac{1}{1-\rho}$	0	$\frac{-\rho}{1-\rho}$
X_{57}	$\frac{2+\rho}{2-\rho}$	0	$\frac{-2\rho}{2-\rho}$
X_{63}	$\frac{-\rho-2}{\rho+1}$	$\frac{3}{\rho+1}$	$\frac{2\rho}{\rho+1}$

X_k	α	β	γ
X_{65}	$\rho+1$	0	$-\rho$
X_{72}	$-\rho-2$	3	ρ
X_{78}	$\frac{\rho+2}{\rho-1}$	$\frac{-3}{\rho-1}$	0
X_{79}	1	$\frac{6\rho}{2\rho+3}$	$\frac{-6\rho}{2\rho+3}$
X_{80}	$\frac{2\rho+1}{1-2\rho}$	$\frac{-6\rho}{1-2\rho}$	$\frac{2\rho}{1-2\rho}$
X_{84}	$\frac{-\rho-2}{\rho}$	$\frac{6}{\rho}$	$\frac{2\rho-4}{\rho}$
X_{90}	$\frac{-(\rho+1)^2}{\rho^2+2\rho-1}$	$\frac{6\rho}{\rho^2+2\rho-1}$	$\frac{2\rho(\rho-1)}{\rho^2+2\rho-1}$
X_{100}	$\frac{2}{2\rho-1}$	$\frac{-3}{2\rho-1}$	$\frac{2\rho}{2\rho-1}$
X_{104}	$\frac{-2}{2\rho-1}$	$\frac{3}{2\rho-1}$	$\frac{2\rho-2}{2\rho-1}$
X_{119}	$\frac{1}{2\rho-1}$	$\frac{3\rho-3}{2\rho-1}$	$\frac{-\rho+1}{2\rho-1}$
X_{140}	0	$\frac{3}{4}$	$\frac{1}{4}$
X_{142}	$\frac{\rho+2}{2\rho+8}$	$\frac{3\rho+6}{2\rho+8}$	$\frac{-2\rho}{2\rho+8}$
X_{144}	$\frac{-4\rho-8}{\rho+4}$	$\frac{12-3\rho}{\rho+4}$	$\frac{8\rho}{\rho+4}$
X_{145}	$\frac{4}{7}$	$\frac{3}{7}$	0
X_{149}	$\frac{-4}{6\rho-3}$	$\frac{-6\rho+9}{6\rho-3}$	$\frac{12\rho-8}{6\rho-3}$
X_{153}	$\frac{4}{6\rho-3}$	$\frac{-6\rho-3}{6\rho-3}$	$\frac{12\rho-4}{6\rho-3}$
X_{165}	$-\frac{1}{3}$	0	$\frac{4}{3}$
X_{191}	-1	$\frac{6}{2\rho+3}$	$\frac{4\rho}{2\rho+3}$
X_{200}	$\frac{\rho+4}{\rho-2}$	$\frac{-6}{\rho-2}$	0

Table 7.2: Triples α, β, γ used to express a given triangle center X_k as the linear combinations $\alpha X_1 + \beta X_2 + \gamma X_3$. Note: $\rho = r/R$. Note also that though the loci of X_{88}, X_{162}, and X_{190} are ellipses over the confocal family (in fact, they sweep the elliptic billiard), they are not included since they are not fixed linear combinations.

Proof. By Theorem 7.5, the locus of $\mathcal{X}$ can be parametrized by $u\lambda + v\frac{1}{\lambda} + w$ for some $u, v, w \in \mathbb{C}$, where λ sweeps the unit circle in $\mathbb{C}$ in the same direction as the 3-periodic vertices sweep the outer ellipse of the Poncelet pair. We can thus parametrize $\mathcal{X}$ as $\mathcal{X}(t) = ue^{it} + ve^{-it} + w$. If either $u = 0$ or $v = 0$, it is clear from this parametrization that $\mathcal{X}$ sweeps its locus monotonically. Thus, we can now assume that $u \neq 0$ and $v \neq 0$.

Denoting $u = u_0 + iu_1$ and $v = v_0 + iv_1$ with $u_0, u_1, v_0, v_1 \in \mathbb{R}$, we can directly compute

$$\left|\frac{d}{dt}\mathcal{X}(t)\right|^2 = |u|^2 + |v|^2 + 2\sin(2t)(u_2v_1 - u_1v_2) - 2\cos(2t)(u_1v_1 + u_2v_2)$$

Since $(u_2v_1 - u_1v_2)^2 + (u_1v_1 + u_2v_2)^2 = (u_1^2 + u_2^2)(v_1^2 + v_2^2) = |u|^2|v|^2$, there is some angle $\phi \in [0, 2\pi)$ (the angle between the vectors (u_1, u_2) and (v_1, v_2)) such that $u_1v_1 + u_2v_2 = |u||v|\cos\phi$ and $u_2v_1 - u_1v_2 = |u||v|\sin\phi$. Substituting this back in the previous equation, we derive

$$\begin{aligned}\left|\frac{d}{dt}\mathcal{X}(t)\right|^2 &= |u||v|\left(\frac{|u|}{|v|} + \frac{|v|}{|u|} + 2\sin(2t)\sin(\phi) - 2\cos(2t)\cos(\phi)\right)\\ &= |u||v|\left(\frac{|u|}{|v|} + \frac{|v|}{|u|} - 2\cos(2t+\phi)\right) \geqslant |u||v|\left(\frac{|u|}{|v|} + \frac{|v|}{|u|} - 2\right)\end{aligned}$$

By AM-GM inequality, this last quantity is always strictly greater than 0 unless $|u| = |v|$. If $|u| \neq |v|$, we will have $\left|\frac{d}{dt}\mathcal{X}(t)\right|^2 > 0$, and hence the velocity vector never vanishes, meaning that the $\mathcal{X}$ sweeps its smooth locus monotonically. By Lemma 7.3, this means that $\mathcal{X}$ sweeps its locus monotonically except when this locus is degenerate.

□

In Section 5.12 we provided a continuity argument for the three turns executed by a triangle center over a traversal of the billiard 3-periodic family.

Remark 7.3. *In Daepp et al. (2019, Lemma 3.4, p. 28) it is shown that (i) the complex argument of the Blaschke product is monotonic on the unit circle, and that (ii) for each λ there are 3 solutions for the equation $B(z) = \lambda$. This means that as λ sweeps the unit circle monotonically, the 3-periodics sweep the outer Poncelet ellipse monotonically and in the same direction as λ. Moreover for every 3 full cycles of λ over the complex the unit circle, each vertex of the 3-periodics sweep the outer ellipse exactly once.*

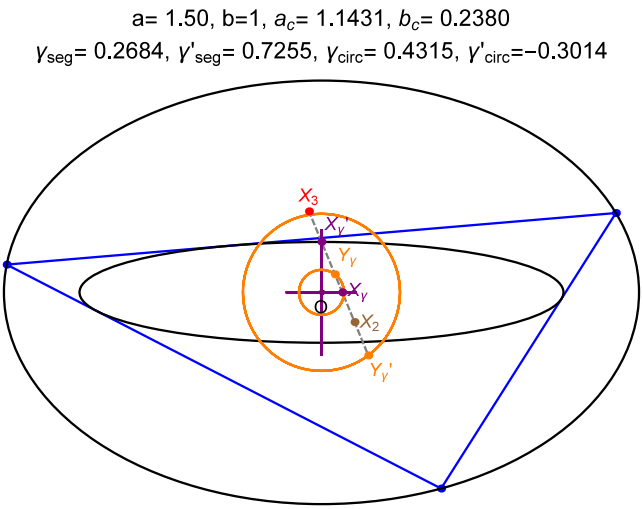

Figure 7.9: A 3-periodic (blue) in a pair of confocal ellipses (black) with $a/b = 1.5$. Also shown are two degenerate (segment-like) loci (purple) obtained with $\gamma \simeq \{.27, .73\}$ and two circular loci (orange), obtained with $\gamma \simeq \{.43, -.3\}$. Video

Proposition 7.8. *Let $\mathcal{X}$ be a fixed linear combination of X_2, X_3, and X_k, where X_k is some stationary center over the family of 3-periodics. Over a full cycle of 3-periodics, the winding number of $\mathcal{X}$ over its elliptical locus is ± 3, except for when this locus is degenerate.*

Proof. By Theorem 7.5, the locus of $\mathcal{X}$ can be parametrized by $u\lambda + v\frac{1}{\lambda} + w$ for some $u, v, w \in \mathbb{C}$. From Remark 7.3, one can see that the winding number of λ associated to 3-periodics is $+3$ for each full cycle of 3-periodics over the outer Poncelet ellipse. Thus, it is sufficient to prove that the winding number of $\mathcal{X}$ over its elliptical locus is ± 1 as λ goes around the complex unit circle just once.

Since w is the center of the elliptic locus of $\mathcal{X}$ (see Lemma 7.3), we compute the winding number of $\mathcal{X}$ around w. Parametrizing $\mathcal{X}$ as $\mathcal{X}(t) = ue^{it} + ve^{-it} + w$ where $\lambda = e^{it}$, one can directly compute the winding number as in Ahlfors (1979, Lemma 1, p. 114):

$$\frac{1}{2\pi i}\oint_{\mathcal{X}} \frac{d\zeta}{\zeta - w} = \frac{1}{2\pi i}\int_0^{2\pi} \frac{\mathcal{X}'(t)}{\mathcal{X}(t) - w} dt = \text{sign}(|u|^2 - |v|^2)$$

By Lemma 7.3, the only way we can have $|u| = |v|$ is if the locus of $\mathcal{X}$ is

degenerate. Thus, whenever this locus is not degenerate, the winding number of $\mathcal{X}$ around its locus as λ sweeps the unit circle once is equal to 1 if $|u| > |v|$ and -1 when $|u| < |v|$, as desired. □

7.7 Exercises

Exercise 7.1. *Consider a cubic polynomial $p(z) = (z-\alpha_1)(z-\alpha_2)(z-\alpha_3)$ with simple roots α_i (i=1,2,3). Let β_1 and β_2 the roots of $p'(z)$. Consider the family of confocal ellipses having foci β_1 and β_2.*

Show that there exists a unique ellipse $\mathcal{E}$ in this family passing through the midpoints $(\alpha_i + \alpha_j)/2$, and that it is tangent to the sides of the triangle $T = \{\alpha_1, \alpha_2, \alpha_3\}$. This ellipse is known as Steiner innelipse of T.

Conclude that the center of $\mathcal{E}$ is the triangular center X_2 of T and that T is a 3-periodic orbit of a homothetic Poncelet pair.

Exercise 7.2. *Consider an ellipse $\mathcal{E}$ and the set of tangent lines. Show that the set of points of intersection between any two perpendicular tangents to $\mathcal{E}$ lie on a circle. Find the radius and the center of this circle.*

Exercise 7.3. *Consider a circle $\mathcal{C}$ and a point P_0. Consider the family of circles passing through P_0 and internally tangent to $\mathcal{C}$. Show that the set of centers of this family of circles is an ellipse. Find the semiaxes and the foci of the ellipse.*

Exercise 7.4. *In the proof of Proposition 7.2, let $z_1(\lambda)$, $z_2(\lambda)$ and $z_3(\lambda)$ the roots of $E_2(z, \lambda) = 0$, $\lambda \in \mathbb{T}$. Show that the trace of these three curves is an ellipse, i.e., they parametrize the excentral locus.*

Exercise 7.5. *Consider a triangle inscribed in $\mathbb{T}^1$ with vertices w_1^2, w_2^2 and w_3^2. Show that:*

- *The incenter X_1 is $-w_1w_2 - w_1w_3 - w_2w_3$.*
- *The excenters are $w_1w_2 - w_1w_3 - w_2w_3$, $-w_1w_2 + w_1w_3 - w_2w_3$ and $-w_1w_2 - w_1w_3 + w_2w_3$.*
- *The barycenter X_2 is $(w_1^2 + w_2^2 + w_3^2)/3$.*
- *The orthocenter X_4 is $w_1^2 + w_2^2 + w_3^2$.*
- *The nine-point center X_5 is $(w_1^2 + w_2^2 + w_3^2)/2$.*

Exercise 7.6. *Derive the conditions under which a locus of a triangle center becomes degenerate (segment-like) over billiard 3-periodics.*

7.8 Research questions

Question 7.1. *In Question 2.1 one is asked to prove that the family of billiard 3-periodic extouch triangles is Ponceletian. Prove that over this family the loci of X_k, $k = 2, 3, 4, 5, 20$ are ellipses, derive their semiaxes. See it Live.*

Question 7.2. *Prove Conjecture 2 and/or Conjecture 3.*

Question 7.3. *Prove (or disprove) Conjecture 4.*

Question 7.4. *Recall the Brocard porism, described in Section 4.4.3. The Brianchon point of the Brocard inellipse is X_6 (stationary over the porism), i.e., the sidelines of the Brocard porism family touch the inellipse at the vertices of the X_6-cevian. Weisstein (2019, Symmmedial triangle) calls this the* symmedial *triangle. Show that over Brocard porism 3-periodics, (i) the symmedial triangles are Ponceletian, (ii) compute the center and semiaxes of its inellipse, (iii) show that the locus of X_k, $k = 13, 14, 15, 16$ are circles. See it Live.*

8 The Focus-Inversive Family

This chapter describes a multi-talented triangle family directly derived from billiard 3-periodics. We call it the *focus-inversive* family of triangles. These are inversive images of billiard N-periodics with respect to a circle centered on (say the left) focus. The $N = 3$ case is shown in Figure 8.1. Amongst its curious properties, we show that: (i) it has a stationary triangle center (the Gergonne point), (ii) its perimeter and sum of cosines is invariant (mirroring the behavior of billiard 3-periodics), (iii) it is also a billiard 3-periodic family but of a gyrating elliptic billiard, (iv) the product of its area with that of focus-inversives with respect to the (right) focus is invariant, (v) that any triangle center whose locus is an ellipse in the elliptic billiard traces out a *circle* over focus-inversives, and finally, that (vi) the loci of its three centroids (vertex, perimeter, and area) are all circles! What's more, most of these properties generalize to focus-inversives for $N > 3$, though we leave these to part II of this book.

8.1 Non-Ponceletian

A known result is that the inversive image of an ellipse with respect to one of its foci is a loopless Pascal's Limaçon, see Weisstein (ibid.). Therefore, the focus-inversive will be inscribed in such a curve and is therefore non-Ponceletian. In-

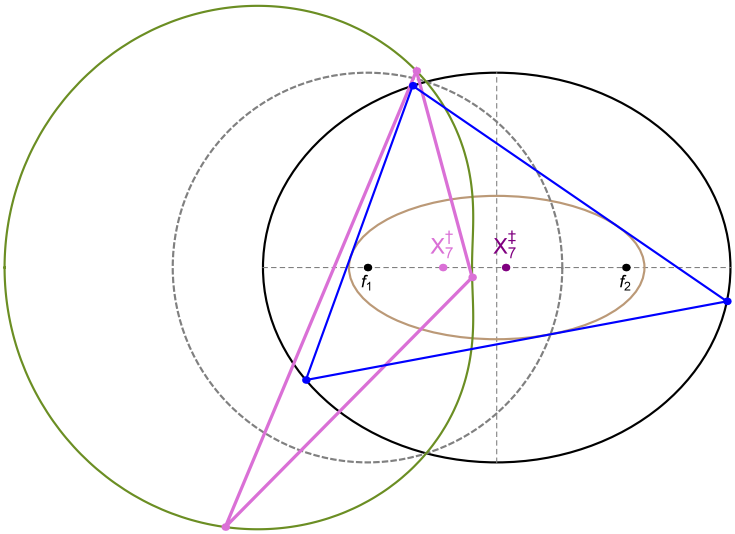

Figure 8.1: The $N = 3$ focus-inversive family (pink), i.e., the inversive image of billiard 3-periodics (blue) with respect to a focused-centered circle $\mathcal{C}$ (dashed gray). Focus-inversives are inscribed in a loopless Pascal's Limaçon (olive green). Both perimeter and sum of cosines are invariant. The Gergonne point $X_7^\dagger$ is stationary. Also shown is $X_7^\ddagger$, the inversive image of $X_7^\dagger$ with respect to $\mathcal{C}$, inquired about in Exercise 8.1. Live

deed, the caustic is also non-elliptic, as shown in Figure 8.2: a continuously increasing billiard aspect ratio will transition the caustic from (i) a regular curve, to (ii) one with a self-intersection and two cusps, to (iii) a non-compact curve with two infinite branches.

8.2 A stationary point

Recall in the confocal family the Mittenpunkt X_9 is stationary. Henceforth we shall append a † to all quantities referring to the focus-inversive family. Let a, b denote the semiaxes of the pre-inversion billiard which we assume to be centered on $[0, 0]$ and be axis-parallel to x, and y respectively. Let ρ denote the radius of $f_1 = [-c, 0]$, the (left) focus-centered inversion circle, $c^2 = a^2 - b^2$. Interestingly:

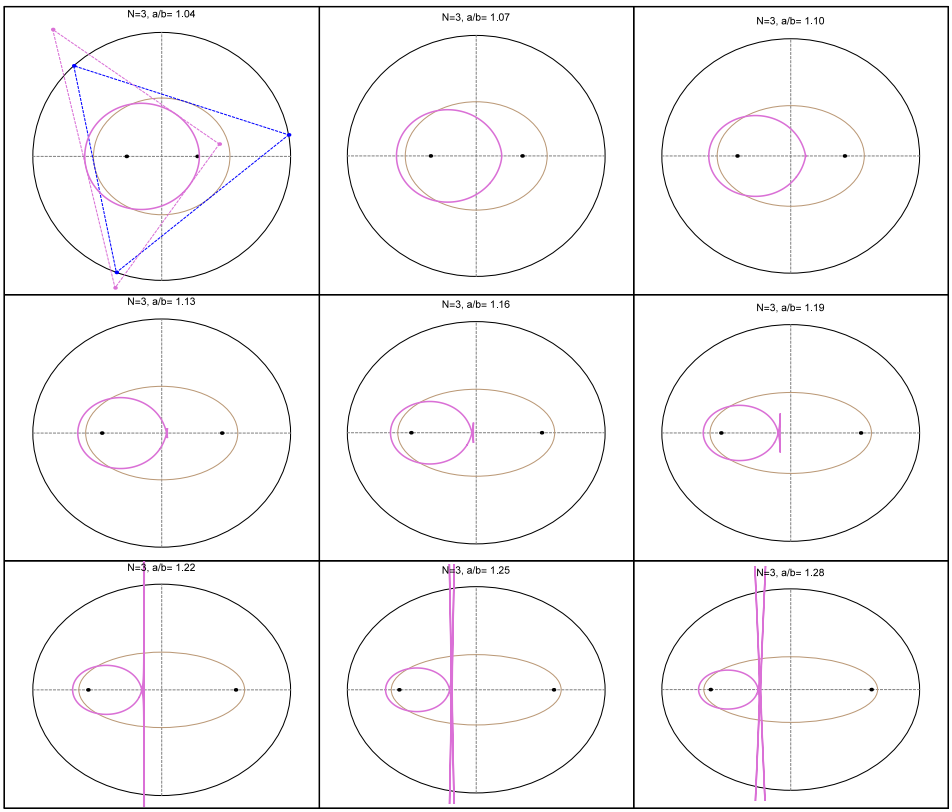

Figure 8.2: Non-conic caustic (pink) to the focus-inversive family (pink). A billiard 3-periodic (dashed blue) and the corresponding focus-inversive triangle are shown at the top-left picture only. The billiard caustic is shown on every frame (brown). From left-to-right, top-to-bottom, a/b is increased in small steps. Over this range, the caustic transitions from (i) a regular curve, to (ii) a curve with one self-intersection and two cusps, to (iii) a non-compact curve. Live

Proposition 8.1. *The Gergonne point $X_7^\dagger$ of focus-inversives is stationary on the major axis of the pre-image confocal pair. Its coordinates are given by:*

$$X_7^\dagger = \left[c\left(1 - \frac{\rho^2}{\delta + c^2}\right), 0 \right]$$

where as before: $\delta^2 = a^4 - (ab)^2 + b^4$.

8.3 Billiard-like invariants

The following two surprising invariants – constant perimeter and sum of cosines – are analogues to those displayed by billiard 3-periodics. Interestingly they are not consequences of elementary principles or transformations.

Proposition 8.2. *The perimeter $L^\dagger$ of focus-inversives is invariant and given by:*

$$L^\dagger = \rho^2 \frac{\sqrt{\left(8\,a^4 + 4\,a^2b^2 + 2\,b^4\right)\delta + 8\,a^6 + 3\,a^2b^4 + 2\,b^6}}{a^2b^2}$$

Let $\theta_i^\dagger$ denote angles internal to focus-inversives.

Proposition 8.3. *The sum of internal angle cosines of focus-inversives is invariant and given by:*

$$\sum \cos\theta_{1,i}^\dagger = \frac{\delta(a^2 + c^2 - \delta)}{a^2c^2}$$

8.4 The rotating billiard table

Recall that in Figure 2.6 we introduced the concept of the *circumbilliard*: given a triangle T, this is the X_9-centered circumellipse of which T is a billiard 3-periodic (circumellipse normals are angular bisectors). Let $\mathcal{C}^\dagger$ denote the (moving) circumbilliard ($X_9^\dagger$-centered circumellipse) of focus-inversives. Indeed, and referring to Figure 8.3, focus-inversives are billiard 3-periodics of a rigidly-moving virtual elliptic billiard (see Exercise 8.4):

Proposition 8.4. *Over focus-inversives, the semiaxes $a^\dagger, b^\dagger$ of $\mathcal{C}^\dagger$ are invariant and given by:*

$$\begin{aligned} a^\dagger &= \rho\, k_1 \sqrt{k_2\,(\delta + a\,c)} \\ b^\dagger &= \rho\, k_1 \sqrt{k_2\,(\delta - a\,c)} \end{aligned}$$

where:

$$\begin{aligned} k_1 &= \frac{c\sqrt{2}}{k_3} \sqrt{\left(8\,a^4 + 4\,a^2b^2 + 2\,b^4\right)\delta + 8\,a^6 + 3\,a^2b^4 + 2\,b^6} \\ k_2 &= 2a^2 - b^2 - \delta \\ k_3 &= 2ab^2 \left(\left(2\,a^2 - b^2\right)\delta + 2\,a^4 - 2\,a^2b^2 - b^4\right) \end{aligned}$$

Proposition 8.5. *Over the 3-periodic family, the Mittenpunkt $X_9^\dagger$ of focus-inversive triangles moves along a circle with center and radius given by:*

$$\begin{aligned} C_9^\dagger &= \left[-c\left(1 + \rho^2 \frac{1}{2b^2}\right), 0\right] \\ R_9^\dagger &= \rho^2\, \frac{2a^2 - b^2 - \delta}{2ab^2} \end{aligned}$$

8.5 Invariant area product

Let $A_1^\dagger$ (resp. $A_2^\dagger$) denote the area of the f_1- (resp. f_2) inversive triangle family. Referring to Figure 8.4:

Proposition 8.6. *For $N = 3$, the area product $A_1^\dagger A_2^\dagger$ of the two focus-inversive triangles is given by:*

$$A_1^\dagger A_2^\dagger = \frac{\rho^8}{8a^8b^2} \left[\left(a^4 + 2\,a^2b^2 + 4\,b^4\right)\delta + \frac{3a^4b^2}{2} + a^6 + 4\,b^6\right]$$

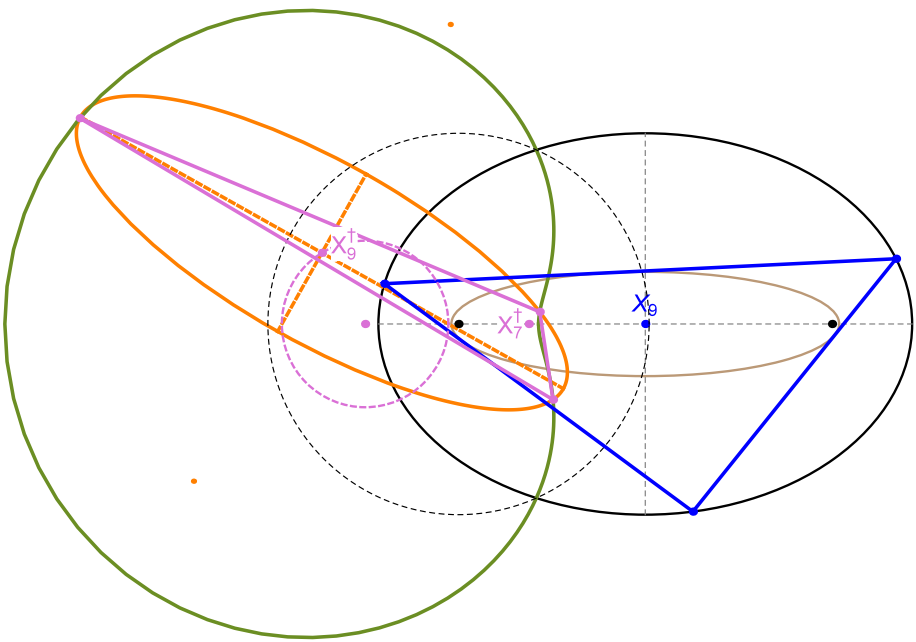

Figure 8.3: The moving circumbilliard (orange) to focus-inversives (pink) rigidly translate and rotate (invariant semiaxes). Their center $X_9^\dagger$ sweeps a circle. The location of the stationary Gergonne point $X_7^\dagger$ is also shown. Video 1, Video 2

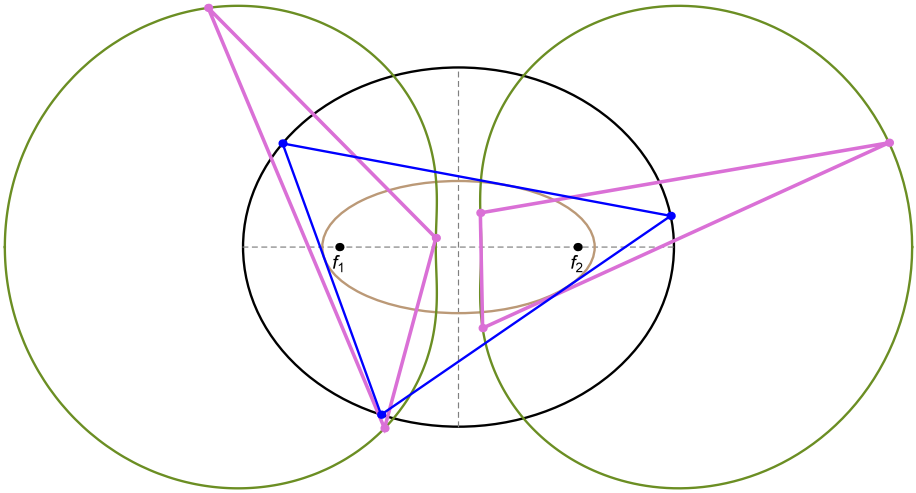

Figure 8.4: The area product of f_1- and f_2-inversive triangles (pink) is invariant. Video, Live

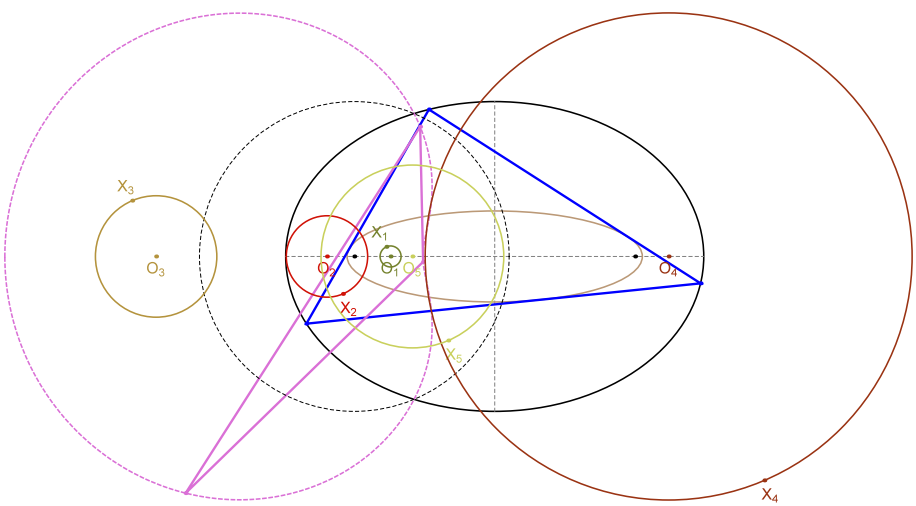

Figure 8.5: A focus-inversive 3-periodic (pink) is shown inscribed in Pascal's Limaçon (dashed pink). Also shown are the circular loci of $X_k^\dagger$, $k = 1, 2, 3, 4, 5$ whose centers O_i all lie on the billiard's major axis. Video, Live

8.6 Circular loci galore!

We saw above that the locus of $X_9^\dagger$ is a circle. A remarkable property of the focus-inversive family is its ability to produce circular loci of many triangle centers. Referring to Figure 8.5, through CAS-assisted simplification we obtain:

Proposition 8.7. *The locus of $X_1^\dagger$ is the circle given by:*

$$C_1^\dagger = \left[c\left(-1+\rho^2\frac{-2a^2+b^2+2\delta}{2b^4}\right),0\right]$$
$$R_1^\dagger = \rho^2\frac{-2\delta^2+b^4+(2a^2-b^2)\delta}{2ab^4}$$

Proposition 8.8. *The locus of $X_2^\dagger$ is the circle given by:*

$$C_2^\dagger = \left[-c\left(1+\rho^2\frac{2a^2-b^2-\delta}{3a^2b^2}\right),0\right]$$
$$R_2^\dagger = \rho^2\frac{2a^2-b^2-\delta}{3ab^2}$$

Proposition 8.9. *The locus of $X_3^\dagger$ is the circle given by:*

$$C_3^\dagger = \left[-c\left(1+\rho^2\frac{a^2+b^2}{2b^4}\right),0\right]$$
$$R_3^\dagger = \rho^2\frac{a(-b^2+\delta)}{2b^4}$$

Proposition 8.10. *The locus of $X_4^\dagger$ is the circle given by:*

$$C_4^\dagger = \left[c\left(-1+\rho^2\frac{(b^2+\delta)\delta}{a^2b^4}\right),0\right]$$
$$R_4^\dagger = \rho^2\frac{c^2(b^2+\delta)}{ab^4}$$

Proposition 8.11. *The locus of $X_5^\dagger$ is the circle given by:*

$$C_5^\dagger = \left[c\left(-1+\rho^2\frac{a^4-3a^2b^2+2b^4+2b^2\delta}{4a^2b^4}\right),0\right]$$
$$R_5^\dagger = \rho^2\frac{(3a^2-2b^2)b^2+(a^2-2b^2)\delta}{4ab^2}$$

Proposition 8.12. *The locus of $X_{100}^{\dagger}$ is the circle given by:*

$$C_{100}^{\dagger} = \left[-c\left(1+\rho^2\frac{1}{b^2}\right), 0\right]$$
$$R_{100}^{\dagger} = \rho^2\frac{a}{b^2}$$

Note: The locus of $X_{11}^{\dagger}$ is also a circle, see Exercise 8.5.

8.7 A rule for circular loci?

Recall Section 6.6.1 where 42 triangle centers are identified (from within the first 200 on Kimberling (2019)), whose loci over billiard 3-periodics are ellipses.

Observation 8.1. *Amongst the first 200 triangle centers listed on Kimberling (ibid.), the following triangle centers $X_k^{\dagger}$ sweep conics over the focus-inversive family:*

- *Circles (40): 1, 2, 3, 4, 5, 8, 9, 10, 11, 12, 20, 21, 35, 36, 40, 46, 55, 56, 57, 63, 65, 72, 78, 79, 80, 84, 90, 100, 104, 119, 140, 142, 144, 145, 149,* ***150***[1]*, 153, 165, 191, 200.*
- *Ellipses (4): 69, 75, 85, 86.*

Comparing these with the list in Section 6.6.1 for the confocal family, one realizes that the only ones missing are X_7 (stationary over the inversive family) and the "swans" X_k, $k=88$, 162, and 190. i.e., triangle centers which by construction lie on the billiard, see Figure 8.6.

Experimentally, in the range $k\leqslant 1000$, if the locus of X_k is an ellipse over billiard 3-periodics (excluding the cases where the locus is the billiard itself), then the locus of $X_k^{\dagger}$ over the focus-inversive family is a circle. Therefore:

Conjecture 5. *If the the locus of some triangle center X is an ellipse over billiard 3-periodics, then the locus of $X^{\dagger}$ over the inversive family is a circle.*

The following cases do not invalidate the conjecture but are noteworthy:

[1] See Question 8.1.

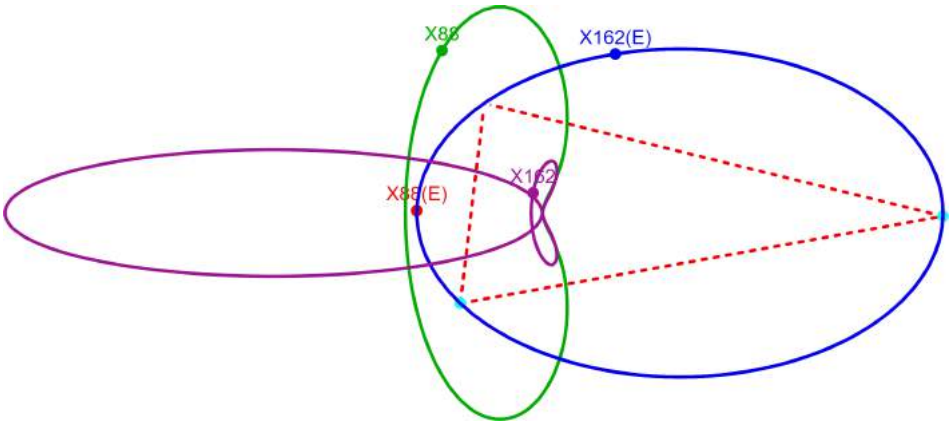

Figure 8.6: Over billiard 3-periodics (dashed red) the loci of both X_{88} and X_{162} coincide with the billiard (blue). However, when taken as centers of the the focus-inversive triangles (not shown), their loci are clearly non-elliptic (green and purple). Live app: X88+X162, X88+X100

- Though X_{100} is a swan, its focus-inversive locus is circular.
- Though X_{658} is swan, its focus-inversive locus is an ellipse.
- Though the locus of X_{150} is non-elliptic over billiard 3-periodics, that of $X_{150}^{\dagger}$ is a circle, see Figure 8.7.
- Though the billiard locus of X_{934} (blue) is a curve with two self-intersections, its focus-inversive locus is a circle, see it Live.

8.7.1 Centroidal loci: a tale of three circles

Let C_0, C_1, C_2 denote the vertex, perimeter, and area centroids of polygon, respectively. In Schwartz and Tabachnikov (2016b, Thm 1) it was shown that the loci of C_0, C_2 over Poncelet families are ellipses, though this not hold in general for C_1.

For triangles, $C_0 = C_2 = X_2$ and $C_1 = X_{10}$, see Weisstein (2019, Spieker Center). Per above we already know that the loci of X_2 and X_{10} over the focus-inversive family are circles. Therefore, and referring to Figure 8.8:

Corollary 8.1. *The loci of the $C_i^{\dagger}$, $i = 1, 2, 3$ of the focus-inversive family are circles.*

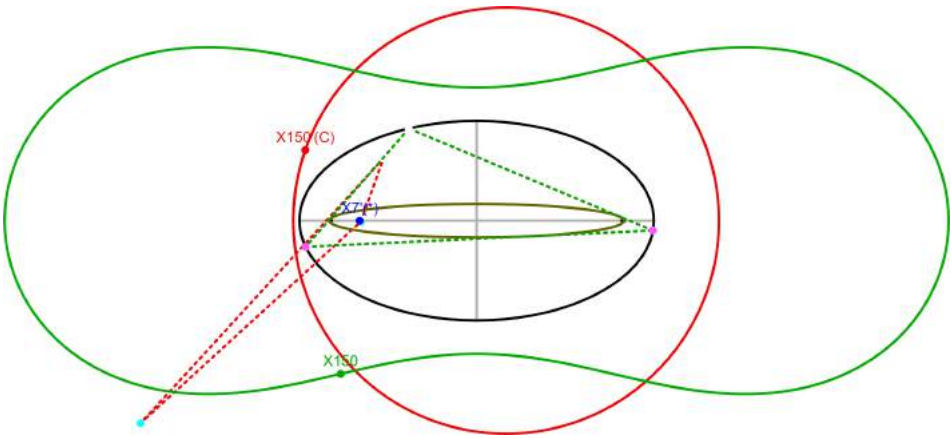

Figure 8.7: Though over billiard 3-periodics the locus of X_{150} is non-elliptic, its locus over the focus-inversive family is a circle. Live.

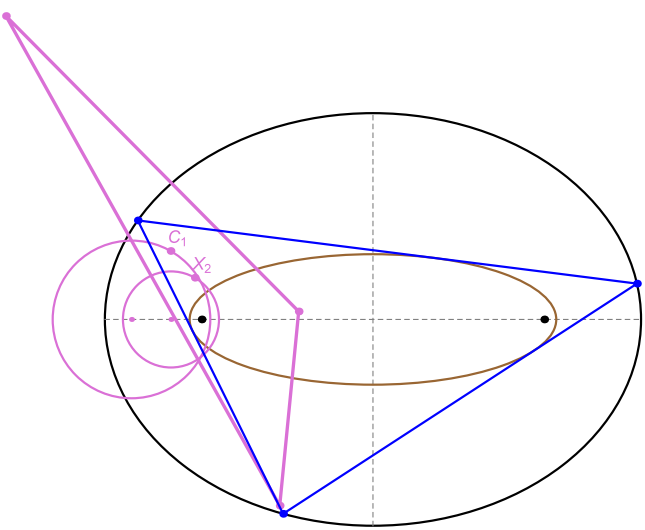

Figure 8.8: Circular locus of the focus-inversive X_2 and the perimeter centroid $C_1^\dagger = X_{10}^\dagger$. Note that for triangles, the former coincides with both the vertex and area centroids. App

8.8 A focus-inversive Doppelgänger

Corollary 4.4 in Section 4.1 states that the poristic family is the polar image of billiard 3-periodics with respect to a circle of radius ρ centered on a focus. Let R and d denote the radius of the poristic circumcircle and $d = |X_3 - X_1|$. If a, b are the semiaxes of the outer ellipse in the confocal pre-image, then these can be expressed as:

Proposition 8.13.

$$\begin{aligned} R &= (2a^4 - 2a^2b^2 + b^4 + (2a^2 - b^2)\delta)a\rho^2/b^6 \\ d &= (2a^2 - b^2 + 2\delta)c\rho^2a^2/b^6 \end{aligned}$$

Recall every pair of circles is associated with two so-called *limiting points* ℓ_1 and ℓ_2 about which the inversion of the pair yields a new pair of concentric circles, see Weisstein (2019, Limiting points). Let $\mathcal{C}$ and $\mathcal{C}'$ denote the incircle and circumcircle of the poristic family. Referring to Figure 8.9, it can be shown:

Observation 8.2. *One of the limiting points – call it ℓ_1 – of the bicentric circle pair coincides with a focus – call it f_1 – of its confocal polar pre-image. Furthermore, ℓ_1 is internal to both circles.*

Classic inversive geometry yields:

Proposition 8.14. *Triangles of the focus-inversive family are identical to the pedal triangles of the poristic family with respect to $f_1 = \ell_1$.*

Let $L^{\dagger\dagger}$ denote the perimeter of the pedal triangle with respect to the non-focal limiting point ℓ_2. Referring to Figure 8.10:

Proposition 8.15. *Over the poristic family, $L^{\dagger\dagger}$ is invariant and given by:*

$$L^{\dagger\dagger} = \frac{\left(9\,R^2 - d^2\right)\left(R^2 - d^2\right)\sqrt{2}\rho^2}{16\,R^4 d}\sqrt{(R^2 - d^2)^{\frac{3}{2}}\sqrt{9\,R^2 - d^2} + 3R^4 + 6R^2d^2 - d^4}$$

Equation (4.2) in Section 4.1 provides an expression for the invariant sum of cosines of the poristic family in terms of the semiaxes a', b' of its billiard polar pre-image. Interestingly:

Proposition 8.16. *The sum of cosines of pedal triangles to the bicentric family with respect to either limiting point is invariant and identical to that of the poristic themselves.*

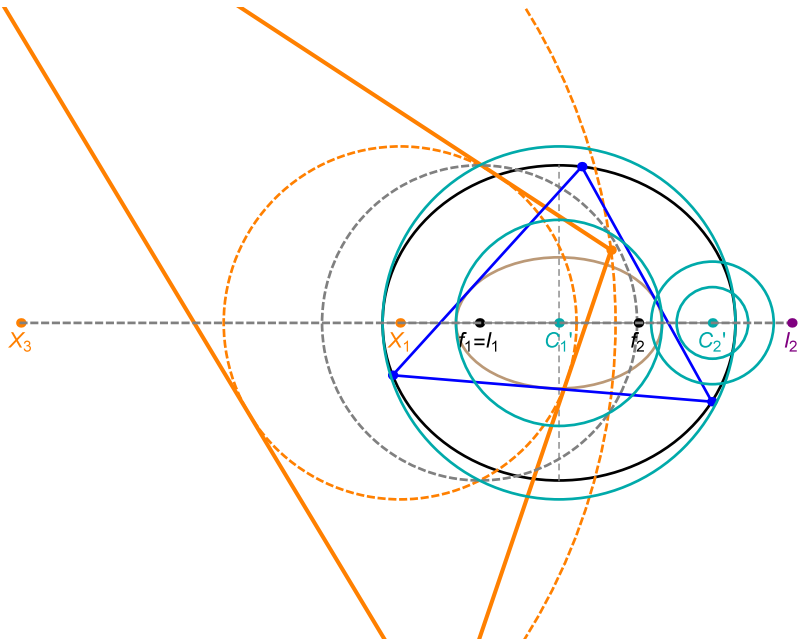

Figure 8.9: Billiard 3-periodic (blue) and its polar image (orange) with respect to a circle (dashed gray) centered on the left focus. Said polar family is poristic and interscribed between two circles $\mathcal{C}$ and $\mathcal{C}'$ (dashed orange) whose centers are labeled X_3 and X_1. Also shown are the two limiting points ℓ_1 and ℓ_2 of this pair of circles. Notice that ℓ_1 (resp. ℓ_2) is internal (resp. external) to $\mathcal{C}$ and $\mathcal{C}'$ and coincides with the billiard left focus (resp. lies to the right of the billiard center). Also shown are the two pairs of concentric circles (light blue) which are inversive images of $\mathcal{C}$ and $\mathcal{C}'$ about ℓ_1 and ℓ_2, respectively. Notice the circles in the first pair are tangent to the billiard (black) and confocal caustic (brown) at their major vertices, respectively.

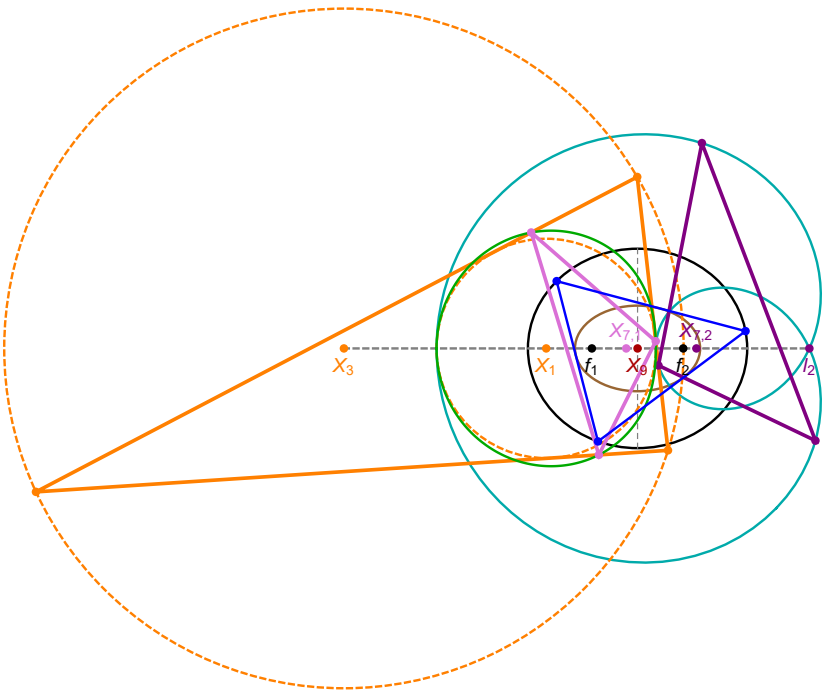

Figure 8.10: A billiard 3-periodic (Blue), and its polar image with respect to the left focus, i.e., the poristic family (solid orange). The focus-inversive family (pink) has invariant perimeter and can also be regarded as the pedal triangle of the poristic family with respect to said focus. The latter coincides with the interior limit point of the poristic circle pair. A second triangle (purple) is shown which is the pedal with respect to the (exterior) limiting point ℓ_2 of the poristic circle pair. Its perimeter is also invariant. The Gergonne points $X_{7,1}$ and $X_{7,2}$ of either pedal family are stationary. live

Let $X_7^{\dagger\dagger}$ denote the Gergonne point of the pedal of bicentrics with respect to their (external) limiting point:

Proposition 8.17. *$X_7^{\dagger\dagger}$ is stationary over the poristic family and given by:*

$$X^{\dagger\dagger} = -\frac{(R^2-d^2)((R^2-d^2)^{3/2}\sqrt{9R^2-d^2}-3R^4-6R^2d^2+d^4)}{16dR^4}$$

8.9 Exercises

Exercise 8.1. *Referring to Figure 8.1, let $X_7^{\ddagger}$ denote the inversion of $X_7^{\dagger}$ with respect to the inversion circle used to produce the focus-inversive family. Show it is given by:*

$$X_7^{\ddagger} = \left[\frac{\delta}{c}, 0\right]$$

Exercise 8.2. *Derive the expression in Proposition 8.2.*

Exercise 8.3. *Derive the expression in Proposition 8.3.*

Exercise 8.4. *Show that the locus of the Mittenpunkt $X_9^{\dagger}$ of focus-inversives is a circle with center $O_9^{\dagger}$ and radius $R_9^{\dagger}$ given by:*

$$O_9^{\dagger} = \left[-c\left(1+\rho^2\frac{1}{2b^2}\right), 0\right]$$
$$R_9^{\dagger} = \rho^2\,\frac{2a^2-b^2-\delta}{2ab^2}$$

Exercise 8.5. *Show that over $N = 3$ focus-inversives, the locus of $X_{11}^{\dagger}$ is the circle given by:*

$$C_{11}^{\dagger} = \left[c\left(-1+\rho^2\frac{-a^2+b^2+\delta}{2a^2b^2}\right), 0\right]$$
$$R_{11}^{\dagger} = \rho^2\frac{-a^2+b^2+\delta}{2ab^2}$$

Exercise 8.6. *Show that over $N = 3$ focus-inversives, the locus of $X_{100}^{\dagger}$ is the circle given by:*

$$C_{100}^{\dagger} = \left[-c\left(1+\rho^2\frac{1}{b^2}\right), 0\right]$$
$$R_{100}^{\dagger} = \rho^2\frac{a}{b^2}$$

Exercise 8.7. *Consider the bicentric (poristic) family which is the polar image of billiard 3-periodics wrt to a focus, see Section 4.1. Show the focus-inversive family are the pedal triangles of said bicentric family wrt to said focus. Bonus: show this focus coincides with one of the limiting points of the bicentric circle pair.*

Exercise 8.8. *Show that poristic pedals with respect to their exterior limiting points are also a constant-perimeter family whose Gergonne point is stationary.*

Exercise 8.9. *Prove Observation 8.2.*

Exercise 8.10. *Prove Proposition 8.14.*

8.10 Research questions

Question 8.1. *Prove that the locus of $X_{150}^{\dagger}$ is a circle. Derive center and radius.*

Question 8.2. *Prove that the locus of $X_{934}^{\dagger}$ is a circle, derive center and radius.*

Question 8.3. *Prove that the locus of $X_{658}^{\dagger}$ is an ellipse. Derive its center and semiaxes.*

Question 8.4. *Prove the loci of $X_k^{\dagger}$, k =69, 75, 85, and 86 are ellipses, derive centers and semiaxes.*

Question 8.5. *Consider the family of inversive images of excentral 3-periodics with respect to a circle centered at a point M in the plane. Show the symmedian point X_6 of such a family will be stationary regardless of M. Compute the location of X_6. See it in this video Video.*

9 A Locus Visualization App

Many insights described in previous chapters were obtained from experimentation and observation of pictures, videos, and interaction with the dynamic geometry of Poncelet configurations. Dozens of notebooks and 100s of small interactive apps were written with Wolfram (2019). Most of our videos, and other digital artifacts are compiled in Reznik (2021b).

To further facilitate exploratory discovery of invariants and locus properties of 3-periodic families, we developed a Javascript-based locus visualization app, originally described in Darlan and Reznik (2021). It borrows many interactivity ideas from Wolfram (2019) `Manipulate`, and the sharing and usability model from Hohenwarter et al. (2013).

A typical screenshot of the application is depicted in Figure 9.1. A large area called here the animation window is where the dynamic geometry of a particular triangular family and its associated loci are drawn To its left is a strip of channel controls, comprising four identical groups, which define which objects are to be used as a basis to compute and draw loci from.

The most common usage pattern is depicted in Figure 9.2, namely: the user selects (i) a triangle family (Poncelet or ellipse-mounted, see below); (ii) the triangle on which computations will be made (the default is "reference" but dozens of derived triangles can be chosen); (iii) the locus type, i.e., whether one wishes

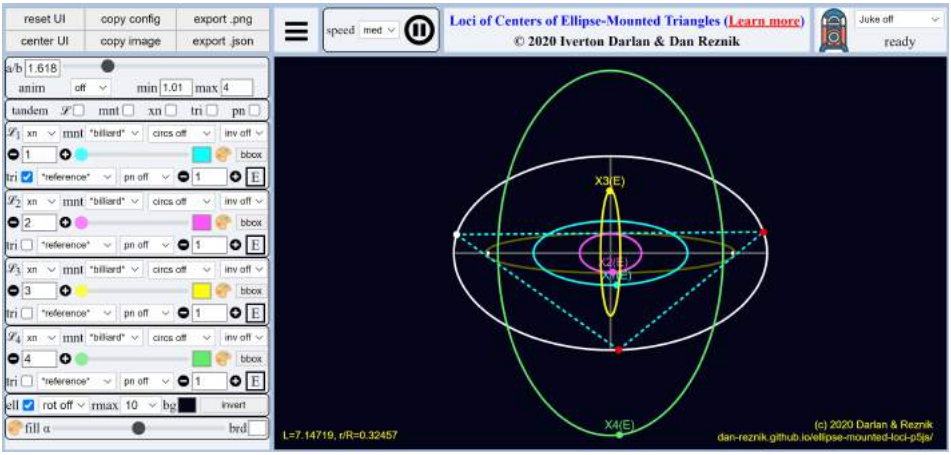

Figure 9.1: Locus Visualization app to explore 3-periodic families. Shown are the loci of X_k, k =1,2,3,4, over billiard 3-periodics. The "(E)" suffix indicated they are numerically ellipses. Live. Also see our tutorial playlist.

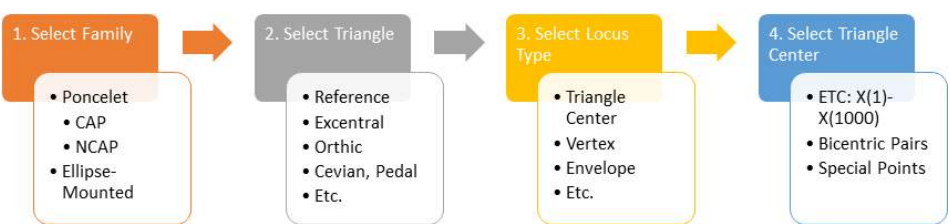

Figure 9.2: Caption

to trace out a triangle center, a vertex, an envelope, etc., and (iv) which triangle center should the locus be drawn for. The first one thousand triangle centers listed on Kimberling (2019) are currently supported.

In the sections below we describe the main functions of the user interface. A video-based tutorial is available in Reznik (2021c).

9.1 Main ellipse and animation controls

Before a particular triangle family can be setup and its loci visualized, one must set certain basic animation controls, using the various areas highlighted in Figure 9.3.

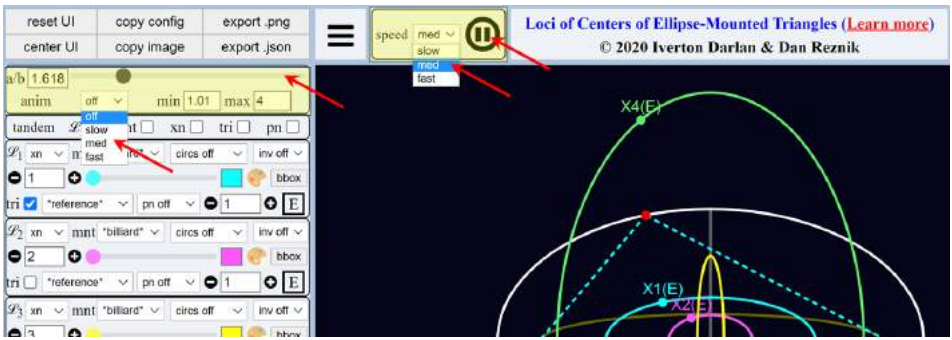

Figure 9.3: Basic animation controls include (i) the setting of the base ellipse aspect ratio `a/b` either via typing into the textbox (showing 1.618 in the picture) or via the scrollbar next to it; (ii) above the animation area, pausing or running the animation and choosing a speed – slow, medium, or fast. Note: a small "anim" dropbox located below the `a/b` scrollbar, when not in the "off" position, triggers a smooth oscillation of the aspect ratio over the range specified in the "min" and "max" input boxes to its right.

These include (i) the setting of the base ellipse aspect ratio `a/b` either via typing into the textbox (showing 1.618 in the picture) or via the scrollbar next to it; (ii) above the animation area, pausing or running the animation and choosing a speed – slow, medium, or fast. Note: a small "anim" dropbox located below the `a/b` scrollbar, when not in the "off" position, triggers a smooth oscillation of the aspect ratio over the range specified in the "min" and "max" input boxes to its right.

9.1.1 Convenience animation controls

If the animation is paused, hitting the up (or right) and down (or left) arrows on the keyboard allows one to carefully step forward or backward over the triangle family.

The mouse wheel allows for the simulation image to be zoomed or unzoomed.

By clicking and dragging into the main animation area one can pan and reposition the image.

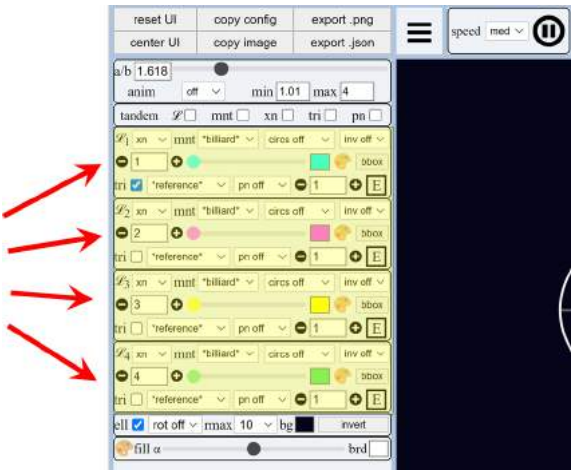

Figure 9.4: Four identical groups of "channel" controls positioned to theleft of the main animation window.

9.2 Channel controls

As shown in Figure 9.4, four identical groups of "channel" controls are positioned to the left of the main animation window. Figure 9.5 zooms in one of them, whose individual settings are explained next.

9.3 Choosing a triangle family

The first step in Figure 9.2 is the choice of a triangle *family*. A specific one is selected via the `mnt` drop-down, see Figure 9.6. Two types of families are supported: (i) Poncelet, and (ii) ellipse "mounted" (see below), which originated the name of the control.

9.3.1 Poncelet families

Currently we support the following 8 types of 3-periodic Poncelet families interscribed between axis-parallel ellipses, whose names are familiar from previous sections: (i) Confocal (i.e., elliptic billiard), (ii) Homothetic, (iii) with Incircle, (iv) with Circumcircle, (v) Dual, (vi) Excentral (to confocals), (vii) Poristic, and (viii) the Brocard Porism. Note (i)-(vi), while the last two are non-concentric.

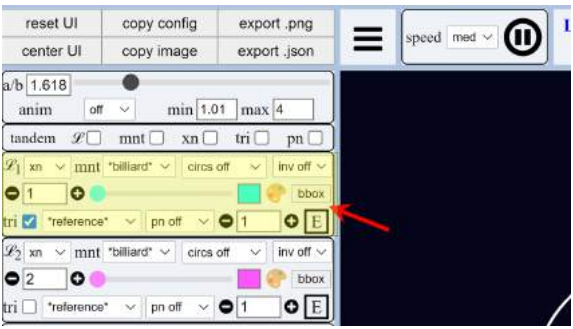

Figure 9.5: Various settings in a single channel control.

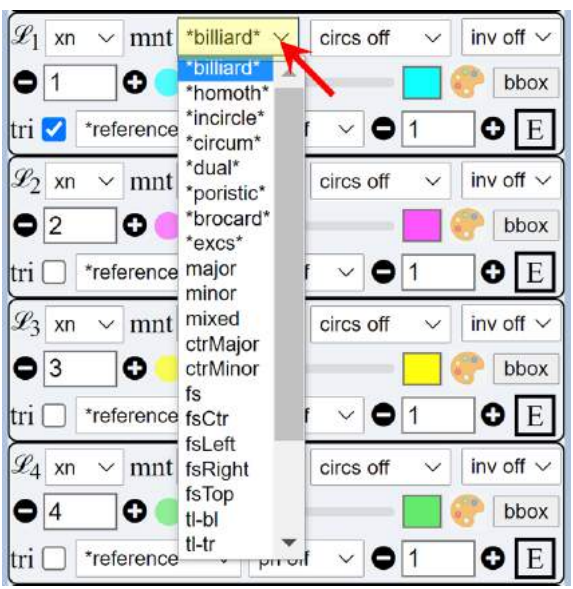

Figure 9.6: The `mnt` drop-down selects a triangle family.

9.3.2 Ellipse "mounted"

Also selectable are triangle families $\mathcal{T}(t) = V_1 V_2 P(t)$, where V_1, V_2 are pinned to two points on or near an ellipse, and $P(t) = [a \cos t, b \sin t]$ sweeps the boundary. Let The following fixed locations for V_1 and V_2 are currently supported:

1. `major`: left and right ellipse vertices (EVs)
2. `minor`: top and bottom EVs
3. `mixed`: left and top EVs
4. `ctrMajor`: center and left EV
5. `ctrMinor`: center and top EV
6. `fs`: the 2 foci f_1 and f_2
7. `fsCtr`: center and right focus (f_2)
8. `fsLeft`: left EV and f_2
9. `fsRight`: right EV and f_2
10. `fsTop`: top EV and f_2
11. `tl-bl`: top left corner of ellipse bounding box (TL) and bottom left of the same (BL)
12. `tl-tr`: TL and top right corner (TR) of ellipse bounding box
13. `tl-l`: TL and left EV
14. `tl-t`: TL and top EV
15. `tl-b`: TL and bottom EV
16. `tl-o`: TL and center of ellipse
17. `tl-br`: TL and center of ellipse

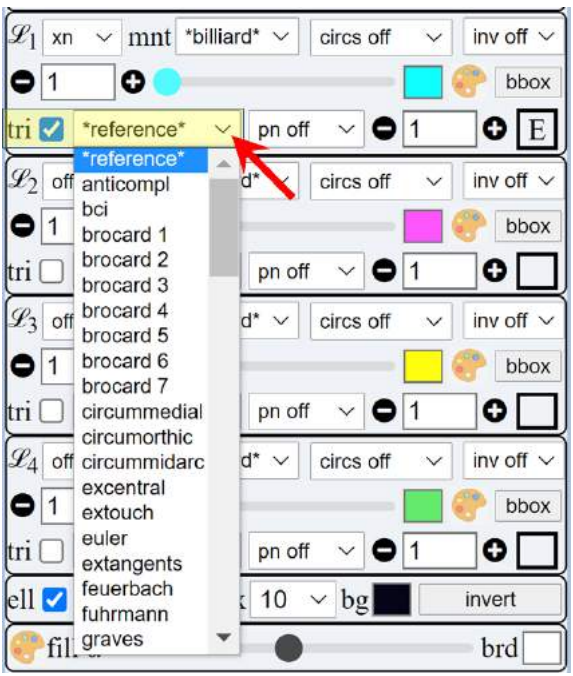

Figure 9.7: The triangle menu selects whether a `*reference*` or some derived triangle should be used to compute loci. The `tri` checkbox immediate to the left selects whether the triangle should be drawn or not.

9.4 Triangle type

The second step in Figure 9.2 is the choice of the type of triangle with respect to which centers and loci will be computed. This is done the `tri` checkbox and drop-down, as shown in Figure 9.7.

While the checkbox controls whether selected triangle is drawn or not, the drop-down contains some four-dozen derived triangles. Below the default setting `*reference*` (this indicates a plain triangle in the family should be used), the choices are organized in three groups:

1. Standard "named" triangles (undecorated abbreviations), such as `anticompl` for anticomplementary, `bci` for BCI triangle, etc., whose construction can be looked up on Weisstein (2019).

2. Exotic triangles (prefixed by a "."): `.andromeda`, `.antlia`, etc., obtained from Lozada (2016).

3. Inversive triangles, e.g., `*inv-f1*`, `*inv-f1c*`, etc. (decorated with asterisks).

Below we document triangles both in the "standard" and "exotic" groups:

9.4.1 Standard triangles

These include: Reference, Anticomplementary, BCI, 1st Brocard, 2nd Brocard, 3rd Brocard, 4th Brocard, 5th Brocard, 6th Brocard, 7th Brocard, Circum-Medial, Circum-Mid-Arc, Circum-Orthic, Excentral, Extouch, Extangents, Feuerbach, Fuhrmann, Half-Altitude, Hexyl, Incentral, Inner Vecten, Intangents, Intouch, Johnson, Lemoine, Lucas Central, Lucas Inner, Lucas Tangents, MacBeath, Medial, Mixtilinear, 1st Morley Adj, 2nd Morley Adj, 3rd Morley Adj, 1st Neuberg, 2nd Neuberg, Orthic, Outer Vecten, Reflection, Steiner, Symmedial, Tangential, Tangential Mid-Arc, Yff Central, Yff Contact.

9.4.2 Exotic triangles

These include: Andromeda, Antlia, Apollonius, Apus, Atik, Ayme, Bevan-Antipodal, 1st Circumperp, 2nd Circumperp, Excenters–Incenter, Reflections, Excenters–Midpoints, Honsberger, Inverse–in–Excircles, Inverse–in–Incircle, Kosnita, Mandart Excircles, Mandart Incircles, Ursa Major, Ursa Minor.

9.4.3 Inversive triangles

The options below are images of the reference triangle in a given family under an inversive-like transformation with respect to unit circle centered on a stationary notable point of the family's underlying ellipse (or caustic), e.g., center, focus, etc.

- `*inv-ctr*,*inv-f1*,*inv-f1c*,*inv-f2*`: inversion of vertices with respect to a unit circle centered on the outer ellipse center, outer ellipse left focus, inner ellipse left focus, or outer ellipse right focus, respectively.

- `*pol-ctr*,*pol-f1*,*pol-f1c*`: a new, "polar" triangle is computed bounded by the polars of the vertices with respect to ellipse center, outer ellipse left focus, or inner ellipse left focus, respectively.

- `*ped-lim2*`: this is specific to the confocal family. Computes the pedal triangle with respect to the non-focal limiting point of the bicentric family which is the polar image of the confocal family.

- `*x3map-ctr*,*x3map-f1*,*x3map-f1c*`: consider a triangulation of the original triangle in 3 subtriangles, each of which contains two vertices of the original triangle and either (i) the center of the outer ellipse, (ii) its left focus, or (iii) the inner ellipse left focus, respectively. These transformations compute a new triangle with vertices at the circumcenter of each subtriangle.

- `*x3inv-ctr*,*x3inv-f1*,*x3inv-f1c*`: these compute the inverses of the previous transform with respect to the same points.

- `*crem-ctr*,*crem-f1*,*crem-f2*`: sends the reference vertices to their images under a quadratic Cremona transformation, which sends $(x, y) \to (1/x, 1/y)$. The origin will be the center of the outer ellipse, its left focus, or its right focus, respectively.

Note: four additional settings `*inf-x*,*inf-y*,*inf-x2*,*inf-y2*` are provided and are experimental and non-inversive. They dynamically set the x or y coordinate of each vertex so they slide along infinity-like Lissajous curves.

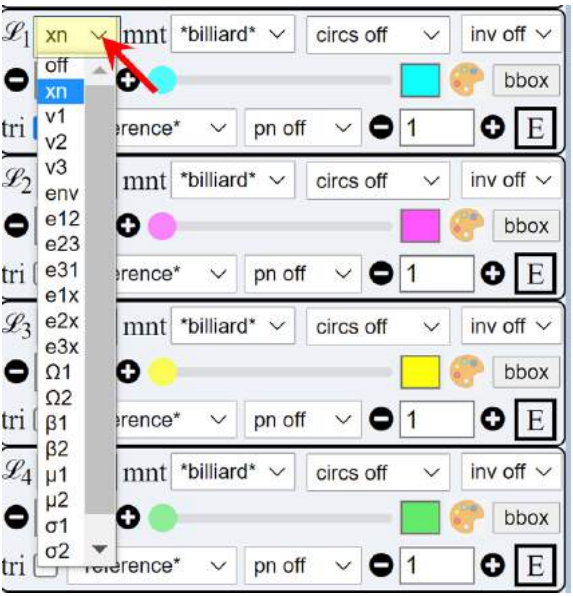

Figure 9.8: The $\mathcal{L}_i$ menu selects the locus type to (triangle center, vertex, envelope, etc.).

9.5 Locus type

The third step in Figure 9.2 is the choice of type of locus to be drawn, or more precisely, the feature selected from the family/triangle combination previously selected. This is done with the $\mathcal{L}_i$ menu at the top of the control group, $i = 1, 2, 3, 4$, shown in Figure 9.8.

There are three conceptual groups of locus types: (i) triangle centers and vertices, (ii) segment envelopes, and (iii) bicentric pairs. These are explained next.

9.5.1 Centers and vertices

1. `off`: it indicates the trace (locus) of this channel should not be drawn. It is the default setting for channels 2, 3, 4 upon startup.

2. `xn`: draw the locus of the selected triangle center, as in Section 9.6;

3. `v1`, `v2`, `v3`: show the trace of one of thee vertices of the triangle family. In Poncelet families, these will sweep out the same curve, but this is not the

case for ellipse-mounted families.

4. `ort`: the *orthopole* of line $X_m X_n$, see Weisstein (2019, Orthopole), where m and n are selected triangle and Cevian centers, see Section 9.6 and Section 9.7.

9.5.2 Envelopes

1. `env`: the envelope of segment $X_m X_n$, $m \neq n$, where m (resp. n) is the selected triangle (resp. Cevian) center.

2. `e12`, `e23`, `e31`: the envelope of side $V_i V_j$ of the triangle family. Note these are one and the same (resp. distinct) for Poncelet (ellipse-mounted) families.

3. `e1x`, `e2x`, `e3x`: the envelope of $V_i X_n$, i.e., the line from a given vertex to a selected triangle center. In a concentric Poncelet family, the envelope of $V_i X_1$ will be the outer ellipse's evolute, see it Live.

9.5.3 Bicentric pairs

Only a few have so far been implemented, from the copious list in Kimberling (2020a).

1. Ω_1, Ω_2: the Brocard points

2. β_1, β_2: the Beltrami points: inversions of the Brocard points with respect to the circumcircle

3. μ_1, μ_2: also known as "Moses" points: inversion of the Brocard points with respect to the incircle.

4. σ_1, σ_2: the two foci of the Steiner circumellipse (aka. the Bickart points)

9.6 Triangle center

The fourth and final step in Figure 9.2 is the choice of triangle center X_k in the region highlighted in Figure 9.9. There are three ways to choose $k \in [1, 1000]$: (i) by typing/editing the text field showing k, (ii) incrementing or decrementing k by

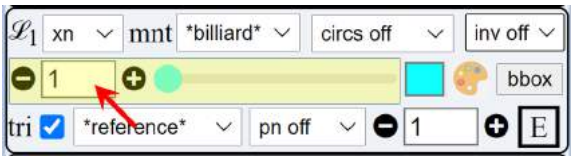

Figure 9.9: Controls used for the selection of a particular triangle center X_k.

clicking on the "-" and "+" symbols around the text field; (iii) using the scrollbar to the right of the "+" control, to quickly scroll through all 1000 values of k. In fact after any of these is performed, this set of controls becomes "focused" in such a way that (iv) left (resp. right) arrow keystrokes will decrement (resp. increment) the value, allowing mouse-free traversal of triangle centers.

9.7 Cevians, pedals, & Co.

An additional "Cevian-like" transformation with respect to an additional triangle center X_m can be applied to the triangle type selected in Section 9.4. Let us call the latter the "parent" triangle. The specific transformation is selected via the drop-down menu in Figure 9.10 (the default setting is `pn off`, meaning this additional transformation is inactive), and X_m via the numeric input box to the right of the menu.

The X_m-transformations possible are grouped into (i) traditional, (ii) inversive, (iv) reflexive, and (iv) triangulated. Below, let T_m denote the transformed triangle, and P_i, $i = 1, 2, 3$, the vertices of the parent triangle.

9.7.1 Traditional

Available in this groups are the standard constructions for (i) Cevian, (ii) Anticevian, (iii) Circumcevian, (iv) Pedal, (v) Antipedal, and (vi) Trilinear Polar triangles described in Weisstein (2019). Recall that the latter produces a degenerate (segment-like) triangle, see Weisstein (ibid., Trilinear Polar).

9.7.2 Inversive

- `invert`: T_m will have vertices at inversions of the parent one with respect to a unit circle centered on X_m.

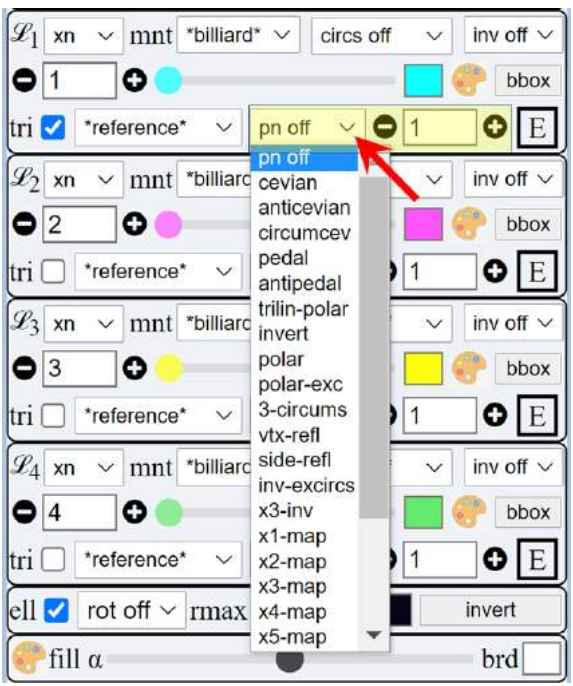

Figure 9.10: Cevian-like triangles and number box to select a triangle center playing the role of Q (see text).

- `polar`: T_m will be bounded by the polars (infinite lines) of the parent's vertices with respect to a unit circle centered on X_m, see Weisstein (2019, Polar).

- `inv-excircs`: T_m will have vertices at inversions of X_m with respect to its excircles, see Weisstein (ibid., Excircle).

- `polar-exc`: T_m will be bounded by the polars (infinite lines) of X_m with respect to each of the parent's excircles.

9.7.3 Reflexive

- `vtx-refl`: T_m has vertices at the reflections of X_m on the parent vertices.

- `side-refl`: T_m has vertices at the reflections of X_m on the sidelines of the parent triangle.

9.7.4 Triangulated

Triangulate the parent with respect to X_m, i.e., consider the following subtriangles: $T_{23} = X_m P_2 P_3$, $T_{31} = X_m P_3 P_1$, and $T_{12} = X_m P_1 P_2$.

- `3-circums`: T_m has vertices at the circumcenters of T_{23}, T_{31}, and T_{12}.

- `3-inv`: The inverse of `3-circums`. T_m is such that the circumcenters of its three subtriangles are the vertices of the parent. The vertices of T_m are the non-X_m intersections of a circle through X_m and P_i with a circle through X_m and P_{i+1}, cyclically.

- X_k-map, $k \in [1, 11]$: T_m has vertices at the X_k of T_{23}, T_{31}, and T_{12}. Note: X_3-map is the same as the `3-circums` setting.

9.8 Notable circles

Dozens of circles can be visualized with respect to the triangle family selected in Section 9.4. These are selected via the (left) drop-down menu highlighted in Figure 9.11. The `circs off` setting is the default. The possible choices are organized in two groups: (i) ellipse-affixed, and (ii) central circles.

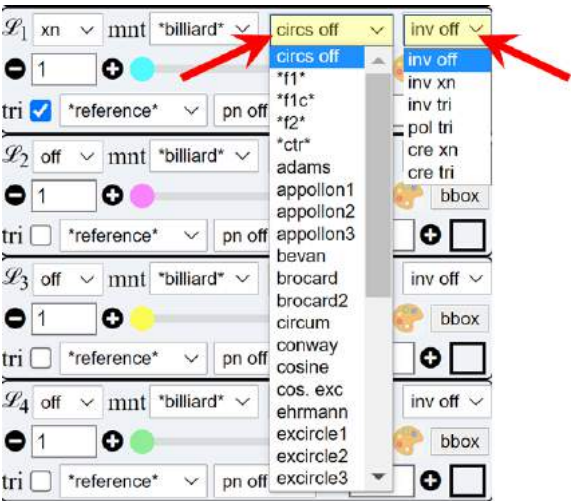

Figure 9.11: The left drop-down selects an ellipse-based circle or a "central" circle for both visualization and/or as references for inversive transformations.

9.8.1 Ellipse-affixed circles

These are asterisk-decorated to indicate that they refer to a unit circle centered on a notable point of the ellipse (or caustic) used to generate a given triangle family, to be sure:

- `*f1*`: the left focus of the outer ellipse. Note: in the poristic (resp. excentral) family this becomes the center of the outer circle (resp. caustic = elliptic billiard).
- `*f1c*`: the left focus of the inner ellipse.
- `*f2*`: the right focus of the outer ellipse. Note: in the poristic (resp. excentral) family this becomes the incenter (resp. a focus of the outer ellipse.
- `*ctr*`: the center of the system.

9.8.2 Central circles

Most of these are defined in Weisstein (ibid., Central Circles):

- `adams`: the Adams circle

- `appollon1,appollon2,appollon3`: 1st, 2nd, and 3rd Apollonius' circles (which intersect on the isodynamic points)
- `bevan`: the Bevan circle, circumcircle of the excentral triangle
- `brocard,brocard2`: the Brocard circle and the so-called "2nd" Brocard circle.
- `circum`: the circumcircle
- `conway`: Conway's circle
- `cosine`: the cosine (or 2nd Lemoine) circle
- `cos.exc`: the cosine circle of the excentral triangle
- `ehrmann`: Ehrmann's 3rd Lemoine circle, see Grinberg (2012).
- `excircle1,excircle2,excircle3`: the three excircles
- `euler`: Euler's circle
- `furhmann`: Furhmann's circle
- `gallatly`: Gallatly's circle
- `gheorghe`: Gheorghe's circle, see Kimberling (2019, X(649))
- `incircle`: Incircle
- `lemoine`: 1st Lemoine circle
- `lester`: Lester's circle
- `mandart`: Mandart's circle
- `moses,moses rad`: Moses's circle and Moses' radical circle
- `parry`: Parry's circle
- `reflection`: the "reflection" circle (circumcircle of the reflection triangle)
- `schoutte`: Schoutte's circle
- `spieker`: Spieker's circle

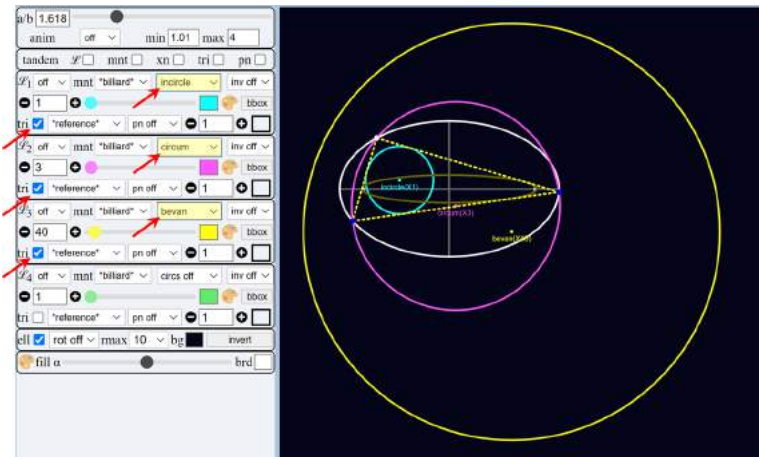

Figure 9.12: The incircle, circumcircle, and Bevan circle are viewer simultaneously, by choosing them on the circle menu in 3 separate channels. Notice that to make the circle appear, one must check the `tri` checkbox in the lower left of that channel control area. Live

- `taylor`: Taylor's circle

As shown in Figure 9.12, several circles can be shown simultaneously. To do this select one for each channel (maintaining the same triangle family and type), and make sure to check the

9.9 Inversive transformations with respect to a circle

Provided a circle $\mathcal{C}$ is selected (see above section), one can add an inversive-type transformation with respect to it. This is done via the (right) drop-down menu highlighted in Figure 9.11. The possible transformations are as follows:

- `inv off`: No transformation is performed.
- `inv xn`: invert the selected triangle center (see Section 9.6) with respect to $\mathcal{C}$.
- `inv tri`: invert the vertices of triangles in the family with respect to $\mathcal{C}$.

- `pol tri`: compute a new triangle bounded by the polars of the original vertices with respect to $\mathcal{C}$.
- `cre xn`: send the selected triangle center to its image under a quadratic Cremona transformation (QCT) $(x, y) \to (1/x, 1/y)$, where (x, y) are the coordinated of the center of $\mathcal{C}$.
- `cre tri`: compute a new triangle whose vertices are images of the QCT with respect to the center of $\mathcal{C}$.

9.10 Conic and invariant detection

9.10.1 Curve type

As shown in Figure 9.13, when one or more loci are displayed, the app indicates in the lower right-hand side of the corresponding control group, the curve type of the locus (detected via least-squares curve fitting). The following codes are used:

- `X`: non-conic
- `E`: ellipse
- `H`: hyperbola
- `P`: parabola (very rare)
- `L`: line or segment
- `*`: a stationary point.

The same code is also appended (in parenthesis) to the (moving) triangle center being displayed, for example, Figure 9.13, `X2(E),X3(E),X4(E)`, indicate the loci of barycenter, circumcenter, and orthocenter are ellipses over billiard 3-periodics.

9.10.2 Detection of metric invariants

The app also reports when certain basic, metric quantities are invariant, currently over triangles in the first channel only. These appear as a single line at the bottom of the animation area of a given experiment, see Figure 9.13. In the example, the following line of text is reported:

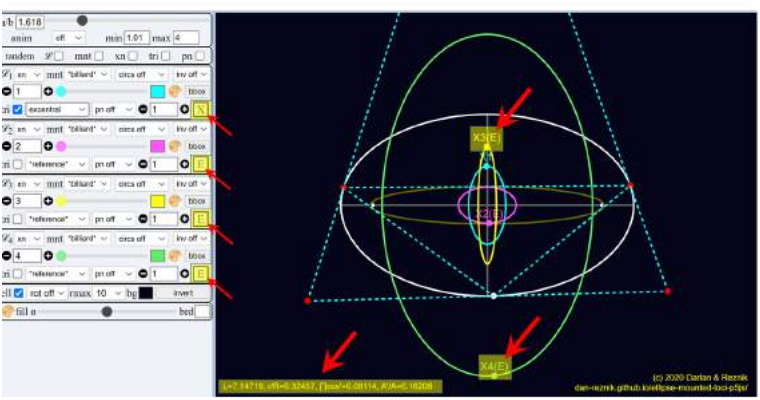

Figure 9.13: An indication as to curve type of each locus appears in a small box in the lower right-hand side of each control group. In the picture, `X` means the first locus (incenter over the excentral family) is non-conic. An `E` in the remainder 3 channels indicates their loci are ellipses. Notice the same indicator is appended to the instantaneous location of the triangle centers being tracked, e.g., `X3(E)` indicates the locus of the circumcenter is an ellipse. Live

$$L = 7.14..., r/R = 0.32..., \prod \cos' = 0.0811, A'/A = 6.6...$$

In turn, this means that perimeter L and ratio r/R of inradius-to-circumradius are numerically invariant over the reference family selected in channel 1, and that the product $\prod \cos'$ of cosines, and ratio A'/A of derived-by-reference areas is constant (these are observations first introduced in Reznik, Garcia, and Koiller (2020a)).

Reported invariants appear unprimed to refer to the reference triangle in a given family. Primed quantities will appear when a derived triangle has been selected (e.g., "excentral"), allowing for mutual comparison.

The following quantities are currently reported, when numerically invariant:

- L, A: perimeter and area
- r, R: inradius and circumradius
- r/R: ratio of inradius-to-circumradius, tantamount to invariant sum of cosines since $\sum \cos = 1 + r/R$.
- $\cot(\omega)$: the cotangent of the Brocard angle
- $\sum s^2, \sum 1/s, \sum s^{-2}$: sum of squared, reciprocal, or reciprocal-squared sidelengths, respectively.
- $\prod \cos$: the product of internal
- $\prod s$: the product of sidelengths
- R_c: if a circle is selected via the circle menu (Section 9.8), whether its radius is constant.

Also reported whenever a derived triangle is selected, are one of L'/L, A'/A, $A'.A$, R'_c/R_c if these are invariant.

9.11 The tandem bar

A common exploratory pattern is to observe the behavior of loci across all channels simultaneously while a single setting is varied, e.g., triangle family, triangle type, etc. This could be done with tedious mouse-based changes (of the varying parameter) across all controls.

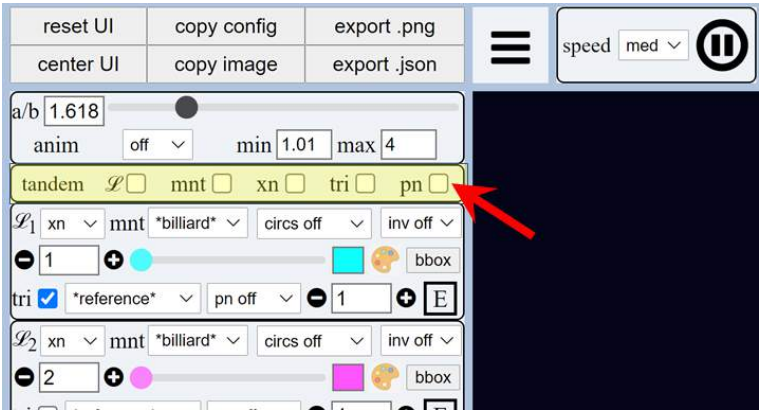

Figure 9.14: The tandem bar. Checking one or more checkboxes ensures locks all corresponding drop-downs in the channel controls to take the same value.

As an example, consider observing the loci of $X_k, k = 1, 2, 3, 4$ for the billiard family and then for the homothetic family. This would require one to reset each of the four `mnt` drop-downs from `billiard` to `homothetic`. If the user now wished to examine said loci over the incircle family, all `mnt` drop-downs wouldhave to be reset to `incircle`, etc.

Referring to Figure 9.14, the tandem bar, makes this rather common usage pattern very efficient.Namely, the user can set one or more tandem checkboxes causing a given setting to be "short circuited" across all channels. Specifically:

- $\mathcal{L}$: the locus type
- `mnt`: the Poncelet or ellipse-mounted family
- `xn`: the triangle center number
- `tri`: the reference or derived triangle
- `pn`: the triangle center with respect to which Cevian-like triangles are calculated

As an example, consider the sequence shown in Figure 9.15. Tandem checkboxes $\mathcal{L}$ and `mnt` are checked, indicating both locus type and triangle family are in unison across all channels. This automatically sets `xn` across all channels, i.e.,

loci will be drawn (as opposed to, e.g., the envelope). The use then needs to manually set the triangle center values of 1,2,3,4 for each channel. To now observe these across all families, since `mnt` is set, the user simply needs to flip through the triangle families using the triangle family drop-down on any one of the channels in the strip. In fact this can be done with the up and down arrows on the keyboard once that control comes into focus (e.g., by expanding the drop-down), allowing for very quick perusal of this phenomenon across all triangle families.

9.12 Odds & ends

9.12.1 Ellipse, locus tange, and animation background

As shown in Figure 9.16, the area immediately below the four sets channel controls the following parameters:

- `ell` checkbox: whether the main ellipse underlying a triangle family of choice should be drawn or not.
- Rotation menu: the default `rot off` setting leaves the animation window as is. Settings 90°,180°,270° apply a global rotation to the picture drawn.
- `rmax` menu: the (half-side) of the square bounding box where points in all loci are evaluated, respective to the minor semiaxis of the ellipse, assume to be of unit length. Ideally, this should be set to as small a value as able to contain all loci.
- `bg`: used to set the background color of the main animation window, dark blue by default. By clicking on the colored square an RGB picker window pops-up permitting fine control of the color.
- `invert` button: single-click inversion (in RGB space) of colors of background and loci currently in being drawn.

9.12.2 Resetting the UI and centering the animation

Figure 9.17 highlights `reset UI` and `center UI` push-buttons are located at the top-left corner of the app. These are used to (i) restore all controls in the app to their default values, and (ii) recenter the geometry drawn to the center of the animation, respectively.

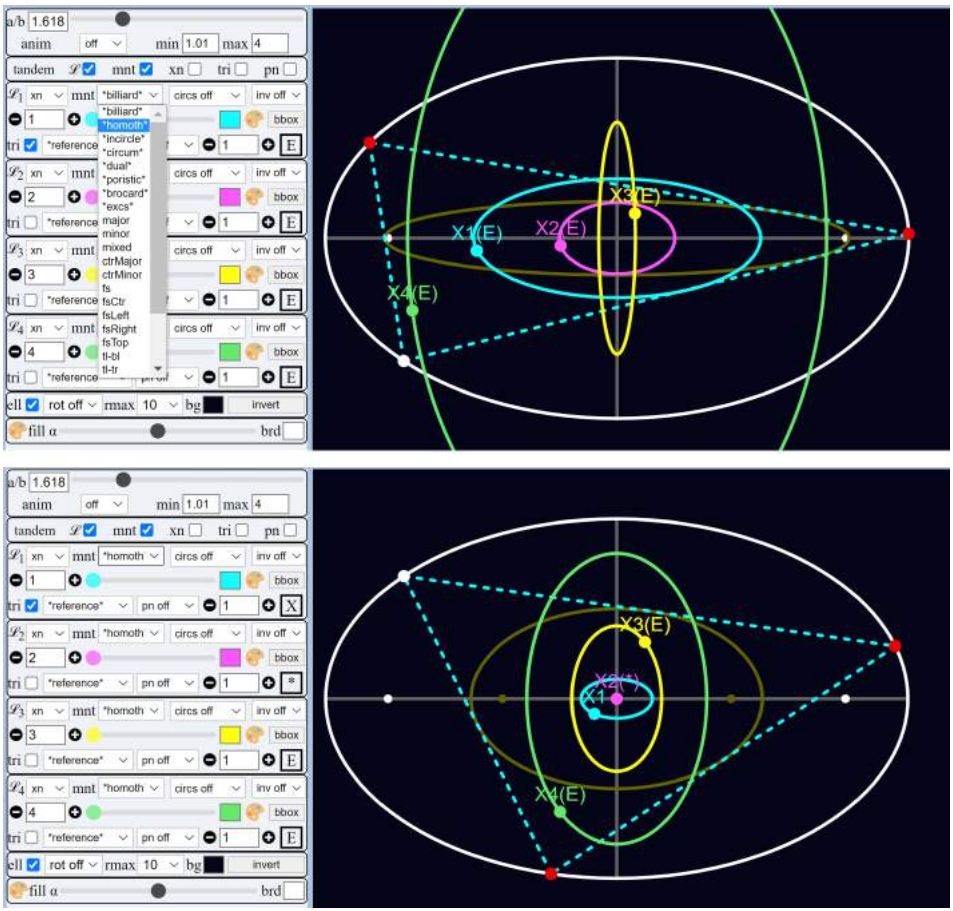

Figure 9.15: Usage of the tandem feature. The user has previously selected triangle centers $k = 1, 2, 3, 4$ for each of the channels. **Top:** the user is about to flip, in tandem, triangle family from "billiard" to "homothetic" for the first channel; **Bottom:** since the tandem `mnt` is checked, all channels flip in unisn to "homothetic", with the visualization being updated in one shot. To quickly flip through all other families, the user can hit the up and down keys on the keyboard.

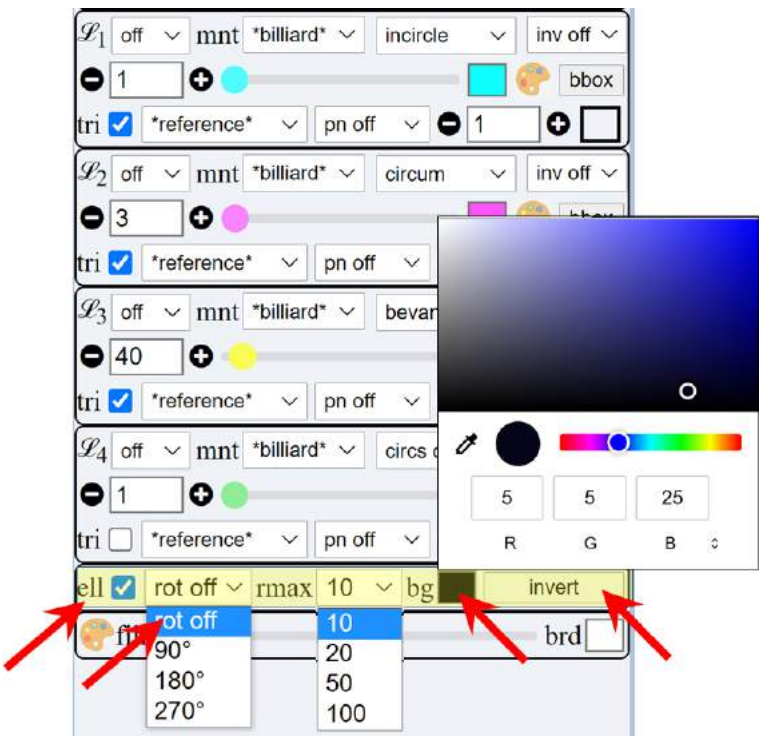

Figure 9.16: In the highlighted area controls are available to (i) `ell`: show or hide the main ellipse, (ii) `rot xxx`: apply a global rotation to the animation widow, (iii) `rmax`: set the bounding box of the area in which loci are computed, (iv) `bg`: set the animation window's background color, and (v) `invert`: invert (RGB negative) colors of background and all loci drawn.

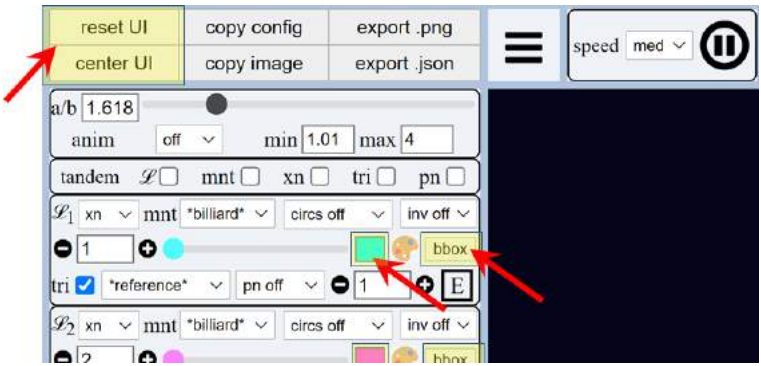

Figure 9.17: Reset and center push-buttons are located at the top-left corner of the app. which (i) `reset UI`: all controls in the app are restored to their default values; (ii) `center UI`: the center of the simulation is panned back to the center of the animation area. This is useful after having previously panned the picture via a mouse drag. Also shown is (iii) a color selector square located to the right of every triangle center scrollbar, through which a new color can be selected for displaying the corresponding locus. Finally, (iv) a `bbox` push button is provided to repositing and scale the geometric scene so as to best fit it in the available space.

9.12.3 Setting the locus color

Also shown in Figure 9.17 are color and rescaling controls to the right of the triangle center scrollbar. These are permit (i) selection of a color specific to a particular locus being drawn, and (ii) a resizing/recentering of the particular locus so as to best fit the animation window.

9.12.4 Collapsing the locus control area

The "hamburger" control shown in Figure 9.18 can be used to hide/expand the set of controls on the left marging of the app, sometimes useful for demonstration purposes.

9.13 Artsy loci

A set of controls, highlighted in Figure 9.19, can be used to color fill connected regions of loci. A first clicking on the palette icon in the middle-right section of

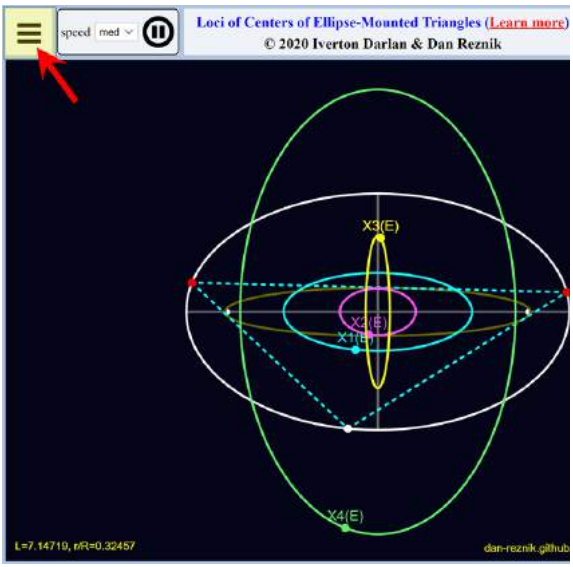

Figure 9.18: The hamburger control (three horizontal bars) located to the right of the the main controls can be clicked to hides/expand the main controls.

a channel's control group selects a random set of pastel colors. Subsequent clicks (or hitting the right arrow key) generate a new random color set. Hitting the left arrow goes back to color sets previously generated. Right-clicking on the palette icon and or changing any other setting in the user interface causes the color fills to disappear.

Also highlighted in Figure 9.19 is a scrollbar and color chooser located below the bottom-most channel control group. These are used to set (i) the transparency of colors fills, and (ii) the color of the border of connected regions (default is white).

A collage of four colored-filled curvaceous loci is shown in Figure 9.20. Some two hundred such "artsy" loci are showcased in Reznik (2021a).

9.14 Sharing and exporting

As shown in Figure 9.21, four buttons on the global control strip (top left of the interface) can be used to copy and export a link, an image, or a vector graphics representation the loci currently rendered. The buttons are as follows:

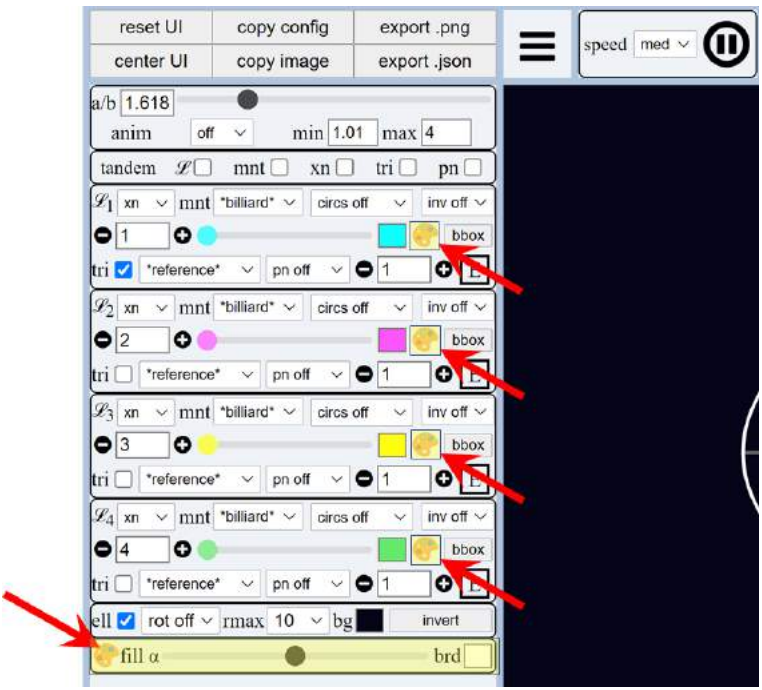

Figure 9.19: Clicking on the highlighted palette icons in the mid-right section of every channel control area triggers color fills in any drawn loci. Clicking it several times (resp. right clicking on it) randomizes colors (resp. removes the color fills). At the bottom of the channel control strip a scrollbar can be used to control the transparency of the fills. A color chooser at its right side can be clicked to select the color of region borders (default is white).

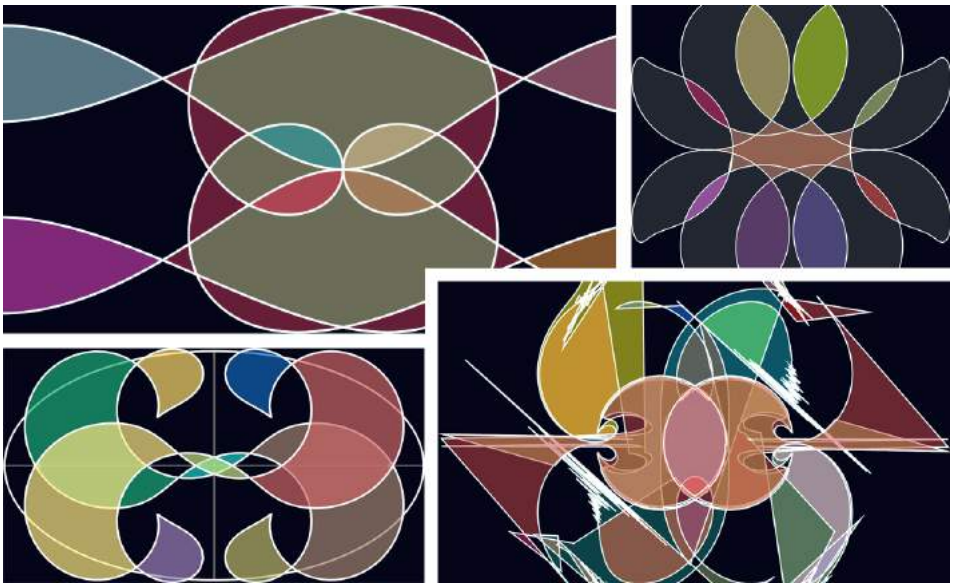

Figure 9.20: Four examples of the kinds of color-filled loci which can be produced with the app. Gallery and Video

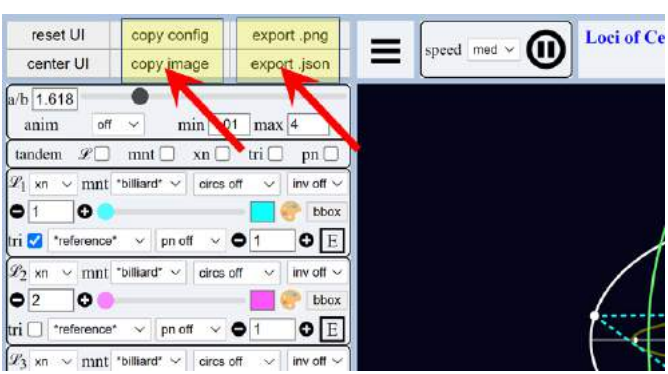

Figure 9.21: Buttons on the upper control strip for copying, sharing, and exporting experiment configuration and images.

- `copy config`: A URL containing all information pertaining to the current geometric scene (as defined by the channel controls and other pieces of UI) is copied to the clipboard. This URL can be shared with another user and/or shortened prior to sharing, e.g., with `bit.ly`.
- `copy image`: the image currently on the animation window is copied to the clipboard. It can then be pasted anywhere else as an image.
- `export .png`: what is currently on the animation window is downloaded to the local file system.
- `export .json`: a vector graphics representation of all loci drawn is exported in human-readable JSON format.

9.15 Jukebox playback

Many experiments constructed with the tool are stored in a database accessible by the app. These are organized in different thematic groups which can be played back in continuously in "jukebox" mode (each experiment being displayed 5-10 seconds). This is initiated by selecting a thematic group from the drop-down at the top right hand side of the app window, highlighted in Figure 9.22. To quickly zip forward or backward thru items in the series, click (or right-click) on the jukebox icon to the left of the drop-down. Jukebox mode can be stopped at anytime by returning the drop-down to the `Juke off` setting.

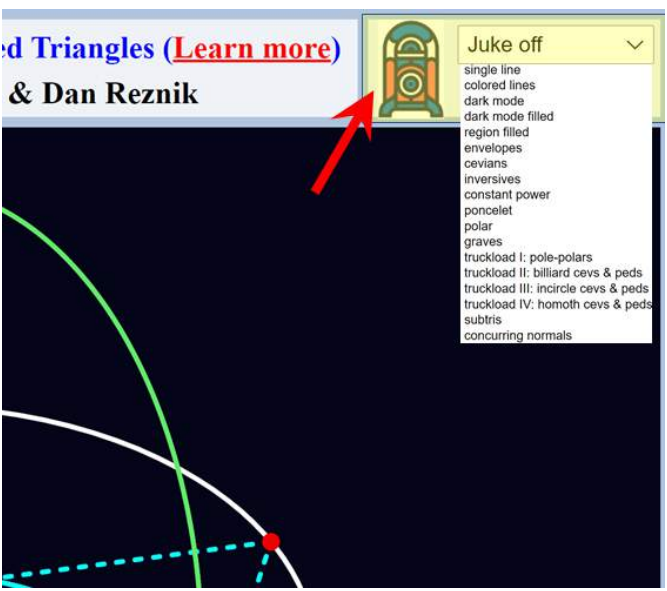

Figure 9.22: To play sequentially through one of many groups of experiments, select an item from the (highlighted) drop-down "jukebox" drop-down menu, at the top right hand corner of the app. To stop the jukebox playback, select `Juke off`. Click (or right-click) on the jukebox icon to quickly move forwards or backwards in a given sequence.

A Notes in Triangle Geometry

A.1 Trilinear coordinates

Let a triangle $\mathcal{T}$ be labeled "Euler style": vertices (and/or angles) A, B, C, and sidelengths a, b, c, where $a = |BC|,\ b = |AC|,\ c = |AB|$.

Note: since in this book triangles are studied within the context of Poncelet 3-periodics, we often refer to vertices (resp. sidelengths) as P_i (resp. s_i), $i = 1, 2, 3$.

If X is a point in the plane $\mathcal{T}$, then its position is completely determined by the ratios of directed distances (with signal) from X to the sidelines. Such ratios can therefore serve as coordinates for X. Any ordered triple $[p, q, r]$ of numbers respectively proportional to the directed distances (with signal) from X to the sidelines BC, CA, AB are called *homogeneous trilinear coordinates*, or, *trilinears*, for short.

Consider a point X whose trilinears are $[p, q, r]$. Then kp, kq and kr are the directed, signed distances to the sidelines of $\mathcal{T}$, where:

$$k = \frac{2\Delta}{ap + bq + cq}.$$

The above distances are known as *exact* trilinear coordinates. Often though, it is sufficient to use trilinears in their unnormalized homogeneous form. The trilinears

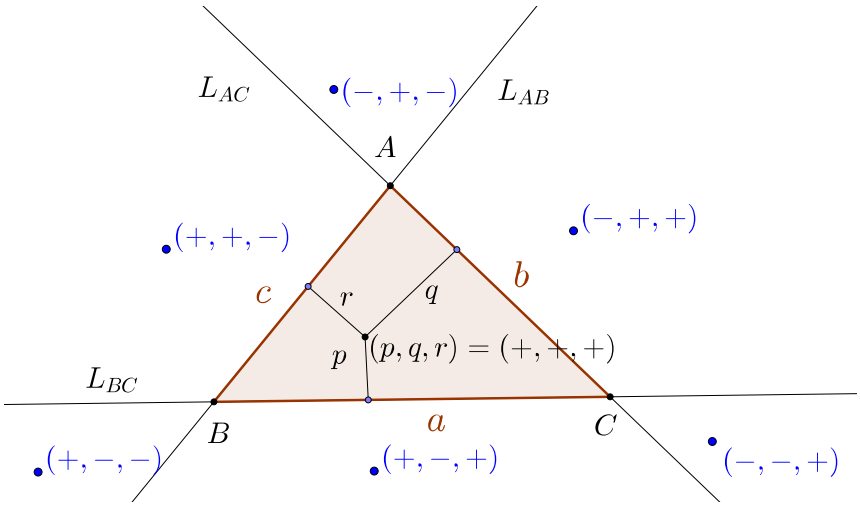

Figure A.1: Trilinear coordinates in the plane.

of A, B, C are given by:

$$A = \left[\frac{2\Delta}{a}, 0, 0\right], \quad B = \left[0, \frac{\Delta}{b}, 0\right], \quad C = \left[0, 0, \frac{2\Delta}{c}, 0\right].$$

As an example, consider the incenter X_1. As the center of the inscribed circle (incircle), the distances from it to the sidelines are one and the same (the inradius), therefore its trilinears are $[1, 1, 1]$. Recall the inradius is given by $r = (a + b + c)/(2\Delta)$, where Δ is the area of $\mathcal{T}$, see Weisstein (2019, Inradius).

A.2 More calculations with distances

Proposition A.1. *Let the trilinear coordinates of two points P and Q be $[p_1, q_1, r_1]$ and $[p_2, q_2, r_2]$. Suppose that $ap_i + bq_i + cr_i = 2\Delta$, i.e., the trilinear coordinates are the actual distances to the sidelines. Then the Euclidean distance $\rho = |P - Q|$ is given by:*

$$\rho^2 \sin^2 B = (p_1 - p_2)^2 + (r_1 - r_2)^2 - 2|(p_1 - p_2)(r_1 - r_2)| \cos B.$$

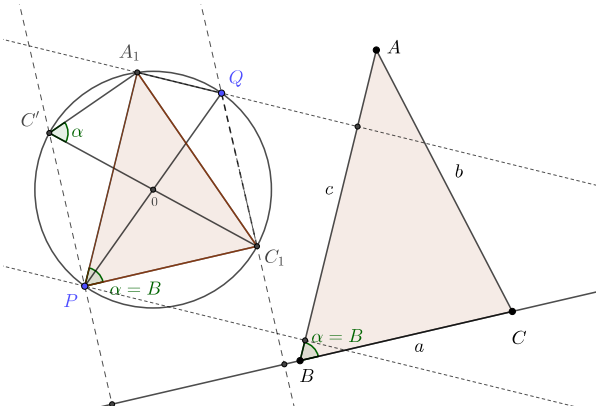

Figure A.2: Distance between points P and Q.

Also we have

$$\rho^2 \sin^2 A = (q_1 - q_2)^2 + (r_1 - r_2)^2 - 2|(r_1 - r_2)(q_1 - q_2)| \cos A.$$
$$\rho^2 \sin^2 C = (p_1 - p_2)^2 + (q_1 - q_2)^2 - 2|(p_1 - p_2)(q_1 - q_2)| \cos C.$$

Referring to Figure A.2:

Proof. Consider the circle having PQ as diameter and center O. Draw the segments PA_1 and PC_1 parallels to the sidelines AB and BC. Let C_1C' be also a diameter.

By the law of cosines we have that

$$|A_1 - C_1|^2 = |P - A_1|^2 + |P - C_1|^2 - 2|P - A_1|\,|P - C_1| \cos\alpha$$

Since C_1C' is a diameter it follows that $\angle A_1PC_1 = \angle A_1C'C_1$. Therefore,

$$|A_1 - C_1| = |C - C'| \sin\alpha = |P - Q| \sin\alpha = \rho \sin B.$$

Now, by the construction of A_1 and C_1, we have that

$$|P - C_1| = |p_1 - p_2|, \quad |P - A_1| = |r_1 - r_2|.$$

This ends the proof. □

Let

$$L = \begin{vmatrix} q_1 & r_1 \\ q_2 & r_2 \end{vmatrix}, \quad M = \begin{vmatrix} r_1 & p_1 \\ r_2 & p_2 \end{vmatrix}, \quad N = \begin{vmatrix} p_1 & q_1 \\ p_2 & q_2 \end{vmatrix}$$

Denote

$$\{L, M, N\} = L^2 + M^2 + N^2 - 2MN\cos A - 2LN\cos B - 2LM\cos C.$$

Proposition A.2.

$$\rho^2 = \frac{R^2\{L, M, N\}}{\Delta^2}.$$

Proof. The result follows from algebraic manipulations of the three formulas obtained in Proposition A.1. The details are left to the reader. □

Proposition A.3. *Let $lx + my + nz = 0$ be a straight line. Then the distances of the vertices of a reference triangle ABC to this line are:*

$$p = \frac{2\Delta}{a}\frac{l}{\{l, m, n\}}, \quad q = \frac{2\Delta}{b}\frac{m}{\{l, m, n\}}, \quad r = \frac{2\Delta}{c}\frac{n}{\{l, m, n\}}.$$

A.3 Barycentric coordinates

If the trilinears of a point are $[p, q, r]$ then its *barycentric coordinates* are $[ap, bq, cq]$. Observe that $2ap$ (resp. $2bq$, $2cr$) is the oriented area of triangle AXB (resp. CXA, BXC).

A.4 Conversion to and from cartesians

Trilinears $[p, q, r]$ of a point $X = (x, y) \in \mathbb{R}^2$ can be converted to cartesians coordinates using Kimberling (2019):

$$X = \frac{paA + qbB + rcC}{pa + qb + rc} \tag{A.1}$$

where $A = (x_a, y_a)$, $B = (x_b, y_b)$, $C = (x_c, y_c)$ are the vertices of the triangle ABC expressed in cartesian coordinates.

To convert cartesians to trilinears, consider a triangle $\mathcal{T} = ABC$ with vertices $A = (x_a, y_a)$, $B = (x_b, y_b)$ and $C = (x_c, y_c)$. The trilinears of $P = (x_0, y_0)$ are given by:

$$\left[\frac{1}{a}((C-B)\wedge P + B\wedge C) : \frac{1}{b}((A-C)\wedge P + C\wedge A) : \frac{1}{c}((B-A)\wedge P + A\wedge B)\right]$$

Where $u \wedge v$ denotes the area of the oriented parallelogram generated by u and v.

A.5 Triangle centers

Let $\mathbb{T}$ be the set of all real triples (a, b, c) which are sidelengths of a triangle ABC. That is,

$$\mathbb{T} = \{(a,b,c) : 0 < a < b + c, 0 < b < c + a, 0 < c < a + b\}.$$

On any subset U of $\mathbb{T}$, define a triangle center function as a nonzero function $f(a, b, c)$ such that:

- f is homogeneous in a, b, c (i.e., $f(ta, tb, tc) = t^n f(a, b, c)$ for some non negative integer n, $t > 0$, and all (a, b, c) in U.
- f is symmetric in b and c (i.e., $f(a, c, b) = f(a, b, c)$ for all (a, b, c) in U.

A center on U is an equivalence class $[p, q, r]$ of ordered triples (p, q, r) given by

$$p = f(a,b,c),\ \ q = f(b,c,a),\ r = f(c,a,b)$$

for some center function f defined on U.

Note: for compactness, sometimes the center function is expressed in terms of sines and cosines of the angles of the triangle.

Constructions for a few triangle centers and related objects are illustrated in Figure A.3.

A.6 Trilinear coordinates for selected triangle centers

Proposition A.4. *The trilinear coordinates for X_2 are given by* $[1/a, 1/b, 1/c]$.

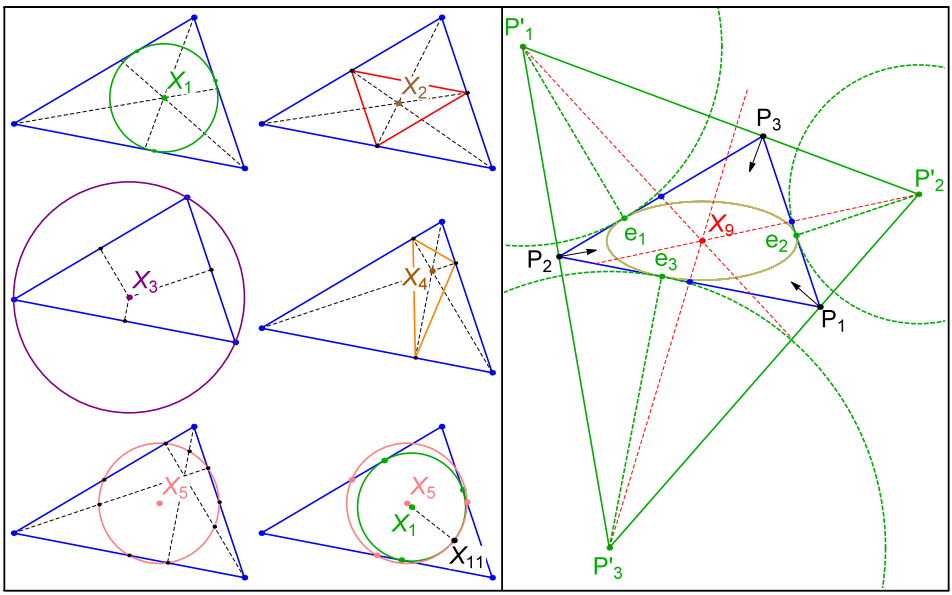

Figure A.3: Constructions for Triangle Centers X_i, $i = 1, 2, 3, 4, 5, 9, 11$, borrowed from Reznik, Garcia, and Koiller (2020a). The incenter X_1 is the intersection of angular bisectors, and center of the incircle (green), whose inradius is denoted r. The barycenter X_2 is where lines drawn from the vertices to opposite sides' midpoints meet. Side midpoints define the medial triangle (red). The circumcenter X_3 is the intersection of perpendicular bisectors, the center of the circumcircle (purple) whose circumradius is denoted R. The orthocenter X_4 is where altitudes concur. Their feet define the orthic (orange). X_5 is the center of the 9-point circle (pink). The Feuerbach point X_{11} is the single point of contact between the Incircle and the 9-Point circle. The *excenters*, i.e., the vertices of the excentral triangle, are pairwise intersections of external bisectors. The *excircles* (dashed green) are centered on the excenters and touch each side at an extouch point. Lines drawn from each excenter through sides' midpoints (dashed red) concur at the mittenpunkt X_9. Also shown (brown) is the triangle's Mandart inellipse, centered on X_9 and internally tangent to each side at an extouchpoint.

Proof. Consider a triangle of reference $\mathcal{T} = ABC$. The midpoint of the segment BC has trilinear coordinates $[0, 1/b, 1/c]$. In fact,

$$\left[0, \frac{a}{2}\sin C, \frac{a}{2}\sin B\right] \equiv [0, \sin C, \sin B] = [0, \sin C, \sin B]$$
$$\equiv \left[0, \frac{R}{b}, \frac{R}{c}\right] \equiv \left[0, \frac{1}{b}, \frac{1}{c}\right].$$

Analogously, $[1/a, 0, 1/c]$ and $[1/a, 1/b, 0]$ are the trilinear coordinates of the other two midpoints of ABC. Therefore, the medial lines are given by $by - cz = 0$, $ax - cz = 0$ and $ax - by = 0$. The intersection of these lines is the point $[1/a, 1/b, 1/c]$. □

Proposition A.5. *The trilinear coordinates of X_3 are given by* $[\cos A, \cos B, \cos C]$.

Proof. Let O be the center of the circumcirle of ABC. Draw a perpendicular line from P to the sideline BC.

As PO is a perpendicular bisector line, it follows that

$$\angle BOP = \frac{1}{2}\angle BOC = \angle BAC = A.$$

Therefore,

$$\frac{|BP|}{OP} = \frac{a}{2}\cot A$$

As $a/\sin A = 2R$ it follows that

$$\frac{a}{2}\cot A = R\sin A\cot A = R\cos A.$$

Performing the same analysis with the other two vertices the result follows. □

Proposition A.6. *The trilinear coordinates of X_4 are given by* $[\sec A, \sec B, \sec C]$.

Proof. The trilinear coordinates of the altitude feet relative to the side BC is given by $[0, \frac{2\Delta}{a}\cos C, \frac{2\Delta}{a}\cos B] \equiv [0, \cos C, \cos B]$. This follows directly by elementary analysis of the geometry of the triangle. Analogously, the other two are given by $[\cos C, 0, \cos A]$ and $[\cos B, \cos A, 0]$. Therefore, computing the intersection of the straight lines $\cos B\, y - \cos C\, z = 0$ and $\cos A\, x - \cos C\, z = 0$ it follows that $X_4 = [\sec A, \sec B, \sec C]$. □

Proposition A.7. *The trilinear coordinates of X_9 are given by* $[b + c - a, a + c - b, a + b - c] \equiv [\cot\frac{A}{2}, \cot\frac{B}{2}, \cot\frac{C}{2}]$.

Proof. Consider the excentral triangle $\mathcal{T}' = A'BC'$ of $\mathcal{T}$ We have that X_9 is the point of concurrence of lines drawn from each excentral point to the midpoint of the corresponding side of ABC. The excentral points have trilinear coordinates $A' = [-1, 1, 1]$, $B' = [1, -1, 1]$ and $C' = [1, 1, -1]$. The lines passing through the excentral points and the correspondent midpoints $[0, 1/b, 1/c]$, $[1/a, 0, 1/c]$ and $[1/a, 1/b, 0]$ of the sides of the triangle $\mathcal{T}$ are given by

$$(b-c)x + by - cz = 0, \quad ax + (a-c)y - cz = 0, \quad ax - by + (a-b)z = 0.$$

Solving the linear system above it follows that $[x, y, z] = [b + c - a, a + c - b, a + b - c]$. Also, using the laws of cosine and sine it follows that

$$\cot\frac{A}{2} = \frac{\cos A + 1}{\sin A} = \frac{(a+b+c)(b+c-a)R}{abc} = k(b+c-a)$$
$$k = \frac{R(a+b+c)}{abc}$$

Analogously, $\cot\frac{B}{2} = k(a+c-b)$ and $\cot\frac{C}{2} = k(a+b-c)$. □

Table A.1 lists trilinears for some centers mentioned above as well as a few others.

A.7 Some derived triangles

A *derived triangle* $\mathcal{T}'$ is constructed from the vertices of a reference triangle $\mathcal{T}$. It can be represented by a 3×3 *vertex matrix*, whose rows the trilinears of the vertices of $\mathcal{T}'$ with respect to $\mathcal{T}$. A few examples include:

- The *excentral* triangle is bounded by the external bisectors of a triangle. Its vertices are known as the *excenters*.
- The *medial* triangle has vertices at the midpoints of the reference's sides.
- The *intouch triangle* has vertices at the points of tangency of the incircle with the sidelines of a reference triangle.
- The *extouch* triangle has vertices at the tangency points of the excircles with the sidelines, see Figure A.4. These are also the midpoints of the perimeter of $\mathcal{T}$. For example, $|A - C| + |A - C_e| = |B - C| + |B - C_e|$.

X_k	triangle center	$f(a,b,c)$
X_1	incenter	1
X_2	barycenter	$1/a$
X_3	circumcenter	$\cos A$
X_4	orthocenter	$\sec A$
X_5	center of Euler's circle	$\cos(B-C)$
X_6	symmedian point	a
X_7	Gergonne point	$(bc)/(b+c-a)$
X_8	Nagel point	$(b+c-a)/a$
X_9	mittenpunkt	$b+c-a$
X_{10}	Spieker center	$bc(b+c)$
X_{11}	Feuerbach point	$1-\cos(B-C)$
X_{15}	1st isodynamic point	$\sin(A+\frac{\pi}{3})$
X_{16}	2nd isodynamic point	$\sin(A-\frac{\pi}{3})$

Table A.1: Some triangle centers and their first trilinear coordinate expressed as a symmetric function $f(a,b,c)$ on the sidelengths. The complete trilinear vector is given cyclically by $[f(a,b,c), f(b,c,a), f(c,a,b)]$. Note that sometimes these are more concisely expressed as trig functions on the angles A, B, C which can be converted back to $f(a,b,c)$ via the law of sines and/or cosines.

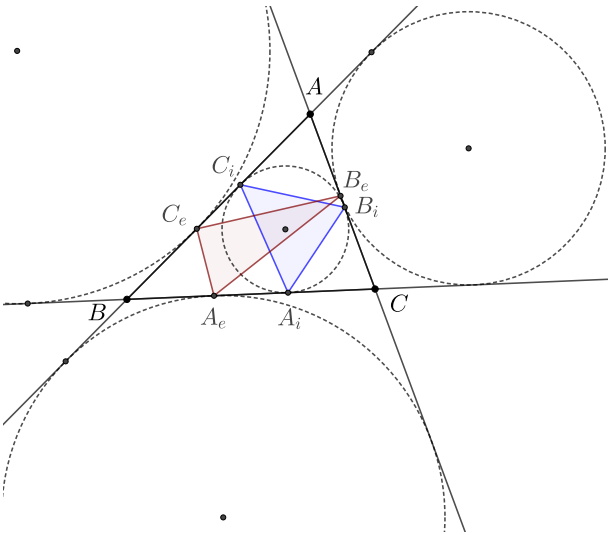

Figure A.4: Intouch triangle (blue) and extouch triangle (brown).

- The *anticomplementary* triangle is such that its medial triangle is the original reference triangle, see Figure A.5.
- The *Feuerbach* triangle has vertices at the points where the 9-point circle touches each of the excircles, Figure A.6.

The vertex matrices for the first three are given by:

$$\begin{bmatrix} -1 & 1 & 1 \\ 1 & -1 & 1 \\ 1 & 1 & -1 \end{bmatrix}, \begin{bmatrix} 0 & b^{-1} & c^{-1} \\ a^{-1} & 0 & c^{-1} \\ a^{-1} & b^{-1} & 0 \end{bmatrix}, \begin{bmatrix} 0 & \frac{ac}{a-b+c} & \frac{ab}{a+b-c} \\ \frac{bc}{b+c-a} & 0 & \frac{ab}{a+b-c} \\ \frac{bc}{b+c-a} & \frac{ac}{a-b+c} & 0 \end{bmatrix}$$

And that for the extouch triangle is:

$$\begin{pmatrix} 0 & \frac{a-b+c}{b} & \frac{a+b-c}{c} \\ \frac{-a+b+c}{a} & 0 & \frac{a+b-c}{c} \\ \frac{-a+b+c}{a} & \frac{a-b+c}{b} & 0 \end{pmatrix}$$

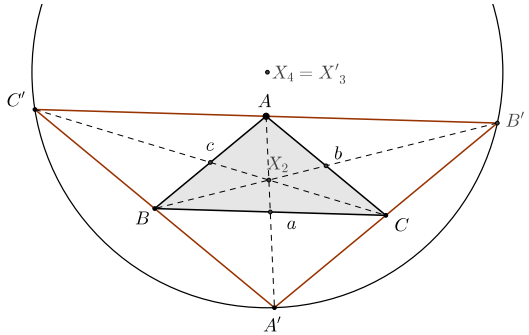

Figure A.5: The anticomplementary triangle $A'B'C'$ of ABC has sides which pass through each vertex of a reference triangle and are parallel to the opposite side. Its circumcenter X'_3 coincides with the reference's orthocenter X_4.

The trilinear vertex matrix of the anticomplementary triangle $\mathcal{T}' = A'B'C'$ is given by Weisstein (2019):

$$\begin{pmatrix} -\frac{1}{a} & \frac{1}{b} & \frac{1}{c} \\ \frac{1}{a} & -\frac{1}{b} & \frac{1}{c} \\ \frac{1}{a} & \frac{1}{b} & -\frac{1}{c} \end{pmatrix}$$

In Weisstein (ibid., Feuerbach triangle), the trilinear vertex matrix for the Feuerbach triangle $A_1B_1C_1$ is defined as:

$$\begin{pmatrix} -\sin^2(\frac{B-C}{2}) & \cos^2(\frac{C-A}{2}) & \cos^2(\frac{A-B}{2}) \\ \cos^2(\frac{B-C}{2}) & -\sin^2(\frac{C-A}{2}) & \cos^2(\frac{A-B}{2}) \\ \cos^2(\frac{B-C}{2}) & \cos^2(\frac{C-A}{2}) & -\sin^2(\frac{A-B}{2}) \end{pmatrix}$$

The trilinear coordinates of X_{11} is given by:

$$[1 - \cos(B - C) : 1 - \cos(C - A) : 1 - \cos(A - B)]$$

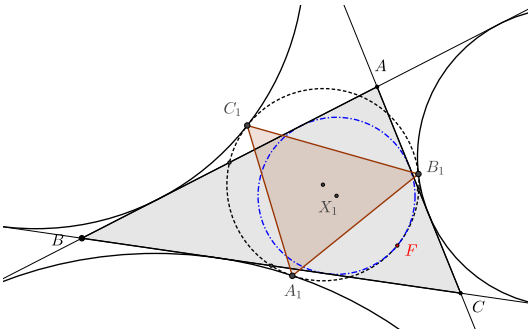

Figure A.6: The Feuerbach triangle $A_1B_1C_1$ of ABC has vertices where the 9-point circle touches the excircles. Point $F = X_{11}$ is the Feuerbach point.

A.8 The (first) Brocard triangle

Referring to Figure A.7, the first Brocard point Ω (resp. second Brocard point Ω') of a triangle $\mathcal{T} = ABC$ (labeled in counterclockwise order) is the unique point interior to $\mathcal{T}$ such that angles $\angle\Omega AB$, $\angle\Omega BC$ and $\angle\Omega CA$ (resp. angles $\angle\Omega' BA$, $\angle\Omega' CB$ and $\angle\Omega' AC$) are equal.

The trilinear coordinates of Ω (resp Ω') are $[c/b : a/c : b/a]$ (resp. $[b/c : c/a : a/b]$.). Since neither is symmetric in the last two coordinates, they are not proper triangle centers. In fact, they are known as a *bicentric* pair, see Kimberling (2020a).

Consider the six straight lines passing through A, B, C and the Brocard points Ω and Ω.

Referring to Figure A.8, the triangle with vertices $B_1 = A\Omega \cap B\Omega'$, $B_2 = C\Omega \cap A\Omega'$ and $B_3 = B\Omega \cap C\Omega'$ is called the *first Brocard triangle*.

The Brocard circle is the circumcircle of the first Brocard triangle, Figure A.8. It contains the two Brocard points and the circumcenter X_3 and the symmedian point X_6. Its center is X_{182}, at the midpoint of X_6 and X_3. Lines X_3X_6 and $\Omega\Omega'$ are orthogonal.

In Johnson (1929), one finds many identities concerning the Brocard points, a few of which are reproduced below:

$$\cot A + \cot B + \cot C = \cot\omega.$$

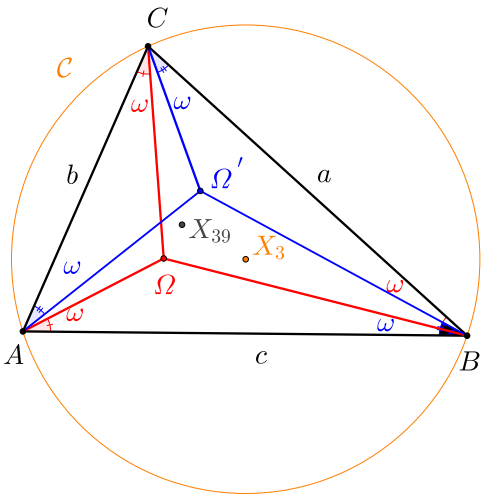

Figure A.7: Brocard points Ω and Ω' of a triangle ABC. X_{39} sits at the midpoint of $\Omega\Omega'$.

$$|\Omega - X_3| = |\Omega' - X_3| = R\sqrt{1 - 4\sin^2\omega}.$$

$$R_B = \frac{R\sqrt{1 - 4\sin^2\omega}}{2\cos\omega}.$$

The trilinear vertex matrix of the Brocard triangle $B_1B_2B_3$ is given by:

$$\begin{pmatrix} abc & c^3 & b^3 \\ c^3 & abc & a^3 \\ b^3 & a^3 & abc \end{pmatrix}$$

A.9 Pedal and antipedal triangles

Referring to Figure A.9(left), the *pedal* triangle with respect to a point P has vertices at the feet of perpendiculars dropped from P onto the sidelines of a reference triangle.

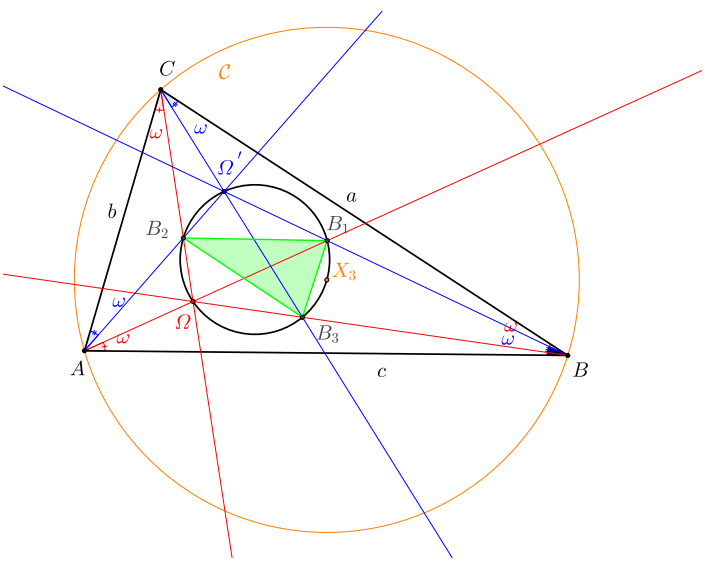

Figure A.8: The first Brocard triangle $B_1B_2B_3$ and its circumcircle, also known as the Brocard circle.

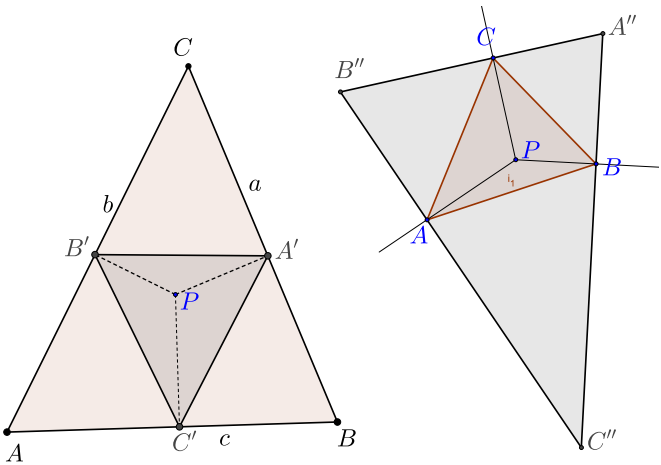

Figure A.9: **Left:** $A'B'C'$ is the pedal triangle of ABC with respect to P. **Right:** $A''B''C''$ is the antipedal of ABC wrt to P, i.e., thepedal of $A''B''C''$ is ABC.

Referring to Figure A.9(right), the *antipedal* triangle is the triangle whose pedal triangle is the reference. One construction for it is as follows: connect P to the vertices of reference $\mathcal{T}$. For each vertex draw a line perpendicular to the corresponding line. The antipedal triangle will be bounded by said lines.

Let $[p, q, r]$ denote the trilinears of a point P. The vertex matrix for the pedal (resp. antipedal) triangle with respect to P will be given by:

$$\begin{pmatrix} 0 & q + p\cos C & r + p\cos B \\ p + q\cos C & 0 & r + q\cos A \\ p + r\cos B & q + r\cos A & 0 \end{pmatrix}$$

Respectively:

$$\begin{pmatrix} -\frac{q+p\cos C}{r+p\cos B} & \frac{r+p\cos B}{p+q\cos C} & \frac{q+p\cos C}{p+r\cos B} \\ \frac{(r+q\cos A)}{q+p\cos C} & -\frac{r+q\cos A}{p+q\cos C} & \frac{q+p\cos C}{q+r\cos A} \\ \frac{q+r\cos A}{r+p\cos B} & \frac{p+r\cos B}{r+q\cos A} & -\frac{p+r\cos B}{q+r\cos A} \end{pmatrix}$$

The pedal triangle with respect to the incenter, circumcenter, and orthocenter are the intouch, medial, and orthic triangles.

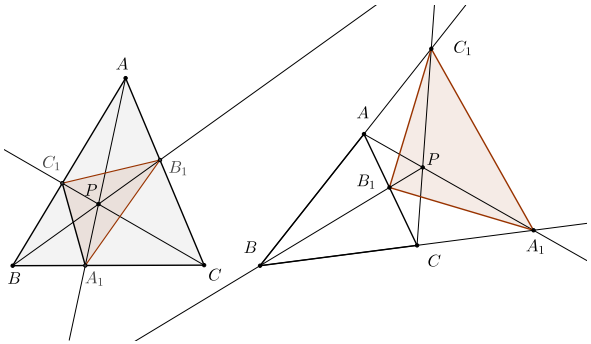

Figure A.10: Ceva triangle $A_1B_1C_1$ of ABC.

A.10 Cevian triangle

Referring to Figure A.10, the Cevian (or Ceva) triangle with respect to a point P has vertices at the intersections of lines from the vertices through P with the opposite sides. These lines are also known as *Cevians*. Let $P = [p, q, r]$. Then the vertex matrix for said Cevian triangle will be given by:

$$\begin{pmatrix} 0 & q & r \\ p & 0 & r \\ p & q & 0 \end{pmatrix}$$

A.11 Perspective triangles

Two triangles $\mathcal{T} = ABC$ and $\mathcal{T}_1 = A_1B_1C_1$ are in perspective when the three lines AA_1, BB_1 and CC_1 are concurrent. This point is called the *perspector* of the pair $\{\mathcal{T}, \mathcal{T}_1\}$. The *perspective axis* of a pair of triangles is the line through the three points of intersection of the corresponding sidelines $AB \cap A_1B_1$, $AC \cap A_1C_1$ and $BC \cap B_1C_1$. See Figure A.11.

A.12 Polar triangle

Referring to Figure A.12, given a reference triangle $\mathcal{T}$ and a conic $\mathcal{E}$, the *polar* triangle is bounded by the polars of the vertices of $\mathcal{T}$ with respect to $\mathcal{E}$. The reference

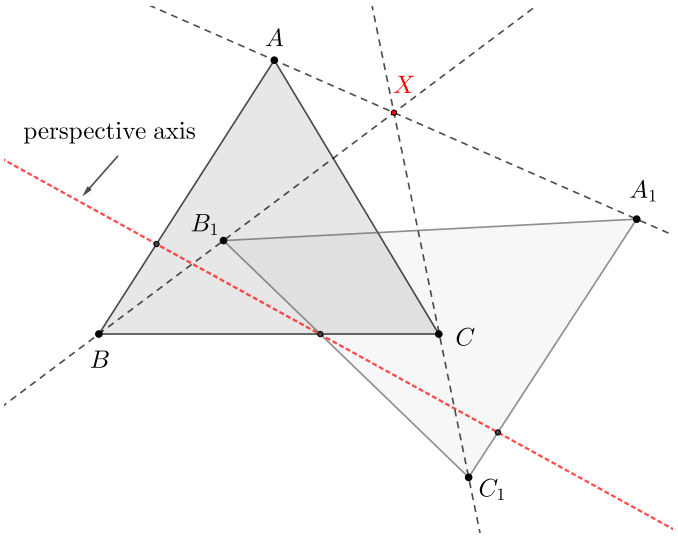

Figure A.11: The perspector X of triangles ABC and $A_1B_1C_1$ and the perspective axis.

and its polar are always perspective at a some point X, known as the perspector of $\mathcal{E}$.

A.13 Circumconic

A *circumconic* of a triangle contains its three vertices. A 2d family of such conics exists. If center (or perspector) is specified, then the circumconic is unique. Points $[x, y, z]$ on a circumconic satisfy:

$$\frac{p}{x} + \frac{q}{y} + \frac{r}{z} = 0$$

If the perspector is supplied, the center of the circumconic is given by:

$$[p(-ap + bq + cr), q(ap - bq + cr), r(ap + bq - cr)]$$

The circumcircle is the circumconic centered on X_3. Its points satisfy:

$$ayz + bxz + cxy = 0.$$

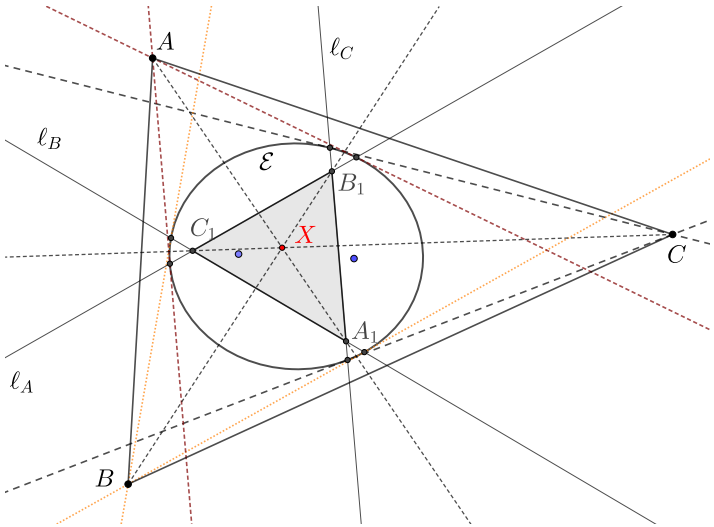

Figure A.12: The polar triangle $A_1B_1C_1$ of ABC with respect to a conic $\mathcal{E}$ are in perspective at X.

A.14 Inconic

The inconic $\mathcal{E}'$ is tangent to the sidelines of a triangle. A 2d family of inconics exists for any triangle. If either center or perspector is specified, then the inconic is unique. For inconics, the perspector is also called the Brianchon point. Let its trilinears be $[\frac{1}{p}, \frac{1}{q}, \frac{1}{r}]$. Then the center is given by $[cq + br : ar + cp : bp + aq]$ and the inconic will satisfy:

$$p^2x^2 + q^2y^2 + r^2z^2 - 2qryz - 2prxz - 2pqxy = 0$$

A.15 Brocard inellipse

The Brocard inellipse is the inconic with parameters $[p, q, r] = [1/a, 1/b, 1/c]$. Points $[x, y, z]$ on it satisify:

$$a^2b^2z^2 - 2a^2bcyz + a^2c^2y^2 - 2ab^2cxz - 2abc^2xy + b^2c^2x^2 = 0$$

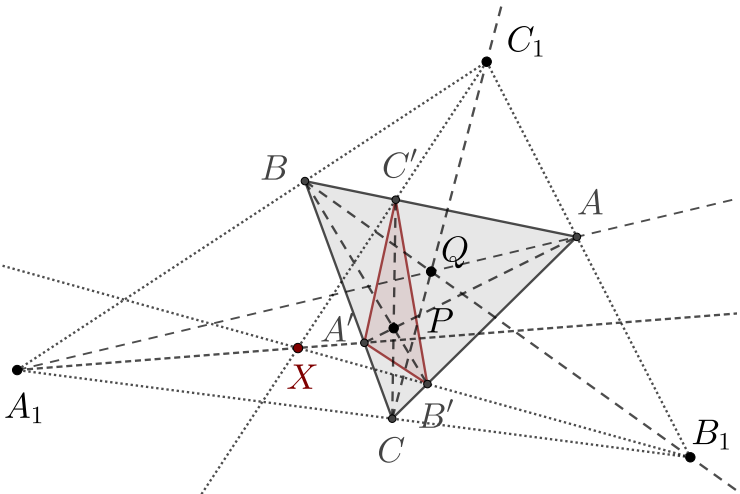

Figure A.13: Point X is the P-Ceva conjugate of Q.

Its center is $X_{39} = [a(b^2 + c^2), b(a^2 + c^2), c(a^2 + b^2)]$ and the perspector is $X_6 = [a, b, c]$.

A.16 Ceva conjugate

Referring to Figure A.13, Let P and Q be points, neither of which lie on a sideline of the reference triangle $\mathcal{T} = ABC$. The P-Ceva conjugate X of Q is the perspector of the Cevian triangle of P and the anticevian triangle of Q, see Kimberling (1998).

A.17 Isogonal conjugation

In the investigation of triangle geometry the isogonal conjugation is an important tool. Referring to Figure A.14, consider a reference triangle $\mathcal{T} = ABC$. Two rays CP and CP' are *isogonal* relative to C when $\angle ACP = \angle BCP'$. Equivalently, the ray CX_1 is the common bisector of $P'CP$ and ACB.

If rays AP and AP' are isogonal ($\angle BAP = \angle BAP'$), we say points P and P' are *isogonal conjugates*. It can be shown that $\angle PBC = \angle P'BC$.

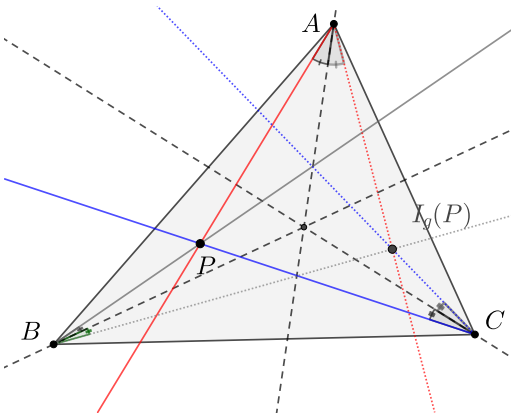

Figure A.14: Isogonal conjugation.

Proposition A.8. *Let P and P' be isogonal conjugates. If $P = [p, q, r]$ then $P' = [1/p, 1/q, 1/r] = [qr, pr, pq]$. The map $\varphi(P) = P'$ is an involution, i.e., $\varphi^2 = id$.*

Proof. Direct from the definition of the map φ. □

The isogonal conjugation is a special quadratic Cremona transformation.

Another useful construction of the isogonal conjugate is as follows. Consider triangle $\mathcal{T} = ABC$ and a point P. Denote by A_1, B_1 and C_1 the contact points of the sidelines of $\mathcal{T}$ with the incircle. Consider the reflection of line AP on AA_1, repeating this cyclically, i.e., reflect line BP (resp. PC) on the bisector BB_1 (resp. CC_1). The intersection of said reflected lines is the *isogonal conjugate* of P.

Proposition A.9. *Let $[p, q, r]$ be the trilinears of a point P. Its isogonal conjugate is given by $[1/p, 1/q, 1/r]$.*

Proof. Consider trilinears $P = [p, q, r]$, $A = [1, 0, 0]$, $B = [0, 1, 0]$ and $C = [0, 0, 1]$. Then $A_1 = [0, 1, 1]$, $B_1 = [1, 0, 1]$ and $C_1 = [1, 0, 0]$. The line AP is given by $qz - ry = 0$ and its reflection relative to the bisector $z = y$ is line $qy - rz = 0$. Cyclically, the other two reflected lines are given by $xp - rz = 0$ and $px - qy = 0$. The intersection of these three lines is

$$\left[\frac{rz}{p}, \frac{rz}{q}, \frac{rz}{r}\right] = \left[\frac{1}{p}, \frac{1}{q}, \frac{1}{r}\right]$$

□

Under isogonal conjugation, it follows that

$$\angle PAB = \angle CAI_g(P),\ \ \angle PBC = \angle ABI_g(P),\ \ \angle PCA = \angle BCI_g(P)$$

The isogonal conjugation is the map

$$I_g([p,q,r]) = [1/p, 1/q, 1/r] = [qr, pr, pq]$$

which is an involution ($I_g \circ I_g = id$).

Referring to Figure A.15:

Proposition A.10. *The circumcenter X_3 and orthocenter X_4 are isogonal conjugates.*

Proof. Let $\mathcal{T} = ABC$. The isosceles triangle BOC has angle $2A$ (or $2\pi - 2A$) at vertex O. Therefore the angle between ray CO and segment BC is equal to $\pi/2 - A$ (or $A - \pi/2$). The angle between ray CX_4 and the segment CA is $\pi/2 - A$ (or $A - \pi/2$). Therefore, X_4 and X_3 are isogonal relative to C. The same conclusion follows for the other vertices. □

A.18 Isotomic conjugation

Referring to Figure A.16, consider a triangle $\mathcal{T} = ABC$ and a point P, consider the intersection A_1 of the line AP with the sideline BC. Reflect A_1 with respect to the midpoint A_m of side BC, obtaining the point A_1'. Repeat cyclically and obtain B_1' and C_1'. The intersection of the three lines AA_1', BB_1' and CC_1' is the isotomic conjugate of P.

Proposition A.11. *Consider $P = [p,q,r]$ specified in trilinear coordinates. Then the isotomic conjugate of P is $[1/(a^2p), 1/(b^2q), 1/(c^2r)]$. If $P = [p,q,r]$ is specified in barycentric coordinates, then the isotomic conjugate of P is simply $[1/p, 1/q, 1/r]$.*

Proof. Let $P = [p,q,r]$, $A = [1,0,0]$, $B = [0,1,0]$ and $C = [0,0,1]$ be the trilinears for said points. The midpoint of the side BC is $A_m = [0,c,b]$. Also, $B_m = [c,0,a]$ and $C_m = [b,a,0]$. The line AP is given by $qz - ry = 0$. Therefore $A_1 = [0,q,r]$ and $A_1' = [0, c^2r, b^2q]$.

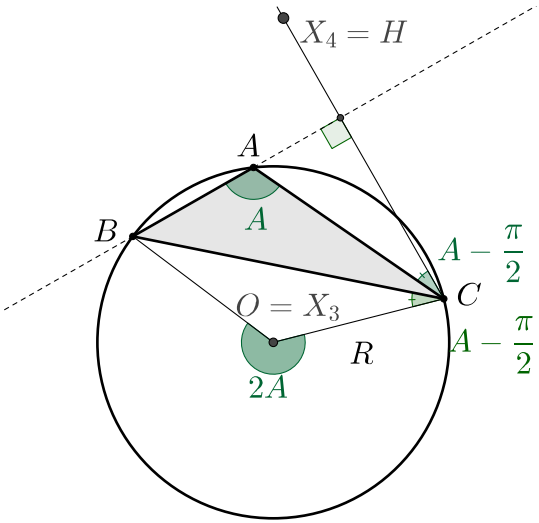

Figure A.15: X_3 and X_4 are isogonal conjugates.

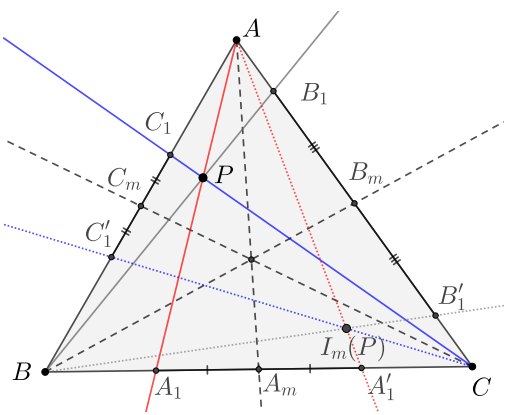

Figure A.16: Isotomic conjugation.

Analogously, the line BP is given by $rx - pz = 0$. Therefore $B_1 = [p, 0, r]$ and $B_1' = [r^2c, 0, a^2p]$. Therefore the intersection of lines AA_1' and BB_1' is the point

$$\left[\frac{1}{a^2p}, \frac{1}{b^2q}, \frac{1}{c^2r}\right]$$

□

The isotomic conjugation is the map $I_m([p, q, r]) = [1/(a^2p), 1/(b^2q), 1/(c^2r)]$ $= [qr/a^2, pr/b^2, pq/c^2]$ which is also an involution.

A.19 The Euler line

The trilinears $[x, y, z]$ of a line passing through points (given in trilinears) $[u, v, w]$ and $[p, q, r]$ satisfy:

$$\begin{vmatrix} x & y & z \\ u & v & w \\ p & q & r \end{vmatrix} = 0,$$

Since the Euler line contains X_3 and X_4, it is given by:

$$\begin{vmatrix} x & y & z \\ \cos A & \cos B & \cos C \\ \frac{1}{\cos A} & \frac{1}{\cos B} & \frac{1}{\cos C} \end{vmatrix} = 0,$$

Equivalently, points $[x, y, z]$ on the Euler line satisfy:

$$\cos A(\cos^2 B - \cos^2 C)x + \cos B\left(\cos^2 C - \cos^2 A\right)y + \cos C\left(\cos^2 A - \cos^2 B\right)z = 0.$$

The Euler line can also be written in terms of the sidelengths a, b, c:

$$a(c^2-b^2)(-a^2+b^2+c^2)x + b(a^2-c^2)(a^2-b^2+c^2)y + c(b^2-a^2)(a^2+b^2-c^2)z = 0$$

The point at infinity on the Euler line is its intersection with the line $ax + by + cz = 0$; equivalently $\sin A\ x + \sin B\ y + \sin C\ z = 0$.

A notable point in the Euler line is the barycenter X_2, whose trilinear are $[1/a, 1/b, 1/c] \equiv [\sin A, \sin B, \sin C]$.

Proposition A.12. *Consider a triangle with vertices at the following cartesian coordinates:* $A = [\alpha, \beta]$, $B = [-1, 0], C = [1, 0]$. *The Euler line is given by:*

$$(3 - 3\alpha^2 - \beta^2)x - 2\alpha\beta y + \alpha(\alpha^2 + \beta^2 - 1) = 0$$

Proof. In cartesians:

$$X_3 = \left[0, \frac{\alpha^2 + \beta^2 - 1}{2\beta}\right], \quad X_4 = \left[\alpha, \frac{1 - \alpha^2}{\beta}\right]$$

The claim follows from direct calculations. □

Proposition A.13. *The image of the Euler line by isogonal conjugation* I_g *is the circumconic (hyperbola) given by*

$$\begin{aligned}\mathcal{I}_E(x, y, z) = &-c\left(a^2 - b^2\right)\left(a^2 + b^2 - c^2\right)xy + b\left(a^2 - c^2\right)\left(a^2 - b^2 + c^2\right)xz \\ &+ a\left(b^2 - c^2\right)\left(a^2 - b^2 - c^2\right)yz = 0\end{aligned}$$

More general, the image of any line by I_g *is a circumconic.*

Proof. Write the Euler line in the parametric form $E(u) = (1 - u)X_3 + uX_4$ and compute $I_g(E(u))$. Now, writing in the implicit form, it is straightforward to obtain the result stated. □

Proposition A.14. *The image of the Euler line under the isotomic conjugation* I_m *is circumconic (hyperbola) by:*

$$\begin{aligned}\mathcal{I}_H(x, y, z) = &ab(a^2 - b^2)(a^2 + b^2 - c^2)xy - ac(a^2 - c^2)(a^2 - b^2 + c^2)xz \\ &- bc(b^2 - c^2)(a^2 - b^2 - c^2)yz = 0\end{aligned}$$

A.20 Circumconic and inconic with conjugation of barycentrics

Let the center $[u, v, w]$ be the barycentrics of a circumconic's center U. Then its perspector is given by $G(U)$, the X_2-Ceva conjugate of U. Algebraically: $G([u, v, w]) = [u(v + w - u), v(w + u - v), w(u + v - w)]$. Let $U = [u, v, w]$ be the barycentrics of an inconic's center. Then its perspector (Brianchon) will be given by $I(A(U))$, where $I([u, v, w]) = [1/u, 1/v, 1/w]$ is the isotomic conjugate of a point and $A([u, v, w]) = [v + w - u, w + u - v, u + v - w]$ is the anticomplement.

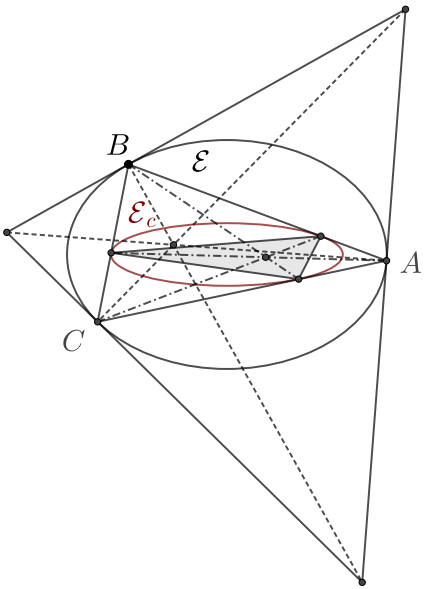

Figure A.17: The elliptic billiard has X_1 as its perspector; the caustic is the Mandart inellipse, whose Brianchon point is the Nagel point X_8.

A.21 Billiard notes

Referring to Figure A.17, the elliptic billiard can be regarded as the (fixed) circumconic centered on X_9, called elsewhere the "circumbilliard". Its perspector is X_1.

The caustic of the elliptic billiard is the Mandart inellipse, whose Brianchon (perspector) is the Nagel point X_8.

Proposition A.15. *The isogonal conjugate of billiard 3-periodics is the antiorthic axis of $\mathcal{T}$.*

Proof. Recall that the antiorthic axis is the perspective axis of $\mathcal{T}$ and its excentral triangle, and that the elliptic billiard is centered at X_9 (mittenpunkt) and its perspector is X_1 (incenter). Therefore, it follows that the antiorthic axis is given by $x + y + z = 0$. The elliptic billiard is $xy + xz + yz = 0$. □

A.22 Exercises

Exercise A.1. *Let $P = [p, q, r]$ be an interior point of an equilateral triangle $\mathcal{T} = ABC$. Show that:*

- *the distances from P to the sidelines are given by $[pk, qk, rk]$, where $k = (2A)/(pa + qb + rc)$ and A is the area of the triangle.*
- *$k(p + q + r)$ is equal to the length of the triangle's altitude, i.e., the sum is independent of the position of the point.*
- *The result is true for P exterior to the triangle, though here we need to consider the signed distance, as in Figure A.1.*
- *If the sum of distances is independent of the point, then the triangle is equilateral.*
- *Generalize the above to regular polygons.*

Exercise A.2. *Show that mittenpunkt X_9 is the symmedian point of the excentral triangle.*

Exercise A.3. *Let P and Q be isogonal conjugates in a triangle ABC. Then the circumcenters of BPC and BQC are inverses with respect to the circumcircle of the triangle ABC.*

Exercise A.4. *Let P and Q be isogonal conjugates in the of triangle ABC. Then the pedal triangles with respect to P and Q share a circumcircle. Moreover, the center of this circle is the midpoint of PQ.*

Exercise A.5. *Let P and Q be isogonal conjugates in a triangle $\mathcal{T} = ABC$. Consider triangle $\mathcal{T}'$ whose vertices lie at the reflections of P with respect to sides AB, BC and AC. Show the circumcenter of $\mathcal{T}'$ is Q.*

Exercise A.6. *Let $\mathcal{E}$ be an ellipse inscribed in a triangle ABC (i.e., an inconic). Then foci f_1 and f_2 of $\mathcal{E}$ are isogonal conjugates.*

Exercise A.7. *Consider two lines x and y passing through a point P_0. Let u and v be conjugate lines with respect to x and y. Let $P \in u$ and $P_x \in x$ and $P_y \in y$ be the pedal points of P. Referring to Figure A.18, show that (i) the points $\{P_0, P, P_x, P_y\}$ are concyclic; (ii) line $h = P_x P_y$ is orthogonal to the line v.*

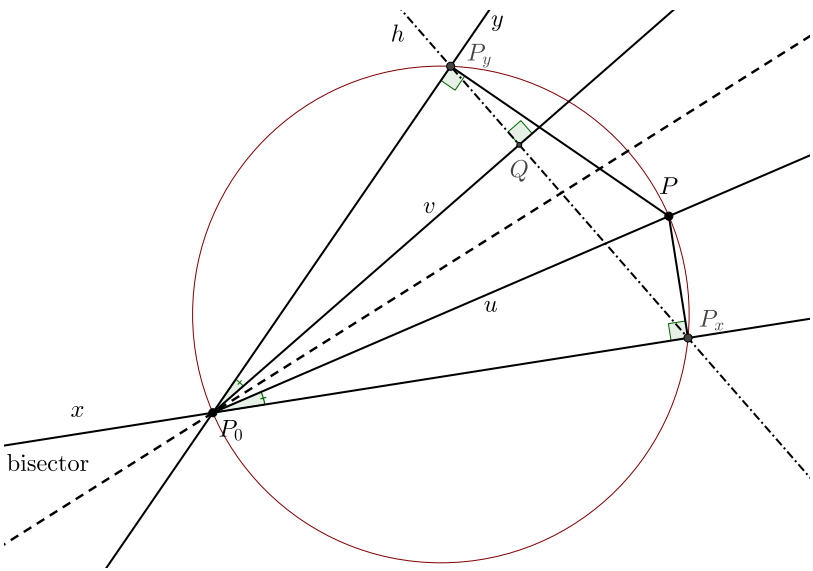

Figure A.18: Isogonal line v is orthogonal to $h = P_x P_y$.

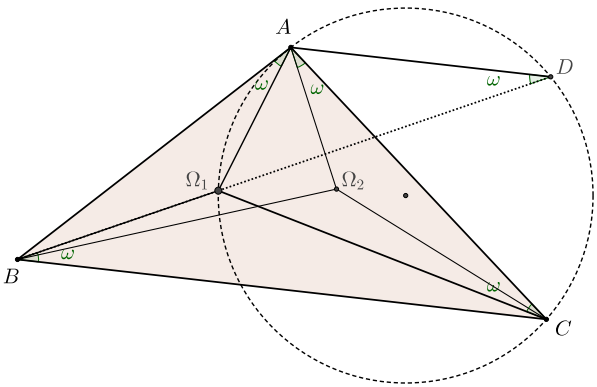

Figure A.19: Geometric construction of Brocard points: let ABC be a triangle. Draw a line through A and parallel to BC. Consider the circle through C and tangent to AB at A. Let D be the intersection of said line and circle. Line BD intersects the circle at Brocard point Ω_1. Repeat this construction for the other vertices and obtain Ω_2.

Exercise A.8. *Show the Brocard points can be obtained through the construction in Figure A.19.*

Exercise A.9. *Let the incircle of triangle ABC touch side BC at A_1, and let A_1A_1' be a diameter of the incircle. Denote by A_2 the intersection of lines AA_1' and BC. Show that $BA_2 = CA_1$. Consider a similar construction with respect to the two other sides. Show that the three lines AA_2, BB_2 and CC_2 are concurrent. Show that this point is X_8 and that it lies on line X_1X_6.*

Exercise A.10. *A similarity about a point O is a composition of a rotation and a dilation, both centered at O. Consider a quadrilateral $ABCD$ which is not a parallelogram. Show that there is a unique similarity sending AC to BD.*

Exercise A.11. *Let A, B, C, D be four distinct points in the plane, such that AC is not parallel to BD. Let X be the intersection of AC and BD. Let the circumcircles of ABX and CDX meet again at O. Show that O is the center of the unique similarity that sends A to C and B to D.*

Exercise A.12. *If O is the center of the similarity that sends A to C and B to D, then O is also the center of the similarity that sends A to B and C to D. See Zhao (2021) and Chavez-Caliz (2020).*

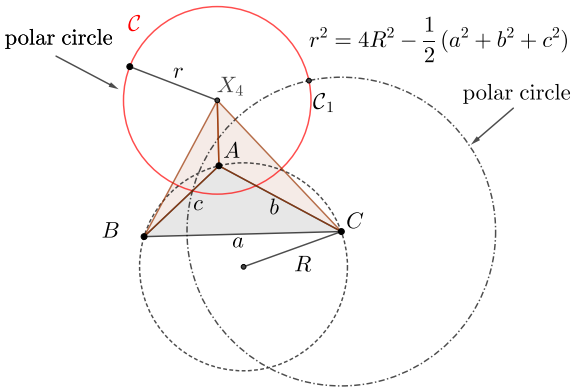

Figure A.20: Polar circles intersecting orthogonally.

Exercise A.13. *Let ABC be a triangle and $\mathcal{C}$ its circumcircle. Let the tangent lines to $\mathcal{C}$ at B and C meet at D. Show that AD is a symmedian of ABC. Use this fact to construct X_6.*

Exercise A.14. *Consider a triangle ABC. On sideline BC construct two points A_1, A_2 such that $A_2 - C = c$ and $A_1 - B = b$. The segment A_1A_2 has length $a + b + c$. Repeat the construction for the other two sidelines. Show that the six points obtained lie on a circle known as Conway's circle.*

Exercise A.15. *A polar circle of an obtuse triangle $\mathcal{T} = ABC$ is the circle centered at the orthocenter X_4 with radius r given by $r^2 = 4R^2 - (a^2 + b^2 + c^2)/2$, where R is the radius of the circumcircle of $\mathcal{T}$. Define analogously the polar circles of triangles ABH, BCH and ACH. Referring to Figure A.20, show that all polar circles intersect orthogonally. Determine the nine-point-circles of the four triangles.*

Exercise A.16. *An orthocentric system is a set of four points $P_i = (x_i, y_i)$ $(i = 1, \ldots, 4)$ in the plane, such that each point P_i is the orthocenter of the triangle defined by the other three points. Show that the set of orthocentric systems is an algebraic set of co-dimension 2 in $\mathbb{R}^8$.*

Exercise A.17. *Show that the circumconic that is the isogonal image of Euler line is never an ellipse.*

Exercise A.18. *Consider the triangle with cartesian vertices* $A = [\alpha, \beta]$, $B = [-1, 0]$ *and* $C = [1, 0]$ *and sides* $a = 2$, $b = \sqrt{(\alpha - 1)^2 + \beta^2}$, $c = \sqrt{(\alpha + 1)^2 + \beta^2}$. *Let* $P_1 = [p_1, q_1, r_1]$ *and* $P_2 = [p_2, q_2, r_2]$ *be the trilinears of three points. Let* $P(u) = uP_1 + (1 - u)P_2$. *Consider the cartesian coordinates for said points obtained with Equation (A.1). Let* $X(P_1) = P_1^*$ *and* $X(P_2) = P_2^*$. *Show that* $P^*(u) = X(P(u))$ *is a line defined by* $wP_1^* + (1 - w)P_2^*$. *Find the relation between parameters* u *and* w, *obtaining that* $w = k_1 u/((k_1 - k_2)u + k_2)$.

Exercise A.19. *Show that the antiorthic axis of a triangle* ABC *is orthogonal to the line* X_1X_3.

Exercise A.20. *Consider the triangle* T *with vertices* $A = [-1, 0]$, $B = [1, 0]$ *and* $C = [u, v]$. *A point* P *is called equilateral if the Ceva triangle with respect to* P *is equilateral. Find an equilateral Ceva triangle with* P *in the interiof of* T. *Find the trilinear coordinates of the equilateral point and confirm that it is* X_{370}. *Analyze the case where* P *is in the exterior of* T. *See Kimberling (2019).*

Exercise A.21. *Let* $I = X_1$ *denote the incenter of a triangle* ABC. *Consider the Euler lines of the four triangles* BCI, CAI, ABI, *and* ABC. *Show that these four lines are concurrent. This point of concurrence is called Schiffler point, and it is* X_{21} *on Kimberling (ibid.). Determine the trilinear coordinates of this point.*

Exercise A.22. *Consider a triangle center given in barycentric coordinates as* $P = [f(a, b, c), f(b, c, a), f(c, a, b)]$ *and define the point* $E(P) = [f(-a, b, c), f(b, c, -a), f(c, -a, b)]$. *(i) Show that* E *is an involution and that* X_2 *is a fixed point of* E. *(ii) Determine the points* $E(X_1)$, $E(X_3)$ *and* $E(X_4)$. *See Kimberling (ibid.).*

Exercise A.23. *Consider a triangle* $\mathcal{T} = ABC$ *and triangular centers* X_1 *and* X_9. *Construct the circumconic* $\mathcal{E}$ *having center* X_9 *and perspector* X_1. *Construct the inconic* $\mathcal{E}_c$ *with the same perspector* X_1. *Show that the center of the inconic is* X_{37} *and that the three points* X_1, X_9, *and* X_{37} *are collinear.*

Exercise A.24. *Consider the space of* 3*-gons (triangles) in* $\mathbb{R}^2$, *up to translations and positive homotheties. Denote this space by* $\mathcal{P}(3, 2)$. *Show that* $\mathcal{P}(3, 2)$ *is diffeomorphic to the unitary sphere* $\mathbb{S}^3$. *Let* $SO(2)$ *be the set of positive rotations in the plane and* S_3 *the set of permutations. Let* $\varphi : S0(2) \times \mathcal{P}(3, 2) \to \mathcal{P}(3, 2)$ *be an action. Analyze the quocient space* $\mathcal{P}(3, 2)/S0(2)$.

Exercise A.25. *Consider a triangle $\mathcal{T} = ABC$, with sidelengths a, b and c. Suppose that $a + b + c$ is normalized to 2. Let $s_a = (b + c - a)/2$, $s_b = (a + c - b)/2$ and $s_c = (a + b - c)/2$. Therefore $s_a \geqslant 0$, $s_b \geqslant 0$ and $s_c \geqslant 0$. Finally, define $x^2 = 1 - a$, $y^2 = 1 - b$ and $z^2 = 1 - c$. Show that the unit sphere $\mathbb{S}^2$ ($x^2 + y^2 + z^2 = 1$) is an eight-fold covering of the space of ordered triangles of the plane up to translations, homotheties and rotations. See Bowden et al. (2019).*

Exercise A.26. *In the family of billiard 3-periodics, analyze properties of the associated spherical curve given in Exercise A.25.*

B Jacobi Elliptic Functions

A well-known reference on this topic is Armitage and Eberlein (2006).

B.1 Jacobi elliptic integral and inverse

The incomplete Jacobi elliptic integral of the first kind is defined as:

$$u = F(\varphi, k) = \int_0^{\varphi} \frac{dx}{\sqrt{1 - k^2 \sin^2 x}}$$

where $0 < k < 1$ is known as the *elliptic modulus*. The complete Jacobi integral of the first kind is obtained by setting $\varphi = \pi/2$.

The Jacobi *amplitude* function $\mathrm{am}(u, k)$ computes the inverse φ of F, i.e., given a u, what is φ such that $F(\varphi, k) = u$.

B.2 Jacobi elliptic functions

Referring to Figure B.1, the following are the three Jacobi *elliptic* functions:

$$\begin{aligned}\mathrm{cn}(u,k) &= \cos(\mathrm{am}(u,k))\\ \mathrm{sn}(u,k) &= \sin(\mathrm{am}(u,k))\\ \mathrm{dn}(u,k) &= \sqrt{1-k^2\mathrm{sn}^2(u,k)}\end{aligned}$$

Note: assuming a given k, we can occasionally omit it when writing the above, e.g., $\mathrm{cn}(u)$ is shorthand for $\mathrm{cn}(u,k)$.

B.3 Basic identities

$$\begin{aligned}\mathrm{cn}(0)=1, \quad \mathrm{sn}(0)=0, \quad \mathrm{dn}(0)=1,\\ \mathrm{cn}(K)=0, \quad \mathrm{sn}(K)=1, \quad \mathrm{dn}(K)=\sqrt{1-k^2}=k_1,\\ \mathrm{cn}(2K)=-1, \quad \mathrm{sn}(2K)=0, \quad \mathrm{dn}(2K)=1.\end{aligned}$$

Also,

$$\begin{aligned}\mathrm{sn}^2(u)+\mathrm{cn}^2(u) &= 1\\ \mathrm{dn}^2(u)+k^2\mathrm{sn}^2(u) &= 1\\ \mathrm{sn}'(u) &= \mathrm{cn}(u)\mathrm{dn}(u)\\ \mathrm{cn}'(u) &= -\mathrm{sn}(u)\mathrm{dn}(u)\\ \mathrm{dn}'(u) &= -k^2\mathrm{sn}(u)\mathrm{cn}(u)\\ \mathrm{am}'(u) &= \mathrm{dn}(u)\end{aligned}$$

$$\begin{aligned}\mathrm{cn}(u+v) &= \frac{\mathrm{cn}(u)\mathrm{cn}(v)-\mathrm{sn}(u)\mathrm{sn}(v)\mathrm{dn}(u)\mathrm{dn}(v)}{\Delta(u,v)}\\ \mathrm{sn}(u+v) &= \frac{\mathrm{sn}(u)\mathrm{cn}(v)\mathrm{dn}(v)+\mathrm{sn}(v)\mathrm{cn}(u)\mathrm{dn}(u)}{\Delta(u,v)}\\ \mathrm{dn}(u+v) &= \frac{\mathrm{dn}(u)\mathrm{dn}(v)-k^2\mathrm{sn}(u)\mathrm{sn}(v)\mathrm{cn}(u)\mathrm{cn}(v)}{\Delta(u,v)}\\ \Delta(u,v) &= 1-k^2\mathrm{sn}^2(u)\,\mathrm{sn}^2(v)\end{aligned}$$

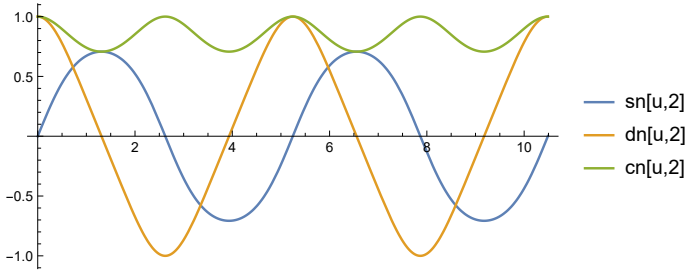

Figure B.1: The three Jacobi elliptic functions sn, cn, and dn.

B.4 Connection with differential equations

It turns out $\mathrm{sn}(u,k)$ is the solution to the implicit differential equation

$$\left(\frac{dy}{du}\right)^2 = (1-y^2)(1-k^2y^2)$$

Likewise, $\mathrm{cn}(u,k)$ is the solution to:

$$\left(\frac{dy}{du}\right)^2 = (1-y^2)(1-k^2+k^2y^2)$$

Finally, $\mathrm{dn}(u,k)$ is the solution to:

$$\left(\frac{dy}{du}\right)^2 = (y^2-1)(1-k^2-y^2)$$

B.5 Inverse Jacobi elliptic functions

The inverse Jacobi elliptic functions are defined as:

$$\operatorname{arcsn}(u,k) = \int_0^u \frac{dy}{\sqrt{(1-y^2)(1-k^2y^2)}}$$
$$\operatorname{arccn}(u,k) = \int_u^1 \frac{dy}{\sqrt{(1-y^2)(1-k^2+k^2y^2)}}$$
$$\operatorname{arcdn}(u,k) = \int_u^1 \frac{dy}{\sqrt{(1-y^2)(k^2-1+y^2)}}$$

B.6 Complex plane extension

Jacobi's elliptic functions can be extended to the complex plane: $sn(z,k) = \sin(\operatorname{am}(z,k))$, $cn(z,k) = \cos(\operatorname{am}(z,k))$ and $dn(z,k) = \sqrt{1-k^2sn^2(z,k)}$, where $z \in \mathbb{C}$, and $0 < k < 1$.

These functions have two independent periods and have simple poles at the same points. In fact:

$$\begin{aligned}
\operatorname{sn}(u+4K) &= \operatorname{sn}(u+2iK') = \operatorname{sn}(u)\\
\operatorname{cn}(u+4K) &= \operatorname{cn}(u+2K+2iK') = \operatorname{cn}(u)\\
\operatorname{dn}(u+2K) &= \operatorname{dn}(u+4iK') = \operatorname{dn}(u)\\
K' &= K(k'),\quad k' = \sqrt{1-k^2}
\end{aligned}$$

The poles of these three functions, which are simple, occur at points

$$2mK + i(2n+1)K',\quad m,n \in \mathbb{Z}$$

They display a certain symmetry around the poles. Namely, if z_p is a pole of $\operatorname{sn}(z)$, $\operatorname{cn}(z)$ and $\operatorname{dn}(z)$, then, for every $w \in \mathbb{C}$, we have Armitage and Eberlein (2006, Chapter 2):

$$\begin{aligned}
\operatorname{sn}(z_p+w) &= -\operatorname{sn}(z_p-w)\\
\operatorname{cn}(z_p+w) &= -\operatorname{cn}(z_p-w)\\
\operatorname{dn}(z_p+w) &= -\operatorname{dn}(z_p-w)
\end{aligned}$$

C Ellipse-Mounted Brocard loci

Let a family of triangles be defined with two vertices V_1, V_2 stationary with respect to an ellipse with semiaxes a, b, and a third vertex $V_3 = P(t)$ which sweeps the boundary, $P(t) = [a\cos t, b\sin t]$. Notice this family is non-Ponceletian. We show that over certain combinations of V_1 and, V_2, the Brocard points sweep beautiful, teardrop-shaped curves.

C.1 Circular sweep, one vertex at center

Referring to Figure C.1 (left):

Proposition C.1. *Let $b = a$. The locus of the Brocard points Ω_1 (resp. Ω_2) with $V_1 = (0,0)$ and $V_2 = (0,a)$ is a circle of radius $\frac{a}{3}$ (resp. a teardrop curve) of area $\frac{\pi a^2}{9}$ (resp. $\frac{2\pi a^2}{9}$).*

Proof. In this case we have that:

$$\Omega_1(t) = a\left[\frac{\cos t}{5-4\,\sin t}, \frac{2-a\sin t}{5-4\,\sin t}\right]$$

$$\Omega_2(t) = a\left[\frac{2\cos t - \sin 2t}{5-4\,\sin t}, \frac{2\sin t + \cos 2t}{5-4\,\sin t}\right]$$

□

Remark C.1. *The above loci intersect at* $a[\pm\sqrt{3}/6, 1/2]$*; along with* $V_2 = (0, a)$ *they define an equilateral. This stems from the fact that when* $P(t) = a[\pm\sqrt{3}/2, 1/2]$, $V_1V_2P(t)$ *is equilateral and the two Brocard points coincide at the Barycenter* X_2.

C.2 Circular sweep, two vertices at 90-degrees

Referring to Figure C.1 (right):

Proposition C.2. *The locus of* Ω_1 *and* Ω_2 *with* $V_1 = [0, a]$ *and* $V_2 = [a, 0]$ *are a pair of identical skewed teardrop shapes given by:*

$$\Omega_1(t) = a\left[\frac{\sin^2 t + \cos t - \sin t}{(\sin t - 2)\cos t - 2\,\sin t + 3}, \frac{1 - \cos t}{(\sin t - 2)\cos t - 2\,\sin t + 3}\right]$$

$$\Omega_2(t) = a\left[\frac{1 - \sin t}{(\cos t - 2)\sin t - 2\,\cos t + 3}, \frac{\left(\cos^2 t - \cos t + \sin t\right)}{(\sin t - 2)\cos t - 2\,\sin t + 3}\right]$$

Let $D([x, y]) = [y, x]$, the reflection about the diagonal. It follows that $\Omega_2(t) = (D \circ \Omega_1)(t - \frac{\pi}{2})$.

In Figure C.2 we show the shape of the locus varies in a complicated way when $V_2 = [0, a]$ and $V_1 = [x, 0]$, with $0 \leqslant x \leqslant a$.

C.3 Circular sweep, antipodal vertices

Referring to Figure C.3 (left), Ferréol (2020) has contributed the following statement:

Proposition C.3. *With* $V_1 = [-a, 0]$ *and* $V_2 = [a, 0]$*, the loci of the Brocard points are a pair of inversely-identical teardrop shapes whose areas are* $\pi a^2/\sqrt{5}$. *The one with a cusp on* V_1 *is given by the following quartic:*

$$x^4 - 2x^3 + 2y^2x^2 + 2x - 2y^2x - 1 + y^4 + 4y^2 = 0$$

Proof.

$$\Omega_1(t) = \left[\frac{-a\cos 2t - 8\,a\cos t + a}{\cos 2t - 9}, \frac{-2\,a\sin 2t - 4\,a\sin t}{\cos 2t - 9}\right]$$

$$\Omega_2(t) = \left[\frac{-8\,a\cos t + a\cos 2t - a}{\cos(2\,u) - 9}, \frac{2\,a\sin 2t - 4\,a\sin t}{\cos 2t - 9}.\right]$$

Let $R([x, y]) = [-x, y]$. Then $\Omega_2(t) = (R \circ \Omega_1)(t)$. The implicit form of Ω_2 is given by

$$B_2([x, y]) = a^2(a^2 - 2ax - 4y^2) + 2ax(x^2 + y^2) - (x^2 + y^2)^2 = 0.$$

Analogously, $B_1([x, y]) = B_2([-x, y]) = 0$ is the implicit form of Ω_1.

The area of the region bounded by Ω_i is given by $\frac{1}{2}\int_{\Omega_i} x\,dy - y\,dx$. It follows that $A(\Omega_i) = \frac{\sqrt{5}\pi a^2}{5}$. □

C.4 Ellipse sweep, two vertices at major endpoints

Figure C.3 (right) depicts the loci of Ω_1 and Ω_2 with $P(t)$ on an ellipse with semi-axes (a, b) and with $V_1 = [-a, 0]$ and $V_2 = [a, 0]$. Their loci are a pair of symmetric teardrop curves whose complicated parametric equations we omit.

C.5 Elliptic sweep, vertices on major axis

Proposition C.4. *The locus of Ω_1 and Ω_2 with $V_1 = [x_1, 0]$, $|x_1| \leqslant a$, $V_2 = [-a, 0]$ and $V_3 = [a\cos t, a\sin t]$ are a pair of singular teardrop curves with the following areas:*

$$A_1 = \frac{4\,(x_1 + a)^2\,a^5\pi}{\left(3\,a^2 + x_1^2\right)^2\sqrt{4\,a^2 + x_1^2}}$$

$$A_2 = \frac{\left(2\,a^2 - a x_1 + x_1^2\right)(x_1 + a)^3\,a^2\pi}{\left(3\,a^2 + x_1^2\right)^2\sqrt{4\,a^2 + x_1^2}}$$

When $x_1 = a$, the ratio of A_1 and A_2 by the area of the circle $a^2\pi$ both reduce to $1/\sqrt{5} \simeq 0.4472$.

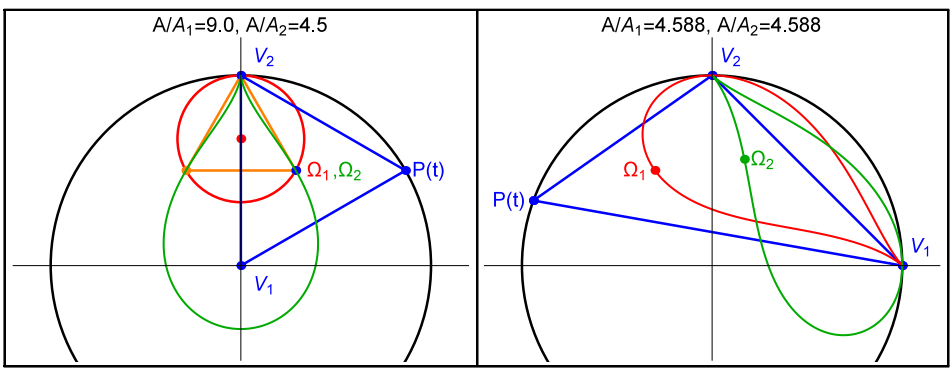

Figure C.1: **Left:** V_1 and V_2 are affixed to the center and top vertex of the unit circle and a third one $P(t)$ revolves around the circumference. The locus of the Brocard points Ω_1, Ω_2 are a circle (red) and a teardrop (green) whose areas are 1/9 and 2/9 that of the generating circle. The sample triangle (blue) shown is equilateral, so the two Brocard points coincide. Notice the curves' two intersections along with the top vertex form an equilateral (orange). **Right:** V_1, V_2 are now placed at the left and top vertices of the unit circle. The Brocard points of the family describe to inversely-similar teardrop shapes. Video, Live

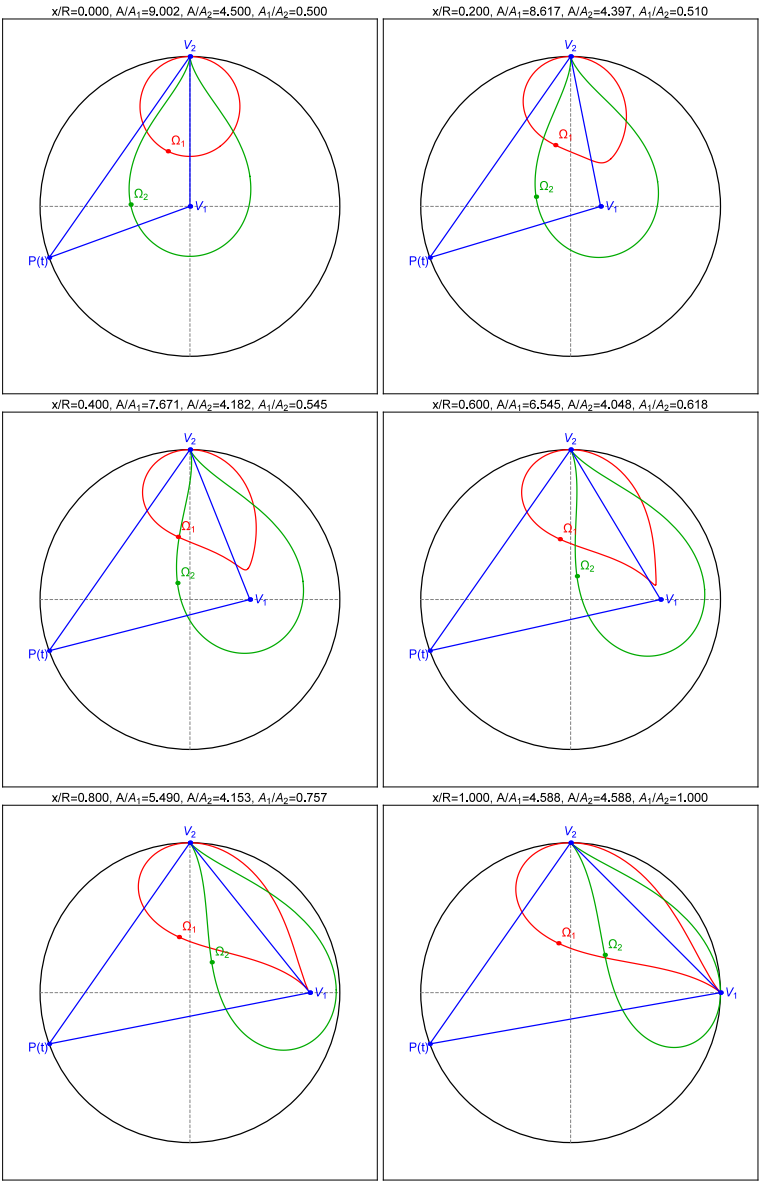

Figure C.2: Loci of Brocard Points Ω_1 (red) and Ω_2 (green) with V_2 fixed at $(0, 1)$ and as V_1 slides from the origin along the x axis toward $[1, 0]$. $P(t)$ performs a complete revolution on a unit circle (black). **Top left:** $V_1 = []0, 0]$, the locus of Ω_1 (resp. Ω_2) is a circle (resp. a teardrop curve) of $1/9$ (resp. $2/9$) the area of the external. **Bottom right:** when $V_1 = [a, 0]$ the two loci are inversely-similar

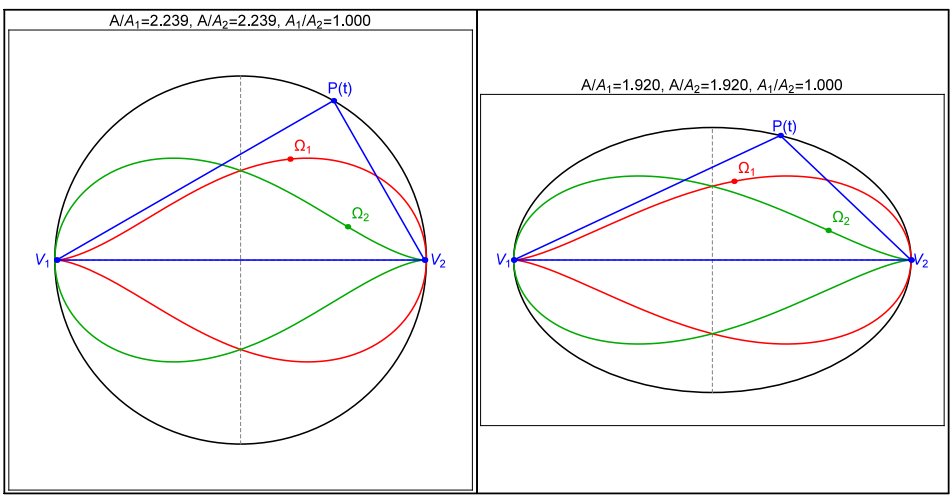

Figure C.3: **Left:** With antipodal V_1 and V_2 and $P(t)$ revolving on the circumference, the loci of the Brocards are symmetric teardrops whose area are $1/\sqrt{5}$ that of the circle. **Right:**. With V_1, V_2 at the major vertices of an ellipse of axes (a, b), and $P(t)$ revolving on its boundary, the the Brocard loci (red and green) are still symmetric (though stretched) teardrop shapes. In this case $a/b = 1.5$. Live

Proof. The above is obtained with direct integration and simplification with a computer algebra system (CAS). □

Bibliography

L. V. Ahlfors (1979). *Complex Analysis: an Introduction to Theory of Analytic Functions of One Complex Variable*. McGraw Hill. Zbl: 0395.30001 (cit. on p. 144).

A. Akopyan, R. Schwartz, and S. Tabachnikov (Sept. 2020). "Billiards in Ellipses Revisited." *Eur. J. Math.* (cit. on pp. 9, 19).

A. Akopyan and A. Zaslavsky (2007). *Geometry of Conics*. Providence, RI: Amer. Math. Soc. (cit. on pp. 7, 53).

J. V. Armitage and W. F. Eberlein (2006). *Elliptic Functions*. London: Cambridge University Press. Zbl: 1105.14001 (cit. on pp. 22, 224, 227).

M. Arnold and S. Tabachnikov (Sept. 2020). "Remarks on Joachimsthal integral and Poritsky property." arXiv: 2009.04988 (cit. on p. 12).

M. Bialy and S. Tabachnikov (Sept. 2020). "Dan Reznik's Identities and More." *Eur. J. Math.* (cit. on p. 9).

H. J. M. Bos, C. Kers, and D. W. Raven (1987). "Poncelet's Closure Theorem." *Expo. Math.* 5, pp. 289–364. Zbl: 0633.51014 (cit. on p. 3).

L. Bowden, A. Haynes, C. Shonkwiler, and A. Shukert (2019). "Spherical geometry and the least symmetric triangle." *Geom. Dedicata* 198, pp. 19–34. Zbl: 1418.53003 (cit. on p. 223).

C. Bradley (2011). "The Geometry of the Brocard Axis and Associated Conics." CJB/2011/170 (cit. on p. 59).

C. Bradley and G. Smith (2007). "On a Construction of Hagge." *Forum Geometricorum* 7, pp. 231–247. Zbl: 1162.51010 (cit. on pp. 59, 63, 116).

W. Chapple (1746). "An essay on the properties of triangles inscribed in, and circumscribed about two given circles." *Miscellanea Curiosa Mathematica, The Gentleman's Magazine* 4, pp. 117–124 (cit. on p. 48).

A. Chavez-Caliz (Aug. 2020). "More About Areas and Centers of Poncelet Polygons." *Arnold Math J.* (cit. on pp. 9, 220).

A. Connes and D. Zagier (2007). "A Property of Parallelograms Inscribed in Ellipses." *The American Mathematical Monthly* 114.10, pp. 909–914. Zbl: 1140.51010 (cit. on p. 26).

H. S. M. Coxeter and S. L. Greitzer (1967). *Geometry Revisited*. Vol. 19. New Mathematical Library. New York: Random House, Inc., pp. xiv+193. MR: 3155265. Zbl: 0166.16402 (cit. on pp. 7, 83).

U. Daepp, P. Gorkin, A. Shaffer, and K. Voss (2019). *Finding Ellipses: What Blaschke Products, Poncelet's Theorem, and the Numerical Range Know about Each Other*. MAA Press/AMS. Zbl: 1419.51001 (cit. on pp. 7, 121, 126, 127, 143).

I. Darlan and D. Reznik (June 2021). "An App for Visual Exploration, Discovery, and Sharing of Poncelet 3-Periodic Phenomena." arXiv: 2106.04521 (cit. on p. 163).

A. Del Centina (2016a). "Poncelet's porism: a long story of renewed discoveries, I." *Arch. Hist. Exact Sci.* 70.1, pp. 1–122. Zbl: 1333.01015 (cit. on pp. i, 50).

— (2016b). "Poncelet's porism: a long story of renewed discoveries, II." *Arch. Hist. Exact Sci.* 70.2, pp. 123–173. Zbl: 1345.01007 (cit. on pp. i, 3).

V. Dragović and M. Radnović (2021). "Poncelet polygons and monotonicity of rotation numbers: iso-periodic confocal pencils of conics, hidden traps, and marvels." arXiv: 2103.01215 (cit. on p. 127).

V. Dragović and M. Radnović (2011). *Poncelet Porisms and Beyond: Integrable Billiards, Hyperelliptic Jacobians and Pencils of Quadrics*. Frontiers in Mathematics. Basel: Springer (cit. on pp. 1, 116).

— (2014). "Bicentennial of the great Poncelet theorem (1813–2013): current advances." *Bull. Amer. Math. Soc. (N.S.)* 51.3, pp. 373–445. Zbl: 1417.37034 (cit. on p. 3).

R. Ferréol (July 2020). *Équation de la larme de Brocard 1*. Private Communication (cit. on p. 229).

C. Fierobe (2021). "On the circumcenters of triangular orbits in elliptic billiard." *Journal of Dynamical and Control Systems*. Accepted. arXiv: 1807.11903 (cit. on p. 9).

W. Gallatly (1914). *The modern geometry of the triangle*. Francis Hodgson. Zbl: 44.0595.17 (cit. on p. 5).

R. Garcia (2019). "Elliptic Billiards and Ellipses Associated to the 3-Periodic Orbits." *American Mathematical Monthly* 126.06, pp. 491–504. Zbl: 1444.37023 (cit. on pp. 9, 13, 20, 140).

R. Garcia and D. Reznik (Oct. 2020). "Invariants of Self-Intersected and Inversive N-Periodics in the Elliptic Billiard." arXiv: 2011.06640 (cit. on p. 26).

— (June 2021). "Related By Similarity I: Poristic Triangles and 3-Periodics in the Elliptic Billiard." *Intl. J. of Geom.* 10.3, pp. 52–70 (cit. on pp. 55, 59).

R. Garcia, D. Reznik, and J. Koiller (2020a). "Loci of 3-periodics in an Elliptic Billiard: why so many ellipses?" arXiv: 2001.08041 (cit. on pp. 88, 116).

— (2020b). "New Properties of Triangular Orbits in Elliptic Billiards." *Amer. Math. Monthly* to appear. arXiv: 2001.08054. Zbl: 1453.37024 (cit. on pp. 9, 17, 104).

— (Jan. 2021). *Companion Website to "Loci of 3-periodics in an Elliptic Billiard: Why so many ellipses?"* GitHub Pages (cit. on pp. 76, 117).

B. Gibert (2021a). *Catalogue of triangle cubics*. URL: https://bernard-gibert.pagesperso-orange.fr/index.html (cit. on pp. 44, 45).

— (2021b). *Thomson cubic*. URL: https://bernard-gibert.pagesperso-orange.fr/Exemples/k002.html (cit. on pp. 46, 47).

G. Glaeser, H. Stachel, and B. Odehnal (2016). *The Universe of Conics: From the ancient Greeks to 21st century developments*. Springer. Zbl: 1354.51001 (cit. on pp. 7, 53).

D. Grinberg (2012). "Ehrmann's third Lemoine Circle." *J. of Classical Geometry* 1, pp. 40–52 (cit. on pp. 73, 178).

M. Helman, D. Laurain, R. Garcia, and D. Reznik (Feb. 2021). *Center power and loci of Poncelet triangles*. arXiv: 2102.09438 (cit. on p. 124).

M. Helman, D. Laurain, D. Reznik, and R. Garcia (June 2021). *A theory for locus ellipticity of Poncelet 3-periodic centers*. arXiv: 2106.00715 (cit. on pp. 121, 140, 141).

M. Hohenwarter et al. (2013). *GeoGebra 4.4* (cit. on p. 163).

R. Honsberger (1995). *Episodes in Nineteenth and Twentieth Century Euclidean Geometry*. Washington, DC: Mathematical Association of America. Zbl: 0829.01001 (cit. on p. 79).

R. A. Johnson (1929). *Modern Geometry: An Elementary Treatise on the Geometry of the Triangle and the Circle*. Boston, MA: Houghton Mifflin (cit. on p. 204).

— (1960). *Advanced Euclidean Geometry*. 2nd. editor John W. Young. New York, NY: Dover. Zbl: 0090.37301 (cit. on pp. 5, 17).

V. Kaloshin and A. Sorrentino (2018). "On the Integrability of Birkhoff Billiards." *Phil. Trans. R. Soc.* A.376. Zbl: 1407.37085 (cit. on p. 3).

C. Kimberling (1998). *Triangle Centers and Central Triangles*. Vol. 129. Congr. Numer. Utilitas Mathematica Publishing, Inc. Zbl: 0912 . 51009 (cit. on p. 211).

— (2019). *Encyclopedia of Triangle Centers*. Zbl: 1423 . 05023. URL: http : // faculty . evansville . edu/ck6/encyclopedia/ETC . html (cit. on pp. 7, 30, 62, 67, 68, 76, 83, 85, 88, 90, 92, 93, 107, 116, 136, 138, 141, 155, 164, 178, 196, 222).

— (2020a). *Bicentric Pairs*. URL: https : //bit . ly/2Svh9Dr (cit. on pp. 173, 204).

— (2020b). *Central Lines of Triangle Centers*. URL: https : //bit . ly/34vVoJ8 (cit. on p. 136).

J. Koiller, D. Reznik, and R. Garcia (2021). "Average Elliptic Billiard Invariants with Spatial Integrals." arXiv: 2102 . 10899 (cit. on p. 22).

C. E. Lozada (Dec. 2016). *Index of Triangles Referenced in ETC*. last update: May 2021. URL: https : //faculty . evansville . edu/ck6/encyclopedia/ IndexOfTrianglesReferencedInETC . html (cit. on p. 170).

P. Moses (Sept. 2020). *Expressions for the Area of Isodynamic Pedal and Isogonic Antipedal Equilaterals*. Private Communication (cit. on p. 67).

B. Odehnal (2011). "Poristic loci of triangle centers." *J. Geom. Graph.* 15.1, pp. 45–67. MR: 2858157. Zbl: 1266 . 51024 (cit. on pp. 9, 51, 55, 116, 118, 131).

D. Reznik (2011). *Path of Incenter for Family of Triangular Orbits in Elliptical Billiard*. YouTube (cit. on p. 140).

— (2021a). *Arful Loci of Triangles in Ellipses* (cit. on p. 188).

— (May 2021b). *Experimental Poncelet Media Assets*. Observable (cit. on p. 163).

— (2021c). *Locus App Tutorial: a Video Walkthrough*. YouTube (cit. on p. 164).

D. Reznik and R. Garcia (2021a). "Circuminvariants of 3-periodics in the elliptic billiard." *Intl. J. Geometry* 10.1, pp. 31–57 (cit. on p. 53).

— (Mar. 2021b). "Related By Similarity II: Poncelet 3-Periodics in the Homothetic Pair and the Brocard Porism." *Intl. J. of Geom.* 10.4, pp. 18–31 (cit. on pp. 64, 111, 116).

D. Reznik, R. Garcia, and J. Koiller (2020a). "Can the Elliptic Billiard still surprise us?" *Math Intelligencer* 42, pp. 6–17. Zbl: 1439 . 37031 (cit. on pp. 9, 140, 182, 198).

— (2020b). "The Ballet of Triangle Centers on the Elliptic Billiard." *Journal for Geometry and Graphics* 24.1, pp. 079–101. Zbl: 1453 . 37024 (cit. on p. 90).

O. Romaskevich (2014). "On the incenters of triangular orbits on elliptic billiards." *Enseign. Math.* 60, pp. 247–255. arXiv: 1304 . 7588. MR: 3342645. Zbl: 1371.37073 (cit. on pp. 9, 13, 140).

— (May 2019). *Proof the Mittenpunkt is Stationary*. Private Communication. Rennes, France (cit. on p. 15).

R. Schwartz and S. Tabachnikov (2016a). "Centers of mass of Poncelet polygons, 200 years after." *Math. Intelligencer* 38.2, pp. 29–34. MR: 3507116. Zbl: 1351.01013 (cit. on p. 9).

— (2016b). "Centers of mass of Poncelet polygons, 200 years after." *Math. Intelligencer* 38.2, pp. 29–34. MR: 3507116. Zbl: 1351.01013 (cit. on p. 156).

R. Shail (1996). "Some properties of Brocard points." *The Mathematical Gazette* 80.489, pp. 485–491. Zbl: 0882.51009 (cit. on pp. 59, 60, 63).

H. Stachel (May 2021a). "On the Motion of Billiards in Ellipses." arXiv: 2105 . 03624v1. Zbl: 07336456 (cit. on p. 22).

— (May 2021b). "The Geometry of Billiards in Ellipses and their Poncelet Grids." arXiv: 2105.03362. Zbl: 07336456 (cit. on pp. 22, 23).

S. Tabachnikov (2005). *Geometry and Billiards*. Vol. 30. Student Mathematical Library. Mathematics Advanced Study Semesters, University Park, PA. Providence, RI: American Mathematical Society, pp. xii+176. MR: 2168892. Zbl: 1119.37001 (cit. on pp. 3, 12).

— (July 2020). *Invariant sum of squared sidelengths for N-periodics in the Homothetic Poncelet Pair.* Private Communication (cit. on p. 38).

S. Tabachnikov and E. Tsukerman (2014). "Circumcenter of Mass and Generalized Euler Line." *Discrete Comput. Geom.* 51, pp. 815–836. Zbl: 1301.51023 (cit. on p. 9).

N. C. Tak (n.d.). *General Formula for Equidistant Locus of Three Points*. Version accessed on: 2016-01-27). URL: https://math.stackexchange.com/q/1628779 (cit. on p. 134).

J. H. Weaver (1927). "Invariants of a poristic system of triangles." *Bull. Amer. Math. Soc.* 33.2, pp. 235–240. MR: 1561353. Zbl: 53.0604.08 (cit. on p. 50).

E. Weisstein (2009). *The CRC Encyclopedia of Mathematics*. 3rd. London: Chapman and Hall/CRC. Zbl: 1179.00007 (cit. on pp. 5, 10).

— (2019). "Mathworld." *MathWorld–A Wolfram Web Resource* (cit. on pp. 5, 19, 20, 25, 27, 30, 34, 35, 38, 43, 45, 50, 53, 55, 58, 60, 62, 63, 70, 73, 74, 82, 83, 85, 93, 100, 110, 111, 138, 146, 147, 156, 158, 170, 173, 174, 176, 177, 194, 203).

S. Wolfram (2019). *Mathematica, Version 10.0*. Champaign, IL (cit. on p. 163).

Y. Zhao (2021). "Three Lemmas in Geometry" (cit. on p. 220).

Index

Glossary

A Poncelet polygon signed area, page 17

A' Poncelet outer polygon signed area, page 17

J Joachimsthal's constant of an elliptic billiard, page 12

L perimeter of a billiard N-periodic, page 12

O center of outer ellipse, page 1

O_c center of inner ellipse, page 1

P_i Poncelet polygon vertex, page 1

R triangle circumradius, page 17

X_i Kimberling center $X(i)$, page 13

$\mathcal{E}$ outer ellipse, page 1

$\mathcal{E}_c$ inner ellipse, page 1

$\mathcal{E}_e$ locus of the excenters over billiard 3-periodics, page 13

$\mathcal{E}_i$ locus of X_i over billiard 3-periodics, page 13

Ω_1, Ω_2 a triangle Brocard points, page 60

ш $\cot\omega$, page 60

δ Darboux's constant of an elliptic billiard , page 12

κ, κ_i ellipse curvature at point $[x, y]$ or at vertex P_i, respectively, page 19

ω Brocard angle, page 62

sn, cn, dn elliptic Jacobi functions, page 23

θ counterclockwise angle from the major axis of $\mathcal{E}$ to that of $\mathcal{E}_c$, page 131

θ_i Poncelet polygon internal angle, page 17

θ_i' Poncelet outer polygon internal angle, page 17

a, b major and minor semiaxes of $\mathcal{E}$, page 12

a_c, b_c major and minor semiaxes of $\mathcal{E}_c$, page 12

a_e, b_e semiaxes of $\mathcal{E}_e$, page 13

a_i, b_i semiaxes of $\mathcal{E}_i$, when elliptic, page 13

c half focal length of $\mathcal{E}$, page 12

c_c half focal lenght of $\mathcal{E}_c$, page 131

$d_{j,i}$ distance from vertex P_i to focus f_j, page 19

f_j a focus of $\mathcal{E}$, page 19

r triangle inradius, page 17

s_i Poncelet polygon sidelength, page 15

x_c, y_c coordinates of O_c, page 131

altitude A segment from a vertex P on a triangle to the foot of a perpendicular dropped from P to the opposite side., page 197

anticomplementary triangle A triangle whose sides contain the reference's vertices and are parallel to the opposite sides, page 100

antiorthic axis The perspective axis of a triangle and its excentral triangle, page 217

antipedal triangle Given a triangle T and a point P, the triangle T' such that T is the pedal triangle of T' with respect to P, page 207

barycenter (X_2) The center of mass of a triangle, obtained by intersecting the medians, page 197

barycentric coordinates Given a triangle ABC and a point P, a triple of numbers proportional to the oriented areas of APB, BPC and CPA, page 196

Brianchon point Point of concurrence of the three lines through the vertices of a triangle and the points of contact of an inconic with the triangle, page 210

Brocard inellipse The inellipse centered on X_{39} with foci on the Brocard points, page 210

Brocard points Unique points Ω_1 and Ω_2 interior to a triangle ABC such that $\angle\Omega_1 AB = \angle\Omega_1 BC = \angle\Omega_1 CA = \omega$ and $\angle\Omega_2 BA = \angle\Omega_1 CB = \angle\Omega_2 AC = \omega$. They are a bicentric pair of points, page 109

CAP A concentric, axis-parallel pair of ellipses admitting Poncelet 3-periodics, page 9

CAS Computer algebra system, page 7

cevian A line from a vertex to a point on opposite sideline of a triangle, page 208

cevian triangle The triangle with vertices at the intersection of cevians through a point P with the opposite sidelines, page 208

circumbilliard The mittenpunkt- (i.e., X_9-) centered circumellipse, page 72

circumcenter (X_3) The center of the circumcircle, obtained by intersecting the perpendicular bisectors, page 197

circumcircle A circle passing through the vertices of a triangle. Its center is X_3, page 7

circumconic A conic passing through each of the vertices of a triangle, page 44

circumconic perspector The perspector of the polar triangle with respect to the circumconic and the reference triangle, page 222

circumellipse A circumconic which is an ellipse, page 53

circumhyperbola An circumconic which is a hyperbola, page 216

circumradius Radius of the circumcircle, page 17

confocal caustic The confocal conic to which all segments of a billiard trajectory are tangent, as implied by Joachimsthal's integral, page 5

contact triangle See intouch triangle, page 200

duality An incidence-preserving transformation with respect to a conic in which points are sent to lines (their polars) or conversely, lines are sent to points (their poles), page 112

ETC Kimberling's Encyclopedia of Triangle Centers, page 76

ETC Kimberling's Encyclopedia of Triangle Centers, page 196

Euler circle See nine-point circle, page 17

excenters The three intersections of the external bisectors to a triangle, page 200

excentral triangle The triangle with vertices at the excenters, page 200

excircles The three circles centered on each excenter and tangent to all sidelines, page 26

extouch triangle The triangle whose vertices are the extouchpoints, page 200

extouchpoints The points of tangency of the excircles with the sidelines, page 200

Feuerbach point (X_{11}) Where the incircle touches the nine-point circle, page 197

Feuerbach triangle The triangle whose vertices are where the 9-point circle touches each of the excircles, page 203

focus-inversive family The inversive image of billiard N-periodics with respect to a circle centered on a focus, page 147

Gergonne point (X_7) The perspector of a triangle and its intouch triangle, page 197

incenter (X_1) The center of the incircle, obtained by intersecting the three internal angle bisectors of a reference triangle, page 197

incircle The circle touching each side of a triangle. Its center is X_1, page 7

inconic A conic tangent to the each of the sidelines of a triangle, page 42

inconic perspector See Brianchon point, page 210

inellipse An inconic which is an ellipse, page 34

inradius Radius of the incircle, page 17

intouch triangle A triangle whose vertices are the intouchpoints, page 200

intouchpoints The points of tangency of the incircle with the sidelines, page 200

invariant a quantity that is conserved in a 1d-family of periodic trajectories, page 17

isogonal conjugate Given a point P, reflect the three P-cevians about the angular bisectors. These meet at the isogonal conjugate of P, page 211

isotomic conjugate Given a triangle P_i, $i = 1, 2, 3$, and a point X, consider the intersections Q_i of cevians through X with the opposite side. Let Q_i' be the reflection of Q_i about the midpoint of the corresponding side side. Lines $P_i Q_i'$ meet at X', the isotomic conjugate of X, page 213

Kimberling center A triangle center catalogued as X_k on Kimberling's Encyclopedia of Triangle Centers (ETC), page 76

MacBeath inconic The inellipse centered on the center X_5 of the nine-point circle. Its foci are X_3 and X_4, page 58

Mandart inellipse The inconic centered on X_9, whose perspector is X_8, page 217

medial triangle A triangle with vertices at the midpoints of the sides of a reference triangle, page 202

mittenpunkt (X_9) Where lines from each excenter through sides' midpoints concur, page 197

Nagel point (X_8) The perspector of a triangle and its extouch triangle, page 197

NCAP A non-concentric, axis-parallel pair of ellipses admitting Poncelet 3-periodics, page 9

nine-point center (X_5) The center of the nine-point circle, page 197

nine-point circle A circle passing through sides' midpoints. It also contains the feet of altitudes and the midpoints between vertices and the orthocenter. Its center is X_5, page 104

orthic triangle A triangle whose vertices are the feet of the three altitudes, page 39

orthocenter (X_4) Where altitudes concur, page 197

Pascal's limaçon Given a point P and a circle $\mathcal{C}$, the limaçon (small snail) is the envelope of all circles with centers on $\mathcal{C}$ which pass through P. The inversive image of an ellipse with respect to a focus-centered circle is a loopless limaçon, page 148

pedal triangle Given a point P, the triangle with vertices at the feet of perpendiculars from P dropped onto the sidelines of a reference triangle, page 207

perpendicular bisector A line through a triangle's side midpoint and perpendicular to said side, page 197

perspective axis For two perspective triangles, the line through the (collinear) intersections of corresponding sidelines, page 208

perspector For two perspective triangles, point of concurrence of lines connecting corresponding vertices, page 208

polar The line which is the dual of a point with respect to conic, page 208

polar triangle The triangle bounded by the polars of the vertices of a triangle with respect to a conic, page 208

pole The point which is the dual of a line with respect to a conic, page 208

poncelet iteration Sends a chord AB of a first conic $\mathcal{E}$ tangent to a second conic $\mathcal{E}'$, to a new chord BC of $\mathcal{E}$, such that BC is also tangent to $\mathcal{E}'$, page 1

Poncelet trajectory The piecewise linear trajectory resulting from sequential Poncelet iterations, page 1

Poncelet's porism A pair of conics which admits a closed Poncelet trajectory after N iterations (N-periodic) is associated with a 1d family of such N-periodic trajectories, page 13

Spieker center (X_{10}) The incenter of the medial triangle, page 197

stationary point A triangle center which remains stationary over the 1d family of 3-periodic trajectories in some conic pair, page 6

Steiner circumellipse The circumellipse centered on the barycenter X_2, page 82

symmedian A cevian through X_6, page 221

symmedian point (X_6) The intersection of the symmedians, page 197

triangle center A point on the plane of a triangle whose trilinears are $[f(a,b,c), f(b,c,a), f(c,a,b)]$ such f is a triangle center function, page 197

triangle center function Given a triangle with sidelenghts a, b, c, a function $f(a,b,c)$ which is both homogeneous and symmetric, i.e., $f(ta,tb,tc) = t^k f(a,b,c)$ and $f(a,b,c) = f(a,c,b)$, page 197

trilinear coordinates Given a triangle and a point P, a triple of numbers proportional to the signed distances from P to the each sideline, page 193

Títulos Publicados — 33º Colóquio Brasileiro de Matemática

Geometria Lipschitz das singularidades – *Lev Birbrair e Edvalter Sena*

Combinatória – *Fábio Botler, Maurício Collares, Taísa Martins, Walner Mendonça, Rob Morris e Guilherme Mota*

Códigos geométricos, uma introdução via corpos de funções algébricas – *Gilberto Brito de Almeida Filho e Saeed Tafazolian*

Topologia e geometria de 3-variedades, uma agradável introdução – *André Salles de Carvalho e Rafał Marian Siejakowski*

Ciência de dados: algoritmos e aplicações – *Luerbio Faria, Fabiano de Souza Oliveira, Paulo Eustáquio Duarte Pinto e Jayme Luiz Szwarcfiter*

Discovering Poncelet invariants in the plane – *Ronaldo A. Garcia e Dan S. Reznik*

Introdução à geometria e topologia dos sistemas dinâmicos em superfícies e além – *Víctor León e Bruno Scárdua*

Equações diferenciais e modelos epidemiológicos – *Marlon M. López-Flores, Dan Marchesin, Vítor Matos e Stephen Schecter*

Differential Equation Models in Epidemiology – *Marlon M. López-Flores, Dan Marchesin, Vítor Matos e Stephen Schecter*

A friendly invitation to Fourier analysis on polytopes – *Sinai Robins*

PI-álgebras: uma introdução à PI-teoria – *Rafael Bezerra dos Santos e Ana Cristina Vieira*

First steps into Model Order Reduction – *Alessandro Alla*

The Einstein Constraint Equations – *Rodrigo Avalos e Jorge H. Lira*

Dynamics of Circle Mappings – *Edson de Faria e Pablo Guarino*

Statistical model selection for stochastic systems with applications to Bioinformatics, Linguistics and Neurobiology – *Antonio Galves, Florencia Leonardi e Guilherme Ost*

Transfer operators in Hyperbolic Dynamics - an introduction – *Mark F. Demers, Niloofar Kiamari e Carlangelo Liverani*

A course in Hodge Theory: Periods of Algebraic Cycles – *Hossein Movasati e Roberto Villaflor Loyola*

A dynamical system approach for Lane-Emden type problems – *Liliane Maia, Gabrielle Nornberg e Filomena Pacella*

Visualizing Thurston's geometries – *Tiago Novello, Vinícius da Silva e Luiz Velho*

Scaling problems, algorithms and applications to Computer Science and Statistics – *Rafael Oliveira e Akshay Ramachandran*

An introduction to Characteristic Classes – *Jean-Paul Brasselet*

impa

Instituto de
Matemática
Pura e Aplicada

ISBN 978-65-89124-43-6